



UNIVERSITAT DE
BARCELONA

Mitochondrial dynamics and quality control mechanisms in Huntington's disease

Laura López Molina

ADVERTIMENT. La consulta d'aquesta tesi queda condicionada a l'acceptació de les següents condicions d'ús: La difusió d'aquesta tesi per mitjà del servei TDX (www.tdx.cat) i a través del Dipòsit Digital de la UB (diposit.ub.edu) ha estat autoritzada pels titulars dels drets de propietat intel·lectual únicament per a usos privats emmarcats en activitats d'investigació i docència. No s'autoritza la seva reproducció amb finalitats de lucre ni la seva difusió i posada a disposició des d'un lloc aliè al servei TDX ni al Dipòsit Digital de la UB. No s'autoritza la presentació del seu contingut en una finestra o marc aliè a TDX o al Dipòsit Digital de la UB (framing). Aquesta reserva de drets afecta tant al resum de presentació de la tesi com als seus continguts. En la utilització o cita de parts de la tesi és obligat indicar el nom de la persona autora.

ADVERTENCIA. La consulta de esta tesis queda condicionada a la aceptación de las siguientes condiciones de uso: La difusión de esta tesis por medio del servicio TDR (www.tdx.cat) y a través del Repositorio Digital de la UB (diposit.ub.edu) ha sido autorizada por los titulares de los derechos de propiedad intelectual únicamente para usos privados enmarcados en actividades de investigación y docencia. No se autoriza su reproducción con finalidades de lucro ni su difusión y puesta a disposición desde un sitio ajeno al servicio TDR o al Repositorio Digital de la UB. No se autoriza la presentación de su contenido en una ventana o marco ajeno a TDR o al Repositorio Digital de la UB (framing). Esta reserva de derechos afecta tanto al resumen de presentación de la tesis como a sus contenidos. En la utilización o cita de partes de la tesis es obligado indicar el nombre de la persona autora.

WARNING. On having consulted this thesis you're accepting the following use conditions: Spreading this thesis by the TDX (www.tdx.cat) service and by the UB Digital Repository (diposit.ub.edu) has been authorized by the titular of the intellectual property rights only for private uses placed in investigation and teaching activities. Reproduction with lucrative aims is not authorized nor its spreading and availability from a site foreign to the TDX service or to the UB Digital Repository. Introducing its content in a window or frame foreign to the TDX service or to the UB Digital Repository is not authorized (framing). Those rights affect to the presentation summary of the thesis as well as to its contents. In the using or citation of parts of the thesis it's obliged to indicate the name of the author.



UNIVERSITAT DE
BARCELONA

MITOCHONDRIAL DYNAMICS AND QUALITY CONTROL MECHANISMS IN HUNTINGTON'S DISEASE

Doctoral degree of Biomedicine in the Faculty of Medicine of the
University of Barcelona

Dissertation submitted by:

Laura López Molina

This work was performed at the Department of Biomedicine in the
Faculty of Medicine of the University of Barcelona under the supervision of
Dr. Silvia Ginés Padrós and Dr. Albert Giralt Torroella

Laura López Molina

Silvia Ginés Padrós

Albert Giralt Torroella

Programa de Doctorat en Biomedicina

“Above all, don’t fear difficult moments. The best comes from them.”

Rita Levi-Montalcini

“Life on earth is such a good story you cannot afford to miss the beginning.”

Lynn Margulis

A mis padres

RESUMEN

INTRODUCCIÓN

La enfermedad de Huntington (EH) es una enfermedad neurodegenerativa causada por la expansión de tripletes CAG en el exón 1 del gen que codifica para Huntingtina (Htt). Los pacientes de EH presentan una tríada de síntomas motores, cognitivos y psiquiátricos que suelen aparecer en la edad adulta y progresan con la enfermedad, hasta ocasionar la muerte en 15-20 años (Roos, 2010).

La característica neuropatológica más destacable de la EH es la atrofia del cuerpo estriado, formado por el putamen y el caudado, debida a la pérdida de neuronas de proyección predominantes en esta región (J. P. Vonsattel et al., 1985). Además de la muerte neuronal, el estriado de los pacientes de EH presenta un aumento de astrocitos reactivos, las células gliales más abundantes (J. P. Vonsattel et al., 1985). A pesar de que otras regiones cerebrales también degeneran, se desconoce por qué estas neuronas son más vulnerables en la EH.

Una de las hipótesis propuestas para explicar esta muerte neuronal selectiva es la disfunción mitocondrial. Estudios previos han demostrado que la Htt mutada (mHtt) altera las dinámicas mitocondriales, aumentando los procesos de fisión (X. Guo et al., 2013; Reddy, 2014). Además, la mHtt provoca un aumento en la liberación de calcio del retículo endoplasmático (RE) y altera la capacidad homeostática del calcio de las mitocondrias en neuronas estriatales (D. Lim et al., 2008; Tang et al., 2003). Teniendo en cuenta estas premisas, hipotetizamos que una alteración en las MAMs (*mitochondria-associated membranes*), regiones donde las mitocondrias interaccionan con el RE y que regulan tanto las dinámicas mitocondriales como el transporte de calcio entre ambos orgánulos (P. Gao et al., 2020), podrían mediar la específica sensibilidad de las neuronas estriatales a la mHtt.

Por otro lado, la alteración de la función astrocitaria podría modular negativamente la actividad de las neuronas estriatales en la EH. En este sentido, uno de los mecanismos de comunicación neuroglial que podría verse afectado es la transferencia de mitocondrias entre estos dos tipos celulares. En otros trastornos neurológicos se ha visto que la transferencia de mitocondrias gliales puede afectar la función neuronal (D. Liu et al., 2021). Sin embargo, no se conoce si la presencia de mHtt alteraría la función mitocondrial en astrocitos ni si la transferencia de mitocondrias de astrocitos con mHtt podría contribuir a la vulnerabilidad de las neuronas estriatales en la EH. En esta Tesis nos proponemos evaluar ambas posibilidades.

Por último, las proteínas de dinámicas mitocondriales están reguladas a través de la fosforilación mediada por quinasas. Pyk2 es una de las quinasas que más se ha estudiado por su papel en el sistema nervioso central tanto en condiciones fisiológicas como patológicas (de Pins et al., 2021). Pyk2 está enriquecida en el cerebro, especialmente en las neuronas hipocámpales y se ha involucrado principalmente en la activación de los receptores NMDA y en la regulación de la plasticidad sináptica (Bartos et al., 2010; Girault, Costa, et al., 1999). Aunque su localización mayoritaria es citosólica, después de la activación neuronal Pyk2 puede translocar a otros subcompartimentos celulares como espinas dendríticas o el núcleo (Camille Faure et al., 2013; S. Lee et al., 2019). En células no neuronales también se ha descrito que puede translocar parcialmente a la mitocondria y fosforilar proteínas relacionadas con el transporte de calcio (Hirschler-Laszkiwicz et al., 2018; O-Uchi et al., 2014). En esta Tesis, proponemos que Pyk2 también se podría localizar en las mitocondrias neuronales, rigiendo así las dinámicas mitocondriales y la homeostasis del calcio. Asimismo, dada la implicación de Pyk2 en los defectos cognitivos de la EH (Giralt et al., 2017), especulamos que la disfunción de Pyk2 podría contribuir a las alteraciones de las dinámicas mitocondriales que ocurren en las neuronas estriatales en esta enfermedad.

METODOLOGÍA

El modelo animal utilizado en esta Tesis para estudiar la disfunción mitocondrial en la EH es el ratón R6/1. Este modelo sobreexpresa el exón 1 humano con 115-145 repeticiones CAG y recapitula tanto la sintomatología motora y cognitiva observada en pacientes de EH como características neuropatológicas. Por otro lado, el estudio de Pyk2 en condiciones fisiológicas de esta tesis se ha realizado en un modelo de ratón deficiente en Pyk2 (Pyk2^{-/-}), que presenta un comportamiento y apariencia general normal. Este modelo ha sido utilizado previamente en otros trabajos para evaluar el papel de Pyk2 en neurodegeneración. En los estudios realizados con ambos modelos murinos se han combinado aproximaciones *in vitro* e *in vivo*.

Para evaluar las dinámicas mitocondriales se han utilizado principalmente técnicas de inmunofluorescencia y análisis por microscopía confocal, así como microscopía electrónica. Para analizar la expresión de distintas proteínas de interés se han realizado estudios bioquímicos y de citometría de flujo. En último lugar, el interactoma de Pyk2 se estudió por espectrometría de masas.

RESULTADOS Y DISCUSIÓN

En el primer estudio, nos hemos centrado en evaluar la implicación de las dinámicas mitocondriales y las MAMs en la regulación defectuosa de calcio en neuronas estriatales del ratón R6/1. Las dinámicas mitocondriales son eventos de fisión y fusión constantes que permiten determinar el tamaño y forma de la mitocondria a la vez que su distribución y función (Chan, 2006). Resultados previos de nuestro grupo y de otros han demostrado que varios modelos celulares y murinos de la EH presentan un aumento en la fragmentación mitocondrial debido a un aumento de los procesos de fisión (Cherubini et al., 2015; Reddy, 2014).

En esta Tesis, analizamos en primer lugar la morfología mitocondrial por inmunofluorescencia en cultivos neuronales estriatales de ratones R6/1. Las neuronas R6/1 mostraron un aumento en el número de mitocondrias, con una forma menos elongada y ramificada que en las control. A continuación, analizamos los contactos entre RE y mitocondria mediante la colocalización de plásmidos que marcan cada uno de los orgánulos, así como la interacción entre las proteínas IP3R3 y VDAC1, presentes en el RE y la mitocondria respectivamente. Ambas técnicas demostraron una reducción en la interacción entre los dos orgánulos en las neuronas estriatales del ratón R6/1. Estos resultados sugieren que el aumento de fragmentación mitocondrial en neuronas de EH podría llevar a la pérdida de contactos entre RE y mitocondrias.

A fin de averiguar si esta pérdida de contactos RE-mitocondria podría ser debida a alteraciones en proteínas propias de las MAMs, evaluamos los niveles de Grp75, IP3R3 y Mfn2 en muestras murinas y humanas de la EH. Estas tres proteínas se encuentran enriquecidas en las MAMs y están implicadas en el transporte de calcio en este subcompartimento celular. En lisados totales cerebrales del ratón R6/1 detectamos una reducción de Grp75, IP3R3 y Mfn2 en el estriado en estadios intermedios de la EH. Sin embargo, ninguna de las proteínas se vio alterada en el córtex o el hipocampo del ratón R6/1 a lo largo de la progresión de la enfermedad. Asimismo, las muestras *post mortem* de pacientes de EH también replicaron esta disminución en putamen y no en córtex o hipocampo. Esta reducción selectiva de proteínas de MAMs en el estriado podría explicar parcialmente la vulnerabilidad estriatal en la EH.

Los resultados obtenidos hasta el momento indicaban que la comunicación entre RE y mitocondria podría estar comprometida. Para comprobar si esta alteración pudiera contribuir a la desregulación de calcio característica del estriado en la EH, evaluamos los niveles de calcio intracelular y el potencial de membrana mitocondrial ($\Delta\psi_m$) en cultivos de neuronas estriatales de ratones WT y R6/1. Detectamos que las neuronas

R6/1 presentaban una disminución en la capacidad de captación de calcio de la mitocondria. En conjunto, nuestros resultados sugieren que la dishomeostasis de calcio en la EH podría depender no solo de la capacidad intrínseca de la mitocondria sino también de la integridad de las MAMs.

Para concluir el primer estudio de esta tesis, evaluamos si la fragmentación mitocondrial estaba mediando todas las alteraciones previamente descritas. Para ello, utilizamos un inhibidor farmacológico de Drp1, la principal proteína responsable de la fisión mitocondrial. El tratamiento con Mdivi-1, inhibidor de la actividad de Drp1, revirtió tanto el aumento de fragmentación mitocondrial como la pérdida de contactos entre RE y mitocondria en cultivos neuronales del ratón R6/1. A su vez, las neuronas R6/1 tratadas con Mdivi-1 también mejoraron la capacidad homeostática del calcio. En definitiva, nuestros resultados indican que la fisión mitocondrial dependiente de la actividad de Drp1 conlleva la perturbación en la comunicación entre RE y mitocondria en el estriado de la EH, señalando que la disfunción mitocondrial está implicada en la vulnerabilidad estriatal que ocurre en esta enfermedad.

En el segundo estudio, quisimos investigar la contribución de los astrocitos a la degeneración selectiva de las neuronas estriatales en la EH. Dada la gran heterogeneidad dentro de población de astrocitos, los estudios más recientes proponen identificarlos mediante perfiles de expresión o la combinación de varios marcadores en lugar de basarse únicamente en el marcador GFAP (Diaz-Castro et al., 2019; Escartin et al., 2021). Para profundizar en esta propuesta, estudiamos la expresión de los marcadores ALDH1L1, GFAP, GLAST y S100 β en el estriado de ratones WT y R6/1. En líneas generales, no detectamos diferencias ni en los niveles de proteína ni en la distribución entre genotipos. A pesar de no ver un aumento en GFAP, el marcador clásico de astrocitos reactivos, no se puede descartar el aumento de astrogliosis ya que se ha observado que no todos los modelos murinos de la EH recapitulan este fenómeno.

Sin embargo, al analizar otros rasgos de astrogliosis como la hipertrofia, sí que vimos un aumento en el área celular de los astrocitos R6/1 en cultivo. Por otro lado, los astrocitos estriatales R6/1 también presentaron un aumento tanto en la respiración mitocondrial, indicando un posible hipermetabolismo. Para descartar que este aumento de respiración mitocondrial es debido a una mayor cantidad de mitocondrias en los astrocitos R6/1, evaluamos la masa mitocondrial combinando técnicas bioquímicas y de inmunofluorescencia. No detectamos diferencias entre genotipos en ninguna de ellas, confirmando la premisa propuesta.

Teniendo en cuenta estos resultados, hipotetizamos que, frente a un exceso de función mitocondrial, los astrocitos R6/1 intentarían disipar el exceso energético iniciando la maquinaria de fisión mitocondrial. Por ello, analizamos proteínas relacionadas con la fisión mitocondrial como Drp1 y Cdk5, y vimos un aumento en su expresión en astrocitos estriatales aislados de ratones adultos R6/1.

Para finalizar esta parte de la tesis, nos propusimos investigar si las mitocondrias de los astrocitos R6/1 podrían ser transferidas a neuronas estriatales y cuál sería el efecto en dichas neuronas. Para ello, comprobamos que los cultivos de astrocitos de ratones WT y R6/1 liberaban mitocondrias funcionales en ambos genotipos. A continuación, tratamos neuronas estriatales WT con estas mitocondrias extracelulares y analizamos su efecto. Aquellas neuronas que recibieron mitocondrias de astrocitos R6/1 presentaron un aumento de estrés oxidativo, así como una disminución en la ramificación de las neuritas. Estos resultados sugieren que las mitocondrias provenientes de astrocitos de la EH contienen propiedades intrínsecas que promueven el daño neuronal, las cuales podrían contribuir a la muerte preferente de las neuronas estriatales en la EH.

En resumen, esta segunda parte demuestra que los astrocitos de la EH, a pesar de no cambiar en los marcadores astrocíticos, presentan algunos rasgos de astrogliosis como la hipertrofia celular o un aumento de la respiración, que provocan un aumento de la fisión mitocondrial. Por último, las alteraciones de la función mitocondrial en astrocitos debidas a la mHtt contribuyen a la degeneración selectiva del estriado en la EH, ya sea por la afectación del propio astrocito o por la comunicación con la neurona mediada por mitocondrias.

En el tercer estudio, nos centramos en el papel de Pyk2 en la regulación de las dinámicas mitocondriales en neuronas. Como Pyk2 es una proteína de anclaje con numerosas interacciones proteicas, primero evaluamos su interactoma en el hipocampo, región donde esta proteína presenta mayor expresión, mediante espectrometría de masas. Además de corroborar la implicación ya descrita en la regulación de receptores NMDA y plasticidad sináptica (Bartos et al., 2010; Heidinger et al., 2002), identificamos una nueva función relacionada con la homeostasis del calcio y la función mitocondria.

A continuación, verificamos por microscopia electrónica la presencia de Pyk2 no solo en las mitocondrias sino también en los contactos entre mitocondrias y RE en neuronas hipocampales. Además, demostramos que la ausencia de Pyk2 en neuronas aumenta la interacción entre RE y mitocondria, lo que podría ocasionar alteraciones en el

transporte de calcio en las MAMs. Para comprobarlo, analizamos los niveles de calcio intracelular y el $\Delta\psi_m$ en cultivos de neuronas hipocampales de ratones control (Pyk2^{+/+}) y Pyk2^{-/-}. Este experimento demostró que la ausencia de Pyk2 dificulta la capacidad de reservorio de calcio del RE, lo que podría alterar el flujo de calcio hacia la mitocondria y conllevar a una desregulación del calcio en la célula.

Finalmente, evaluamos las dinámicas y morfología de las mitocondrias. Por una parte, observamos que los ratones Pyk2^{-/-} presentaban un aumento en la proteína de fisión Drp1 mientras las proteínas de fusión Mfn2 y Opa1 no se veían alteradas. Por la otra, las neuronas Pyk2^{-/-} tanto en secciones hipocampales como en cultivo mostraron un aumento en el número de mitocondrias y una morfología más redondeada y menos compleja, características de la fragmentación mitocondrial. En conjunto, los resultados del tercer estudio de esta tesis demuestran que Pyk2 es una molécula crucial en la regulación de las dinámicas mitocondriales y en la formación de contactos entre RE y mitocondria en las neuronas en contexto fisiológico.

CONCLUSIONES

Los resultados presentados en esta tesis señalan las alteraciones en la función y las dinámicas de las mitocondrias como mecanismo patológico de la vulnerabilidad estriatal en la EH, que afectan tanto a neuronas como a astrocitos.

Asimismo, hemos aportado evidencias del nuevo rol de Pyk2 en la función mitocondrial de las neuronas en condiciones fisiológicas. Dado que las alteraciones en la homeostasis del calcio y en la función mitocondrial son características comunes en neurodegeneración, es probable que las alteraciones mitocondriales reguladas por Pyk2 contribuyan en los mecanismos patológicos de la EH. Además, ya se han descrito previamente alteraciones de Pyk2 en otras enfermedades neurológicas como Alzheimer o estrés crónico (Giralt et al., 2018; Montalban et al., 2019; Salazar et al., 2019). Por todo ello, proponemos Pyk2 como pieza clave en la perturbación de las dinámicas mitocondriales y de los contactos RE-mitocondria que ocurre en el estriado de la EH.

ABBREVIATIONS

ABBREVIATIONS

3-NP	3-nitropropionic acid
ACSA-2	Astrocyte cell surface antigen-2
A β	Amyloid β
AD	Alzheimer's disease
ALDH1L1	Aldehyde Dehydrogenase 1 Family Member L1
ALDOC	Aldolase C
ANOVA	Analysis of variance
AR	Aspect Ratio
ATP	Adenosine triphosphate
AU	Airy unit
BAC	Bacterial artificial chromosome
CA1	Cornu Ammonis 1
Ca ²⁺	Calcium ion
cADPR	Cyclic ADP-ribose
Ca _i ²⁺	Intracellular calcium
CCCP	Carbonyl cyanide m-chlorophenyl hydrazone
cDNA	Complementary DNA
CNS	Central nervous system
DIV	Days in vitro
DMSO	Dimethyl sulfoxide
DNA	Deoxyribonucleic acid
Drp1	Dynamamin-related protein 1
ER	Endoplasmic reticulum
ETC	Electron transport chain
FADH ₂	Reduced Flavin adenine dinucleotide
FAT	Focal adhesion targeting

ABBREVIATIONS

FCCP	Carbonyl cyanide-4-(trifluoromethoxy)phenylhydrazine
FERM	Four-point-one/ezrin/radixin/moesin
FF	Form Factor
Fis1	Mitochondrial fission protein 1
FMO	Fluorescence minus one
GFAP	Glial Fibrillary Acidic Protein
GFP	Green fluorescent protein
GLAST	Glutamate/aspartate transporter
GLT-1	Glutamate transporter 1
Grp75	Glucose-regulated protein 75
GWAS	Genome-wide association studies
H ⁺	Hydrogen
HD	Huntington's disease
Hdh	Huntington's disease homolog
Htt	Huntingtin
IMM	Inner mitochondrial membrane
IMS	Intramembrane space
IP3R	Inositol (1,4,5)-triphosphate receptor
KI	Knock-in
kDa	Kilodalton
KO	Knock-out
LTD	Long-term depression
LTP	Long-term potentiation
M	Molar
MAMs	Mitochondria-associated membranes
MAP2	Microtubule-associated protein 2

ABBREVIATIONS

MCU	Mitochondrial calcium uniporter
Mdivi-1	Mitochondrial division inhibitor 1
MFI	Mean fluorescence intensity
Mfn1	Mitofusin 1
Mfn2	Mitofusin 2
mHtt	Mutant huntingtin
mPTP	Mitochondrial permeability transition pore
MSN	Medium spiny neuron
mtDNA	Mitochondrial DNA
NADH	Reduced Nicotinamide adenine dinucleotide
NES	Nuclear export signal
NLS	Nuclear localization sequence
NMDAR	N-methyl-D-aspartate receptors
NTS	Nuclear targeting sequence
OMM	Outer mitochondrial membrane
OXPHOS	Oxidative phosphorylation
p	Phosphorylation
PBS	Phosphate buffer saline
PCR	Polymerase chain reaction
PD	Parkinson's disease
PFA	Paraformaldehyde
PINK1	PTEN-induced kinase 1
PKC	Protein kinase C
PLA	Proximity Ligation Assay
PolyQ	Polyglutamine
PR	Proline-rich

ABBREVIATIONS

PSD	Post synaptic densities
Pyk2	Proline-rich protein Tyrosine Kinase 2
RNA	Ribonucleic acid
ROI	Region of interest
ROS	Reactive oxygen species
rpm	Rotation per minute
RT	Room temperature
RT-qPCR	Quantitative reverse transcription polymerase chain reaction
SERCA	Sarco/endoplasmic reticulum Ca ²⁺ -ATPase
SEM	Standard error of the mean
SFK	Src-family kinases
STEP	Striatal-enriched phosphatase
TBS-T	Tris-buffered saline-Tween 20
TG	Thapsigargin
TMRM	Tetramethylrhodamine methyl ester
TNT	Tunneling nanotubes
VDAC	Voltage dependent-anion channels
WT	Wild type
YAC	Yeast artificial chromosome
$\Delta\Psi$	Membrane potential
$\Delta\Psi_m$	Mitochondrial membrane potential

TABLE OF CONTENTS

TABLE OF CONTENTS

INTRODUCTION	1
1. Role of mitochondria in the CNS	3
1.1. Mitochondrial functions	3
1.2. Mitochondrial dynamics and quality control mechanisms	6
1.3. Mitochondria-associated membranes	9
1.4. Mitochondrial transfer and transmitophagy	11
1.5. Mitochondrial defects in neurodegeneration	13
2. Huntington's Disease	17
2.1. Clinical features	17
2.2. Huntingtin gene and protein	19
2.3. Neuropathology	21
2.4. Huntington's disease models	22
2.5. Striatal vulnerability in Huntington's disease	26
3. Role of Pyk2 in the CNS	33
3.1. Structure of Pyk2	33
3.2. Activation of Pyk2	35
3.3. Physiological function of Pyk2 in the CNS	36
3.4. Regulation of Pyk2 localisation	38
3.5. Pathological role of Pyk2 in CNS	39
METHODS	47
1. Human HD <i>post-mortem</i> brain samples	49
2. Animal models	49
2.1. HD mouse model	50
2.2. Pyk2 ^{-/-} mouse	50
3. Cultures	51
3.1. Primary neuronal cultures	51
3.2. Primary astrocytic cultures	51
4. Cellular biology methods	52

TABLE OF CONTENTS

4.1. Plasmids and transfections	52
4.2. Mitochondrial ros production	54
4.3. Calcium and mitochondrial membrane potential imaging	54
4.4. Pharmacological treatments <i>in vitro</i>	55
4.5. Mitochondrial oxygen consumption	55
4.6. Measurement of metabolites in culture medium	56
4.7. Isolation of astrocytes from adult mouse brain.....	56
4.8. Mitotracker incubation	57
4.9. Oxidative stress production in live cells	58
5. Immunofluorescence	59
5.1. Immunocytochemistry	59
5.2. Proximity ligation assay.....	60
5.3. Flow citometry	61
6. Microscopy technics	65
6.1. Confocal image acquisition and analysis	65
6.2. Electron microscopy	67
7. Molecular biology methods	68
7.1. Protein extraction	68
7.2. Protein quantification.....	69
7.3. Western blot.....	69
7.4. Subcellular fractionation of nucleus, cytosol and mitochondria.....	71
7.5. Lipid peroxidase for oxidative stress production	72
7.6. Citrate synthase activity	72
7.7. Quantitative reverse transcription pcr (rt-qpcr).....	73
7.8. Immunoprecipitation.....	74
7.9. Mass spectrometry.....	74
8. Statistical analysis	75

TABLE OF CONTENTS

RESULTS	77
1. Role of mitochondrial dynamics and MAMs in HD striatal neuronal vulnerability	79
1.1. Mitochondrial morphology in R6/1 neuronal culture	79
1.2. Loss of ER-mitochondria contact sites in R6/1 striatal neurons	82
1.3. MAMs proteins are decreased specifically in the striatum of HD mice and HD patients.....	84
1.4. ER-mitochondrial calcium transfer is altered in R6/1 striatal neurons.....	90
1.5. Increased Drp1 activity mediates excessive mitochondrial fragmentation in R6/1 striatal neurons.....	92
1.6. Inhibition of Drp1 prevents alterations in mams and mitochondrial function	95
2. Contribution of astrocytic mitochondria to striatal vulnerability in HD	98
2.1. Characterization of astrocyte population in R6/1 striatum.....	98
2.2. Oxidative and glycolytic metabolisms are increased in R6/1 striatal astrocytes	102
2.3. Mitochondria in adult R6/1 striatal astrocytes are not less functional	103
2.4. Mitochondrial dynamics are altered in R6/1 striatal astrocytes	105
2.5. Mitochondrial release from R6/1 astrocytes contributes to striatal neuronal vulnerability	109
3. Role of Pyk2 in mitochondria and MAMS	115
3.1. Pyk2 is reduced in the striatum of HD patients	115
3.2. Pyk2 interacts with mitochondrial proteins in hippocampus	116
3.3. Pyk2 is localised in mitochondria and MAMS	118
3.4. ER-mitochondrial contact sites formation is regulated by Pyk2	120
3.5. Pyk2 is involved in ER-mitochondria calcium transfer in hippocampal neuronal cultures.....	122
3.6. Pyk2 regulates mitochondrial dynamics and morphology <i>in vivo</i> and <i>in vitro</i> hippocampal neurons.....	124
3.7. Nuclear translocation and location domains of Pyk2 control dynamics of hippocampal mitochondria	126

TABLE OF CONTENTS

DISCUSSION	131
1. Role of mitochondrial dynamics and MAMs in HD striatal neuronal vulnerability	133
2. Contribution of astrocytic mitochondria to striatal vulnerability in HD	137
3. Role of Pyk2 in mitochondria and MAMs	145
4. Pyk2: a new player in the disruption of mitochondrial dynamics and MAMs in HD?	148
CONCLUSIONS	153
REFERENCES	157
ANNEX	193
Supplementary Table 1.....	195
Supplementary Table 2.....	197
Publications	210

INTRODUCTION

INTRODUCTION

Mitochondria are ancestral organelles originated 1.45 billion years ago that gave rise to eukaryotic cells as Lynn Margulis explain with the endosymbiotic theory (Margulis, 1967). Since they are descendants from proteobacteria, mitochondria conserve some prokaryotic characteristics and are considered as semi-autonomous organelles. The brain is the most energetic demanding organ of the human body, requiring up to 20% of total ATP, out of which 96% is consumed by neurons (X. H. Zhu et al., 2012), and mitochondria are crucial to provide the immense necessity of nutrients and energy for neural function. Thus, mitochondria arise as fundamental regulators in the CNS. In this Thesis, we aim to understand the role of mitochondria in Huntington's disease and how alterations of their function may underlie selective striatal vulnerability, affecting both neurons and astrocytes.

1. ROLE OF MITOCHONDRIA IN THE CNS

1.1. Mitochondrial functions

Mitochondria are double membrane organelles placed in the cytoplasm, presenting an outer mitochondrial membrane (OMM) and an inner mitochondrial membrane (IMM). These structures delimit the mitochondrial matrix, surrounded by the IMM, and the intramembrane space (IMS), between OMM and IMM (Figure 1). Each of these compartments is highly specialized and required for vital cellular functions. The OMM is a lipid bilayer that resembles to other eukaryotic membranes that separates the organelle from the cytosol (Scorrano, 2013). The IMM presents a similar composition to prokaryotic membranes, with high contents of cardiolipin. Cardiolipin is responsible for the IMM curvature, forming invaginations called cristae, that expand into the matrix and where oxidative phosphorylation (OXPHOS) occurs (Dimmer et al., 2011). In the IMS, protons pumped during the electron transport chain (ETC) are accumulated. Finally, the matrix is where numerous metabolic pathways occur, as the Krebs cycle and the fatty acid oxidation. In addition, the mitochondrial matrix contains circular small genome, the mitochondrial DNA (mtDNA), that is maternally inherited. mtDNA contains 37 genes encoding 13 proteins, 22 transfer RNA and 2 ribosomal RNA involved in the function and structure of ETC (Taanman, 1999). Thus, mitochondria are considered as semi-autonomous organelles. Mitochondria are involved in many crucial mechanisms for the cell, but the two principal functions are ATP production and calcium homeostasis. Hereunder, these two processes are detailed.

INTRODUCTION

1.1.1. ATP production

Mitochondria are actively implicated in energy metabolism, being considered as the powerhouse of the cell. Mitochondrial energy conversion occurs in the IMM through the OXPHOS (Figure 1). Oxidation of nutrients provides electron in the form of NADH and FADH₂ to the ETC that are transported from complex I or II respectively. Complexes I, III and IV pump protons to the IMS creating an electrochemical gradient, and proton re-entry drives synthesis of ATP from ADP in the complex V or ATP synthase (Kühlbrandt, 2015; Liesa & Shirihai, 2013).

During OXPHOS, reactive oxidative species (ROS) are generated and the main form of ROS, superoxide anion (O₂⁻), is produced by the electron leakage in complex I and III. ROS participate in physiological cellular signalling regulating autophagy, immunity and cell differentiation (Sena & Chandel, 2012). However, high levels of ROS can cause oxidative stress and hamper normal functions, contributing to pathological processes in ageing, cancer, diabetes or neurodegeneration (Sena & Chandel, 2012).

1.1.2. Calcium homeostasis

Calcium ion (Ca²⁺) is an intracellular messenger involved in cellular processes including secretion, metabolism, membrane excitability, contraction in the muscle, and gene expression and neurotransmitter release in neurons (reviewed in (M. J. Berridge et al., 2000)). Intracellular Ca²⁺ is mainly stored in the ER, the larger reservoir that is constantly refilled by the sarco/endoplasmic reticulum Ca²⁺-ATPase (SERCA) pump (Raffaello et al., 2016). Mitochondria play a fundamental role in buffering the cytosolic calcium and oscillations in cytosolic Ca²⁺ are tightly controlled by a balance between mitochondrial Ca²⁺ uptake and release (Figure 1).

Ca²⁺ entry in the mitochondria thanks to the electrochemical gradient of protons translocation during ETC, which creates a large potential gradient, called the mitochondrial membrane potential ($\Delta\Psi_m$) (Contreras et al., 2010). The resulting $\Delta\Psi_m$ represents a driving force for Ca²⁺ to accumulate in the mitochondria, crossing both OMM and IMM. The most abundant Ca²⁺ channels in the OMM are voltage dependent anion channel (VDAC) (Shoshan-Barmatz & Ben-Hail, 2012). Subsequently, Ca²⁺ is absorbed inside the mitochondria through the mitochondrial calcium uniporter (MCU), placed in the IMM.

INTRODUCTION

Accumulation of Ca^{2+} in the matrix is counteracted by efflux mechanisms that maintain intramitochondrial homeostasis. In excitable cells like neurons, the main system to extrude Ca^{2+} to the cytosol is the mitochondrial $\text{Na}^+/\text{Ca}^{2+}$ exchanger (Castaldo et al., 2009). Non-excitable cells as astrocytes and oligodendrocytes use $\text{Ca}^{2+}/\text{H}^+$ exchanger as Ca^{2+} efflux mediator (Chaudhuri et al., 2021). In addition, overload of Ca^{2+} uptake induces a bioenergetic failure of the organelle, opening the mitochondrial permeability transition pore (mPTP). Prolonged opening of mPTP might result into a loss of $\Delta\Psi_m$ and enables the release of pro-apoptotic factors from the mitochondria to the cytoplasm (Rozzi et al., 2018).

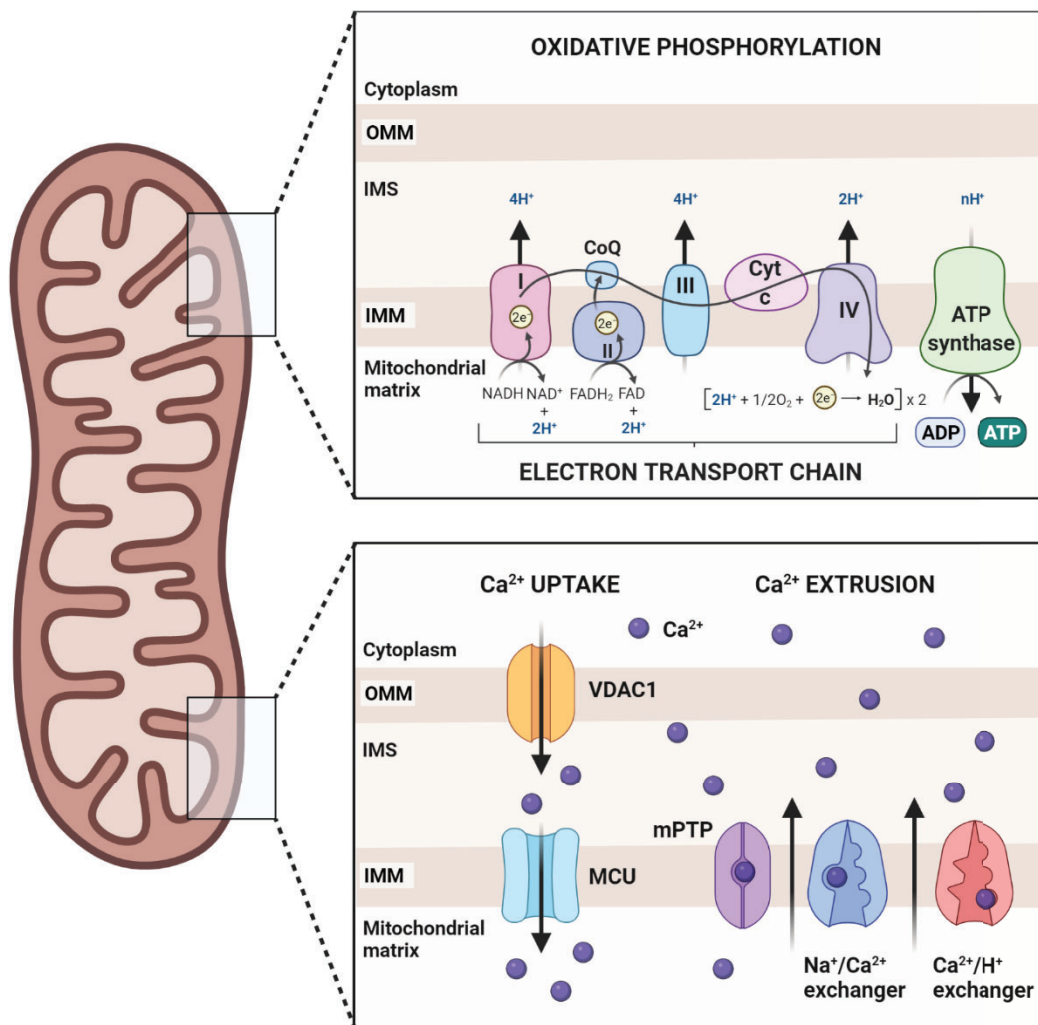


Figure 1. General functions of mitochondria. Mitochondria produce energy through oxidative phosphorylation (OXPHOS). In the IMM, electrons are transported through complexes I-IV to ATP synthase to generate ATP. To ensure calcium homeostasis, mitochondria regulate calcium uptake and extrusion. Ca^{2+} enters the mitochondria crossing VDAC1 in the OMM and MCU in the IMM. Ca^{2+} is released through $\text{Na}^+/\text{Ca}^{2+}$ exchanger and in some cells also through $\text{Ca}^{2+}/\text{H}^+$ exchange. In case of Ca^{2+} overload, mPTP is induced.

INTRODUCTION

1.2. Mitochondrial dynamics and quality control mechanisms

Far from being static and rigid structures, mitochondria are dynamic organelles that constantly move within the cell and undergo coordinated turnover. For ensuring proper function and number, mitochondrial dynamics and quality control must be regulated. Mitochondrial dynamics comprise the balance between fission and fusion events, shaping the organelles according to cell's necessities. Fission enables the division of mitochondrial network into smaller entities, facilitating their transport and distribution to distant locations. In turn, mitochondrial fusion allows mixing of genetic content, preventing from detrimental effects of mtDNA mutations, and dissipation of excess of metabolic energy (Oliveira et al., 2007; D. Yang et al., 2021).

The master regulator of mitochondrial fission is Drp1, a GTPase mainly located in the cytosol but also in the mitochondria. To initiate fission, Drp1 reorganises into a ring-like structure around mitochondrion, constraining the organelle and inducing division. In the OMM, proteins Fis1 and Mff act as adaptors for oligomeric forms of Drp1, thus enhancing Drp1 recruitment. The constant relocation of Drp1 and its GTPase activation have been postulated to be modulated by multiple post-translation modifications, including phosphorylation. Initially, Drp1 was reported to be phosphorylated at serine 616 by Cdk1/Cyclin B during mitosis, inducing its oligomerization and dividing mitochondria (Lackner & Nunnari, 2010). Later, several investigations in murine neurons pointed out Cdk5 as a modulator of this phosphorylation site, affecting Drp1 localisation and therefore mitochondrial morphology (Cho et al., 2014; Jahani-Asl et al., 2015). In addition, a recent investigation in fibroblasts suggested that PINK1 could also phosphorylate Drp1 on serine 616 site (Han et al., 2020). On the contrary, Drp1 phosphorylation at serine 637 by PKA seemed to inhibit fission either by impediment of Drp1 translocation or reduction of the GTPase activity (Cereghetti et al., 2008; C. R. Chang & Blackstone, 2007; L. C. Gomes et al., 2011).

Since mitochondria are double membrane organelles, fusion of OMM and IMM are tightly synchronised but regulated by independent machinery. The fusion of OMM is upon the activity of mitofusin (Mfn) proteins. Mfn1 and Mfn2 are GTPase located in the OMM that can form homotypic or heterotypic interactions with adjacent mitochondria (H. Chen et al., 2005). Following OMM fusion, Opa1 orchestrates IMM fusion. Opa1 is a dynamin-related GTPase present as integral protein in the IMM and as soluble form in the IMS and it is in charge of cristae remodelling (Frezza et al., 2006). To better understand their role, Chen and colleagues showed that mouse embryonic fibroblasts with null mutations in Mfn1 or Mfn2 displayed highly fragmented mitochondria with loss of $\Delta\Psi_m$ and lower

INTRODUCTION

cellular respiration (H. Chen et al., 2005) while lack of Opa1 impeded mitochondrial fusion that drove to poor cellular functionality (H. Chen et al., 2005).

On the other side, quality of mitochondria is assessed by mitophagy and biogenesis. Mitophagy is a subcellular process that selectively degrades damaged mitochondria. In mitophagy, organelles with low $\Delta\Psi_m$ accumulates PINK1 in the OMM and triggers recruitment of Parkin. The complex PINK1/Parkin leads to autophagic sequestration, lysosomal fusion and degradation (Gottlieb & Bernstein, 2016). Biogenesis refers to the *de novo* formation of organelles and depends on the coordinated expression of nuclear and mitochondrial genes. It is mostly controlled by PGC-1 α , which translocates to the nucleus and interacts with transcription factors NRF1 and NRF2 to enhance transcription of genes related to mitochondrial biogenesis (Y. Wang et al., 2019).

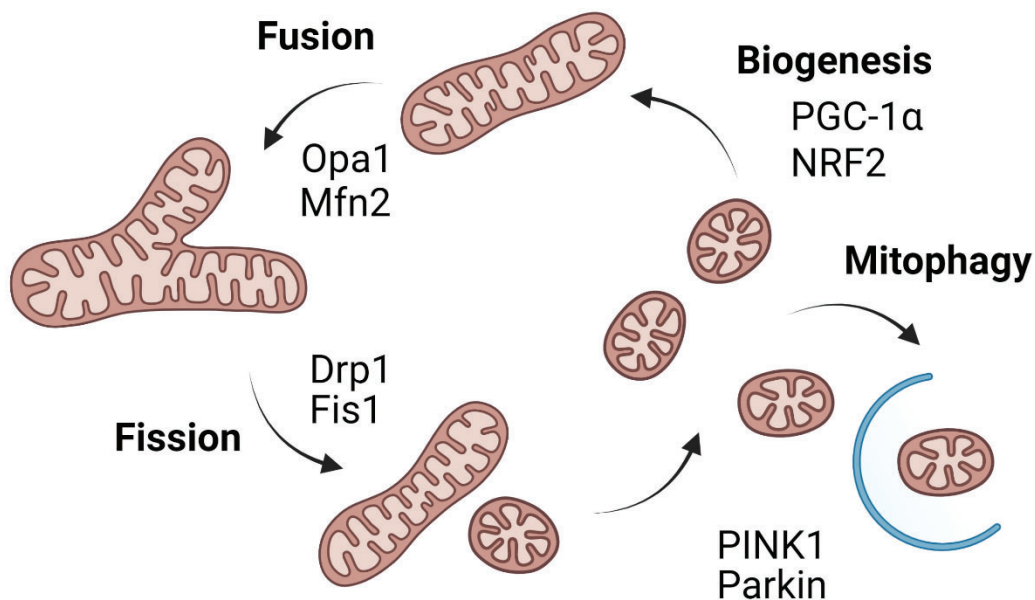


Figure 2. Mitochondrial dynamics and quality control mechanisms. Mitochondria undergo dynamic changes in the number and the morphology. To control mitochondrial mass and size, fission and fusion events are balanced. Fission is regulated by Drp1 and Fis1 while fusion is induced by Opa1 and Mfn2. To ensure the quality of these organelles, damaged mitochondria are tagged with PINK1 and Parkin and processed for degradation through the selective autophagy named mitophagy. In turn, new mitochondria are synthesised through the biogenesis, a process mediated by PGC-1 α and NRF2.

INTRODUCTION

As a result of all these cyclic events, mitochondria constantly remodel their morphology, meaning that in a healthy cell coexists a wide variety of shapes and sizes. Indeed, mitochondrial shape and number differ upon cell type or tissue. Hence, alterations in mitochondrial dynamics machinery culminate in abnormal shapes in the mitochondrial pool, entailing that unbalanced fission will lead to fragmentation whereas unopposed fusion will cause elongation (Figure 3).

In the CNS, most of investigations on mitochondrial morphology have been conducted in neuronal models. However, mitochondria from neurons and astrocytes, the major glial cell in the brain, present distinctions in mitochondrial dynamics. In neurons, up to 40-50% of the whole mitochondrial pool are mobile, in a direct motion combined with brief pauses. Neuronal mitochondria can be transported anterogradely at $0.55 \mu\text{m/s}$ and retrogradely at $0.65 \mu\text{m/s}$ (Jackson et al., 2014; Stephen et al., 2015). Conversely, only 20-30% of mitochondria in astrocytes are mobile, following an oscillatory pattern of movement and with lower motion speed in anterograde ($0.15 \mu\text{m/sec}$) and retrograde ($0.2 \mu\text{m/sec}$) transport (Jackson et al., 2014; Jackson & Robinson, 2018; Stephen et al., 2015). These differences in mitochondrial motility suggest that fusion events could be less frequent in astrocytes than in neurons, indicating differential regulation of mitochondria upon cellular type in the CNS.

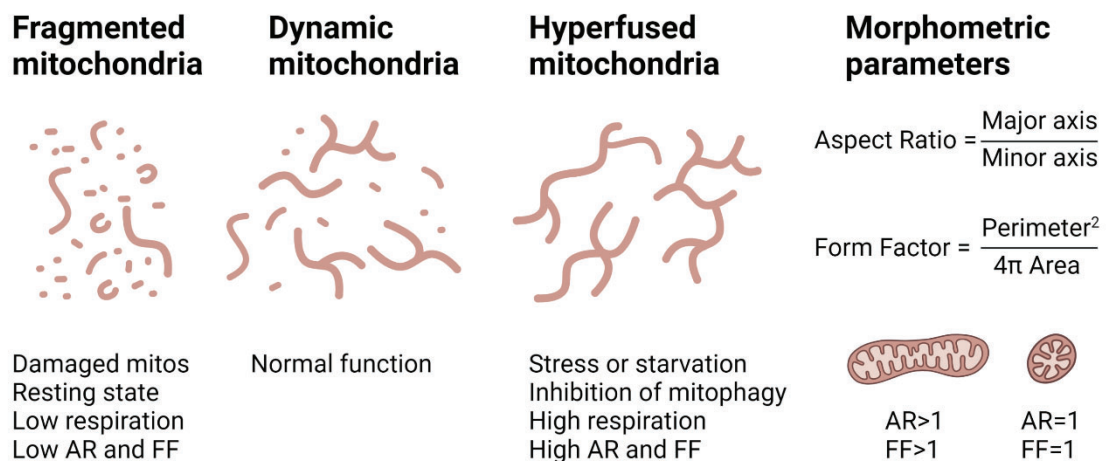


Figure 3. Mitochondrial morphology and morphometric parameters. Imbalance in fission/fusion machinery promotes alterations in mitochondrial morphology. Excessive fission leads to fragmented mitochondria, with smaller and rounder shapes and decreased function. Excessive fusion drives to elongated mitochondria and inhibited mitophagy. To evaluate morphology of mitochondria, parameters as Aspect Ratio and Form Factor are calculated as a measure of mitochondrial elongation and branching.

1.3. Mitochondria-associated membranes

Once thought to be solitary organelles, mitochondria interact with other cellular compartments forming contact sites. The most studied ones are those with the endoplasmic reticulum (ER), called mitochondria associated membranes (MAMs). It is estimated that 5-20% of total mitochondrial surface is in close apposition to the ER (Rizzuto et al., 1998). OMM tethers at a distance of 9-16 nm with the smooth ER and 19-30 nm with the rough ER (Csordás et al., 2006). Adequate distance is highly regulated by specific linking proteins since excessive juxtaposition (<5 nm) may lead to a Ca^{2+} overload of mitochondria (Csordás et al., 2006). Enrichment of resident proteins confers this region with a specific biochemical composition, proven with its isolation through cell fractionation in 1990 by Jean Vance, who described it as a sedimenting ER fraction associated with mitochondria (Rusiñol et al., 1994). Initially reported as key components in lipid synthesis (Rusiñol et al., 1994), MAMs are known to be in charge of many more functions as Ca^{2+} transport, mitochondrial dynamics and biogenesis, ER stress, inflammation and autophagy (reviewed in (P. Gao et al., 2020)). In this Thesis, Ca^{2+} transfer in MAMs is of particular interest due to the relevance of Ca^{2+} in neuronal function and neurodegenerative processes (Figure 4).

Mitochondrial Ca^{2+} absorption strongly depends on the intracellular calcium concentration and mitochondria must be exposed to high levels of Ca^{2+} to uptake it. Hence, mitochondrial Ca^{2+} absorption is most likely to take place nearby compartments with Ca^{2+} release such as the ER (Giorgi et al., 2018). For this reason, MAMs are microdomains with higher Ca^{2+} concentrations than in the bulk of the cytosol (Rizzuto et al., 1993). In these hotspots, Ca^{2+} effluxes from the ER through the main calcium channel, the inositol 1,4,5 trisphosphate receptor (IP3R) and enters mitochondria crossing the VDAC1 channel in the OMM. Notably, there are three IP3R isoforms, being IP3R2 only expressed in glia and IP3R3 predominantly neuronal (Sharp et al., 1999) and specialized in transmitting Ca^{2+} to mitochondria (D. A. Gomes et al., 2005). The complex IP3R3/VDAC1 is physically strength by the molecular chaperone glucose-regulated protein 75 (Grp75). Other MAMs resident proteins as Mfn2 reinforce the link that maintains the proper distance between both organelles (De Brito & Scorrano, 2008).

Moreover, MAMs participate in mitochondrial dynamics (Figure 4). ER is described to physically wrap around mitochondria, helping in their division (Rowland & Voeltz, 2012a). Friedman et al. demonstrated that ER tubules mark mitochondrial fission sites prior to the recruitment of mitochondrial division machinery and thus, ER tubules that contact mitochondria might define the location of mitochondrial fission sites (Friedman et al.,

INTRODUCTION

2011). On the other hand, mitochondrial fusion protein Mfn2 is enriched in ER-mitochondria surface. Mfn2 in the ER can form homotypic or heterotypic unions with Mfn2 or Mfn1 in OMM. Thus, these complexes enable regulation of MAMs distance but also ER shape and mitochondrial fusion (H. Chen et al., 2003; De Brito & Scorrano, 2008). Indeed, ablation of Mfn2 in mouse embryonic fibroblasts and HeLa cells demonstrated loosening of ER-mitochondrial interaction as well as disruption of ER morphology (De Brito & Scorrano, 2008).

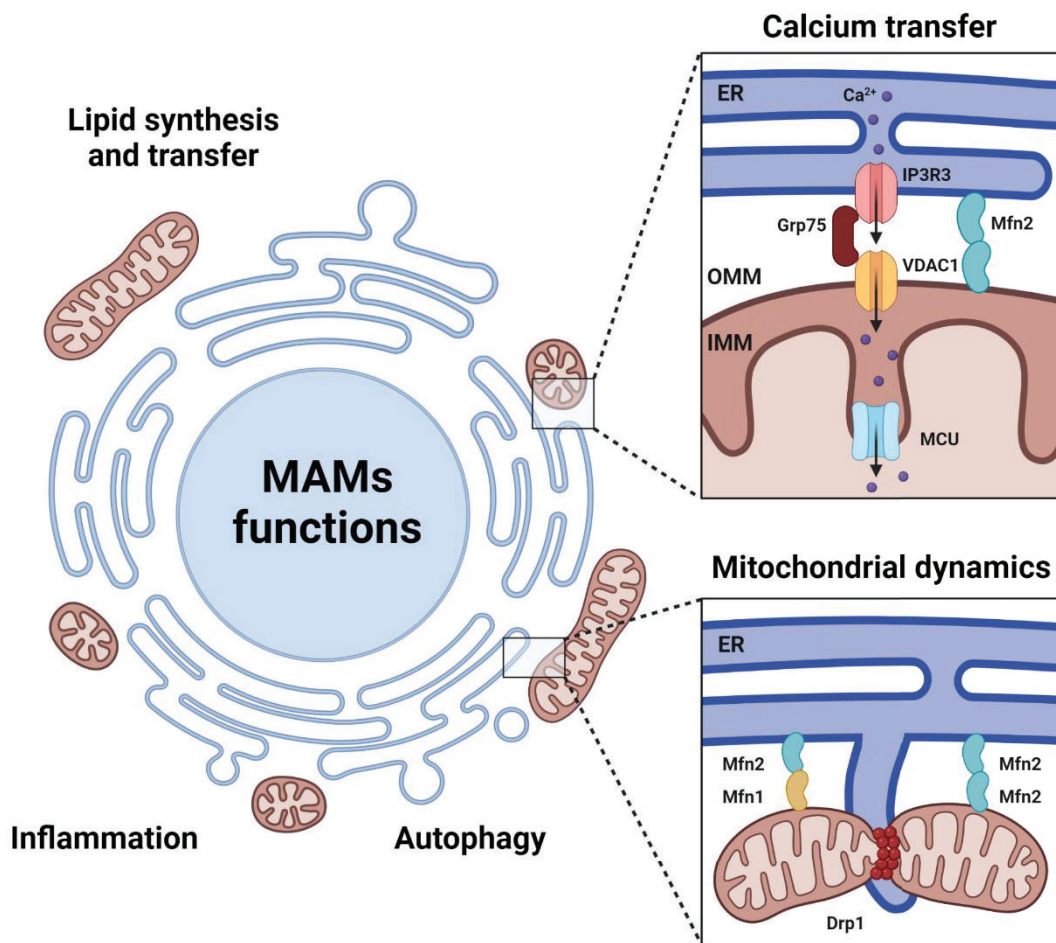


Figure 4. Function of MAMs and proteins mediating calcium transfer and mitochondrial dynamics. ER and mitochondria closely interact forming microdomains called MAMs. These regions tightly control Ca²⁺ homeostasis and transfer from the ER to the mitochondria. Ca²⁺ is released by IP3R3, crosses VDAC1 in the IMM and accumulates in the mitochondria via MCU. Grp75 and Mfn2 strengthen the interaction between ER and mitochondria. MAMs are also involved in mitochondrial dynamics since the ER can constrain the mitochondrion and helps in the mitochondrial fission. Mfn2 in the ER can either interact with Mfn1 or Mfn2 in the OMM.

1.4. Mitochondrial transfer and transmitophagy

It is widely accepted that healthy cells control their own mitochondrial quality control mechanisms. However, some years ago a new concept called “transmitophagy” arose and challenged this current dogma. Transmitophagy has been described as the horizontal transfer of mitochondria between cells. In the horizontal transfer, whole mitochondria and mtDNA are transported from a donor cell and incorporated in the acceptor cell (M. V. Berridge et al., 2016). Transmitophagy is proposed to be as a part of the machinery that regulates mitochondrial quantity and quality in physiological conditions, meaning that mitochondrial biogenesis and mitophagy could be simultaneously occurring intracellular and intercellular.

It was first noticed by Gerdes' lab that nanotubular structures (tunnelling nanotubes, TNT) mediated cell-to-cell communication and facilitated selective transport of intracellular organelles (Rustom et al., 2004). TNT seemed as ultrafine structures formed *de novo* and appeared as a continuous membrane connecting two cells. Then, Speed and colleagues demonstrated mitochondrial transfer *in vitro*, showing how mitochondria or mtDNA were transferred from mesenchymal stem cells to carcinoma cells depleted of mtDNA (A549 ρ^0 cells) and consequently, aerobic respiration in acceptor cells was rescued (Spees et al., 2006). Since then, growing evidence support the existence of mitochondrial transfer between mammal cells *in vitro* (reviewed in (D. Liu et al., 2021)). In the CNS, transmitophagy has been postulated to occur as a neuro-glial crosstalk (Figure 5). Hence, damaged mitochondria from neurons could be degraded by astrocytes and astrocytes would supply neurons with healthy and fully functional *de novo* mitochondria (Davis et al., 2014; Hayakawa et al., 2016).

INTRODUCTION

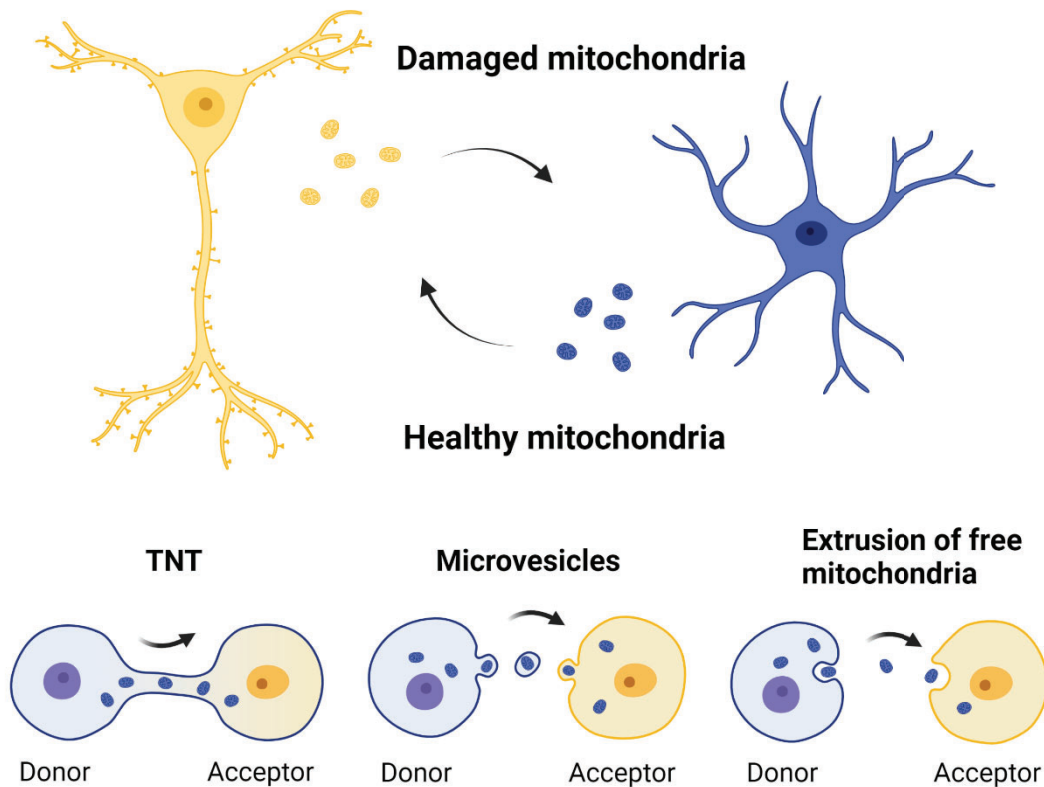


Figure 5. Proposed mechanisms of transmitophagy between astrocyte and neurons. Astrocytes could represent a support for neurons by degrading defective neuronal mitochondria and by providing new and healthy mitochondria. Mitochondria can be transfer from donor cell to acceptor cell through tunnelling nanotubes (TNT), microvesicles fused with plasma membrane or internalization of free mitochondria.

So far, it has not been fully understood how mitochondria can move from one cell to another. TNT are the major structure for mitochondrial transfer, being cell membrane protrusions connecting two cells. Other mechanisms proposed are the release of extracellular vesicles and extrusion of free mitochondrion or mitochondrial content (Shanmughapriya et al., 2020) (Figure 5). Regarding the molecular pathways underlying this process, CD38 has been shown to be an indispensable player in the release of extracellular mitochondrial (Hayakawa et al., 2016). CD38 is a multifunctional enzyme that catalyses NAD to cyclic ADP-ribose (cADPR), which is a second messenger that mobilizes intracellular Ca^{2+} by coupling to the ER ryanodine receptor (Guerreiro et al., 2020; Mészáros et al., 1993). In the brain, CD38 is predominantly expressed in astrocytes and to a lesser extend in neuron and microglia (Akimoto et al., 2013; Yamada et al., 1997). CD38 mediates astrocyte-to-neuron communication by the activation of intracellular calcium responses in the astrocyte. In turn, glutamate released from neurons up-regulates CD38 expression in astrocytes (Bruzzone et al., 2004). Thus, CD38 plays a role in neuroglia crosstalk in a bidirectional manner.

1.5. Mitochondrial defects in neurodegeneration

Neurodegenerative diseases are characterized by the progressive loss function and structure of the nervous system. Mitochondrial dysfunction is a common feature in most of them and it is becoming one of the emerging mechanisms to understand the neuropathology process associated to Alzheimer's disease (AD), Parkinson's disease (PD) or Huntington's disease (HD) among others. Although defects in mitochondria may not be the primary cause, failure of these organelles seems to be an early event in the pathophysiology of these neurodegenerative disorders and could be one of the main triggering phenomena leading to neuronal dysfunction and death. Among many disturbances, brains of AD, PD and HD patients show decreased ATP production, high levels of oxidative stress and defective metabolism, finally compromising neuronal viability (M. Flint Beal, 2000; Browne & Beal, 2004; X. Zhu et al., 2006). Below, mitochondrial affectation in AD and PD, the most frequent neurodegenerative disease, are detailed whereas alterations in HD will be further elaborated in section 2.5.4 in this chapter.

1.5.1. Mitochondrial dynamics and quality control in neurodegeneration

As mentioned above, alterations in mitochondrial dynamics can result in fatal repercussion for the cell. Hence, mutations in genes related to mitochondrial fission and fusion are highly detrimental and have been associated with several neuronal affections (reviewed in (Zorzano & Claret, 2015)).

Although ablation of fission protein Drp1 is lethal (Ishihara et al., 2009), mutations in this protein in *Drosophila* recapitulated neurodegenerative phenotypes and a hyperfused mitochondrial network (Fowler et al., 2020). Conversely, mutations in fusion protein Mfn2 in mice cause Charcot-Marie-Tooth disease subtype 2A, a peripheral neuropathy characterized by chronic axonal degeneration of motor and sensory neurons. Consistently, mutations in Opa1 induces autosomal dominant optic atrophy, reporting a progressive degeneration of retinal ganglion cells and disrupted mitochondrial cristae in axons of optic nerve. In this context of impaired fusion, mitochondria are excessively fragmented and trafficking is hampered (Alavi et al., 2007; Zorzano & Claret, 2015).

Compelling evidence show affection of mitochondrial dynamics and quality control in AD. In AD brain of mouse and patients, it was reported reduction of Mfn1 and Mfn2 and increment of Drp1 in protein and mRNA levels (Manczak et al., 2011; Watanabe et al.,

INTRODUCTION

2016) along with an excessive mitochondrial fragmentation and aberrant distribution, that could be reverted with pharmacological Drp1 inhibition (W. Wang et al., 2017). In addition, AD models present impaired mitophagy accompanied by diminished levels of Parkin (Du et al., 2017; D. Yang et al., 2021). Similarly, increased Drp1 levels have been observed in brains of PD patients (F. Zhao et al., 2017) while in PD mouse models mutations in α -synuclein and LRKK2 trigger Drp1 translocation to mitochondria, causing mitochondrial fragmentation (Ordonez et al., 2018; X. Wang et al., 2012). In addition, it has been reported that loss of Mfn2 contributes to degeneration of dopaminergic neurons in the brain of PD mouse models. Moreover, mutations in Parkin and PINK1 in *Drosophila* reproduced many of the characteristics of PD such as loss of dopaminergic neurons and mitochondrial pathology (Yufeng Yang et al., 2006).

1.5.2. MAMs and calcium homeostasis in neurodegeneration

Defects in calcium homeostasis are a hallmark in neurodegenerative diseases and intracellular calcium overload has been described as a component in neurotoxicity. Therefore, mitochondrial mishandling of calcium has been tightly related to neurodegeneration processes and growing evidence links calcium dyshomeostasis with alterations in MAMs (Esteras & Abramov, 2020; Hees, 2019).

In AD, amyloid β ($A\beta$) has been found to interact with mitochondria and to promote mitochondrial Ca^{2+} overload (Sanz-Blasco et al., 2008) as well as massive Ca^{2+} release from the ER (Ferreiro et al., 2008). Moreover, AD-related proteins presenilin 1 (PS1) and presenilin 2 (PS2) are enriched in MAMs. Indeed, upregulation of MAMs function and increased ER-mitochondrial contacts were detected in presenilin-mutant cells and fibroblasts from PD patients (Area-Gomez et al., 2012). IP3R3 and VDAC1 also showed enhanced protein expression in hippocampal neurons exposed to $A\beta$, causing an increment in contact sites between ER and mitochondria (Hedskog et al., 2013). Levels of Mfn2 are controverted, since human AD brains showed a reduction in mRNA and protein levels (Manczak et al., 2011) while FAD mice reported a significant raise (Filadi et al., 2016). Discrepancies in the outcome could be due to difference in the severity of the AD mice models. Nonetheless, Mfn2 is postulated to play a fundamental role in AD pathological mechanisms (Eysert et al., 2020).

Likewise, PD-related proteins α -synuclein, Parkin and PINK1 are highly located in ER-mitochondrial interaction sites (Calì et al., 2012, 2013; Celardo et al., 2016). Mutations in α -synuclein seem to impair mitochondrial Ca^{2+} uptake whereas defects in Parkin

INTRODUCTION

function trigger loss of ER-mitochondrial contact sites and Ca^{2+} mishandling (Gandhi et al., 2009; Rodríguez-Arribas et al., 2017). Several studies have reported the interaction of α -synuclein with MAMs-resident proteins VDAC1 and Grp75 (F. T. Liu et al., 2015; Lu et al., 2013). In addition, overexpression of α -synuclein diminished ER-mitochondria association, hampering Ca^{2+} buffering and ATP production (Guardia-Laguarta et al., 2014; Paillusson et al., 2017). On the contrary, Cali et al. described that overexpression of α -synuclein induced a physical and functional increment in ER-mitochondrial contact sites together with an enhancement in mitochondrial Ca^{2+} uptake (Cali et al., 2012). As with AD, current studies differ whether MAMs are up or downregulated in PD. Further investigations should clarify if these discrepancies are due to stages in neurodegeneration or if the diversity in the PD models are activating different molecular mechanisms. Altogether indicate that despite one direction or the other, dysregulation of MAMs formation results in detrimental consequences for the cell, that contribute to neurodegeneration.

1.5.3. Mitochondrial transfer in neurodegeneration

While in physiological conditions mitochondrial transfer represents a part of the recycling cycle, under pathological situations can constitute a replacement of dysfunctional mitochondria for functional ones, protecting the damage cell from mitochondrial dysfunction (Davis et al., 2014). Although mitochondrial transfer in neurodegenerations has been insufficiently explored, many investigations have studied this cellular process in other pathological contexts in the CNS. For instance, mitochondria released from astrocytes conferred neuroprotection in a mouse model of ischemia (Hayakawa et al., 2016). Moreover, beneficial transfer of mitochondria from astrocytes to neurons have been described in ischemic stroke (Hayakawa et al., 2016; Lippert & Borlongan, 2019), and after cisplatin treatment (English et al., 2020), resulting in the improvement of neuronal viability and restoring of ATP production and calcium homeostasis. On the other direction, transport of defective mitochondria from neurons to astrocyte were reported in optic nerve (Davis et al., 2014) and PD rat model (Morales et al., 2020), preventing neuro-inflammation.

Interestingly, extracellular mitochondria have been proposed as a therapeutical approach for diseases with neuronal vulnerability. Recently, a study performed in human patients and in a rat model of stroke reported extracellular mitochondria in the CSF after subarachnoid haemorrhage (Chou et al., 2017). The same authors also suggested the use of these extracellular mitochondrial as biomarkers since higher levels of $\Delta\Psi_m$

INTRODUCTION

correlated with better clinical recovery after stroke injury. Other reports successfully attempted *in vivo* transplant of healthy mitochondria to damaged brain tissues and recovered neuronal functionality in murine models of PD (J. C. Chang et al., 2016; Shi et al., 2017), and ischemic stroke (Huang et al., 2016). Indeed, mitochondrial transplantation in human has already been tested and currently an on-going clinical trial is recruiting patients to investigate amelioration of myocardial ischemia after direct injection of autologous mitochondria into the ischemic myocardium (NCT#02851758) (C. Y. Chang et al., 2019). Therefore, it would be interesting to extend this knowledge to neural diseases, particularly to neurodegenerative diseases, and translate these potential therapeutic applications.

As mentioned in the previous section, one of the few proposed molecular mechanisms to modulate the transfer of extracellular mitochondria is CD38 (Hayakawa et al., 2016). Although no investigation has implicated CD38 in neurodegenerative diseases yet, levels of CD38 increase with aging and correlate with a reduction of NAD, a neuroprotective metabolite degraded by CD38, as well as with mitochondrial dysfunction (Barbosa et al., 2007; Camacho-Pereira et al., 2016). Interestingly, low levels of NAD were reported in AD, PD, HD and ALS (Guerreiro et al., 2020; Lautrup et al., 2019) as well as in normal aging (X. H. Zhu et al., 2015). Since CD38 is the main player of NAD degradation, this reduction could be linked to a higher CD38 activity in neurodegenerative disorders, that would lead to alterations in mitochondrial transfer between astrocytes and neurons. Nevertheless, further research on this topic would be required to unravel the role of CD38 in neurodegenerative processes.

2. HUNTINGTON'S DISEASE

Huntington's disease (HD) is a rare neurodegenerative disease characterized by the triad of progressive motor, cognitive and psychiatric symptoms. HD was first mentioned in 1842 by Charles Walter, but George Huntington was the first reporting a detailed description of HD in 1878, highlighting the hereditary pattern, the existence of chorea along with cognitive and psychiatric perturbations and the progressive nature of the disease (Huntington, 2003). The causative gene causing HD was mapped in 1983 (Gusella et al., 1983) but it was not until 1993 when the mutations in the gene were identified (The Huntington's Disease Collaborative, 1993). To date, available treatments for HD are only addressed to alleviate symptomatology, but no effective cure has been developed yet.

2.1. Clinical features

Huntington's disease has a prevalence of 10.6–13.7 individuals per 100,000 in Western populations. However, prevalence ratios are largely heterogeneous worldwide and Asian countries have a much lower incidence of HD with a prevalence of 1–7 cases per million whereas the highest occurrence documented is in the region of Lake Maracaibo, Venezuela, where the prevalence is about 700 per 100,000 (P. McColgan & Tabrizi, 2018; Okun & Thommi, 2004).

Diagnosis of HD is generally based on a positive genetic test and the onset of motor disturbance. Symptoms typically develop in middle age, between 30 and 50 years old, and it is followed by the disease progression until death, usually 15-20 years later (Figure 6). The initial motor symptomatology occurs as involuntary and excessive movements in distal extremities as fingers, toes and facial muscles that gradually extend to proximal and finally to all other muscles. At later stages of the disease, hyperkinetic movements dissipate and shift to hypokinesia, showing bradykinesia, dystonia, and rigidity (Roos, 2010). Secondly, cognitive disturbances appear up to 20 years before the onset of chorea and are those related to executive functions including alterations in attention and emotion recognition, impairments in working and spatial memory, deficits in language comprehension and verbal fluency, which gradually worsen to severe dementia (Giralt et al., 2012; Jane S. Paulsen et al., 2017). Thirdly, psychiatric symptoms appear up to 20 years before the onset of chorea and comprise a wide variety of manifestations being depression the most reported, follow by anxiety and apathy. In addition, HD patients can also suffer from irritability, aggressivity, obsessive-compulsive behaviours and suicidal

INTRODUCTION

thoughts (J. S. Paulsen, 2005; Van Duijn et al., 2007). Notably, rates of suicide in HD patients are higher than in the general population (Wetzel et al., 2011). HD patients can present other clinical manifestations less known as changes in sexual behaviour and circadian circles, and even non-brain related symptoms as unintended weight loss, hyperhidrosis, heat and cold intolerance, sialorrhoea and urinary difficulties (Aziz et al., 2010). Finally, the main cause of death in HD patients is aspiration pneumonia, as a complication of dysphagia, followed by suicide (P. McColgan & Tabrizi, 2018; Roos, 2010).

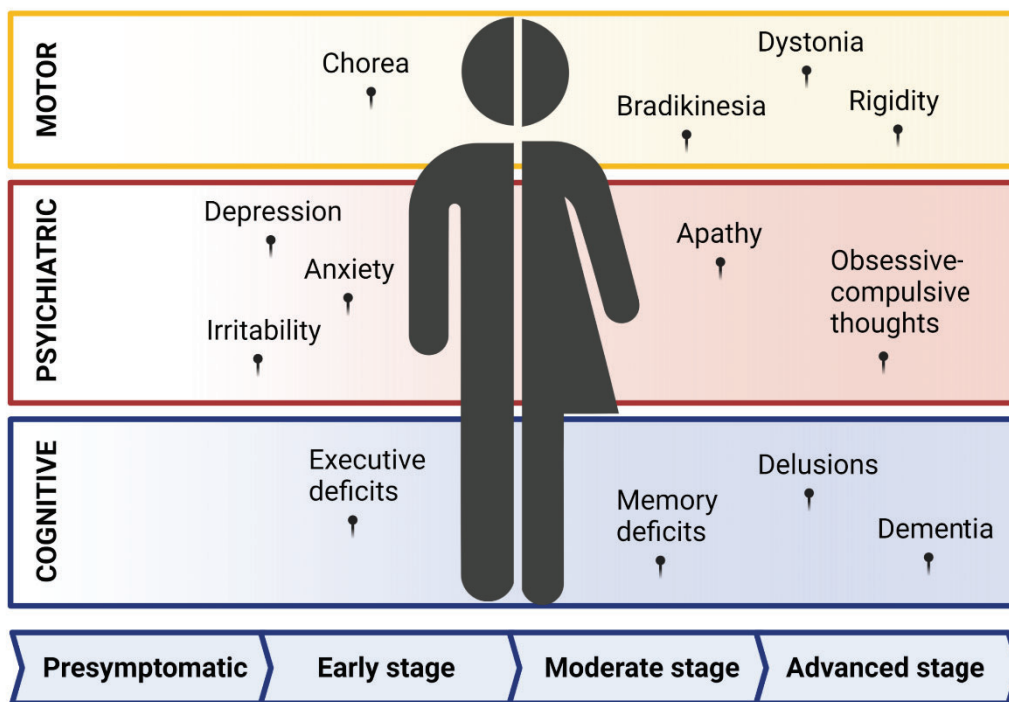


Figure 6. Progression of HD symptoms in humans. Schematic representation of the progression of motor, cognitive and psychiatric symptoms in HD patients through the different stages of the disease. See main text for references in section 2.1.

To date, no neuroprotective or disease-delaying drug has been developed and available therapeutical approaches for HD only aim to restrain the symptoms. Hence, clinical care of patients focuses on multidisciplinary management of symptoms in order to upgrade their quality life, combining pharmacological and non-pharmacological interventions (Bates et al., 2015). To treat chorea, tetrabenazine, a dopamine depleting drug, is the only drug specifically licensed for this purpose. In turn, psychiatric alterations may be treated with cognitive behaviour therapy along with selective serotonin uptake inhibitors and antipsychotics (Ross & Tabrizi, 2011).

2.2. Huntingtin gene and protein

HD is caused by an autosomal dominantly inherited expansion in the CAG trinucleotide repeat in the *Huntingtin* gene (*IT15*), which codifies for the huntingtin protein (Htt). The *IT15* gene is localised in the short arm of chromosome 4, in 4p16.3 and contains 67 exons, being the mutations located in the first exon.

Non-HD subjects normally present between 9 and 35 CAG repeats. Individuals presenting 27-35 are considered as “intermediate allele”, meaning it is insufficient to develop the phenotype, but due to CAG repeat instability their progeny may inherit the allele in the HD range. Repeats of 36 or more units are pathogenic. Range of 36 to 39 CAG repeats are considered as reduced penetrance, meaning a delayed onset of symptoms, while patients with 40 or more repeats present full penetrance of the disease (Tabrizi et al., 2020) (Figure 7). Length of CAG repeats is inversely correlated to the age of onset of the disease, meaning the more repeats, the earlier the disease manifests (M. Duyao et al., 1993). Importantly, although most of the patients present 40-50 CAG units (Wheeler et al., 1999), patients with 60 or more CAGs present the most aggressive form and usually starts at the age of 20 or earlier, thus called juvenile HD (Cronin et al., 2019).

Wild type Htt is a large protein of 350 kDa containing 3,144 amino acids with an expandable polyglutamine (polyQ) tract in the N-terminal. Htt is ubiquitously expressed throughout the body but at different levels, being the highest at brain and testis. In the brain, most expression is found in the cortex, hippocampus and striatum (Borrell-Pagès et al., 2006). Within the cell, Htt was firstly thought to be mainly cytoplasmatic, but later other locations have been described as in nucleus, the Golgi apparatus, ER, or mitochondria (Borrell-Pagès et al., 2006). According to this spread subcellular localisation, Htt can interact with many partners and is involved in numerous cellular functions. Most of the protein interactors are related to cellular dynamics, metabolism, protein turnover, and gene expression. Hence, it is not surprisingly that Htt plays a role in vesicle trafficking, endocytosis, cell division, autophagy, and transcription (Saudou & Humbert, 2016). Notably, complete ablation of Htt in mice results in embryonic lethality, pointing out the essential role of Htt in development (M. P. Duyao et al., 1995; Zeitlin et al., 1995).

The presence of expanded CAG trinucleotides in the exon 1 of the gene *IT15* causes a mutant form of Htt protein (mHtt). Although some research has suggested a loss of physiological function, expansion in polyQ in Htt is primarily considered as a toxic gain-of-function mutation (Tabrizi et al., 2020). mHtt has a propensity to misfold in abnormal conformations, resulting in soluble monomers combining to form oligomers, gradually

INTRODUCTION

increasing the size and finally forming large inclusions or aggregates (Figure 7). Aggregates are mainly found in the cytoplasm and the nucleus (Cooper et al., 1998). Whether the role of mHtt aggregates is pathogenic or protective remains under debate. On the one hand, inclusions are thought to be crucial in the pathogenesis of HD, hampering normal Htt function (Ross, 1997). On the other hand, other studies suggest that oligomeric mHtt is a more toxic form and accumulation into aggregates could be a protective mechanism (Arrasate et al., 2004).

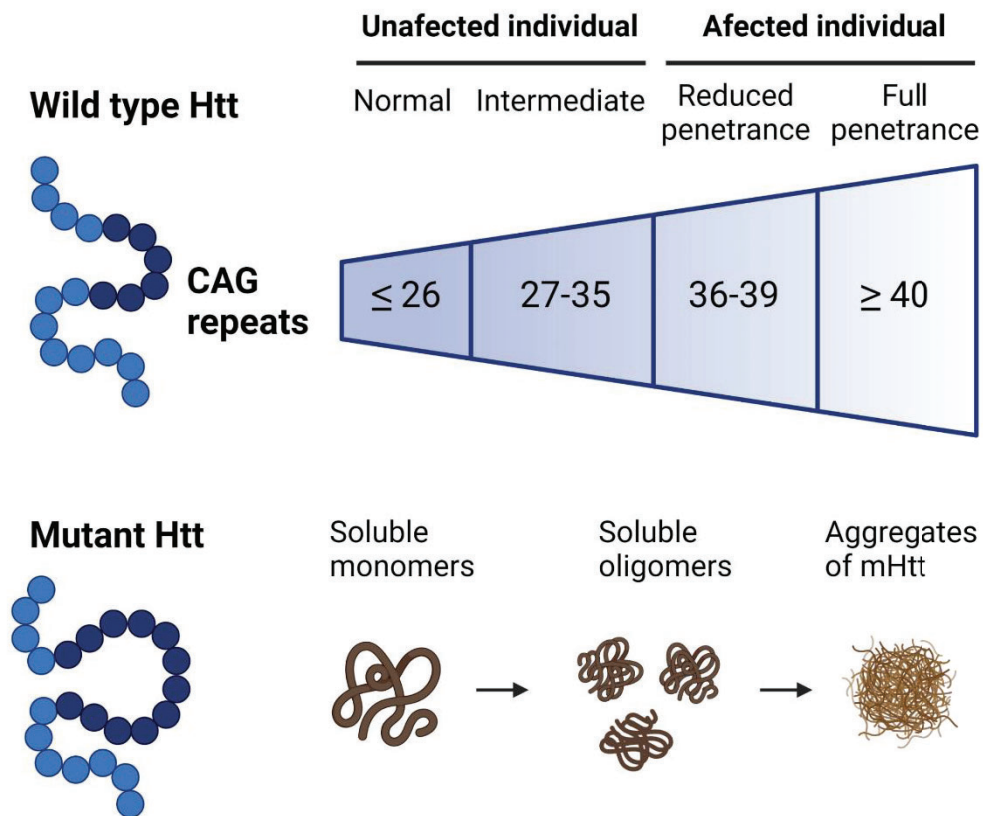


Figure 7. Generation of mutant Htt. HD is caused by the expansion of CAG trinucleotides in the gene encoding for Htt protein. Based on the clinical manifestation of HD, length of CAG repeats can be classified in normal, intermediate, reduced, or full penetrance. Thus, the more CAGs, the more severe is the symptomatology. As a result of the CAG expansion, mutant Htt (mHtt) misfolds and generates soluble monomers that combines in oligomers, finally resulting in insoluble aggregates. The effect of mHtt aggregates remains under debate since they have been demonstrated to be pathogenic and protective simultaneously.

2.3. Neuropathology

The most remarkable trait in HD neuropathology is the selective and gradual atrophy of the striatum, in humans composed by the putamen and caudate regions, along with neuronal loss and astrogliosis. To evaluate the severity and progression of neuropathological changes in *post-mortem* HD brains, Vonsattel et al. established a grading system based in macroscopical and microscopical observations, resulting in 5 stages in ascending order of severity (J. P. Vonsattel et al., 1985). Grade 0 includes those brains with no gross alterations related to HD although there is a loss of 30-40% neurons in the caudate. In grade 1, caudate present 50% of neuronal loss along with moderate astrogliosis. In grade 2 and 3, atrophy, neuronal loss and astrogliosis are gradually more prominent until in grade 4 the striatum presents up to 95% of neuronal loss (J. P. Vonsattel et al., 1985; J. P. G. Vonsattel & Marian, 1998). To a lesser extent, other regions as cerebral cortex, globus pallidus and hippocampus also present shrinkage in HD patients (E. H. Kim et al., 2014; Nana et al., 2014; J. P. Vonsattel et al., 1985; J. P. G. Vonsattel & Marian, 1998) (Figure 8). Hence, while degeneration of striatum could explain motor symptomatology, affection of cortex and hippocampus correlates with cognitive and psychiatric alterations (Z. Guo et al., 2012; Harrington et al., 2014; Peter McColgan et al., 2017; Mehrabi et al., 2016).

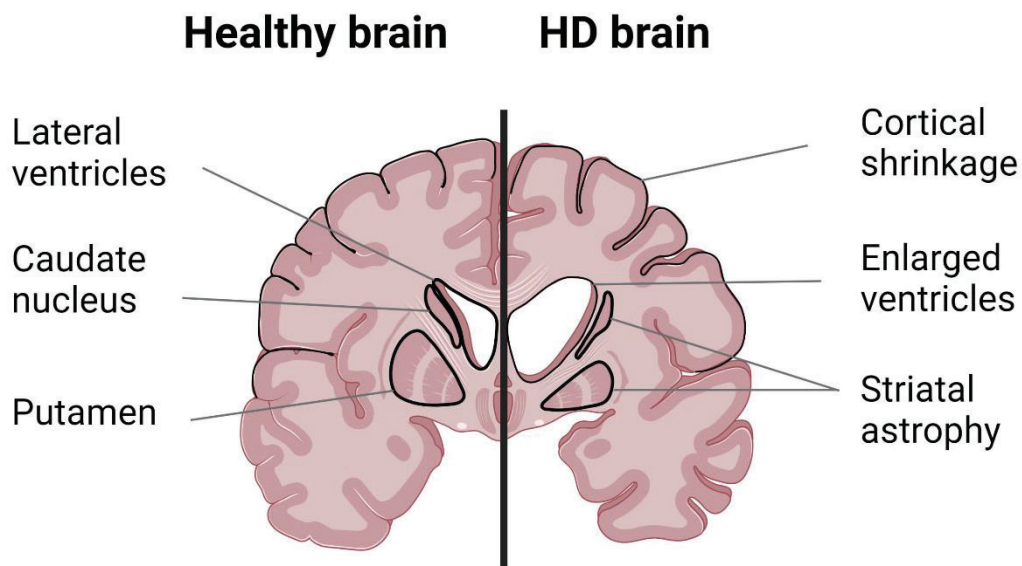


Figure 8. Schematic representation of the brain neuropathology in HD. In humans, the striatum is composed of the putamen and the caudate nucleus. Compared to healthy brains, caudate and putamen in HD patients are progressively degenerated. In advanced stages, the massive striatal atrophy leads to an expansion of the ventricles. Shrinkage of cortex is also observed in HD brains.

INTRODUCTION

The main cell type that degenerates in HD are the medium spiny neurons (MSN) (reviewed in (Morigaki & Goto, 2017)), being the 90-95% of total neurons within the striatum (Dubé et al., 1988; Gerfen, 1988). MSNs can be divided into two populations depending on the projections to other brain areas: the direct and the indirect pathway. MSN from the indirect pathway express dopamine D2 receptor and project to the *globus pallidus pars externa*. In turn, MSN from the direct pathway expresses dopamine D1 receptor and directly project to *globus pallidus pars interna* and *substantia nigra reticulata*. These mentioned brain regions where MSN project, together with the striatum and the subthalamic nucleus form the basal ganglia, the hub of movement control (Gerfen et al., 1990). In early stages of the disease, MSN forming the indirect pathway are the first to degenerate, developing the hyperkinetic movements (Reiner et al., 1988; Richfield et al., 1995). At advanced stages of HD, MSN from the direct pathway also degenerate, provoking the hypokinesia (Deng et al., 2004). Cellular composition and pathology of the HD striatum will be further explained in section 2.5 in this chapter.

2.4. Huntington's disease models

Although analysis of *post-mortem* human brains largely contributes to the understanding of molecular mechanisms involved, research on HD mainly rely on cellular and animal models. Prior to the identification of mutation in Htt gene, the HD models of preferences were chemically-induced lesions models, such as those using 3-nitropropionic acid (3-NP) (Borlongan et al., 1997) or quinolonic acid (M. Flint Beal et al., 1986). Indeed, the contribution of mitochondrial defects to HD pathogenic mechanisms was proposed after seeing that the use of mitochondrial toxin 3-NP promoted selective loss of MSN (M. F. Beal et al., 1993). Although these toxins induce vulnerability of the striatum, these models cannot reproduce slow disease progression or mHtt-related pathogenesis.

The discovery of the gene causing HD enabled the creation of several genetic murine models that accurately replicate the progression of the disease. These models tremendously help in the understanding of HD molecular pathogenesis but also represents a suitable tool for potential pharmacological development. Genetic mouse models can be divided into three groups depending on the technology used for their generation: N-terminal transgenic, full-length transgenic and knock-in. Although all three types reproduce motor and behaviour impediment resembling the HD symptoms in humans, they differ in the origin of mHtt, the promoter, the number of CAG repeats, and in severity and onset of the disease (Table 1).

2.4.1. N-terminal transgenic mouse models

N-terminal transgenic mouse expresses the 5' fragment of the human *IT15* gene, including exon 1 with CAG repeats region, proving that N-terminal fragment of mHtt is sufficient to mimic HD pathology in mice. This transgenic mouse presents an early onset and rapid disease progression compared to other murine models and the symptoms that are recapitulated include loss of coordination, tremors, hypokinesia, abnormal gait, neuropathology and shortened lifespan (L. Menalled et al., 2014). This category comprises R6/1, R6/2 and N171-82Q lines.

R6/1 and R6/2 were the first genetically modified HD mice, inserting mutant human exon 1 of the *Htt* gene containing 116 and 144 CAG repeats respectively. Both lines recapitulate HD pathology items as choreiform-like movements, resting tremors, brain weight loss, and neuronal atrophy (Mangiarini et al., 1996). Because of the early onset and rapid symptomatology progression, R6 lines are better chosen for testing therapeutical strategies. The major inconvenient of these mice is the absence of neuronal death.

N171-82Q mice express a fragment of human Htt, containing the first 171 amino acids with 82 glutamines, under the regulation of the mouse prion promoter. These mice develop similar neuropathological and behavioural phenotypes to those in R6 mice (Schilling et al., 1999) along with some cell death in the cortex and the striatum (Z. X. Yu et al., 2003). Conversely, as they present less CAG repeats than R6, symptomatology starts later in N171-82Q mice. Thus, this mouse line is more suitable for studies of premanifest than R6/1 and R6/2.

2.4.2. Full-length transgenic mouse models

Full-length models express the full-length *Htt* gene containing expanded CAG triplets carried in either a yeast (YAC) or a bacterial artificial chromosome (BAC). These transgenic mice progressively develop disease phenotypes over months and show relatively normal survival. The most studied YAC derived murine model is YAC128, which expresses the full *mHtt* gene with 128 CAG repeats (Hodgson et al., 1999; Slow et al., 2003). In turn, the BACHD mouse model expresses full-length human *Htt* gene with 97 CAG triplets (Gray et al., 2008). Besides motor and cognitive impediment, both lines shows selective but slight neuronal loss in the striatum (Gray et al., 2008; Hodgson et al., 1999; Slow et al., 2003). Due to the appearance of gain of body weight, the major

INTRODUCTION

drawback of these mice is the impossibility to study mechanisms related to metabolism changes in HD (Gray et al., 2008; L. Menalled et al., 2014).

2.4.3. Knock-in mouse models

The third category of genetically modified HD mice are knock-in models, in which, unlike previous described models, the HD mutation is replicated by directly modification of CAG repeats into the mouse *Htt* gene, replacing the murine exon 1 of the *Htt* gene with a mutant human copy that contains the expansion of CAG (White et al., 1997). Like HD patients, these HD knock-in mice also are heterozygous for one wild type *Htt* allele and one CAG-expanded allele (L. Menalled et al., 2014). Therefore, knock-in mouse model is the one with the closest expression reproducibility to HD in humans in its appropriate genomic context. However, the more genetically accurate the model is, the more subtle the phenotype. Several knock-in lines have been generated but the most commonly used is the HdhQ111, which expresses 111 CAG repeats (Wheeler et al., 2000). These mice present a slower progression of symptomatology and neuropathology compared to the N-terminal models, making them more suitable to study early stages of the disease.

Table 1. Genetic HD mouse models. Characteristics of most used HD mouse model. Ages are given in weeks (W) or months (M).

Model	Transgenic product	Promoter	CAG repeats	Aggregates	Cognitive deficits	Motor deficits	Neuropathology	Lifespan
R6/2	67 amino acids of N-terminal fragment (human <i>Htt</i>), 3 copies	Human <i>Htt</i>	144	4W	4W	5-6W	Loss of brain weight and neuronal atrophy. Reduce dopamine levels. Astrogliosis.	13-16W
R6/1	67 amino acids of N-terminal fragment (human <i>Htt</i>), 1 copy	Human <i>Htt</i>	116	9W	12W	14W	Loss of brain weight and neuronal atrophy. Reduce dopamine levels.	32-40W
N171-82Q	171 amino acids of N-terminal fragment (human <i>Htt</i>)	Mouse prion protein	82	16W	14W	11W	Gross brain atrophy and striatal neuron loss. Hyperventricular enlargement.	16-24W
YAC128	Full-length human <i>Htt</i> with yeast artificial chromosome	Human <i>Htt</i>	128	12M	2M	3-6M	Striatal atrophy and neuronal loss. Nuclear aggregates at 12M.	Normal
BACHD	Full-length human <i>Htt</i> with bacteria artificial chromosome	Human <i>Htt</i>	97	12M	2-6M	3-6M	Loss of brain weight. Cytoplasmatic aggregates but not nuclear inclusions of mHtt.	Normal
HdhQ111	Replacement of mouse <i>Htt</i> exon 1 with chimeric human/mouse exon 1	Endogenous mouse <i>Htt</i>	111	6M	6M	8M	Nuclear but not cytoplasmic mHtt aggregates. Astrogliosis at 24M.	Normal

INTRODUCTION

2.5. Striatal vulnerability in Huntington's disease

One of the main questions in HD research that remains to be elucidated is why striatal neurons are more susceptible to mHtt toxicity. It has been proposed that the presence of mHtt could activate both cell-autonomous and non-cell autonomous pathogenic mechanisms that drive to neuronal death of the MSN. In this section, several pathogenic mechanisms occurring in neurons and astrocytes of the HD striatum will be examined.

2.5.1. Neural population in the striatum

The striatum is the largest input nucleus of the basal ganglia (BG), a group of interconnected sub-cortical nuclei. Single-cell RNA seq studies in the mouse striatum revealed that the most prevalent cell type is the neuron, followed by astrocytes (Gokce et al., 2016). The principal striatal neurons are the MSN, GABAergic neurons that comprise up to 95% of striatal neurons while the resting 5% corresponds to GABAergic and cholinergic interneurons. Conventionally, MSN have been classified depending on the expression of dopamine receptors D1 or D2 (Khakh, 2019).

Regarding astrocytes, categorization is more complex since it is a highly heterogeneous cell population. So far, several classifications have been proposed based on morphology (protoplasmic or fibrous), location (grey or white matter), or reactivity state (A1 neurotoxic or A2 neuroprotective). However, none of them has truly encompassed the nature of astrocytes and recent studies attempt to establish subtypes of astrocytes based on transcriptional and proteomic profiles (Chai et al., 2017; Gokce et al., 2016; Khakh, 2019). Moreover, astrocytes differ between brain regions, showing differential gene and protein expression patterns for instance between striatal, cortical and hippocampal astrocytes (Batiuk et al., 2020; Diaz-Castro et al., 2019; Zengli Zhang et al., 2019).

Striatal astrocytes are characterized by a “bushy” morphology, with numerous branches and branchlets, and low GFAP expression (Khakh, 2019; Khakh & Sofroniew, 2015). In fact, although GFAP is the most commonly used marker for astrocytes, it only labels about 15% of the total astrocyte volume (Bushong et al., 2002) and it is preferentially expressed in the main stem branches, underrepresenting the whole extent of astrocyte territory compared to other staining (Sofroniew & Vinters, 2010). Despite scarce levels of GFAP, other markers as GLT-1, GLAST, ALDH1L1 or S100 β label most of striatal astrocytes (Khakh & Sofroniew, 2015). GLT-1 and GLAST are the main astrocytic glutamate transporter located in the plasmatic membrane. While GLT-1 highest

INTRODUCTION

expression is in the hippocampus, cortex and striatum, GLAST expression is higher in the cerebellum (Khakh & Sofroniew, 2015; Pajarillo et al., 2019). ALDH1L1 is a metabolic enzyme involved in the folate metabolism widely distributed in the whole cell and expressed in most astrocytes but not in other cell types (Matias et al., 2019). Finally, S100 β is a calcium binding protein abundant in the cytoplasm and nucleus of astrocytes, generally related to maturation of astrocytes although can also be expressed in oligodendrocytes and ependymal cells (Hachem et al., 2005; Raponi et al., 2007).

Another matter of controversy is the role of astrogliosis in a pathological context. Astrogliosis or reactive gliosis refers to functional, morphological and molecular changes that undergo the astrocytes to respond to abnormal events in the CNS (Escartin et al., 2021). Traditionally, reactive astrocytes have been linked to increased GFAP expression and hypertrophy. Whether neuroprotection or neurotoxic responses are triggered with astrogliosis remains to be elucidated.

2.5.2. Alterations in neurons in Huntington's disease

MSN are extremely sensitive to the toxic effect of mHtt. Although specific mechanisms underlying selective neuronal vulnerability in the striatum are still not fully understood, excitotoxicity, mHtt aggregate formation or mitochondrial dysfunction have been proposed as potential pathological processes (Figure 9).

Excitotoxicity refers to the excessive excitatory amino acids signalling, mainly glutamate that triggers overload of intracellular Ca²⁺ and promotes neuronal death. After its release from synaptic terminals, glutamate activates N-methyl-D-aspartate (NMDA) receptors (NMDAR), allowing the entry of Ca²⁺ to the cell. Studies in *post-mortem* samples of putamen from HD patients revealed losses of NMDAR levels up to 90% compared to healthy brains (Young et al., 1988). Similarly, striatum of HD animals showed decreased expression of NMDAR subunits NR2A and NR2B (Ali & Levine, 2006; Cepeda et al., 2001). In HD rodents, striatal injections of NMDA agonists as quinolinic acid have proven that MSN are highly vulnerable to glutamate-induced excitotoxicity, reproducing the neurochemical characteristics of neuronal damage observed in HD (M. F. Beal et al., 1991; M. Flint Beal et al., 1986). In addition, NMDAR mislocalisation can enhance excitotoxicity since the increment of NMDAR at extrasynaptic sites increases the toxic soluble form of mHtt and activates neuronal death pathways (Milnerwood et al., 2010; Okamoto et al., 2009).

INTRODUCTION

Secondly, generation of mHtt aggregates are a hallmark of HD and may contribute to the striatal vulnerability in this disease (J. P. G. Vonsattel & Marian, 1998) (see section 2.2 for details on aggregate formation). Inclusions of mHtt have been observed in both nucleus and cytoplasm of mouse and human HD striatum (Hackam et al., 1999; L. B. Menalled et al., 2003; Schilling et al., 1999) and exhibit different biochemical composition and ultrastructural properties depending on the cellular compartment (Hackam et al., 1999; Riguet et al., 2021). Nuclear inclusions have been associated with sequestering of transcription factors whereas cytosolic aggregates impair functions as axonal transport (Gunawardena et al., 2003; W. C. M. Lee et al., 2004). Moreover, striatal neurons seem to clear mHtt aggregates slower than their counterparts in the cortex (T. Zhao et al., 2016). Finally, mitochondrial dysfunction has been traditionally linked to selective loss of MSN in HD and it will be further explained in the following section 2.5.4.

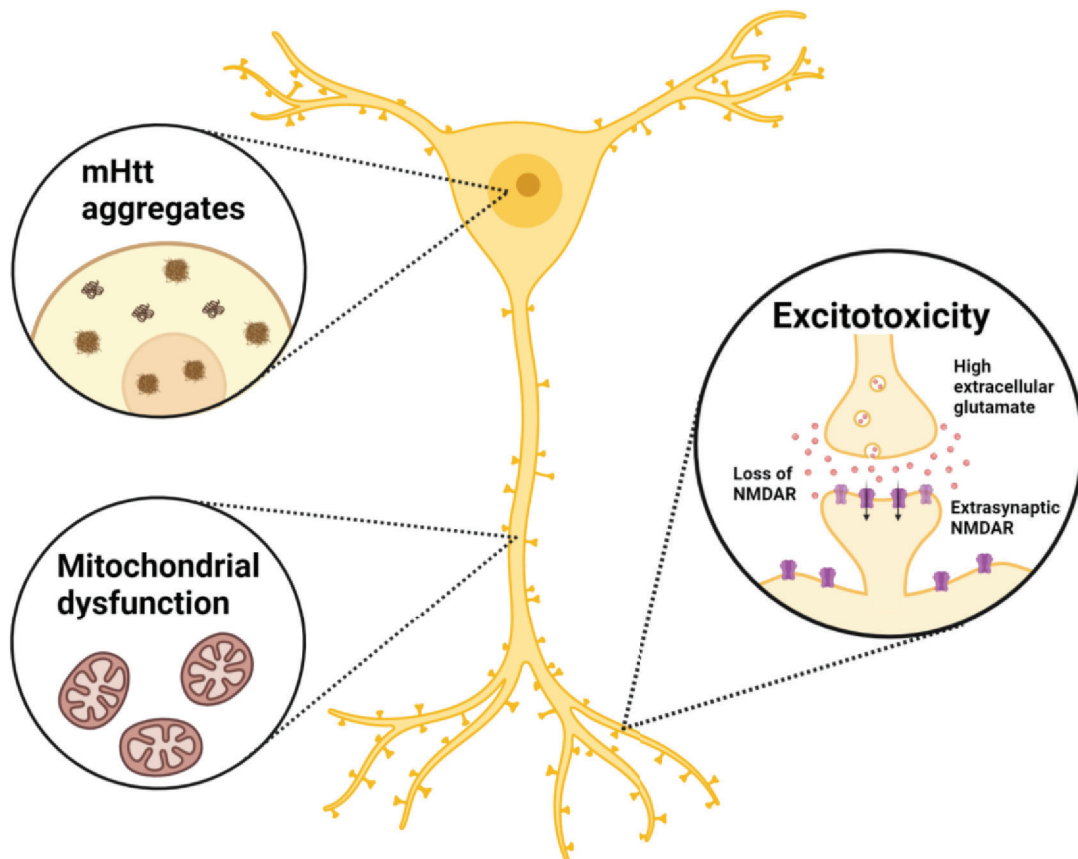


Figure 9. Pathogenic mechanisms that contribute to MSN selective loss in HD. The presence of mHtt in neurons induces the loss of NMDAR, accumulation of extracellular glutamate and mislocalisation of NMDAR at extrasynaptic sites, altogether enhancing the excitotoxicity. In addition, mHtt forms aggregates that localise in the cytosol and the nucleus of striatal neurons. Finally, mHtt triggers alterations in mitochondrial function, leading to a mishandling of Ca^{2+} buffering. Although other cellular pathways are disrupted in HD neurons, these three alterations have been currently hypothesised as key factors in the striatal vulnerability that occurs in HD.

2.5.3. Alterations in astrocytes in Huntington's disease

As Vonsattel et al. noticed in *post-mortem* human samples, loss of MSN in HD putamen is accompanied by an increment of astrogliosis that becomes more prominent throughout the disease (J. P. Vonsattel et al., 1985). In line with this observation, increased levels of GFAP and colocalisation of GFAP with mHtt were found in HD putamen of all grades of severity compared to healthy subjects (Faideau et al., 2010). On the contrary, not all HD mouse model recapitulate astrogliosis although they display dysfunctional astrocytes (Khakh et al., 2017; Tong et al., 2014) (Figure 10). Despite this controversy, a recent study focused on the transcriptional profile of striatal astrocytes from HD mouse and showed significant changes along the disease (Diaz-Castro et al., 2019).

Astrocytes also contribute to the neuronal excitotoxicity since they take up the glutamate, metabolize it to glutamine and release the glutamine to the extracellular space for the consequent uptake by the neurons (Estrada-Sánchez & Rebec, 2012; Estrada Sánchez et al., 2008). Hence, astrocytes are crucial for the clearance of excessive extracellular glutamate. In the striatum of several HD mouse models it has been reported a diminution in the mRNA and protein expression as well as in the functionality of glutamate transporters GLT-1 and GLAST (Arzberger et al., 1997; Behrens et al., 2002; Bradford et al., 2009; Estrada-Sánchez et al., 2009; Shin et al., 2005). In addition, *post-mortem* samples of caudate and putamen of HD patients showed progressive loss of GLT-1 along the disease (Arzberger et al., 1997). This reduction of transporters results in impaired glutamate uptake by the astrocytes, thus increasing extracellular glutamate levels and triggering the death of MSN (Behrens et al., 2002; Faideau et al., 2010; Liévens et al., 2001; Shin et al., 2005). In addition, HD astrocytes also release more pro-oxidative factors while produce less antioxidants (Ben Haim et al., 2015).

Similarly to neurons, mHtt aggregates have been found in the cytoplasm and the nucleus of striatal astrocytes both in HD mice and HD patients brains, although nuclear inclusions are less frequent than in neurons (Jansen et al., 2017; Shin et al., 2005; Tong et al., 2014). However, nuclear inclusions of mHtt found in striatal astrocytes of transgenic and knock-in HD mouse models, proved to contribute to age-dependent neurological symptoms (Bradford et al., 2009). This same work showed that expression of mHtt under the control of the GFAP promoter induced some HD neurological symptoms in mice as motor deficits, demonstrating a pathological role of mHtt in astrocytes and suggesting that neuroglial communication could be affected in HD (Bradford et al., 2009).

Following this idea, other authors reduced mHtt in the astrocytes of the BACHD mouse model and reported an improvement in motor and neuropsychiatric features along with

INTRODUCTION

a restoration in the striatal volume, indicating the contribution of astrocytes to the behavioural and neuropathological phenotype in HD (Wood et al., 2019). Moreover, in chimeric animals, mice engrafted with human astrocyte progenitors expressing mHtt demonstrated impaired motor coordination and hyperexcitability of MSN. On the contrary, striatal engraftment of R6/2 mice with healthy glia improved motor deficits and survival (Benraiss et al., 2016). Altogether, these investigations proved that the expression of mHtt in striatal astrocytes hampers neuroglia crosstalk and drives to pathogenic features of HD.

Furthermore, alterations in the generation of antioxidants mediated by astrocytes, has been reported. HD *post-mortem* striatum showed loss of antioxidant agents along with increased oxidative stress (Ehrnhoefer et al., 2018; Rotblat et al., 2014). Boussicault et al. showed in BACHD mice that expression of mHtt in astrocytes, and not in neurons, was sufficient to start an oxidative stress response in neurons by diffusible factors (Boussicault et al., 2014). Likewise, R6/2 mice displayed defects in the flux of ascorbic acid, a protector agent against oxidative damage, from astrocytes to neurons that triggered metabolic failure and redox imbalance in HD striatal neurons (Acuña et al., 2013). Additionally, reactive astrocytes in HD brain may also release pro-oxidant factors (Ben Haim et al., 2015). Altogether, these works suggest that deficient astrocyte-to-neuron signalling is involved in early energy metabolic alterations in HD.

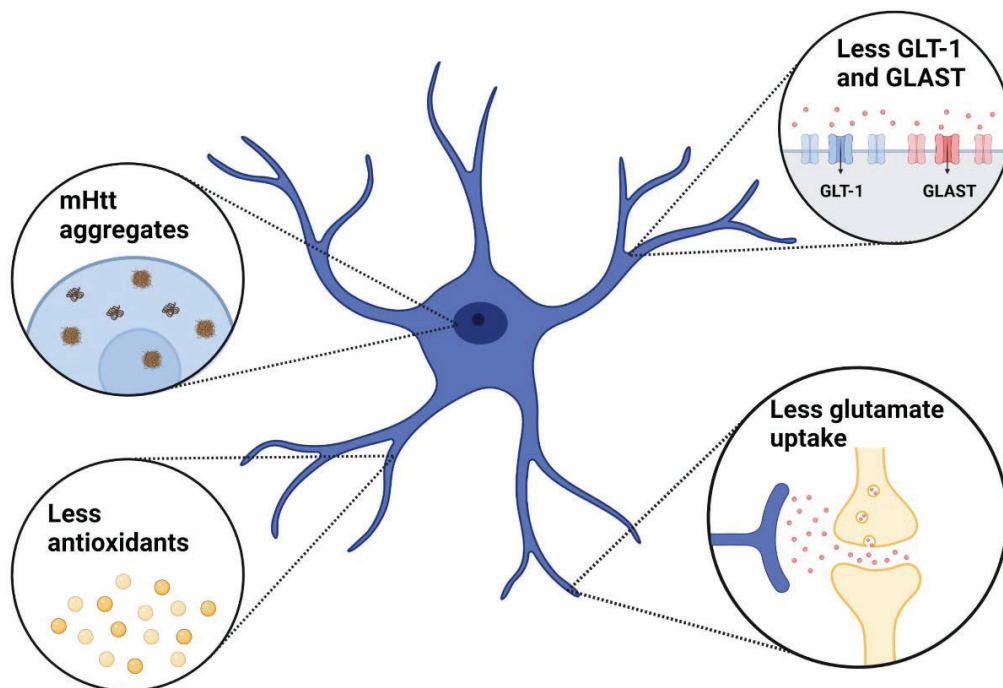


Figure 10. Alterations in HD astrocytes. The presence of mHtt in striatal astrocytes induces the loss of glutamate transporters GLT-1 and GLAST, hampering the uptake of extracellular glutamate. In addition, HD astrocytes show cytosolic and nuclear mHtt aggregates and produce less antioxidant protection for neurons. All these pathological mechanisms could contribute to the selective neuronal loss in the striatum of HD.

2.5.4. Mitochondrial dysfunction in HD

Mitochondrial dysfunction has been largely related to striatal vulnerability in HD since the treatment with 3-NP, an irreversible inhibitor of OXPHOS complex III, resembled neuronal death occurring in HD (M. F. Beal et al., 1991). In turn, brain biopsies of HD patients revealed a decreased activity in mitochondrial respiratory chain complexes II, III, and IV (Browne et al., 1997; Gu et al., 1996) as well as decreased glucose metabolism (Browne & Beal, 2004). Indeed, length of CAG repeats in mHtt can determine severity in mitochondrial metabolism deficit (Seong et al., 2005). In addition, mHtt was detected to directly interact with the OMM, inducing the opening of the mPTP and an aberrant Ca^{2+} release (Choo et al., 2004).

Moreover, alterations in mitochondrial ultrastructure and dynamics have been found in HD striatum, suggesting an imbalance towards fission (Goebel et al., 1978; Guedes-Dias et al., 2016). Putamen of HD patients showed increased Drp1 and Fis (Costa et al., 2010; J. Kim et al., 2010) along with reduction of Mfn1, Mfn2, and Opa1 levels (J. Kim et al., 2010; Shirendeb et al., 2011).

On the other side, lymphoblasts from HD patients and HD immortalized cells display mitochondrial fragmentation and disruption of cristae (Costa et al., 2010). Additionally, it was reported in HD human fibroblasts that mHtt directly binds Drp1, increasing its GTPase activity and resulting in more but smaller mitochondria (Song et al., 2011). Indeed, immunoprecipitation of Drp1 in brain lysates from HD patients and HD mice showed that mHtt presented a higher affinity for Drp1 compared to wild type Htt (Song et al., 2011). Regarding mitophagy, several studies have proposed that this aberrant mitochondrial fragmentation could be linked to defective axonal transport and abnormal distribution of mitochondria, triggering mitochondrial accumulation and defective removal of organelles in striatal HD neurons (Franco-Iborra et al., 2021; Reddy & Shirendeb, 2012; Trushina et al., 2004). Likewise, biogenesis of mitochondria in HD also seems to be impaired since levels of PGC-1 α are diminished in the striatum of HD patients and HD mouse models (Chaturvedi et al., 2010; Cui et al., 2006; J. Kim et al., 2010; Weydt et al., 2006).

Besides disruption of dynamics, HD neuronal mitochondria also show Ca^{2+} mishandling. Isolated mitochondria from the striatum of HD rodents proved to be more sensitive to Ca^{2+} overload than their counterparts in the cortex, suggesting that striatal neurons are more vulnerable to metabolic stress (Brustovetsky et al., 2003). In addition, mHtt but not wild-type Htt activates IP3R and induces Ca^{2+} release from the ER, mediating Ca^{2+} overload (D. Lim et al., 2008; Tang et al., 2003; H. Zhang et al., 2008). Thus, ER-

INTRODUCTION

mitochondria contact sites are likely to be affected by the expression of mHtt and this possibility is explored in this Thesis.

Since most studies have been conducted in neurons or the whole striatum, little is known about mitochondrial function specifically in HD astrocyte. However, HD striatal astrocytes seem to replicate some of the characteristics of mitochondrial dysfunction observed in neurons. Thus, as in neurons, striatal astrocytes show higher susceptibility than cortical astrocytes to mitochondrial toxin (Saba et al., 2020). Furthermore, not only mitochondria in striatal neurons, but also in striatal astrocytes, buffer less Ca^{2+} before undergoing mPTP compared to cortical cells (Oliveira & Gonçalves, 2009). Hence, selective vulnerability of striatal mitochondria relies simultaneously in neurons and astrocytes.

Finally, neuroglial crosstalk mediated by mitochondria is a recent field of research. Transfer of healthy glial mitochondria has been postulated as a potential rescue of neuronal damage in front of several neurological insults as stroke or AD (Lippert & Borlongan, 2019; Nitzan et al., 2019). On the contrary, transfer of damaged glial mitochondria seems to propagate neuroinflammation and neuronal dysfunction in models of AD and amyotrophic lateral sclerosis (Joshi et al., 2019). However, transfer of extracellular mitochondria has been barely explored in the neuropathology of HD. So far, Joshi et al. described in an *in vitro* HD mouse model that disrupted mitochondria from microglia trigger inflammatory activation of astrocytes, contributing to neuronal damage (Joshi et al., 2019). In this Thesis we aimed to further investigate the mechanisms mediating mitochondrial communication between astrocytes and neurons, that could support the hypothesis that disruption of mitochondrial function in astrocytes contributes to the striatal vulnerability in HD.

3. ROLE OF PYK2 IN THE CNS

As the cellular environment changes, mitochondria are constantly modifying their shape and size to provide a rapid adaptative response to the cell's requirements. One of the mechanisms underlying this phenomenon is the modulation of mitochondrial proteins through post-translational modifications (Kotrasová et al., 2021). Phosphorylation is the most common post-translational modification, inducing changes in the protein conformation and, consequently, in its function. Kinases are the enzymes in charge of the phosphorylation, catalysing the transfer of phosphate groups from ATP to specific amino acids of the target protein. According to the nature of the substrate, kinases can be divided into serine/threonine kinases and tyrosine kinases, meaning that the phosphorylation site will be certain residues of serine/threonine or residues of tyrosine, respectively (Cheng et al., 2011).

Among many kinases, proline-rich tyrosine kinase 2 (Pyk2) has been largely studied in health and disease in the CNS (reviewed in (de Pins et al., 2021)). Pyk2 is considered a scaffolding protein highly expressed in neuron and its phosphoregulation is tightly related to the neuronal plasticity. Considering that regulation of mitochondrial dynamics by phosphorylation has been widely linked to mitochondrial dysfunction in several diseases, including neurodegenerative ones (Kotrasová et al., 2021), the potential role of Pyk2 in mitochondrial dynamics could be fundamental to understand the alterations in mitochondria that occur in HD. As a prelude to this hypothesis, in this Thesis we aimed to identify the implication of Pyk2 in mitochondrial function in a physiological context.

3.1. Structure of Pyk2

Pyk2 was initially isolated from a human brain complementary DNA library by PCR and described as a tyrosine kinase activated by increments in Ca^{2+} concentration and by protein kinase C (PKC) (Lev et al., 1995). Simultaneously, other three independent investigations identified the same protein by using different approaches. Therefore, Pyk2 can also be referred as (1) cell adhesion kinase β (CAK β), isolated from a rat brain cDNA library (Sasaki et al., 1995); (2) related adhesion focal tyrosine kinase (RAFTK), isolated from human megakaryocytes and cloned by homology in murine cDNA (Avraham et al., 1995), and (3) calcium-dependent protein- tyrosine kinase (CADTK) by purification of rat liver cell lines (H. Yu et al., 1996).

INTRODUCTION

Pyk2 is a non-receptor tyrosine kinase highly expressed in hematopoietic cells and in the CNS (Avraham et al., 1995; Dikic et al., 1998; Lev et al., 1995), being specially enriched in the pyramidal hippocampal neurons but also in neurons of other brain regions as cerebral cortex, thalamus, amygdala, and striatum. Although to a lesser extent, Pyk2 is also expressed in other cells present in the CNS as astrocytes (Cazaubon et al., 1997; Giralt et al., 2016) and microglia (Rolón-Reyes et al., 2015; Tian et al., 2000).

Pyk2 is a 110 kDa protein containing 1,009 amino acids that is comprised by three structural domains: an N-terminal FERM (four-point-one/ezrin/radixin/moesin) domain, a central kinase fragment and a C-terminal focal adhesion targeting (FAT) domain. In between the three domains, there are two linker regions including proline-rich (PR) motifs. The FERM domain comprises three structural modules (F1, F2, and F3). FERM domain mediates intermolecular interactions with transmembrane proteins but also intramolecular interactions with other proteins (Girault, Labesse, et al., 1999; Kohno et al., 2008). Since mutations in the Pyk2 FERM domain induces inhibition of Pyk2 phosphorylation, FERM domain has been suggested to regulate Pyk2 activity (Dunty & Schaller, 2002; Lipinski et al., 2006). Moreover, the FERM domain seems to interact with several cytosolic and nuclear proteins. Indeed, F1 presents a nuclear localisation sequence (NLS) and a nuclear export signal (NES) (Camille Faure et al., 2013; Ossovskaya et al., 2008).

The shorter linker between FERM and kinase domains, with 43 residues, contains a PR sequence (PR1) and a tyrosine residue at position 402 (Tyr-402), which is the major autophosphorylation site of Pyk2, but also a direct binding of Src, one of the positive activators of Pyk2 activity (Dikic et al., 1996, 1998). The kinase domain is the central region and contains two sites of phosphorylation at Tyr-579 and Tyr-580 that enhance Pyk2 kinase activity (Lipinski & Loftus, 2010). Following kinase domain, the longer linker connects kinase and FAT domains and presents two more PR sequences, PR2 and PR3. In addition, this linker also presents NES and nuclear translocation sequence (NTS) for nucleocytoplasmic shuttling (Ossovskaya et al., 2008). Finally, the FAT domain of Pyk2 mediates its interaction with the scaffolding protein paxillin, a protein enriched in focal adhesions (Lipinski & Loftus, 2010) (Figure 11).

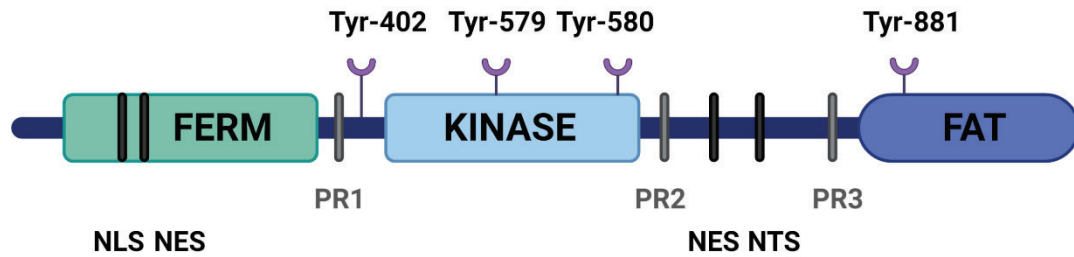


Figure 11. Structure of Pyk2. Schematic representation of Pyk2 structural domains FERM, kinase and FAT and linkers between them. Proline-rich (PR) motifs, and tyrosine (Tyr) residues for phosphorylation are indicated. Nuclear localisation sequence (NLS), nuclear export sequence (NES), and nuclear targeting sequence (NTS) are also depicted.

3.2. Activation of Pyk2

Pyk2 is activated in response to a variety of extracellular stimuli that elevate the intracellular Ca^{2+} concentration. However, precise mechanisms that triggers this activation are not completely understood yet. It is believed that increment of Ca_i^{2+} induces dimerization of Pyk2 and autophosphorylation at Tyr-402 (Kohno et al., 2008; Lev et al., 1995). Indeed, immunoprecipitation assays proved that Ca^{2+} /calmodulin directly binds to Pyk2 at the FERM domain, forming homodimers and enhancing autophosphorylation (Kohno et al., 2008). Moreover, phosphorylation in Tyr-402 can be executed by various enzymes from the Src-family kinases (SFK), including Src, Fyn, Lck, Lyn, and Yes (reviewed in (de Pins et al., 2021)). Additionally, SFK also phosphorylate Pyk2 at Tyr-579, Tyr-580 and Tyr-881 (Dikic et al., 1996; S. S. Wu et al., 2006; Zhao Zhang et al., 2014). In turn, activated Pyk2 recruits SFK that phosphorylate Pyk2 at other sites (Li et al., 1999; S. Y. Park et al., 2004). Thus, the interactions between Pyk2 and SFK bring a positive loop of activation, pointing out that the regulation of these kinases is mutually dependent.

Besides canonical activation, Pyk2 in neurons can be activated alternatively. It has been shown in brain lysates that Pyk2 interacts with PSD-95 (Bartos et al., 2010; Seabold et al., 2003). When Ca_i^{2+} rises, Ca^{2+} /calmodulin interacts with PSD-95 and promotes its dimerization and the recruitment of Pyk2. Clustering of Pyk2 enables its autophosphorylation at Tyr-402 and consequently, its activation. In addition, although PSD-95 is sufficient for the activation of Pyk2, it was observed that Ca^{2+} /calmodulin stimulates PSD-95 binding to Pyk2 (Bartos et al., 2010) (Figure 12).

INTRODUCTION

Conversely, Pyk2 can be negatively regulated by dephosphorylation through tyrosine phosphatases and serine-threonine phosphatases. Among all phosphatases, striatal-enriched protein-tyrosine phosphatase (STEP), arise as a major contributor and it is enriched in neuronal population of the forebrain (Lombroso et al., 2016), similarly to Pyk2. STEP binds to Pyk2 at Tyr-402 and dephosphorylates it. Accordingly, Xu et al. reported that STEP KO mice showed increased Pyk2 phosphorylation (Xu et al., 2012).

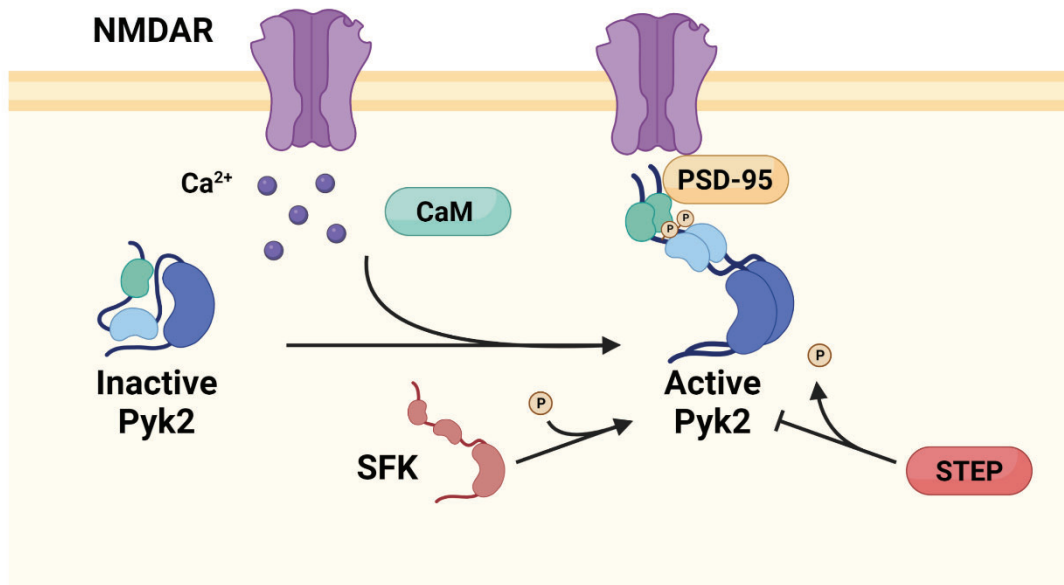


Figure 12. Mechanisms of activation of Pyk2 in neurons. Pyk2 is activated by interaction with Ca²⁺/calmodulin (CaM), which induces its dimerization and facilitates its phosphorylation. Active Pyk2 can then interact with PSD-95, a scaffold protein in the NMDAR complex. Pyk2 is phosphorylated by Src-family kinases (SFK) and dephosphorylated through phosphatases as STEP.

3.3. Physiological function of Pyk2 in the CNS

Pyk2 is a key factor in many cellular mechanisms, regulating cell adhesion, proliferation, survival, and migration. However, in this Thesis we will focus on the role of Pyk2 in the CNS in physiological conditions and its possible implication in neurodegeneration, and thus, specific functions related to neuronal activation are detailed hereunder.

Pyk2 has been described to be involved in NMDAR activation. Initially, proteomic studies in mouse forebrain identified Pyk2 as one of the components of the NMDAR complex as well as Src (Husi et al., 2000). Indeed, PSD-95, a scaffold protein that tethers NMDAR, interacts with Pyk2 in the NMDAR complex by binding to the C-terminal domain of Pyk2

INTRODUCTION

(Seabold et al., 2003). Moreover, PSD-95 phosphorylation by Src triggers Pyk2 recruitment and its consequent activation (C. Zhao et al., 2015). Therefore, various studies point out that activation of Pyk2 in neurons enhances NMDAR function (Bartos et al., 2010; Heidinger et al., 2002).

Following implication in NMDAR, Pyk2 has also been reported to play a role in synaptic plasticity (Girault, Costa, et al., 1999). Synaptic plasticity refers to the activity-dependent modifications of the existing synapses, adapting their effectivity or strength, and leading to their appearance or disappearance. NMDAR contribute to the induction of long-term plasticity as long-term potentiation (LTP) or long-term depression (LTD). Activity of NMDAR can be up-regulated by phosphorylation mediated by Src, resulting in the induction of LTP (X. M. Yu et al., 1997). For the induction of LTP, clustering of Pyk2 with PSD-95 and NMDAR has proved to be necessary (Bartos et al., 2010). Indeed, mice depleted of Pyk2 showed impeded LTP when the stimulation was induced with high-frequency stimulation (Giralt et al., 2017; Mastrolia et al., 2021). Likewise, Pyk2 also contributes to LTD at neuronal synapses. Hsin et al. showed in hippocampal neurons that chemical LTD boosted Pyk2 phosphorylation at Tyr-402 while knockdown of Pyk2 blocked LTP (Hsin et al., 2010). Thus, activity of Pyk2 is necessary for both LTP and LTD.

To better understand the physiological functions in which Pyk2 is implicated, genetic full knock-out mice have been generated. Girault's laboratory developed knockout mice for Pyk2 by flanking exons 15-18, which correspond to the central kinase domain, with LoxP sequence. Resulting *Pyk2^{f/f}* mice were then crossed with a Cre line, thus deleting exons 15-19 and generating genetic knockout of Pyk2. When comparing wild type (*Pyk2^{+/+}*), heterozygous (*Pyk2^{+/-}*) and knockout (*Pyk2^{-/-}*) mice for Pyk2, no major alterations were detected in body weight or general behaviour and health. Immunoblot and immunofluorescence analysis showed a reduction about 50% of Pyk2 in *Pyk2^{+/-}* whereas signal was barely undetectable in *Pyk2^{-/-}* mice, proving that the target protein was successfully knocked out (Giralt et al., 2016). Different studies have used this model to evaluate the implication of Pyk2 in the pathological mechanisms of neurological diseases as AD, HD or chronic stress (Giralt et al., 2017, 2018; Montalban et al., 2019). In this Thesis, these *Pyk2^{-/-}* mice were used to study the role of Pyk2 in mitochondria in physiological conditions.

INTRODUCTION

3.4. Regulation of Pyk2 localisation

Although Pyk2 is a cytosolic protein, it can translocate to other subcellular compartments after neuronal activation. As mentioned above, Pyk2 is required for synaptic plasticity and thus, this kinase needs to translocate to synapses. Increments in Ca^{2+} induces translocation of Pyk2 from the cytoplasm to postsynaptic sites, where PSD-95 is concentrated. In addition, NMDAR activation has been reported to cluster Pyk2 at postsynaptic sites (Bartos et al., 2010).

Moreover, several studies demonstrated that Pyk2 is involved in spine and neurite formation, suggesting both positive and negative effect. Although $Pyk2^{-/-}$ mice did not report impeded brain development, ablation of Pyk2 led to a reduction in the number of dendritic spines (Giralt et al., 2016). Conversely, an overexpression of Pyk2 in primary culture of mouse hippocampal neurons was reported to hamper spine formation and to induce synapse loss (S. Lee et al., 2019). These experiments indicated that a tight regulation of Pyk2 is necessary for a proper synaptic density and function. In neuronal cell lines PC12 and SH-SY5Y, Pyk2 is localised in the neurite growth cone and regulates neurite outgrowth induced by growth factors (Ivankovic-Dikic et al., 2000). On the contrary, Pyk2 also promotes neurite retraction by phosphorylating GSK-3 (Sayas et al., 2006). Thus, it seems that Pyk2 could be mediating neurite remodelling, both outgrowth and retraction.

As mentioned in section 3.1 in this chapter, Pyk2 contains several nuclear import and export signals. Thus, Pyk2 can shuttle between the nucleus and the cytoplasm. In PC12 cells and hippocampal cultured neurons, depolarization induced a Ca^{2+} -dependent nuclear translocation of Pyk2 (C. Faure et al., 2007). This translocation was demonstrated to be independent of Pyk2 autophosphorylation or kinase activity but depended on the regulation of the NES by the phosphorylation of residue Ser-778 (Camille Faure et al., 2013). Upon neuronal stimulation, calcineurin dephosphorylates Ser-778, promoting the inactivation of the nuclear export motif and the accumulation of Pyk2 in the nucleus by the NLS and NES present in the FERM and longer linker respectively (Camille Faure et al., 2013; Ossovskaya et al., 2008). Although some molecular mechanisms of nuclear accumulation have been identified, nuclear function of Pyk2 remains to be elucidated.

Localisation of Pyk2 in other organelles have been relatively unexplored. In non-neuronal cells, it was described that following Ca^{2+} entry into the cell via the transient receptor potential (TRP) channel, Pyk2 can be phosphorylated and partially translocated to mitochondria (Hirschler-Laszkiwicz et al., 2018; B. A. Miller et al., 2019). So far, Pyk2

translocation to mitochondria has been described in cardiac cells, where Pyk2 can be activated and phosphorylate the MCU (Arcucci et al., 2006; B. A. Miller et al., 2019; O-Uchi et al., 2014) enhancing mitochondrial Ca^{2+} uptake and mitochondrial ROS production (O-Uchi et al., 2014). Thus, in this Thesis we aimed to study the localisation of Pyk2 in mitochondria and whether it can regulate mitochondrial morphology and function in neurons.

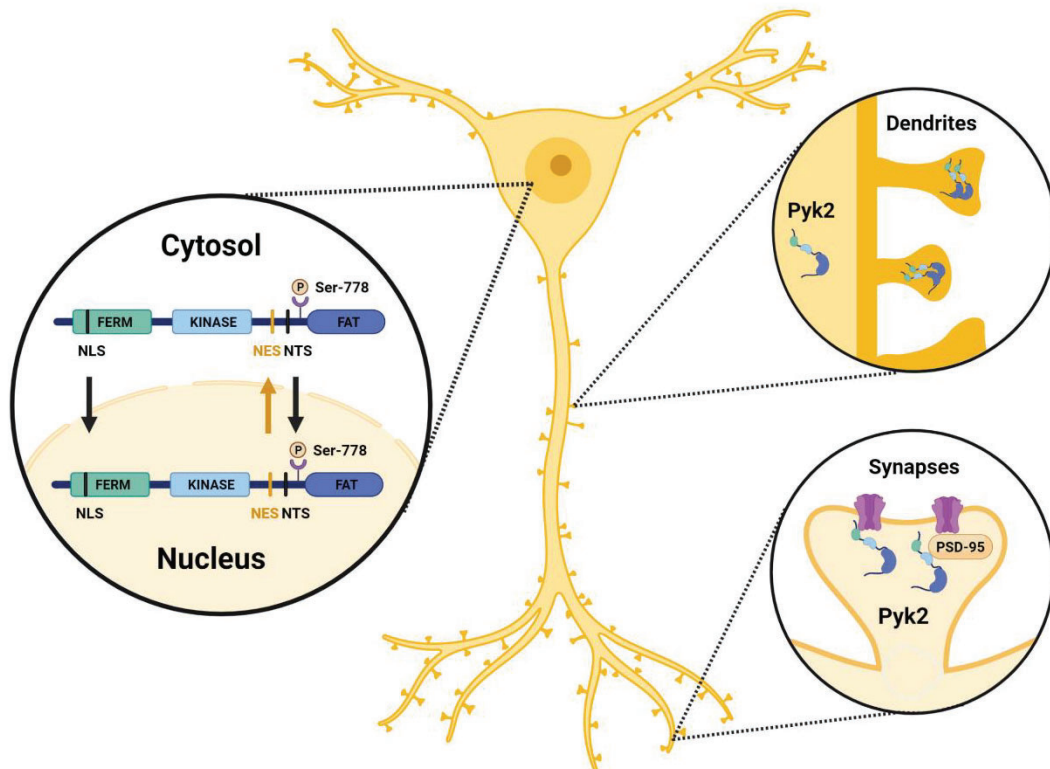


Figure 13. Localisation of Pyk2 in the neuron. Although main localisation of Pyk2 is the cytosol, Pyk2 can translocate to the nucleus in response to changes in intracellular Ca^{2+} levels. NLS and NTS motifs signals for nuclear import while NES for export to the cytosol. NES motif is enhanced by phosphorylation at site Ser-778. Pyk2 can also be recruited in dendrites and post-synaptic sites, where it interacts with PSD-95 and NMDAR.

3.5. Pathological role of Pyk2 in CNS

Since Pyk2 is involved in essential cellular functions in the neuron, it is not surprising that alterations in Pyk2 may lead to pathological situations, as neurodegenerative disease including AD, PD and HD.

PTK2B, the human gene encoding Pyk2, has been identified as a risk factor for late onset AD by many genome-wide association studies (GWAS) (Beecham et al., 2014; De Jager et al., 2014; Lambert et al., 2013). While the involvement of Pyk2 in AD pathology has

INTRODUCTION

been widely demonstrated, whether it has a neurotoxic or neuroprotective effect remains under debate. Our group has shown that 5XFAD transgenic mice presented a reduction in the phosphorylation of Pyk2 and the overexpression of Pyk2 reverted behavioural deficits related to AD (Giralt et al., 2018). On the contrary, other authors described the deletion of Pyk2 as a positive effect for AD pathological mechanisms. Deletion of Pyk2 in APP/PS1 mouse model protected from the detrimental effect of A β on loss of dendritic spines and memory impediments (S. Lee et al., 2019; Salazar et al., 2019). These discrepancies could be derived by the differences displayed in the transgenic mouse models of AD: 5XFAD mice present an aggressive phenotype with an early onset whereas in APP/PS1 mice the phenotype starts at six months of age (Kumar et al., 2021).

Moreover, Pyk2 has also been related to protein Tau. Tau is the major component of neurofibrillary tangles in AD and its excessive phosphorylation is considered as an early event in the pathogenesis of tauopathies (Wegmann et al., 2021). Pyk2 colocalises with hyperphosphorylated and oligomeric Tau in the brain of AD patients as well as in neurons of transgenic Tau mice (Dourlen et al., 2017; Köhler et al., 2013). Simultaneously, expression of STEP seems to be increased in brains of patients and mouse models of AD while inhibition of STEP boosts Pyk2 phosphorylation, improving cognitive impediments in transgenic AD mice (P. Kurup et al., 2010; Xu et al., 2014).

Pyk2 involvement in PD pathogenesis has been less explored. However, it has been proved that activation of Pyk2 induces tyrosine phosphorylation of α -synuclein via SFK (Nakamura et al., 2002). While no alterations in Pyk2 levels have been detected, brains of PD patients show higher levels of STEP, suggesting a reduction in Pyk2 function in this disease (P. K. Kurup et al., 2015).

Finally, previous work of our group showed that Pyk2 is reduced in the hippocampus of HD patients and R6/1 mice (Giralt et al., 2017). Indeed, previous work from our group showed that memory and synaptic alterations in the hippocampus of R6/1 mice were reverted when Pyk2 was overexpressed, indicating that lack of Pyk2 could be underlying the regulation of cognitive deficits in HD. In accordance with these results, a recent report from our group has involved Src in cognitive perturbances of HD in HdhQ111 mice, showing decreased levels of the phosphorylated form of Src in cortex of HD mice (Alvarez-Periel et al., 2018). Moreover, this same study described Cdk5 as a player in learning and memory deficits in HD by the modulation of NMDAR. Finally, we have also proved that Cdk5 mediates mitochondrial fragmentation in HD striatal cells (Cherubini et al., 2015). Taken together, in this Thesis we aimed to follow these promising results in HD together with the potential role of Pyk2 in the regulation of mitochondrial dynamics.

AIMS

The main aims of this Thesis are the following:

1. To study the role of mitochondrial dynamics and MAMs in the striatal neuronal vulnerability in HD.

- 1.1. To evaluate mitochondrial morphology in HD primary striatal neurons.
- 1.2. To analyse ER-mitochondrial contact sites and MAMs proteins in the striatum of HD models.
- 1.3. To determine alterations in ER-mitochondrial Ca^{2+} transport in primary striatal neurons of HD mouse models.
- 1.4. To explore whether alterations in MAMs in HD striatum are dependent of aberrant Drp1 activity.

2. To explore the contribution of astrocytic mitochondria to striatal vulnerability in HD.

- 2.1. To characterize the astrocyte population in the striatum of R6/1 mice.
- 2.2. To evaluate the metabolism and mitochondrial dynamics in R6/1 striatal astrocytes.
- 2.3. To assess transmitophagy in HD *in vitro* models from astrocytes to neurons and the impact on neuronal viability.

3. To study the role of Pyk2 in the regulation of mitochondrial dynamics and MAMs.

- 3.1. To study the subcellular localization of Pyk2 in neurons.
- 3.2. To evaluate the function of Pyk2 in MAMs formation in *in vivo* and *in vitro* neuronal models.
- 3.3. To explore the contribution of Pyk2 to the ER-mitochondrial Ca^{2+} transport in primary neurons.
- 3.4. To assess the involvement of Pyk2 in mitochondrial dynamics and morphology in *in vivo* and *in vitro* neuronal models.

METHODS

1. HUMAN HD *POST-MORTEM* BRAIN SAMPLES

Samples of caudate, putamen, hippocampus and cortex from control subjects and HD patients were obtained from Neurological Tissue Bank of the Biobank-Hospital Clínic-Institut d'Investigacions Biomèdiques August Pi i Sunyer (IDIBAPS) following the guidelines and approval of the local ethic committee (Hospital Clínic Barcelona's Clinical Research Ethics Committee). Details from these samples are provided in Table 2. Notice that male and female subjects were included in both diagnostics to avoid sex derived effects.

Table 2. Human samples from control subjects and HD patients. For each individual, an identification number is assigned together with gender, age (years) and *post-mortem* delay (PMD, h). For HD patients, Vonsattel grades and CAG repeats are specified.

ID	Diagnostic	Sex	Age	CAG repeats	PDM
CS-081	Control	Female	81	-	23:30
CS-1491	Control	Male	83	-	13
CS-1563	Control	Male	79	-	5
CS-1570	Control	Female	86	-	4
CS-1679	Control	Female	90	-	12:20
CS-1697	Control	Male	78	-	6
CS-1733	Control	Male	76	-	11:30
CS-1774	Control	Female	74	-	5
CS-1120	HD Vonsattel grade 3	Male	55	48	15
CS-1193	HD Vonsattel grade 3-4	Male	55	-	7
CS-1294	HD Vonsattel grade 3	Male	53	45+/-2	7
CS-1334	HD Vonsattel grade 1	Male	73	40+/-2	7
CS-1438	HD Vonsattel grade 3	Male	85	40	5:30
CS-1630	HD Vonsattel grade 2	Male	76	41	6
CS-1638	HD Vonsattel grade 2	Male	72	-	13:10
CS-1758	HD Vonsattel grade 2-3	Male	68	42+/-2	6:10

2. ANIMAL MODELS

Animals were genotyped from a tail biopsy by PCR analysis. For the *in vivo* studies, all mice used in the experiments were males. For the *in vitro* studies, both male and female mice were included in the experiments. Mice were housed together in numerical birth

METHODS

order in groups of mixed genotypes. Housing room was kept at 19-22°C, under 12:12h light/dark cycle and animals had *ad libitum* access to food and water. All procedures involving animals were performed in compliance with the National Institutes of Health Guide for the Care and Use of Laboratory Animals and approved by the local animal care committee of the Universitat de Barcelona (447/17 and 315/18) and the Generalitat de Catalunya (9878 and 10141-P7), in accordance with the European (2010/63/EU) and Spanish (RD53/2013) regulations for the care and use of laboratory animals.

2.1. HD MOUSE MODEL

2.1.1. R6/1

R6/1 transgenic mice were originally obtained from Jackson Laboratory (Bar Harbor, ME, USA). R6/1 expressed the N-terminal exon 1 fragment of mHtt with 115 or 145 glutamines. In the first study of this Thesis, R6/1 mice colony expressed 145 CAG repeats instead of 115 CAG repeats of the original R6/1 mice due to CAG repeat instability as has been previously described by other groups (Møllersen et al., 2010; Morton et al., 2009). In the second study of this Thesis, excessive expansion of CAG was corrected, and R6/1 colony expressed 115 CAG. Female WT were crossmated with male R6/1 to generate age-matched heterozygous WT and R6/1 littermates. Animals were maintained in a B6CBA genetic background.

2.1.2. HdhQ111

HdhQ111 knock-in mice were originally obtained from Dr. M. MacDonald's lab (Lloret et al., 2006). HdhQ111 knock-in mice presented targeted insertion of 109 CAG repeats that extends the glutamine segment in murine huntingtin to 111 residues. Female HdhQ7/Q7 wild type (WT) were crossmated with male HdhQ7/Q111 knock-in (KI) to generate age-matched heterozygous WT and KI littermates. Animals were maintained on a C57BL/6 genetic background.

2.2. PYK2^{-/-} MOUSE

For Pyk2 deletion, Pyk2^{fl/fl} C57Bl/6 mice were generated in which the *PTK2B* exons 15b-18 were flanked with LoxP sequences (Gen-O-way, Lyon, France) leading to a deletion that disrupts the protein kinase domain when crossed with an expressing Cre line. Pyk2^{-/-} mice and Pyk2^{fl/fl} mice were genotyped, and heterozygous mice were crossed to generate +/+, and -/- mice. Animals were maintained on a C57BL/6 genetic background.

3. CULTURES

3.1. PRIMARY NEURONAL CULTURES

Brains from mouse embryos at day 18 of embryonic development (E18) were removed and placed in Neurobasal medium (Gibco, Cat #21103-049). Hippocampal, striatum and cortex were dissected and gently mechanically dissociated with a fire-polished glass Pasteur pipette. Cells were seeded at different densities depending on the experiment (Table 3) onto coverslips or onto plates pre-coated with 0.1 mg/mL poly-D-lysine (Sigma-Aldrich, Cat. #P0899). Neurons were cultured in Neurobasal medium supplemented with 2% B27 (Gibco, Cat. #17504-044) and 1% Glutamax (Gibco, Cat. #35050-038) to grow cells in serum-free condition. Cultures were maintained at 37°C in a humidified atmosphere containing 5% CO₂. Embryos' genotype was determined by PCR from tail biopsy.

Table 3. Cell density of neuronal cultures.

CELL NUMBER	PLATE	DENSITY	EXPERIMENT
40,000 cells	12 mm coverslip	20,000 cells/cm ²	Immunocytochemistry
80,000 cells	12 mm coverslip	40,000 cells/cm ²	Treatment with ACM
120,000 cells	12 mm coverslip	60,000 cells/cm ²	Transfections
180,000 cells	25 mm coverslip	20,000 cells/cm ²	Calcium imaging
750,000 cells	6-well plate	80,000 cells/cm ²	Western Blot

3.2. PRIMARY ASTROCYTIC CULTURES

Brains from mouse pups at postnatal day 2 (P2) were removed and striatum was dissected and gently mechanically dissociated with a fire-polished glass Pasteur pipette (0.2-0.4 mm of diameter). Cells were seeded onto a 6-well plate precoated with 0.1 mg/mL poly-D-lysine in MEM medium (Gibco, Cat. #31095-029) supplemented with 20% FBS (PAN Biotech, Cat. #P40-37500), 90 mM glucose (Sigma, Cat. #G5400) and 1% penicillin/streptavidin (Gibco, Cat. #15090-046). At DIV5, cells were under horizontal shaking overnight in order to detach other cell types from the astrocytic culture. To passage the cell at DIV7, astrocytes were trypsinized for 2 min and neutralised with supplemented media. Cells were then centrifuged 10 min at 500 g and seeded at different densities depending on the experiment (Table 4) onto new coverslips or onto

METHODS

new plates pre-coated with 0.1 mg/mL poly-D-lysine. Medium changes were carried out every 3-4 days for nutrient replacement. Astrocytes were processed for further experiments at DIV14, DIV21 or DIV28. Cultures were maintained at 37°C in a humidified atmosphere containing 5% CO₂. Pups' genotype was determined by PCR from tail biopsy.

Table 4. Cell density of astrocytic cultures at passage day.

CELL NUMBER	PLATE	DENSITY	EXPERIMENT
20,000 cells	12 mm coverslip	10,000 cells/cm ²	Immunocytochemistry, DIV14
200,000 cells	6-well plate	20,000 cells/cm ²	ACM to treat neurons, DIV14
300,000 cells	p60	15,000 cells/cm ²	ACM for flow cytometry, DIV14
250,000 cells	p60	12,000 cells/cm ²	Western Blot, DIV14
100,000 cells	6-well plate	10,000 cells/cm ²	Western Blot, DIV21
60,000 cells	6-well plate	6,000 cells/cm ²	Western Blot, DIV28

4. CELLULAR BIOLOGY METHODS

4.1. PLASMIDS AND TRANSFECTIONS

Plasmids were obtained from expanded DH5α Competent *E. coli* (Invitrogen, Cat. #18265017). To transform bacteria, 200 ng of plasmid were added to 50 µl of cultured bacteria and incubated for 30 min on ice. To induce transformation by heat shock, mixture was incubated for 20 sec at 42°C and placed again on ice for 2 min. 800 µl of Lysogenic Broth (LB containing 10 g Tryptone, 5 g yeast extract and 10 g NaCl in 1 L distilled water) were added and transformed bacteria were growing for 1 h at 250 rpm at 37°C. Bacteria were seeded on agar plates containing 20 µg/mL kanamycin and grown overnight at 37°C. Then, isolated colonies were collected and grown in 5 mL of LB for 8 h and then in 200 mL of LB overnight at 37°C. Next day, pellet of the grown bacteria was lysed to isolate the plasmid with Pure Yield Plasmid Miniprep System (Promega, Cat. #A1223) and DNA was purified with Pure Yield Plasmid Maxiprep System (Promega, Cat. #A2393).

4.1.1. ER AND MITOCHONDRIA PLASMIDS

Striatal primary neurons were transfected to label mitochondria and ER for further colocalization analysis with pDsRed2-Mito and GFPSec61- β plasmids, respectively. The pDsRed2-Mito vector (Clontech Laboratories Inc, Cat. #632421) encodes a mitochondrial targeting sequence of human cytochrome c oxidase subunit VIII (Mito) that is fused to the 5'-end of *Dicosoma* sp. red fluorescent protein (DsRed2). The GFPSec61- β vector expresses the protein transport protein GFPSec61- β , located in the ER membrane, and is tagged with green-fluorescent protein (GFP). GFPSec61- β plasmid was a gift from Dr Tom Rapoport through the Addgene platform (Addgene, Cat. #15108).

The day prior to transfection (DIV10), half of the media was replaced with fresh medium. Neurons were transfected at DIV11 using Neuromag (OZ Bioscience, Cat. #NM50500) according to manufacturer's instructions. 1 μ g pDsRed2-Mito and 1 μ g GFPSec61- β were mixed with 4 μ l of Neuromag and incubated for 20 min at RT in the dark. Mixture was added to cells and incubated on a Magnetic Plate (Oz Bioscience, Cat. #MF10000) for 20 min at RT in the dark. Cells were then placed in the incubator at 37°C until DIV14, when they were fixed with 4% paraformaldehyde and analysed by confocal microscopy (see sections 5.1 and 6.1.1 in this chapter).

4.1.2. PYK2 CONSTRUCTS

To analyse the role of Pyk2 in mitochondrial dynamics regulation, hippocampal primary neurons from Pyk2^{-/-} cultures were transfected with different truncated forms of Pyk2 previously described (Camille Faure et al., 2013; Giralt et al., 2017): GFP (control), GFP-Pyk2, GFP-Pyk2^{-DFAT} (FAT domain and the third proline-rich motif were deleted from Pyk2), GFP-Pyk2^{YF} (Pyk2 with a point mutation of the autophosphorylated tyrosine-402) and GFP-Pyk2^{RRST} (Pyk2 with four point mutations in nuclear transport and location motifs). GFP was fused to the N-terminus of Pyk2. Pyk2^{+/+} neurons were transfected only with GFP as control.

Neurons were transfected at DIV18 using Transfectin (Bio-Rad, Cat. #170-3351) following manufacturer's instructions. 1 μ g of plasmid was mixed with 3 μ l of transfectin and incubated for 20 min at RT in the dark. Mixture was added to cells and incubated for 45 min at 37°C. Then, medium was replaced for fresh supplemented media and cells were placed in the incubator at 37°C until DIV21, when they were fixed with 4% paraformaldehyde and analysed by confocal microscopy (see sections 5.1 and 6.1.1 in this chapter).

METHODS

4.2. MITOCHONDRIAL ROS PRODUCTION

In order to measure mitochondrial ROS production in neuronal cultures, MitoSOX™ Red Indicator (Molecular Probes, Invitrogen, Cat. #M36008) was used. MitoSox is a fluorogenic dye that selectively detect superoxide, the predominant mitochondrial ROS. Once MitoSOX reaches mitochondria, the dye is oxidised by superoxide and becomes highly fluorescent.

Striatal primary neurons at DIV14 were incubated with MitoSOX at a final concentration of 5 μ M for 30 min at 37°C. Medium was removed and cells were washed twice. Neurons were then fixed with 4% paraformaldehyde/phosphate buffer saline (PFA/PBS) and nuclei stained with DAPI (see details at section 5.1 in this chapter). Digital images with 4.0 digital zoom and stacks of 0.4 μ m were processed through a convolve filter, subtraction of background and automatically thresholded using ImageJ software (Figure 14). MitoSOX intensity was calculated as Integrated Density/Area of cell. For each condition, 15 neurons were analysed from 7-8 independent experiments.

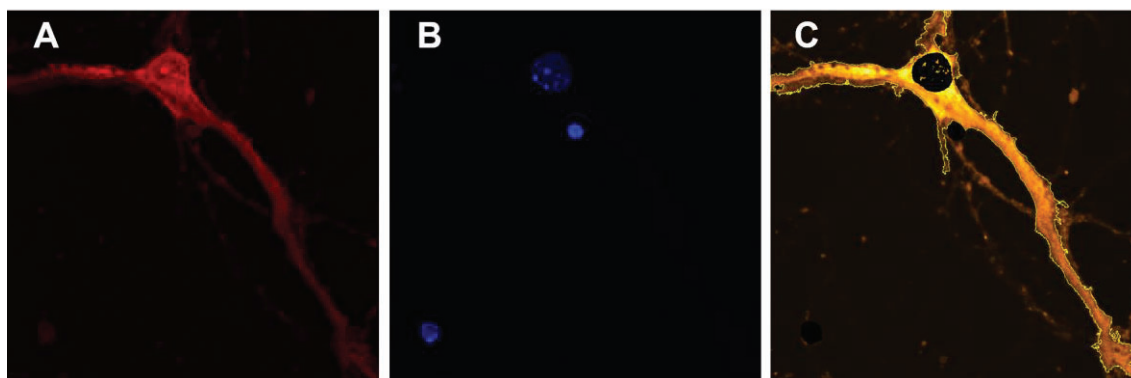


Figure 14. Analysis of digital images of MitoSOX fluorescence in primary neurons. Original image of MitoSOX staining (A) and nuclei (B) were segmented. In the processed image (C), intensity of MitoSOX was measured in the detected area (outlined in yellow in C) and nuclei area was subtracted from total area.

4.3. CALCIUM AND MITOCHONDRIAL MEMBRANE POTENTIAL IMAGING

To study calcium transfer from ER to mitochondria, calcium imaging was performed in neuronal cultures. Neurons at DIV14 or DIV21 were washed with Krebs buffer (145 mM NaCl, 5 mM KCl, 10 mM HEPES, 1 mM MgCl₂, 1 mM CaCl₂, 5.6 mM glucose and pH 7.4/NaOH) and loaded with 5 μ M Fluo-4 (Invitrogen, Cat. #F-14201) for 30 min and then with 20 nM TMRM (Invitrogen, Cat. #T668) for 20 min at RT to detect intracellular Ca²⁺ changes (Ca²⁺) and mitochondrial membrane potential ($\Delta\Psi$ m) respectively. 25 mm glass

coverslips were assembled in a chamber filled with 500 μ l of Krebs buffer on the stage of confocal microscope with an incubator system that controls temperature and CO₂. After 50 sec of recording, 0.5 μ M Thapsigargin (TG, Sigma-Aldrich T9033) was injected to inhibit SERCA ATPase and block Ca²⁺ storage at the ER. Then, 2 μ M FCCP (Sigma-Aldrich C2920), an uncoupler of mitochondrial respiratory chain, was added at 450 sec to depolarize mitochondrial membrane and inducing Ca²⁺ release to the cytosol. Images were captured every 2.5 sec throughout 750 sec of experiment. Fluorescence intensity was quantified using ImageJ software and values were normalized to the baseline. Fluo4 and TMRM fluorescence changes are presented as fold change of normalized response F1/F0 (F0 is the fluorescence intensity at time zero; F1 is the corrected fluorescence intensity at a given time point).

4.4. PHARMACOLOGICAL TREATMENTS *IN VITRO*

4.4.1. Mdivi-1

To assess the effect of Drp1 inhibition on mitochondrial dynamics and function, primary striatal neurons at DIV 14 were exposed to Mitochondrial division inhibitor 1 (Mdivi-1; Sigma-Aldrich, Cat. #M0199). Striatal cultures from WT or R6/1 embryos were treated with vehicle (DMSO) or 25 μ M Mdivi-1 for 1 hour. After treatment, cells were fixed and immunostained (see section 5.1 in this chapter) or prepared for calcium measurement assays (see section 4.3 in this chapter).

4.4.2. Glutamate

To study Pyk2 translocation to mitochondria, hippocampal primary neurons from Pyk2^{+/+} embryos were stimulated with glutamate. Neurons at DIV21 were treated with 40 μ M glutamate or vehicle for 15 min. After treatment, cells were then washed twice with PBS and processed for electron microscopy analysis, using the same fixative and post-fixative solutions as in tissue samples (see section 6.2.2 in this chapter).

4.5. MITOCHONDRIAL OXYGEN CONSUMPTION

Mitochondrial respiration was measured by high-resolution respirometry using Oroboros Oxygraph-2k. Striatal primary astrocytes from WT and R6/1 mice at DIV15 were cultured. 500,000 cells were obtained and resuspended in respiration MiR05 medium (0.5 mM EGTA, 3 mM MgCl₂, 60 mM lactobionic acid, 20 mM taurine, 10 mM KH₂PO₄, 20 mM HEPES, 110 mM sucrose and 0.1% BSA (w/v), pH 7.1). First, the oxygen consumption

METHODS

was measured in basal conditions. Then, 2.5 μM oligomycin was added to block complex V and measure leak respiration. Next, CCCP was titrated with sequential doses of 1 μM to obtain maximum uncoupled respiration and finally 0.5 μM rotenone and 2.5 μM antimycin were added to block complex I and complex III and measure non mitochondrial oxygen consumption. Data recording and analysis were performed using DatLab software v5.1.1.9 (Oroboros Instruments). Results were normalized to number of cells and expressed as $\text{pmol}\cdot\text{s}^{-1}/10^6$ cells. Residual oxygen consumption (ROX) due to non-mitochondrial respiration was measured and subtracted from all other measurements. Routine respiration refers to basal consumption of oxygen while ETC corresponds to maximal respiratory capacity after CCCP injection. In each assay, WT and R6/1 were monitored simultaneously.

4.6. MEASUREMENT OF METABOLITES IN CULTURE MEDIUM

To evaluate changes in glycolytic metabolism in astrocytes, levels of glucose, lactate and pH were measured in the medium using microfluidic epoc Blood Gas Electrolyte and Metabolite (BGEM) Test Card (Epcal, Cat. #CT-1006-00-00). Medium from WT and R6/1 striatal astrocytic cultures was obtained at DIV14 and centrifuged at 2000 g. Supernatant was injected in the microfluidic card with a 1 mL syringe and metabolites were measured with an epoc Reader. Levels of glucose and lactate are expressed in $\mu\text{g}/\text{mL}$ and $\mu\text{mol}/\text{mL}$ respectively.

4.7. ISOLATION OF ASTROCYTES FROM ADULT MOUSE BRAIN

Mice were sacrificed at different ages by cervical dislocation. Striatum of adult WT and R6/1 mice was dissected, placed in ice-cold PBS and disaggregated using the Adult Brain Dissociation Kit (Miltenyi, Cat. #130-107-677). Tissue was enzymatically and mechanically disaggregated for 30 min at 37°C. Dissociated cells were filtered with a 70 μm filter and debris were removed by a gradient with Debris Removal Solution and an overlay of ice-cold PBS. After centrifugation, cells were pelleted and washed with cold PBS.

To isolate astrocytes from striatum of adult mice, cells were magnetically isolated using the Anti-ACSA-2 MicroBead Kit (Miltenyi, Cat. #130-097-678). The ACSA-2 antigen is expressed specifically on astrocytes in a similar pattern to GLAST expression. Cells were

first blocked with FcR Blocking Reagent for 10 min at 4°C and then magnetically labelled with Anti-ACSA-2-Microbeads for 15 min at 4°C. Then, cell suspension was loaded onto a MACS MS Column (Miltenyi, Cat. #130-042-201) and ACSA-2+ fraction was retained within the column. Column was removed from the magnetic field and the magnetically retained ACSA-2+ cells were eluted with PBS 0.5% BSA (Miltenyi, Cat. #130-091-376), pH 7.2. Finally, ACSA-2+ cells were lysed in the appropriated buffer either for Western Blot (see section 7.3 in this chapter) or RNA extraction (see section 7.7 in this chapter). For MitoTracker labelling, striatal astrocytes were isolated from each animal individually. For extraction of protein and RNA, a pool of 3 striata was required.

4.8. MITOTRACKER INCUBATION

MitoTrackers are dyes that passively cross the plasmatic membrane and accumulate in mitochondria. MitoTracker Green (Invitrogen, Cat. #M7514) and MitoTracker Red CMXRos (Invitrogen, Cat. #M7512) were used in combination to track mitochondrial mass and mitochondrial membrane potential simultaneously for flow cytometry assays as described in (Monteiro et al., 2020). MitoTracker Green binds mitochondrial proteins and accumulates in the mitochondrial matrix, independently of $\Delta\Psi_m$, and thus, it is a marker of mitochondrial content. On the other side, MitoTracker Red is dependent on $\Delta\Psi_m$ since it is accumulated on polarized mitochondria and therefore, can be used to determine mitochondrial viability. Hence, using both dyes, functional and dysfunctional mitochondria can be evaluated in live cells.

4.8.1. MitoTracker to assess functionality of intracellular mitochondria in adult striatal astrocytes.

To assess functional and dysfunctional mitochondria in adult striatal astrocytes, MitoTracker Red and MitoTracker Green were incubated following the protocol from de Brito Monteiro et al. (Monteiro et al., 2020). Adult astrocytes were isolated from striatum of WT and R6/1 mice at 20W as described in section 4.7. Then, cells were incubated with 50 nM MitoTracker Red and 100 nM MitoTracker Green, together with Live/Dead Aqua (Invitrogen, Cat. #L34957) to assess cellular viability, for 15 min at 37°C. Cells were washed with 2% FBS in PBS and centrifuge at 1,500 rpm for 5 min. Pellet was resuspended in 2% FBS in PBS and immediately observed by flow-cytometry (see 5.3.2 in this chapter).

METHODS

4.8.2. MitoTracker to assess functionality of extracellular mitochondria in astrocyte conditioned medium.

To analyse functionality of extracellular mitochondria present in the astrocyte conditioned medium (ACM), striatal primary astrocytes from WT and R6/1 mice were incubated with MitoTracker Red and MitoTracker Green. Both MitoTrackers were incubated in non-supplemented MEM at a final concentration of 200 nM for 30 min at 37°C and cells were then washed twice with PBS. Medium was changed to fresh supplemented MEM and incubated for 24 h at 37°C. Next day, astrocyte conditioned medium (ACM) was collected and centrifuged for 10 min at 2,000 g to pellet mitochondria. Pellet was resuspended in PBS and immediately observed by flow-cytometry (see 5.3.3 in this chapter).

4.8.3. MitoTracker to assess mitochondrial transfer from astrocytes to neurons.

To observe the effect of transfer of mitochondria from astrocytes to neurons, WT striatal neuronal cultures were treated with ACM from striatal astrocytes incubated with MitoTracker Red. Striatal astrocytic cultures of WT and R6/1 mice were obtained (see section 3.2 in this chapter) and at DIV18, astrocytic mitochondria were labelled with 200 nM MitoTracker Red in non-supplemented MEM for 30 min at 37°C and then cells were washed twice with PBS. Medium was changed to fresh Neurobasal without supplementing and was incubated for 24h at 37°C. Then, ACM was collected and centrifuged for 10 min at 1,000 g to pellet cellular debris. The resulting supernatant was transferred to WT neurons, replacing only half medium change. Neurons were incubated with the ACM for 24h h at 37°C and then cells were processed to assess oxidative stress in live cells (see section **¡Error! No se encuentra el origen de la referencia.** in this chapter) or neuronal branching (see section 6.1.4 in this chapter).

4.9. OXIDATIVE STRESS PRODUCTION IN LIVE CELLS

Production of oxidative stress was measured in neuronal cultures using CellROX Green Reagent (Invitrogen, #C10444). CellROX Green is a fluorogenic DNA dye that detects reactive oxygen species (ROS), and its signal localizes mainly in the nucleus and mitochondria.

Striatal neurons at DIV16 were incubated with CellROX Green at a final concentration of 5 µM for 30 min at 37°C. Then, medium was removed, and cells were washed twice with PBS. Neurons were fixed with 4% PFA/PBS and nuclei stained with DAPI (see details at

section 5.1 in this chapter). Confocal images were taken in the following 24 h to evaluate intensity of fluorescence with a Zeiss LSM880 confocal microscope. Stacks of 0.3 μm were acquired using a 63x OIL objective. Digital images were processed through a convolve filter, subtraction of background and automatically thresholded using ImageJ software. CellROX intensity was calculated as Integrated Density/Area of cell. For each condition, 60-140 neurons were analysed from 2 independent experiments.

5. IMMUNOFLUORESCENCE

5.1. IMMUNOCYTOCHEMISTRY

Primary neuronal cultures grown on 12 mm glass coverslips were fixed at DIV14 or DIV21 with 4% paraformaldehyde (PFA) in PBS for 10 min, rinse in PBS and treated with 0.1 M glycine-PBS for 15 min to quench formaldehyde crosslinking. Coverslips were washed thrice with PBS. Next, cells were permeabilised with 0.1% saponin for 10 min and blocked with PBS containing Normal Horse Serum 15% for 30 min at RT. Then, cells were washed in PBS and incubated overnight at 4°C with primary antibodies diluted in Normal Horse Serum 5%-PBS (

Table 5).

Table 5. Primary antibodies used for immunocytochemistry.

ANTIGEN	SPECIE	DILUTION	SOURCE	ID
GFAP-488	-	1:250	Invitrogen	53-9892-82
GLAST-PE	-	1:50	Miltenyi	130-118-344
MAP2	Mouse	1:500	Sigma-Aldrich	M 1406
TOM20	Rabbit	1:250	Protein Tech	11802-1-AP

Remaining primary antibody was removed with three washes with PBS and incubated 1 h at RT with the appropriated fluorescent secondary antibodies (Table 6). Finally, coverslips were rinsed thrice with PBS and mounted on microscope slides with DAPI-Fluoromount-G® (Southern Biotech, Cat. #0100-20).

METHODS

Table 6. Secondary antibodies used for immunocytochemistry.

ANTIGEN	DILUTION	SOURCE	ID
Alexa Fluor® 488	1:100	Jackson	715-545-150
AffiniPure Donkey Anti-Mouse IgG		ImmunoResearch	
Alexa Fluor® 488	1:100	Jackson	711-545-152
AffiniPure Donkey Anti-Rabbit IgG		ImmunoResearch	
Alexa Fluor® 647	1:100	Jackson	711-605-152
AffiniPure Donkey Anti-Rabbit IgG		ImmunoResearch	
Cy™3 AffiniPure Donkey Anti-Mouse IgG	1:100	Jackson ImmunoResearch	715-165-150
Cy™3 AffiniPure Donkey Anti-Rabbit IgG	1:100	Jackson ImmunoResearch	711-165-152

5.2. PROXIMITY LIGATION ASSAY

To measure contacts between ER and mitochondria, proximity ligation assay (PLA) was performed using Duolink® detection kit with red fluorophore λ excitation 594 nm/ λ emission 624 nm (Sigma-Aldrich, Cat. #DUO92101-1KT). PLA is an *in situ* assay that generates a fluorescent signal only when the two targeted proteins are in close proximity, up to 40 nm.

Prior to PLA assay, cells were fixated and labelled with MAP2 to stain neurites as previously described. Then, primary antibodies IP3R3 (1:500, rabbit, Milipore, Cat. #AB9076) and VDAC1 (1:500, mouse, Abcam, Cat. #ab14734) were incubated overnight to target ER and mitochondria respectively. After washing with PBS, PLA probes anti-rabbit MINUS and anti-mouse PLUS were added for 1 h and hybridization was amplified by rolling circle amplification. Nuclei were stained with DAPI using mounting media provided in the kit.

Digital images were taking with 3.0 digital zoom and stacks of 0.4 μ m. Fluorescent dots were analysed using the plugin “Analyse particles” of ImageJ. Number of particles was

relativized to cell area (Figure 15). As a negative control, one of the primary antibodies was omitted and no signal was detected.

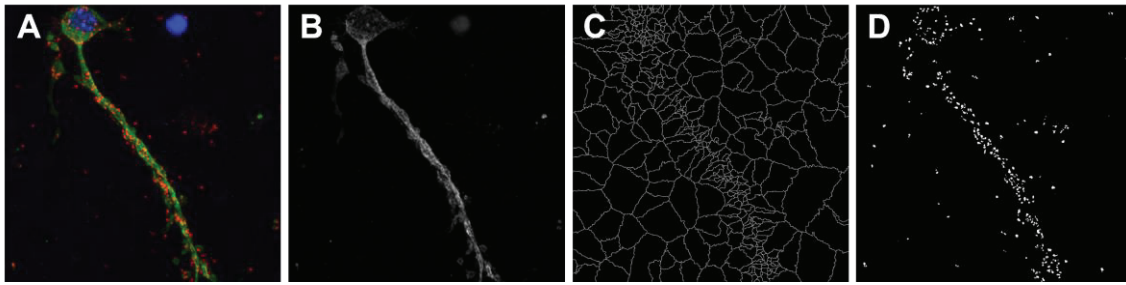


Figure 15. Processing of confocal images for PLA analysis. Original image (A) was processed with split channels. Cell area labelled with MAP2 in green was subjected to background subtraction (B) and PLA signal in red was segmented and thresholded (C). Only PLA particles overlapping cell area were analysed (D).

5.3. FLOW CITOMETRY

Analysis by flow cytometry was performed using a BD LSR Fortessa flow cytometer (Becton, Dickinson and Company, BD Biosciences, San Jose, CA) and software FACSDiva™ v. 8.0.1 (Becton, Dickinson and Company). The instrument was equipped with 355, 405, 488, 561 and 640 nm LASERS. Unstained and single-stained samples for each fluorochrome were used to set voltages, compensations, and gating strategy.

5.3.1. Astrocyte markers

Expression of several astrocyte markers (Table 7) were assessed by flow cytometry in striatum from WT and R6/1 mice at 20W. Striatal cells were disaggregated using the Adult Brain Dissociation Kit (Miltenyi, Cat. #130-107-677) as described in section 4.7 in this chapter. Cells were stained with Live/Dead Aqua (Invitrogen, Cat. #L34957) for 30 min at RT. Surface antibody GLAST was incubated for 15 min at RT and washed with PBS-0.1% NaN₃-5% FBS. Cells were fixated and permeabilized using FIX&PERM Cell Permeabilization Kit (Life Technologies, Cat. #GAS003). Intracellular antibodies ALDH1L1, GFAP, and S100β were incubated 20 min at RT and Brilliant Violet 711 Streptavidin was added to detect the streptavidin conjugated to ALDH1L1 for 20 min at RT (Table 2). Samples were washed with PBS-0.1% NaN₃-5% FBS and centrifuged at 500 g for 10 min at 4°C. Pellet was resuspended in PBS-0.1% NaN₃-5% FBS and immediately observed by flow cytometry.

METHODS

Cells were gated based on FSC-H versus SSC-H parameters. Dead cells were removed by gating Live/Dead Aqua negative cells. Autofluorescence (no probe) was used as negative control and fluorescence minus one (FMOs) as gating controls. FACS data were analysed by FlowJo software DiVa v8.0.1 software.

Table 7. Conjugated antibodies used for flow cytometry.

ANTIGEN	FLUOROPHORE	DILUTION	SOURCE	ID
ALDH1L1	Streptavidin	1:500	Invitrogen	13-9595-82
GFAP	Alexa 488	1:100	Invitrogen	53-9892-82
GLAST	PE	1:50	Miltenyi	130-118-344
S100 β	Alexa 700	1:100	Novus Biologicals	NBP2- 54579AF700

5.3.2. MitoTracker Green and MitoTracker Red

Mitochondria from adult striatal astrocytes or from ACM of WT and R6/1 mice were labelled with MitoTracker Green and MitoTracker Red (see section 4.8.1 and 4.8.2 respectively).

To exclude debris, mitochondria particles were gated based on light-scattering properties in the FSC-H versus SSC-H parameters and P1 gate was established using controls beads in size from 3 μ m to 500 nm. Events within P1 gate were collected, and analysed using MitoTracker Green (LASER 488nm, 525/50 bandpass filter) and MitoTracker Red (LASER 561nm, 582/15 bandpass filter). Autofluorescence (no probe) was used as negative control. MitoTracker Green positive events were gated based on their MitoTracker Green mean fluorescence intensity (MFI) compared with the MFI of the Autofluorescence (no probe) negative control. MitoTracker Red positive events were gated based on their MitoTracker Red MFI compared with the MFI of the Autofluorescence (no probe) negative control. MitoTracker Green positive events were selected according to their MitoTracker Red MFI. FACS data were analysed by DiVa v8.0.1 software (Figure 16 and Figure 17.).

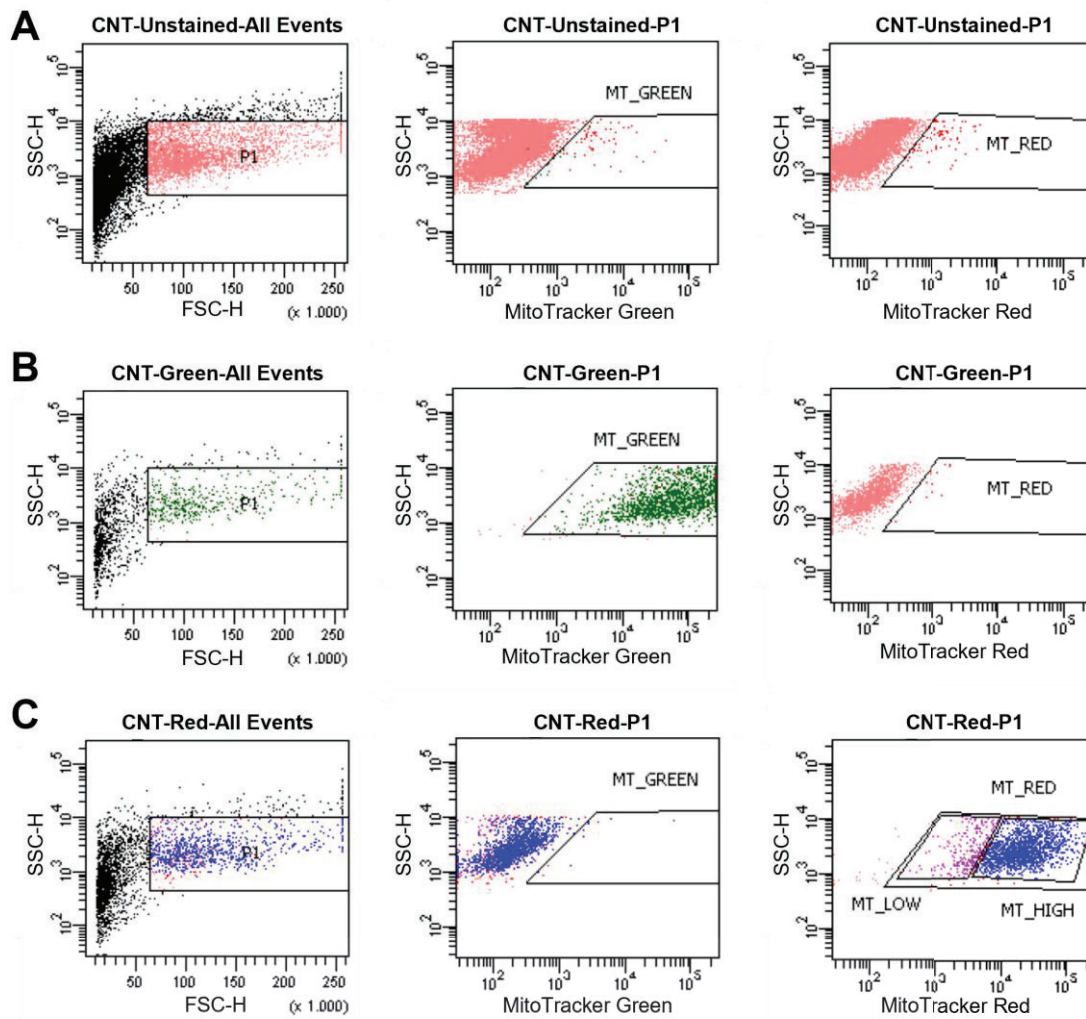


Figure 16. Selection of MitoTracker Green and MitoTracker Red populations in isolated astrocytes from the striatum of adult mice at 20W. Representative plots of mean intensity fluorescence for autofluorescence (A), MitoTracker Green (B) and MitoTracker Red (C) samples. In the left panels, particles with a size similar to mitochondria (500 nm-3 μ m) are gated (P1). In middle panels, gating of MitoTracker Green positive events. In right panels, gating of MitoTracker Red positive events with two subpopulations (low and high) based on the mean intensity fluorescence.

METHODS

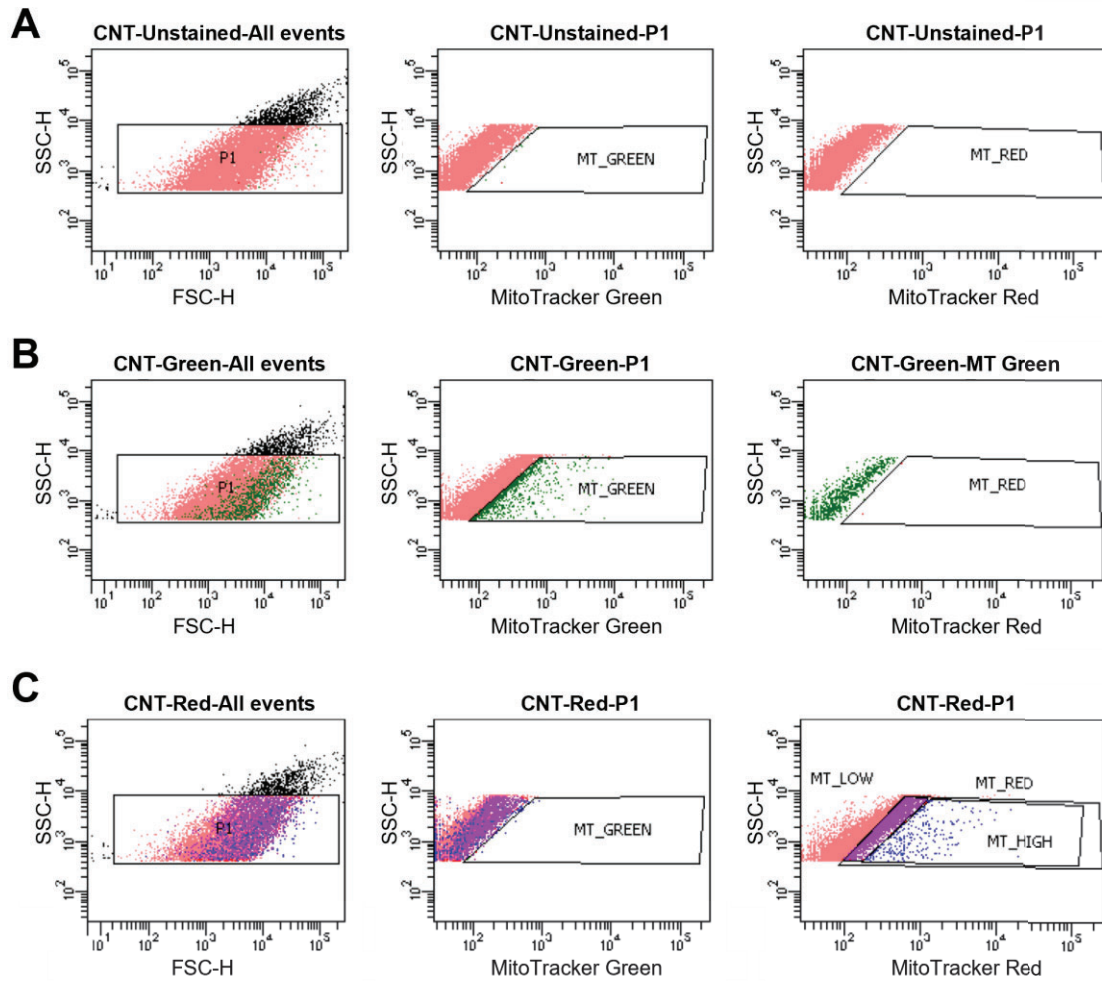


Figure 17. Selection of MitoTracker Green and MitoTracker Red populations in the ACM of primary astrocytic cultures. Representative plots of mean intensity fluorescence for autofluorescence (**A**), MitoTracker Green (**B**) and MitoTracker Red (**C**) samples. In the left panels, particles with a size similar to mitochondria (500 nm-3 μ m) are gated (P1, in pink). In middle panels, gating of MitoTracker Green positive events. In right panels, gating of MitoTracker Red positive events with two subpopulations (low and high) based on the mean intensity fluorescence.

6. MICROSCOPY TECHNIQS

6.1. CONFOCAL IMAGE ACQUISITION AND ANALYSIS

Immunofluorescence was examined by confocal microscopy using a Leica TCS SP5 confocal microscope (Leica Microsystems) or Zeiss LSM880 confocal microscope (Zeiss). Digital images were obtained with 63.0x 1.40 OIL or 63.0x glycerol objective depending on the experiment. For each image, z-stacks were taken from the entire three-dimensional structure. Digital zoom and size of stack depended on the experiment.

6.1.1. MITOCHONDRIAL MORPHOLOGY IN NEURONAL CULTURES

To analyse mitochondrial morphology, digital images from striatal and hippocampal primary neuronal cultures at DIV14 and DIV21 respectively were acquired with 3.0 digital zoom and stacks of 0.4 μm using a 63x OIL objective in a LEICA SP5 confocal microscope. Images were then processed through a convolve filter and automatically thresholded using ImageJ software. The resulting image was a binary image with black particles (mitochondria) in a white background. From binary image, individual mitochondria were subjected to particle analyses to obtain number of mitochondria per cell, Aspect Ratio (AR, length-to-width ratio), and Form Factor (FF, $(Pm^2/4 \pi \times Am)$), where Pm is the perimeter and Am is the surface area of mitochondrion (Figure 18). AR values of 1 mean a perfect circle, and the higher AR, the more elongated mitochondria. FF values of 1 indicate unbranched mitochondrion, and higher FF correspond to more complex mitochondria network. For each condition, 10-15 neurons were analysed from 6-8 different embryos.

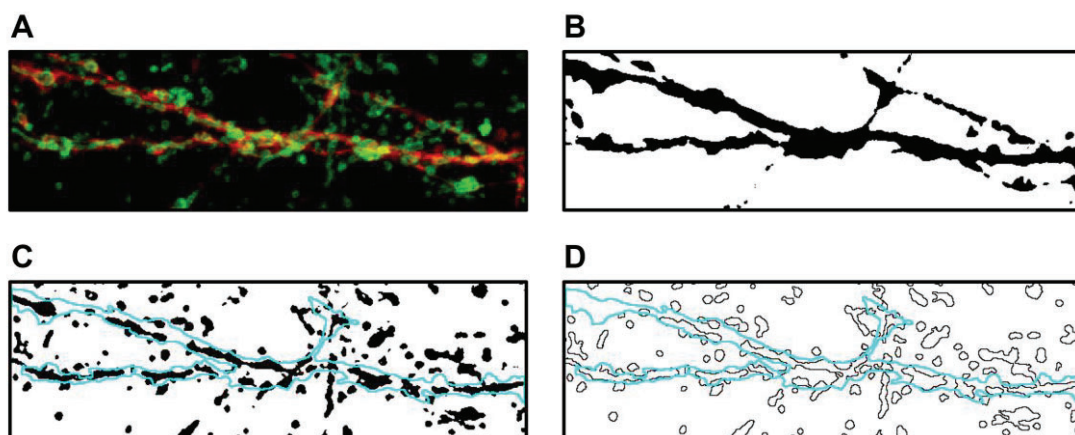


Figure 18. Processing of confocal images for mitochondrial morphology analysis in primary neurons. (A) Original digital images with mitochondria in green and neuronal area in red were processed with split channels. (B) Neuronal area was thresholded. (C) Mitochondria were converted to binary image in a white background and (D) particles were measured with morphometric parameters. In C and D, blue line delimits the area subjected to the analysis.

METHODS

6.1.2. MITOCHONDRIAL MORPHOLOGY IN ASTROCYTIC CULTURES

To analyse mitochondrial morphology in primary astrocytes, striatal astrocytic cultures at DIV14 were immunolabelled with GLAST-PE (Miltenyi, Cat. #130-118-344), GFAP-488 (Invitrogen, Cat. #53-9892-82), TOM20 (ProteinTech, Cat. #11802-1-AP) and Fluoromount. Digital images were acquired with stacks of 0.33 μm using a 63x OIL objective a Zeiss LSM880 confocal microscope. Digital mosaics were performed tiling 4x4 images. Images were processed through a convolve filter and automatically thresholded using ImageJ software. Cells were segmented for GLAST and GFAP signal and cell area and intensity were measured. Mitochondrial morphology was analysed in the maxima projection and segmented by machine learning using WEKA software. Number of mitochondria, mitochondrial mass and circularity were calculated. For each genotype, 8 mosaics were analysed from 3-4 different pups.

6.1.3. ER-MITOCHONDRIAL CONTACT SITES

Contact sites between ER and mitochondria were analysed in striatal neurons at DIV14 by measuring colocalisation of the plasmids GFPsec61- β and pDsRed2-Mito respectively. Digital images were acquired with 4.0 digital zoom and stacks of 0.2 μm using a 63x OIL objective in a LEICA SP5 confocal microscope. Stacks were filtered, automatically thresholded, deconvolved and background was subtracted using ImageJ software. Interaction between organelles were quantified as overlapping of plasmids measured with Mander's coefficient (M2) from the ImageJ plugin "JACoP". For each condition, 10-15 neurons were analysed from 5-9 independent experiments.

6.1.4. NEURONAL BRANCHING

Neuronal branching was evaluated in WT primary striatal neurons at DIV17 after treatment with WT or R6/1 ACM. Neurons were stained with MAP2 (see section 5.1 in this chapter) and digital images were acquired with 63x OIL objective in a Zeiss LSM880 confocal microscope with a 0.6 zoom and 0.3 μm stacks. To quantify the branching, Sholl analysis was performed using ImageJ software with the plugins "Concentric Circles" and "Cell Counter". Concentric circles were placed with the soma in the centre and 8 circles were analysed (inner circle: 50; outer radius: 400). Intersections of neurites with the circles were counted with the "Cell Counter" plugin.

6.2. ELECTRON MICROSCOPY

6.2.1. EXTRACELLULAR MITOCHONDRIAL

Extracellular mitochondria were processed for electron microscopy similarly to previous descriptions of extracellular particle and mitochondria detection in astrocyte cultures (Hayakawa et al., 2016). Medium from striatal astrocytic culture was collected at DIV14 after 4 days in culture. Cellular debris were pelleted and discarded by centrifugation of the sample for 10 min at 2.000 g. Then, the resulting supernatant was washed in phosphate buffer (PB) 0.1 M and centrifuged again for 10 min at 2.000 g. Pellet was processed for electron microscopy analysis. Sample was fixed in 1% osmium tetroxide 0.8% potassium ferrocyanide in PB 0.1 M, pH 7.4 for 1.5 h at 4°C and then rinsed in double distilled water to remove osmium excess.

Samples were then dehydrated through a graded series of acetone to 100%. They were infiltrated with Spurr resin mixed with acetone. For the correct resin polymerization, samples were embedded in Spurr resin at 60°C for three consecutive days. Thin sections were cut at 50 nm thickness using an ultramicrotome (Ultracut E Leica). Samples were observed with a J1010 Jeol electron microscopy. Digital images were obtained with a CCD camera (Gatan Orius).

6.2.2. MITOCHONDRIAL MORPHOLOGY AND MAMS

To evaluate the subcellular location of Pyk2, hippocampal sections from Pyk2^{+/+} mice were obtained, processed and analysed by electron microscopy. First, mice were transcardially perfused with a solution containing 4% paraformaldehyde and 0.1% glutaraldehyde made up in 0.1 M PB, pH 7.4. After perfusion, brains were removed from the skull, and immersed in the same fixative 12 h 4°C. Tissue blocks containing the hippocampus were dissected, washed with PB and cut with a vibratome to obtain samples of 1mm³. Samples were post-fixed with 2% osmium tetroxide in PB 0.1 M for 20 min and then were dehydrated in a series of ethanol and finally flat embedded in epoxy resin (EPON 812 Polysciences). After polymerization, blocks from the CA1 region or blocks from cell cultures were cut at 70 nm thickness using an ultramicrotome (Ultracut E Leica). Sections were cut with a diamond knife, picked up on formvar-coated 200 mesh nickel grids. Sections were then immunostained by indirect immunolabeling using protein gold as immunomarker. Protein A-gold probes (20 nm) were obtained from CMC Utrecht (Netherlands). After immunolabeling, sections were double stained with uranyl acetate and lead citrate prior to observation with a Philips (CM-100) electron microscope. Digital

METHODS

images were obtained with a CCD camera (Gatan Orius). EPON embedded sections were ultrathin-sectioned and reacted with anti-Pyk2 (Sigma-Aldrich, #P3902) antibody revealed with protein A coupled to 10 nm gold particles.

Mitochondrial morphology and MAMs were evaluated in hippocampal sections of Pyk2^{+/+} and Pyk2^{-/-} mice by electron microscopy. Number of mitochondria, AR and FF were quantified by counting the total number of visible mitochondria present in a fixed size surface of the *stratum radiatum* from the CA1 region. Aspect Ratio (AR, length-to-width ratio) and Form Factor (FF, $Pm^2/4 Am$) were determined manually tracing individual mitochondria using ImageJ software (NIH, Bethesda, MD, USA). Aspect Ratio (AR, length-to-width ratio), and Form Factor (FF, $Pm^2/4 Am$), where Pm is perimeter and Am is area of mitochondrion. To determine the number of MAMs in neuronal cultures, mitochondrial contacts closely associated to ER were manually counted. Contacts were considered when the distance between both organelles was less than 30 nm as previously described (Watanabe et al., 2016). 50 mitochondria from 6 different cells per genotype were analysed. To measure Pyk2 density in mitochondria in neuronal cultures, the number of individual gold particles (10-nm) localised in morphometrically determined areas was hand counted and the labelling density was calculated as the number of gold particles per μm and then relativized the values as a percentage.

For Pyk2 particles counting in neuronal cultures, the number of individual gold particles (10-nm) localised in morphometrically determined areas was hand counted and the labelling density was calculated as the number of gold particles per area of the mitochondria and then values were relativized to a percentage.

7. MOLECULAR BIOLOGY METHODS

7.1. PROTEIN EXTRACTION

7.1.1. EXTRACTION FROM ANIMAL AND HUMAN BRAINS

Mice were sacrificed at different ages by cervical dislocation. Brain was rapidly removed, and striatum, hippocampus and cortex were dissected, frozen on dry ice, and stored at $-80^{\circ} C$ until used. Both mouse and human brain frozen tissue were homogenised by sonication in ice-cold lysis buffer containing 50 mM Tris-HCl (pH 7.5), 150 mM NaCl, 10 mM EGTA and 1% Triton X-100 and supplemented with 1mM sodium orthovanadate and protease inhibitor cocktail (Sigma-Aldrich, Cat. #P8340). Samples were centrifuged at 16,100 g at $4^{\circ} C$ for 15 minutes and supernatants were collected.

7.1.2. EXTRACTION FROM PRIMARY CULTURES

To obtain protein extracts, primary cultures were washed with PBS and incubated with ice-cold lysis buffer containing 50 mM Tris base (pH 7.5), 150 mM NaCl, 2 mM EDTA, 1% NP-40 and supplemented with 1mM sodium orthovanadate and protease inhibitor cocktail (Sigma-Aldrich, Cat. #P8340). Cells were detached from plates using a scraper and then disaggregated by pipetting up and down with an insulin syringe. Finally, samples were centrifuged at 13,200 g at 4°C for 15 min and supernatants were collected.

7.2. PROTEIN QUANTIFICATION

Quantification of protein extracts was performed using a colorimetric assay with the Detergent-Compatible Protein Assay kit (Biorad, Cat. #5000116) as instructed by manufacturer. Reagents were added to the samples, and, after 15 min incubation, absorbance was measured at 650-750 nm using the spectrophotometer Synergy™ 2 Multi-Detection Microplate Reader (BioTek). A serial dilution of BSA (0.5 µg/µl, 1 µg/µl, 2 µg/µl, 4 µg/µl, 8 µg/µl and 16 µg/µl) was used to perform a standard curve as reference for protein concentration. Each sample was measured in duplicates and only those quantifications with a standard deviation lower than 0.5 were considered valid.

7.3. WESTERN BLOT

Protein extract (10-20 µg) were denatured in SDS sample buffer containing 62.5 mM TrisHCl (pH 6.8), 10% glycerol, 2% Sodium dodecyl sulphate (SDS), 140 mM β-mercaptoethanol and 0.1% bromophenol blue. Protein samples were boiled at 100°C for 5 min and resolved on 6-12% SDS-polyacrylamide gel electrophoresis (SDS-PAGE), depending on the molecular weight of the protein of interest, at 30 mA/gel for approximately 1 h. Marker (Biorad, Cat. #1610394) was loaded together with protein samples to indicate molecular weight along the SDS-PAGE. Next, proteins were transferred onto nitrocellulose membranes (Amersham, Cat. #10600002) at 100 V for 1-1.5 h at 4°C. To block nonspecific protein binding sites, membranes were incubated with 10% non-fat powdered milk in Tris-buffer saline 0.1% Tween-20 (TBS-T) for 1 h at RT. After washing thrice with TBS-T for 10 min at RT, membranes were blotted with primary antibodies (Table 8) overnight at 4°C.

METHODS

Table 8. Primary antibodies used for Western Blot. List with molecular weight, host specie, dilution used, source and reference of each primary antibody.

ANTIGEN	MW (KDA)	HOST	DILUTION	SOURCE	ID
ALDH1L1	100	Mouse	1:500	NeuroMab	N103/39
CD38	45	Mouse	1:500	ProteinTech	60006-1-Ig
Cdk5	30	Mouse	1:1000	Santa Cruz	sc-6247
Drp1	79-84	Mouse	1:1000	BD Biosciences	611113
GFAP	50	Rabbit	1:1000	DAKO	z0334
GLAST	60	Rabbit	1:1000	Abcam	ab416
Grp75	75	Mouse	1:1000	Abcam	ab 2799
IP3R3	300	Mouse	1:500	BD Biosciences	610312
LC3B	14-16	Rabbit	1:1000	Cell Signaling	2775
Mfn2	86	Mouse	1:500	Abcam	ab 56889
Opa1	80-100	Mouse	1:8000	BD Biosciences	610312
p62	62	Mouse	1:500	Abcam	ab56416
Parkin	50	Rabbit	1:1000	Assay Biotech	B0542
Pyk2	110-116	Rabbit	1:1000	Sigma- Aldrich	P3902
S100β	20-25	Mouse	1:500	Sigma- Aldrich	S2532
TOM20	16	Rabbit	1:1000	Abcam	ab56783
VDAC1	31	Rabbit	1:1000	Abcam	ab15895

After primary antibody incubation, membranes were rinsed thrice with TBS-T and incubated for 1 h at RT with the corresponding horseradish conjugated secondary antibody (Table 9). After three more washes at RT, immunoreactive bands were developed using Western Blot Luminol Reagent (Santa Cruz, Cat. #sc-2048).

Table 9. Secondary antibodies used for Western Blot. List of secondary antibodies with the used dilution, source and identifier.

ANTIGEN	DILUTION	SOURCE	ID
Anti-goat IgG	1:3000	Promega	V8051
Anti-mouse IgG	1:3000	Promega	W4021
Anti-rabbit IgG	1:3000	Promega	W4011

Loading control was performed by reproving membranes with different antibodies, depending on the type of sample that was analysed (Table 10). Loading control antibodies were incubated for 20 min at RT and then washed and developed as the others primary antibodies. Image Lab software (BioRad) was used to quantify densitometry of immunoreactive bands relative to the intensity of loading control band in the same membrane.

Table 10. Primary antibodies used as loading control for Western Blot. List with cellular compartment, molecular weight, host specie, dilution used, source and identifier of each primary antibody.

ANTIGEN	SAMPLE	MW (KDA)	HOST	DILUTION	SOURCE	ID
Actin	Total lysate	42	Mouse	1:50000	Sigma	A3854
CoxV	Mitochondrial fraction	17	Mouse	1:1000	Invitrogen	A21350
Lamin B	Nuclear fraction	61	Goat	1:1000	Santa Cruz	sc-6217
Tubulin	Total lysate and cytosolic fraction	55	Mouse	1:50000	Sigma- Aldrich	6074

7.4. SUBCELLULAR FRACTIONATION OF NUCLEUS, CYTOSOL AND MITOCHONDRIA

Hippocampal samples from adult Pyk2^{+/+} mice of 4 month of age were removed and homogenized in Buffer A (20mM HEPES, 2mM EDTA, 1,5mM MgCl₂, 10mM KCL, pH 7,5, 1mM PMSF, 10 µg/mL aprotinin, 1 µg/mL leupeptin, 2mM sodium orthovanadate) using two steps of mechanical disintegration. The homogenates were centrifuged at 500 g for 5 min at 4°C and the resulting pellet (P1) was considered as nuclear fraction.

METHODS

Supernatant (S1) was centrifuged at 13,000 g for 20 min at 4°C. The resulting second supernatant (S2) was centrifuged at 100,000 g for 1 h at 4°C and supernatant (S3) corresponded to cytosolic fraction. The previously obtained pellet (P2) was washed with Buffer D (250 mM Sucrose) and mitochondria fraction was pelleted centrifuging at 13,000 g for 20 min at 4°C and resuspended in Buffer D.

7.5. LIPID PEROXIDASE FOR OXIDATIVE STRESS PRODUCTION

Lipid peroxidation is indicative of oxidative stress in cells and tissues and levels of malondialdehyde (MDA) are used as a measure of lipid oxidation. Lipid peroxidation levels were measured in primary striatal astrocytes from WT and R6/1 animals using the BIOXYTECH LPO-586™ colorimetric assay (Oxys Research, Cat. #21012). The BIOXYTECH LPO-586™ assay is based on the reaction of a chromogenic reagent, N-methyl-2-phenylindole, with MDA, a peroxide derived from fatty acid oxidation, to yield a stable chromophore with maximal absorbance at 586 nm. Following manufacturer's instructions, samples at concentration of 2 µg/µl were mixed with N-methyl-2-phenylindole and HCl. Mixture was incubated at 45°C for 1 h and absorbance was measured with a spectrophotometer at 586nm. Values were normalized to protein content (µM MDA/µg protein). Each sample was measured in duplicates.

7.6. CITRATE SYNTHASE ACTIVITY

To determine mitochondrial content in primary striatal astrocyte cultures from WT and R6/1 mice, the enzymatic activity of citrate synthase (CS) was measured. CS is an enzyme of the Krebs cycle that catalyses the formation of citrate from oxalacetate and acetyl-CoA. The resulting reduced CoA (CoA-SH) transforms 5,5'-dithiobis-2-nitrobenzoic acid (DTNB) into 2-nitro-5-thiobenzoic acid (TNB). The increase of TNB can be then read at 412 nm as the citrate synthase activity.

Reaction mix was prepared with 100 µM DTNB, 300 µM acetyl-CoA, 0.1% Triton X-100, and 100 mM Tris HCl pH 8.1. Cell samples were added to the mix in a final concentration of 4µg/µl, incubated at 37°C for 5 min, and basal absorbance was measured at 412 nm for 4 minutes. Then, 500 µM oxalacetate was added to initiate the reaction and absorbance was read again for 4 minutes. Absorbance was measured with a HITACHI U2900 spectrophotometer and the software UV-Solutions v2.2. Variations in

absorbances were calculated as total activity minus basal activity. Values were expressed as nanomoles of consumed substrate or generated product per minute and milligram of protein (nmol/minute·mg protein). All reactions were performed in parallel with internal quality controls and following national standardized methods (González-Casacuberta et al., 2019; Medja et al., 2009).

7.7. QUANTITATIVE REVERSE TRANSCRIPTION PCR (RT-qPCR)

Total RNA was extracted from primary neuronal striatal cultures from E18 WT and R6/1 embryos using the RNeasy Lipid Tissue Mini Kit (QIAGEN, Cat. #74804). Concentration of RNA was measured with Nanodrop 1000 spectrophotometer (Thermo Fisher). 500 ng of purified RNA was reverse transcribed using the High Capacity cDNA Reverse Transcription Kit (Applied Biosystems, Cat. #436814). The cDNA synthesis was performed at 25°C for 10 min, at 37°C for 120 min and a final step at 85°C for 5 min in a final volume of 20 µl as instructed by manufacturer. Then, cDNA was analysed by quantitative RT-PCR using PrimeTime qPCR Assays (Integrated DNA Technologies) (Table 11). Quantitative PCR was performed in a final volume of 12 µl on 96-well plates with Premix Ex Taq (Takara Biotechnology, Cat. #RR037A). Reactions included Segment 1: 1 cycle of 30 seconds at 95°C and Segment 2: 40 cycles of 5 seconds at 95°C and 20 seconds at 60°C. All RT-PCR assays were run in duplicate. To provide negative control and exclude contamination by genomic DNA, the PrimeScript RT enzyme was omitted in the cDNA synthesis step and samples were subjected to the PCR reaction in the same manner with each probe. RT-PCR data were quantified using the comparative quantitation analysis program of 64 MxPro™ quantitative PCR software version 3.0 (Stratagene) and 18S and actinβ gene expression were used as housekeeping gene.

Table 11. Probes used for gene expression assays. For each gene, reference assay and source are given.

GENE	ASSAY	SOURCE
18S	Hs.PT.39a.22214856.g	Integrated DNA Technologies
Actinβ	Mm.PT.39a.22214843.g	Integrated DNA Technologies
Cdk5r	Mm.PT.58.30657823.g	Integrated DNA Technologies
Dnm1l	Mm.PT.56a.16160059	Integrated DNA Technologies

METHODS

7.8. IMMUNOPRECIPITATION

Mouse hippocampal tissue was homogenized on ice-cold immunoprecipitation (IP) buffer (50mM Tris, 150mM NaCl, 2mM EDTA, 1% Triton, pH 7.4, 1mM PMSF, 10 µg/mL aprotinin, 1 µg/mL leupeptin). 400 µg protein were incubated overnight at 4°C under rotary agitation with 2 µg of Pyk2 antibody (Sigma-Aldrich, #P3902) or rabbit IgG (Jackson ImmunoResearch, Cat. #309-005-082) as a negative control. Sepharose beads (GE Healthcare, Cat. #17-0618-01) were incubated with the immune complex at 4°C overnight under rotary agitation. Beads were washed once on IP buffer, IP/PBS (1:1) and PBS and collected by centrifugation at 3,000 rpm 5 min. Immunocomplexes were boiled 10 min at 100°C and resolved on SDS-PAGE or resuspended in PBS for mass spectrometry analysis.

7.9. MASS SPECTROMETRY

Immunoprecipitated protein extracts from hippocampus of Pyk2^{+/+} and Pyk2^{-/-} were diluted in Laemmli sample buffer and loaded into a 0.75 mm thick polyacrylamide gel with a 4% stacking gel casted over a 12.5% resolving gel. The run was stopped as soon as the front entered 3 mm into the resolving gel so that the whole proteome became concentrated in the stacking/resolving gel interface. Bands were stained with Coomassie Brilliant Blue, excised from the gel and protein enzymatic cleavage was carried out with trypsin (Promega; 1:20, w/w) at 37 °C for 16 h as previously described (Shevchenko et al., 2007). Purification and concentration of peptides was performed using C18 Zip Tip Solid Phase Extraction (Millipore). Peptide mixtures were separated by reverse phase chromatography using an UltiMate 3000 UHPLC System (Thermo Scientific) fitted with an Aurora packed emitter column (Ionopticks, 25 cm x 75 µm ID, 1.6 µm C18). Samples were first loaded for desalting and concentration into an Acclaim PepMap column (ThermoFisher, 0.5 cm x 300 µm ID, 5 µm C18) packed with the same chemistry as the separating column. Mobile phases were 100% water 0.1% formic acid (FA) (buffer A) and 100% Acetonitrile 0.1% FA (buffer B). Column gradient was developed in a 120 min two step gradient from 5% B to 20% B in 90 min and 20%B to 32% B in 30 min. Column was equilibrated in 95% B for 10 min and 5% B for 20 min. During all process, precolumn was in line with column and flow maintained all along the gradient at 300 nl/min. The column temperature was maintained at 40 °C using an integrated column oven (PRSO-V2, Sonation, Biberach, Germany) and interfaced online with the Orbitrap Exploris 480 MS. Spray voltage were set to 2 kV, funnel RF level at 40, and heated capillary temperature at 300 °C. For DDA experiments full MS resolutions were set to 1200,000

at m/z 200 and full MS AGC target was set to Standard with an IT mode Auto. Mass range was set to 375–1500. AGC target value for fragment spectra was set to Standard with a resolution of 15,000 and 3 seconds for cycle time. Intensity threshold was kept at 8E3. Isolation width was set at 1.4 m/z. Normalized collision energy was set at 30 %. All data were acquired in centroid mode using positive polarity and peptide match was set to off, and isotope exclusion was on.

Raw files were processed with MaxQuant (Jürgen Cox & Mann, 2008) v1.6.17.0 using the integrated Andromeda Search engine (Jürgen Cox et al., 2011) . All data were searched against a target/decoy version of the mouse Uniprot Reference Proteome without isoforms (55,366 entries) with March 2021 release. First search peptide tolerance was set to 20 ppm, main search peptide tolerance was set to 4.5 ppm. Fragment mass tolerance was set to 20 ppm. Trypsin was specified as enzyme, cleaving after all lysine and arginine residues and allowing up to two missed cleavages. Carbamidomethylation of cysteine was specified as fixed modification and peptide N-terminal acetylation, oxidation of methionine, deamidation of asparagine and glutamine and pyro-glutamate formation from glutamine and glutamate were considered variable modifications with a total of 2 variable modifications per peptide. “Maximum peptide mass” were set to 7500 Da, the “modified peptide minimum score” and “unmodified peptide minimum score” were set to 25 and everything else was set to the default values, including the false discovery rate limit of 1% on both the peptide and protein levels. The Perseus software (version 1.6.14.0) (Tyanova et al., 2016) (Tyanova, S et al. Nat. Methods 2016, 13, 731–740) was used for statistical analysis and data visualization.

8. STATISTICAL ANALYSIS

All results were analysed using GraphPad Prism software version 8.0. Data are represented as mean \pm standard error of the means (SEM). Outliers were identified with the ROUT method and normality of data was analysed following the Shapiro-Wilk test. Statistical analysis was performed using Student’s t-test or Mann-Whitney test for comparison between two groups. For multi-component variables comparison, Kruskal-Wallis, One-way ANOVA or Two-way ANOVA were applied followed by the *post hoc* Dunn’s test or Tukey’s test. A 95 % confidence interval was used and a *p* value <0.05 was considered significant. Number of samples (*n*) and *p* values are specified in each figure legend.

Schematic illustrations were created with BioRender.com.

RESULTS

1. ROLE OF MITOCHONDRIAL DYNAMICS AND MAMs IN HD STRIATAL NEURONAL VULNERABILITY

HD is characterized by the preferential degeneration of the striatum. Compelling evidence suggest that mitochondrial dysfunction could be underlying the striatal vulnerability in HD since this brain area displays a high sensitivity to alterations in mitochondrial dynamics and in Ca^{2+} homeostasis. Indeed, striatal HD mitochondrion seems to be more sensitive to Ca^{2+} loads, presents less membrane potential and are more likely to undergo fragmentation. The aim of this first study was to explore whether previously reported disruption of mitochondrial dynamics in HD striatal neurons could compromise the formation of ER-mitochondrial contact sites, hampering Ca^{2+} transfer between these two subcellular compartments. To test this hypothesis, we evaluated ER-mitochondria contact sites (MAMs), MAMs protein levels and Ca^{2+} transport between organelles. Moreover, we investigated whether these alterations could be a result of an excessive Drp1 activity.

1.1. Mitochondrial morphology in R6/1 neuronal culture

1.1.1. R6/1 striatal neurons present mitochondrial fragmentation

To assess mitochondrial morphology in HD neurons, WT and R6/1 striatal neuronal cultures were transfected with pDsRed2-mito and stained with MAP2 to label mitochondria and neurites respectively (Figure 19A). Morphometrical analysis by confocal microscopy showed an increase in the number of mitochondria per neurite (Figure 19B), together with a lower Aspect Ratio (Figure 19C), and lower Form Factor (Figure 19D). Reduced values of Aspect Ratio indicated a more spherical shape whereas lower Form Factor associated with less mitochondrial network branching and complexity. Altogether, these results suggest an excessive mitochondrial fragmentation in R6/1 striatal neurons.

RESULTS

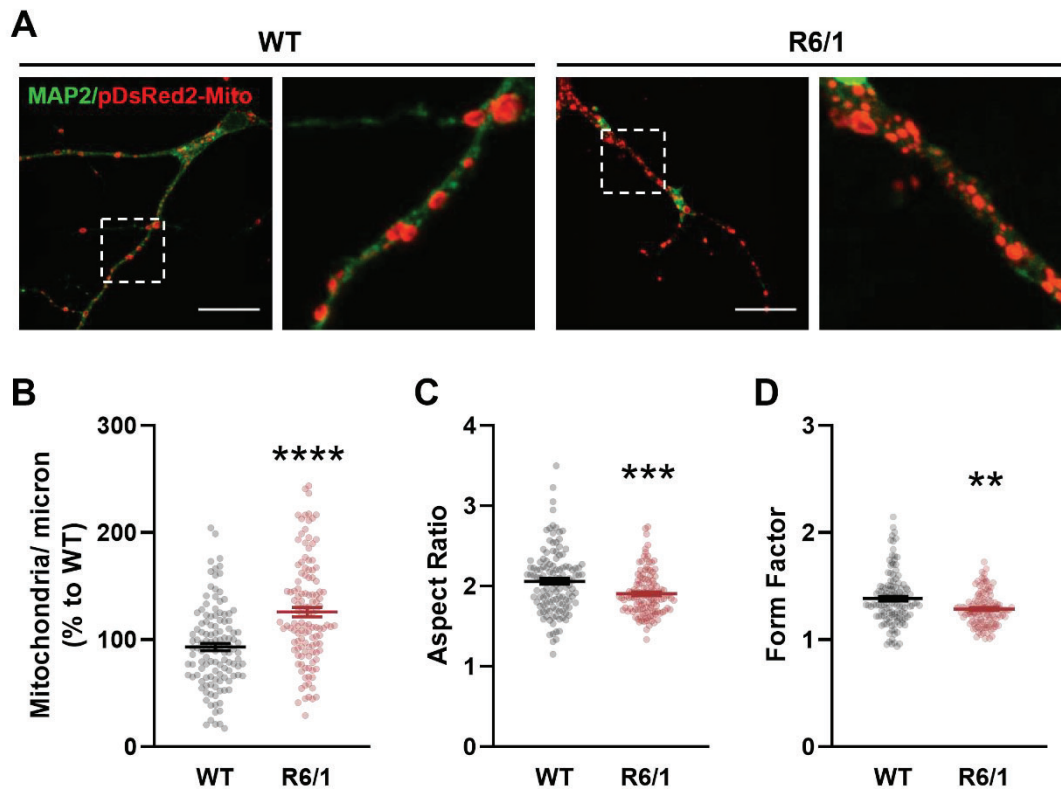


Figure 19. Increased mitochondrial fragmentation in R6/1 striatal primary neurons. (A) Confocal images of striatal primary neurons from WT and R6/1 at DIV14 in basal conditions transfected with pDsRed2-mito in red and immunolabeled with MAP2 in green. Panels on the right show magnification of the boxed areas in white. Scale bar, 20 μ m. R6/1 neurons presented increased (B) number of mitochondria per micron of neurite as a percentage (Mann-Whitney test, A, B=12042, 18339, U=4539; $p < 0.0001$), lower (C) Aspect Ratio (Mann-Whitney test, A, B=18163, 13968, U=5967; $p = 0.0005$) and lower (D) Form Factor (Mann-Whitney test, A, B=17886, 13489, U=5863; $p = 0.0007$). Data represent mean \pm SEM of 15-17 neurons from 8 different embryos per genotype ($n = 122-124$). Each point represents the mean of all mitochondria in each neuron. ** $p < 0.01$, *** $p < 0.001$, **** $p < 0.0001$ vs WT.

1.1.2. R6/1 cortical and hippocampal neurons do not show alterations in mitochondrial morphology

We wondered if the aberrant mitochondrial fragmentation detected in R6/1 striatal neurons was also present in other brain regions affected in HD. To this aim, we evaluated mitochondrial dynamics in neurons of cortical (Figure 20A-D) and hippocampal (Figure 20E-H) primary cultures. Neurons from WT and R6/1 mice were immunostained with TOM20 in green and MAP2 in red (Figure 20A and Figure 20E). No differences between genotypes were observed either in the number of mitochondria (Figure 20B and Figure 20F) or morphological parameters as Aspect Ratio (Figure 20C and Figure 20G) and Form Factor (Figure 20D and Figure 20H). Hence, alterations in mitochondrial dynamics in HD seem to be specific of the striatum.

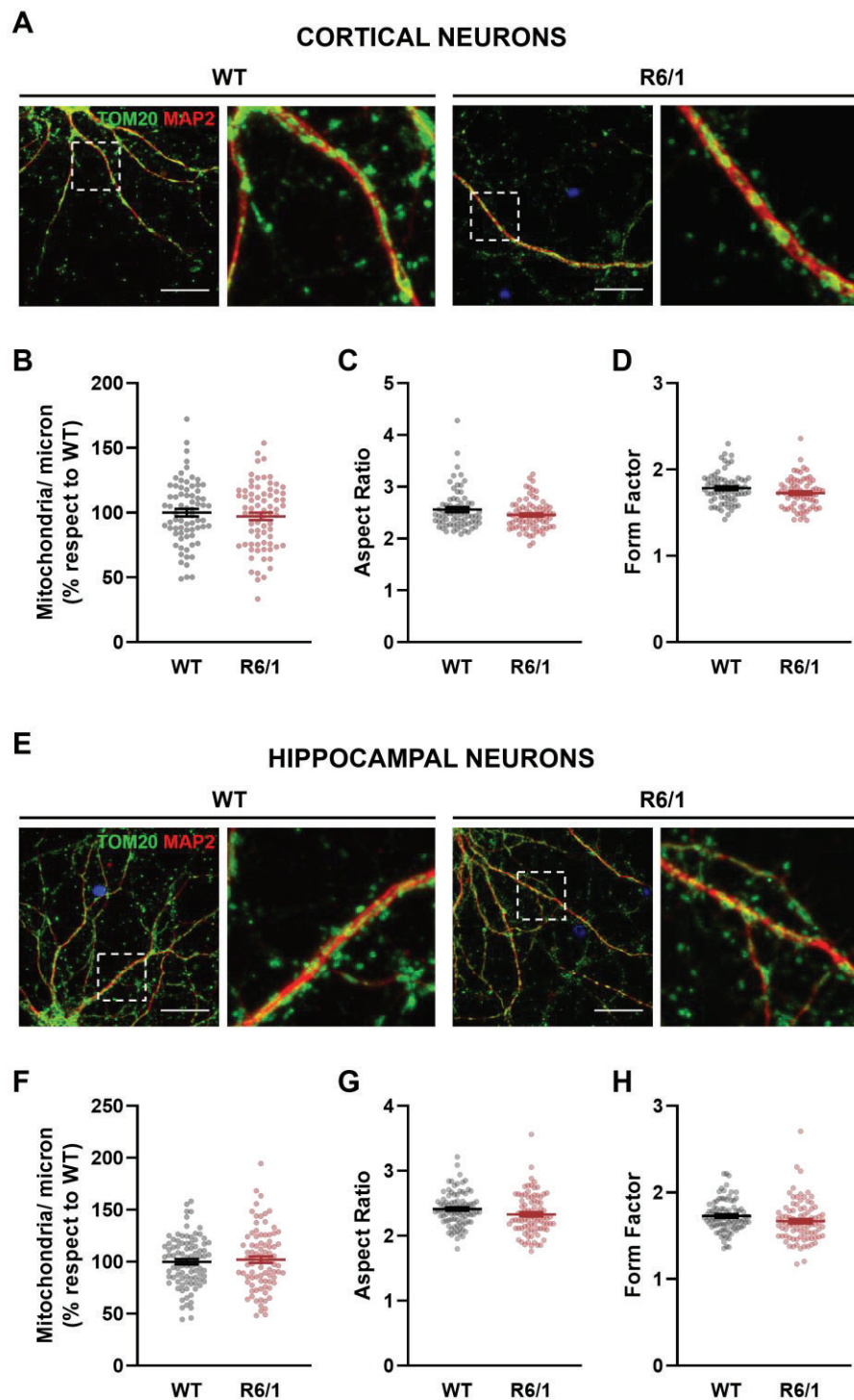


Figure 20. R6/1 cortical and hippocampal primary neurons do not present alterations in mitochondrial morphology. Confocal images of cortical (**A**) and hippocampal (**E**) primary neurons from WT and R6/1 at DIV14 in basal conditions. Neurons were immunolabeled with TOM20 in green, MAP2 in red and nuclei in blue. Panels on the right show magnification of the boxed areas in white. Scale bar, 20 μ m. No differences were found in any of the morphological parameters evaluated. (**B**, **F**) Number of mitochondria (**B**: Student t-test, $t=0.6872$, $df=142$, $p=0.4931$; **F**: Student t-test, $t=0.4914$, $df=173$, $p=0.6237$). (**C**, **G**) Aspect Ratio (**C**: Student t-test, $t=1.851$, $df=143$, $p=0.0663$; **G**: Student t-test, $t=1.891$, $df=173$; $p=0.0602$). (**D**, **H**) Form Factor (**D**: Student t-test, $t=1.864$, $df=136$, $p=0.0645$; **H**: Student t-test, $t=1.908$, $df=174$; $p=0.0580$). Data represent mean \pm SEM of 5-6 different embryos with 12-15 neurons per genotype (cortical neurons $n=70-73$; hippocampal neurons $n=85-90$). Each point represents the mean of all mitochondria in each neuron.

RESULTS

1.2. Loss of ER-mitochondria contact sites in R6/1 striatal neurons

Given the increase in mitochondrial fission observed in R6/1 striatal neurons, we wondered whether disrupted mitochondrial network could hamper ER-mitochondria association. To this aim, we transfected WT and R6/1 primary striatal neurons with two plasmids, GFP-Sec61 and pDsRed2-Mito to label ER in green and mitochondria in red respectively (Figure 21A). Yellow signal indicated the regions where both organelles were in close contact. Colocalisation between plasmids was analysed by confocal microscopy and quantified with Mander's coefficient as the proportion of ER that overlaps with mitochondria. Comparing levels of colocalisation, R6/1 neurons displayed a reduction in ER-mitochondria contact sites (Figure 21B).

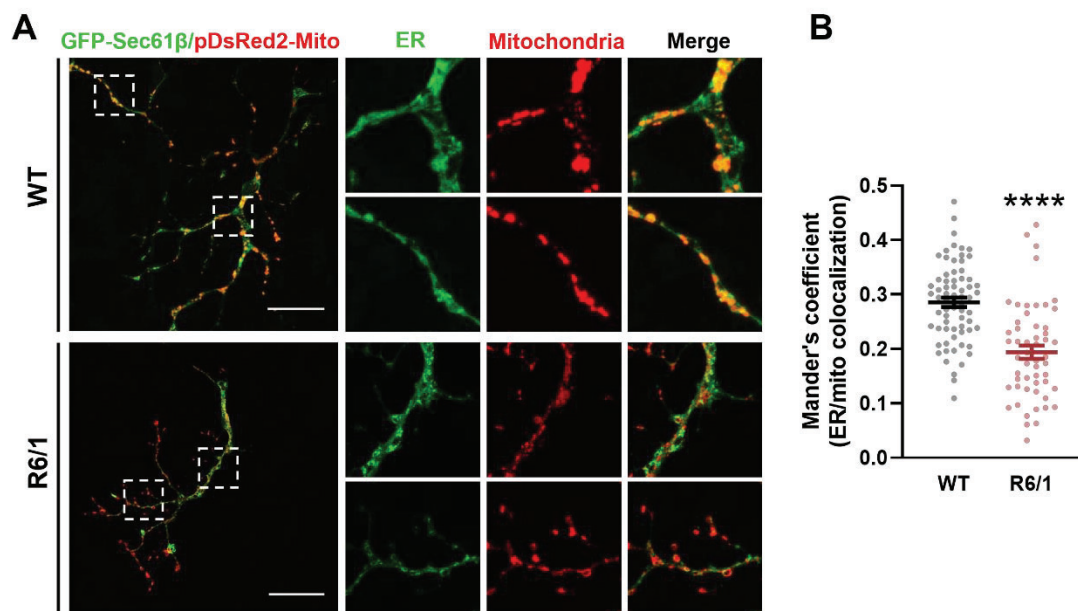


Figure 21. ER-mitochondria colocalisation is decreased in R6/1 striatal neurons. (A) Confocal images of primary striatal cultures from WT and R6/1 embryos transfected with GFP-Sec61- β in green and pDsRed2-mito in red labelling ER and mitochondria respectively. Single and merged channels magnifications from the boxed area in white are shown in the right panels. Scale bar, 50 μ m. (B) Quantification of plasmids colocalisation by Mander's coefficient (Student t-test, $t=6.254$, $df=120$; $p<0.0001$). Data represent mean \pm SEM of 5-12 neurons from 8 different embryos per genotype ($n=68-54$). Each point represents a neuron. **** $p<0.0001$ vs WT.

We then verified these results with an *in situ* technic with higher sensitivity. Proximity ligation assay (PLA) was performed in primary striatal neurons from WT and R6/1 mice. IP3R3 and VDAC1 were targeted as markers for ER and mitochondria respectively (Figure 22A) since these are enriched proteins MAMs (Hedskog et al., 2013). Red fluorescence signal was generated if both cellular compartments were closer than 40 nm and IP3R3 and VDAC1 could interact, thus, indicating ER-mitochondria contact sites.

Neurite area was immunostained with MAP2 in green and used to normalize number of PLA particles. In line with colocalisation analysis, R6/1 neurons showed lower number of PLA signal (Figure 22B).

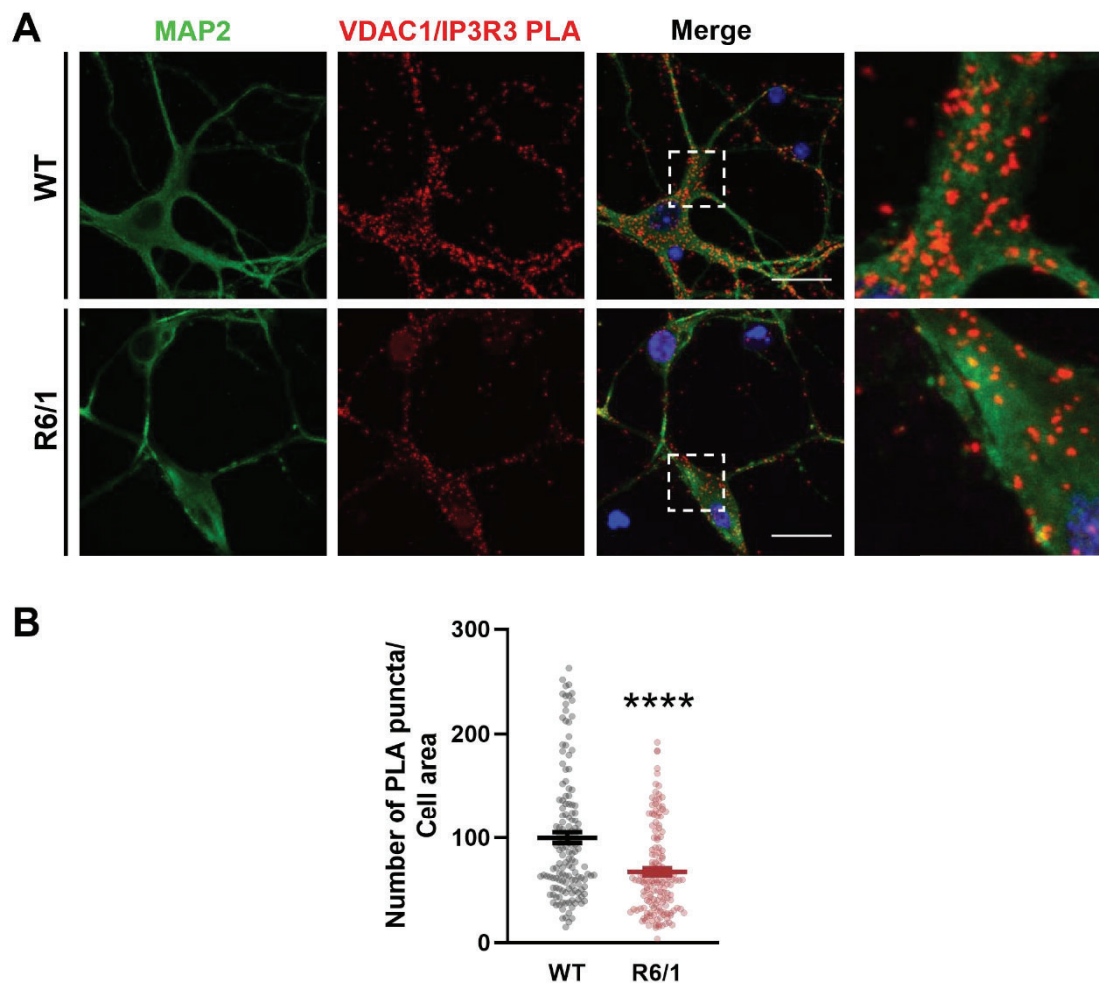


Figure 22. ER-mitochondrial contacts are diminished in R6/1 striatal neurons. (A) Confocal images of VDAC1/IP3R3 interaction by in situ *proximity ligation assay* (PLA) in WT and R6/1 primary striatal neurons. Interaction between the two targeted proteins is shown in red, neurons were immunolabeled with MAP2 in green and nuclei appear in blue. Scale bar, 20 μ m. (B) Quantification of ER-mitochondrial contact sites by PLA (Mann-Whitney test, A, B=24949, 18711, U=7235; $p < 0.0001$). Number of PLA particles is relativized to cell area. Data represent mean \pm SEM of 20 neurons from 8 different embryos per genotype (n=144-151). Each point represents a neuron. **** $p < 0.0001$ vs WT.

Since reduced PLA could be a consequence of a lower expression of the targeted proteins, we assessed the protein levels of IP3R3 and VDAC1 in total lysates from WT and R6/1 striatal neuronal cultures by Western Blot (Figure 23). No differences were found when comparing genotypes in none of the proteins. Hence, the observed diminution of PLA signal was likely due to a loss in the interaction between ER and mitochondria.

RESULTS

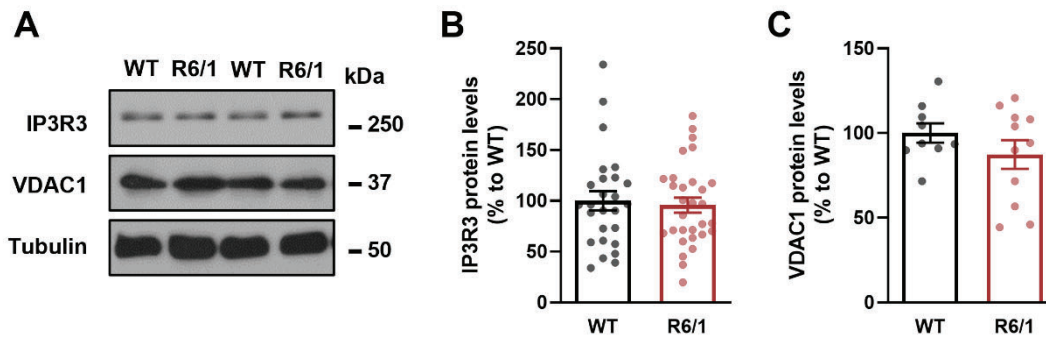


Figure 23. No differences in IP3R3 and VDAC1 protein levels between WT and R6/1 striatal primary neurons. (A) Representative immunoblotting of IP3R3, VDAC1 and tubulin in total lysates of striatal neuronal cultures from WT and R6/1 embryos. (B, C) Densitometry quantification of IP3R3 (Student t-test, $t=0.3718$, $df=54$; $p=0.7115$) and VDAC1 (Student t-test, $t=1.180$, $df=18$; $p=0.2535$). Tubulin was used as loading control. Molecular weight markers positions are indicated in kDa. Data represent mean \pm SEM. In B, $n=26-30$; in C, $n=9-11$.

Altogether, these data suggest that increased mitochondrial fission due to mHtt toxicity is associated with the loss of ER-mitochondria contacts in striatal neurons, leading to alterations of mechanisms regulated by MAMs such as Ca^{2+} handling.

1.3. MAMs proteins are decreased specifically in the striatum of HD mice and HD patients

The structural integrity of MAMs depends on proteins that tether both cellular compartments and are enriched at these areas (Csordás et al., 2006). Therefore, mutation of MAMs proteins can impact on the formation of contact sites (De Brito & Scorrano, 2008). To further understand how loss of ER-mitochondria contacts could be affected in the HD striatum over the course of the disease, we evaluated levels of several MAM-resident proteins involved in Ca^{2+} homeostasis, namely Grp75, IP3R3 and Mfn2. IP3R3 is a Ca^{2+} channel located in the ER that interacts with VDAC1 in the OMM, whereas Grp75 and Mfn2 strengthen the close contact between organelles, thus improving the efficiency of Ca^{2+} transfer.

Levels of Grp75, IP3R3, and Mfn2 proteins were analysed in total lysates of striatum from WT and R6/1 mice at different stages of the disease (8, 12, 20, 30 weeks of age) (Figure 24A). These ages were chosen to evaluate pre-symptomatic (8 weeks), onset of cognitive deficits (12 weeks), motor deficits (20 weeks) and late stages (30 weeks) respectively. Grp75 protein levels showed a decrease in R6/1 mice at 12 and 20 weeks of age while at 30 weeks this reduction was no longer detectable. Regarding IP3R3, R6/1

RESULTS

mice exhibited a diminution of IP3R3 levels that began at 12 weeks and was sustained at 20 and 30 weeks of age. Lastly, Mfn2 levels were only reduced in the R6/1 mice at 20 weeks of age.

Additionally, we tested levels of these MAMs proteins in the striatum of a different HD mouse model, the knock-in HdhQ111 mice with a slower HD progression (Figure 24B). In line with the outcome from R6/1 mice, Grp75 was reduced in the HdhQ111 mice at 9 months of age, with a tendency to decrease at 13 months and no alterations at 18 months of age. Similarly, IP3R3 diminution started at 9 months while maintained at latter disease stages. Finally, Mfn2 levels were exclusively decreased at 9 months of age.

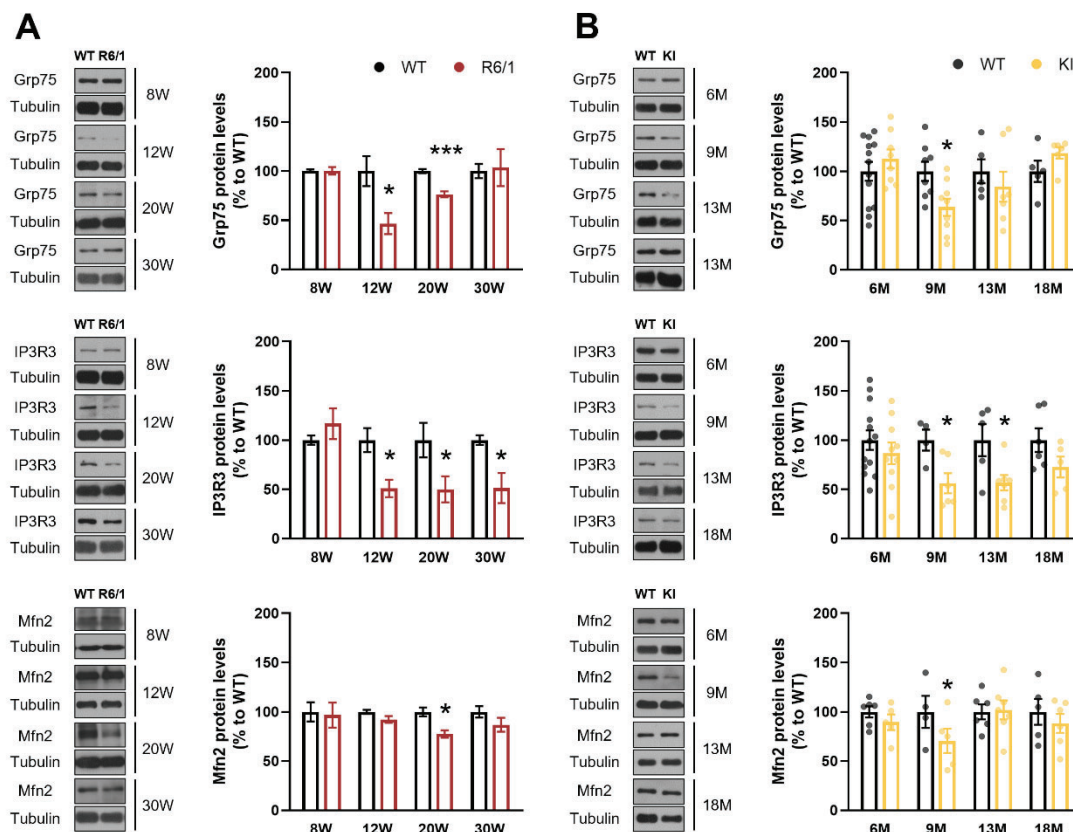


Figure 24. MAMs proteins are decreased in the striatum of HD mouse models R6/1 and HdhQ111. (A) Immunoblotting and densitometry quantification of protein levels of Grp75, IP3R3, and Mfn2 in the striatum of WT (black) and R6/1 (red) mice at different stages of the disease (W, weeks). (B) Immunoblotting and densitometry quantification of protein levels of Grp75, IP3R3, and Mfn2 in the striatum of WT (black) and HdhQ111 (yellow) mice at different stages of the disease (M, months). Tubulin was used as loading control. Relative protein levels are expressed as percentage to WT mice at every age. Data represent mean \pm SEM, $n=5-13$ animals. * $p<0.05$, *** $p<0.001$ vs WT as determined by Student's t-test.

RESULTS

These MAMs proteins were also analysed in *post-mortem* tissue from the putamen of control subjects and HD patients (Figure 25). All analysed proteins Grp75 (Figure 25A), IP3R3 (Figure 25B), and Mfn2 (Figure 25C) were found to be diminished in HD patients compared to control individuals.

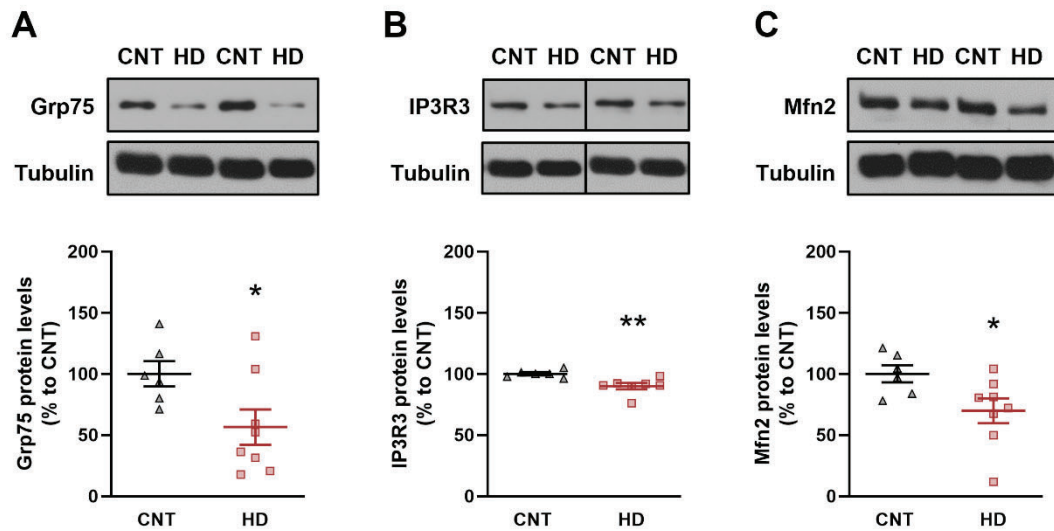


Figure 25. MAMs proteins levels are decreased in *post-mortem* putamen of HD patients. Immunoblotting and the corresponding densitometry quantification of (A) Grp75 (Student t-test, $t=2.294$, $df=12$; $p=0.0407$), (B) IP3R3 (Mann-Whitney test, $A, B=61, 30, U=2$; $p=0.0047$), and (C) Mfn2 (Student t-test, $t=2.293$, $df=12$; $p=0.0407$). Tubulin was used as loading control. Relative protein levels are expressed as percentage to control subjects. Data represent mean \pm SEM, $n=6-8$ subjects. * $p < 0.05$, ** $p < 0.01$ vs CNT.

Our previous *in vitro* findings showed that HD striatal but not cortical nor hippocampal neurons presented mitochondrial morphology alterations (Figure 19 and Figure 20). Thus, we also wondered whether disturbances in MAMs proteins were exclusively striatal or also occurred in other brain regions affected in HD as cortex and hippocampus. To this aim, we first assessed levels of Grp75, IP3R3 and Mfn2 in the cortex of R6/1 (Figure 26A) and HdhQ111 mice (Figure 26B). No major disturbances were found when comparing between genotypes except for an occasional drop in Gr75 levels at 12 weeks of age in the cortex of R6/1.

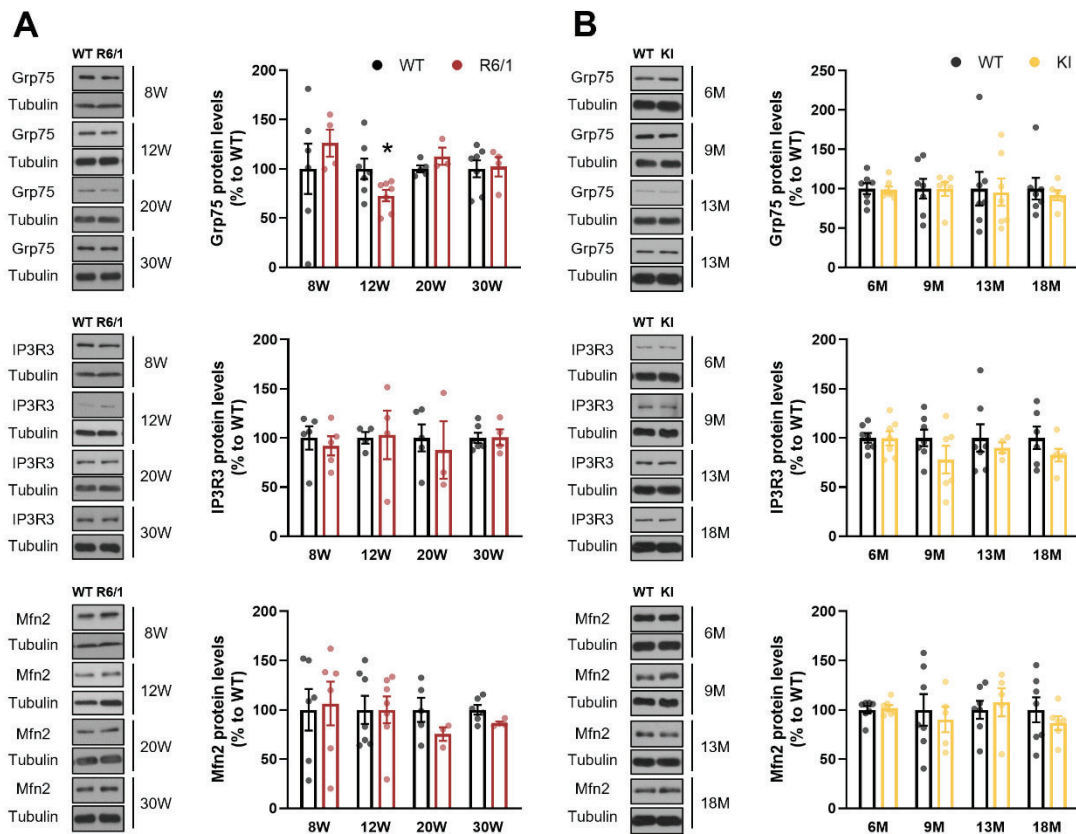


Figure 26. Levels of MAMs proteins Grp75, IP3R3 and Mfn2 are not altered in the cortex of HD mouse models R6/1 and HdhQ111. (A) Immunoblotting and densitometry quantification of protein levels of Grp75, IP3R3, and Mfn2 in the cortex of WT (black) and R6/1 (red) mice at different stages of the disease (W, weeks). (B) Immunoblotting and densitometry quantification of protein levels of Grp75, IP3R3, and Mfn2 in the cortex of WT (black) and HdhQ111 (yellow) mice at different stages of the disease (M, months). Tubulin was used as loading control. Relative protein levels are expressed as percentage to WT mice at every age. Data represent mean \pm SEM, n=4-7 animals. * $p < 0.05$ vs WT as determined by Student's t-test or Mann-Whitney test.

Then, hippocampus of R6/1 (Figure 27A) and HdhQ111 mice (Figure 27B) were analysed. As expected, protein levels of Grp75, IP3R3, and Mfn2 remained unchanged between genotypes throughout the different disease stages.

RESULTS

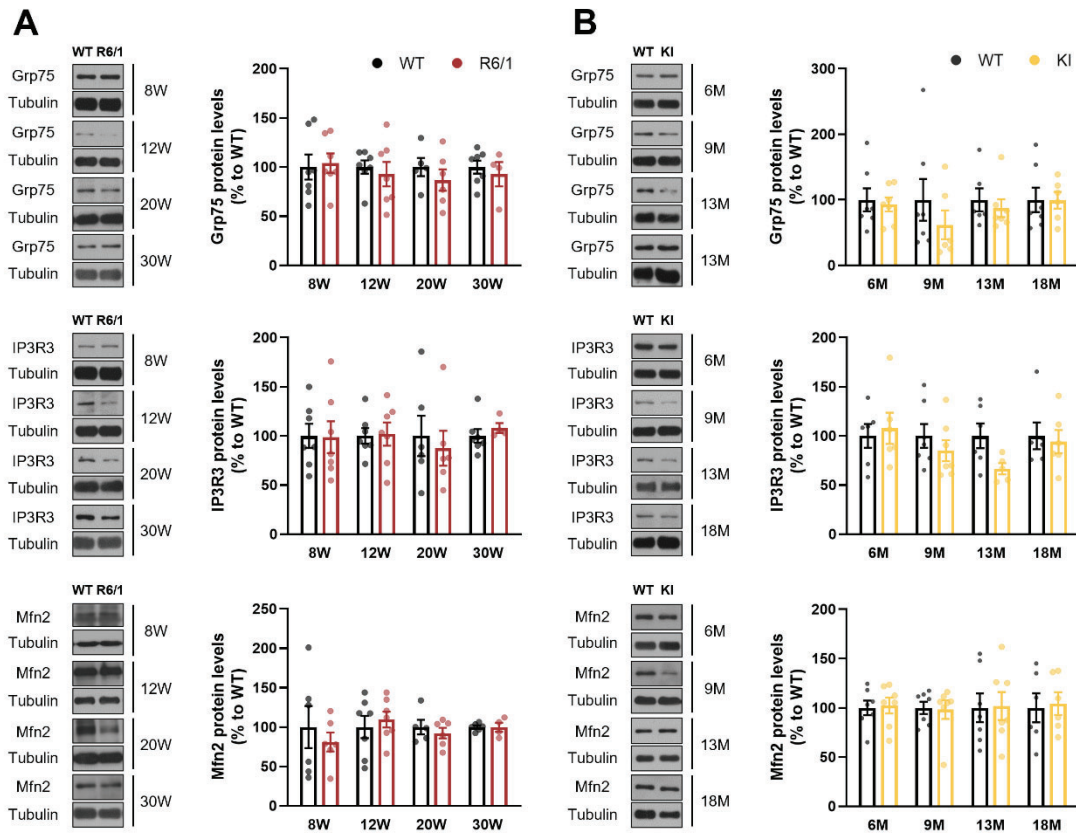


Figure 27. Levels of MAMs proteins Grp75, IP3R3 and Mfn2 are not altered in the hippocampus of HD mouse models R6/1 and HdhQ111. (A) Immunoblotting and densitometry quantification of protein levels of Grp75, IP3R3, and Mfn2 in the hippocampus of WT (black) and R6/1 (red) mice at different stages of the disease (W, weeks). (B) Immunoblotting and densitometry quantification of protein levels of Grp75, IP3R3, and Mfn2 in the hippocampus of WT (black) and HdhQ111 (yellow) mice at different stages of the disease (M, months). Tubulin was used as loading control. Relative protein levels are expressed as percentage to WT mice at every age. Data represent mean \pm SEM, n=4-7 animals.

Finally, *post-mortem* samples of cortex and hippocampus from control subjects and HD patients were analysed by Western Blot. Neither of the proteins Grp75, IP3R3, or Mfn2 were altered in cortex (Figure 28A) nor in hippocampus (Figure 28B).

Taken together, these data strengthen the fact that MAMs alterations in HD arise specifically in the striatum and not in other brain regions affected by the disease as the cortex and the hippocampus.

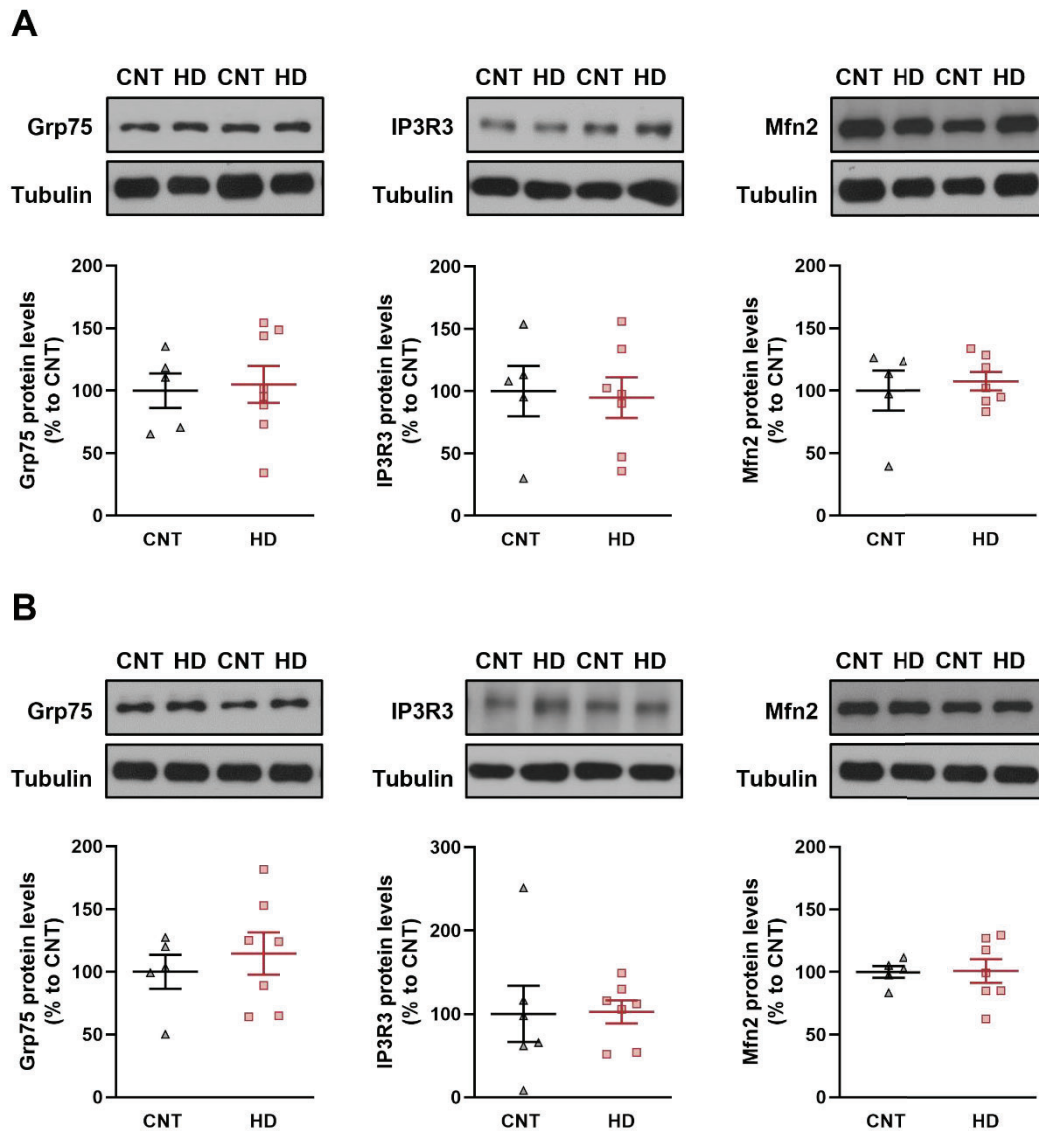


Figure 28. MAMs protein levels of Grp75, IP3R3 and Mfn2 do not change in cortical and hippocampal brain samples of HD patients. (A) Immunoblotting and densitometry quantification of protein levels of Grp75 (Student t-test, $t=0.2253$, $df=11$; $p=0.8259$), IP3R3 (Student t-test, $t=0.2038$, $df=10$; $p=0.8426$), and Mfn2 (Student t-test, $t=0.4635$, $df=10$; $p=0.6529$) in the cortex of control (CNT) and HD subjects. (B) Immunoblotting and densitometry quantification of protein levels of Grp75 (Student t-test, $t=0.6276$, $df=10$; $p=0.5443$), IP3R3 (Student t-test, $t=0.07175$, $df=11$; $p=0.9441$), and Mfn2 (Student t-test, $t=0.09735$, $df=10$; $p=0.9244$) in the hippocampus of control and HD subjects. Tubulin was used as loading control. Relative protein levels are expressed as percentage to control subjects. Data represent mean \pm SEM, $n=5-8$ subjects.

RESULTS

1.4. ER-mitochondrial calcium transfer is altered in R6/1 striatal neurons

Considering that R6/1 striatal neurons presented a loss in ER-mitochondria contact sites together with a reduction in MAM-resident proteins involved in Ca^{2+} , we hypothesised that calcium transfer between both organelles could be disrupted. To better understand ER-mitochondrial crosstalk from a functional perspective, we aimed to track calcium and mitochondrial membrane potential ($\Delta\psi_m$) in live cells from striatal neuronal cultures of WT and R6/1 mice. Neurons were stained with Fluo4 and TMRM as indicators of intracellular calcium (Ca_i^{2+}) and $\Delta\psi_m$ respectively (Figure 29A). In basal conditions, no differences in neither of the dyes were detected when comparing WT and R6/1 cultures (Figure 29B). Thapsigargin (TG), an inhibitor of SERCA activity, was added to induce release of Ca^{2+} from the ER to the cytoplasm. As expected, in WT neurons we detected an increase of Fluo4 as well as a drop in TMRM following thapsigargin treatment. Conversely, R6/1 neurons revealed higher Ca_i^{2+} and lower $\Delta\psi_m$ when compared to WT neurons, suggesting a possible attenuation in the mitochondrial capacity of calcium uptake (Figure 29B). Finally, FCCP, an uncoupler of OXPHOS, was added to the culture to induce maximal depolarization and to force release of calcium accumulated in mitochondria. WT neurons responded to this stimulus with a boost in Fluo4 associated with a depolarization of $\Delta\psi_m$. However, R6/1 neurons showed lower levels of Ca_i^{2+} together with lower $\Delta\psi_m$ compared to WT neurons (Figure 29B).

Overall, these findings demonstrate that the presence of mHtt induces mishandling in calcium homeostasis along with weakened capacity of calcium retention in the mitochondria in R6/1 neurons.

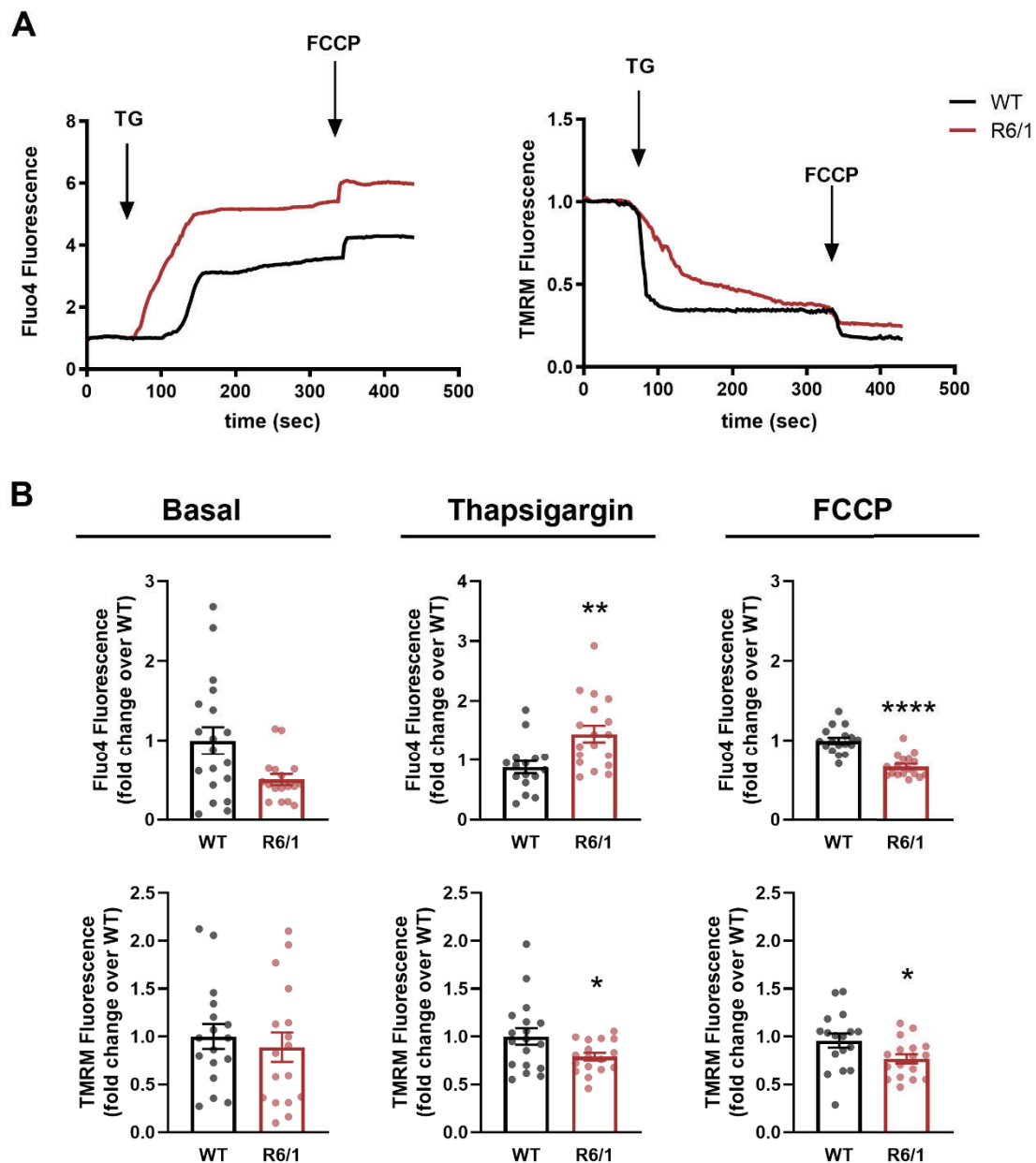


Figure 29. Alterations in ER-mitochondrial calcium transfer in striatal neurons of R6/1 mice. Primary neurons from WT and R6/1 mice were labelled with 5 μ M Fluo4 and 20 nM TMRM to trace intracellular calcium and mitochondrial membrane potential respectively. Cells were stimulated with thapsigargin (TG, 0.5 μ M) at 40 sec and with FCCP (2 μ M) at 360 sec. (A) Representative fluorescence traces of Fluo4 (left panel) and TMRM (right panel) from individual WT and R6/1 neurons, in black and red respectively, through the experiment. Black arrows indicate the injection point of the treatment. (B) Quantification of fluorescence fold change of Fluo4 (upper panel) and TMRM (lower panel) before (basal) and after TG or FCCP treatment. Values are normalized to WT neurons in each condition. Data represent mean \pm SEM. n=16-19 cultures per genotype from 6 different embryos. * p<0.05, ** p<0.01, **** p<0.0001 vs WT as determined by Student's t-test.

RESULTS

1.5. Increased Drp1 activity mediates excessive mitochondrial fragmentation in R6/1 striatal neurons

Drp1 is a GTPase that represents the principal component of the mitochondrial fission machinery. It has been described that mHtt can bind Drp1, enhancing its GTPase activity (Song et al., 2011). Moreover, previous results from our group and others have demonstrated that HD models show increased Drp1 activity (Cherubini et al., 2015; Song et al., 2011). We hypothesised that the enhanced Drp1 activity could underlie the exacerbated mitochondrial fission in HD that leads to an aberrant interaction with the ER.

1.5.1. Levels of Drp1 RNA and protein in R6/1 striatal neuronal cultures

To analyse whether expression and levels of Drp1 were altered in our HD *in vitro* model, RT-PCR and Western blot analysis were performed in cultured striatal neurons from WT and R6/1 mice. According to Drp1 dysregulation in HD, mRNA levels of *Dnm1l*, the gene encoding for Drp1, was upregulated in R6/1 striatal neurons (Figure 30A). However, when protein levels were analysed, similar levels of the monomeric Drp1 forms were found between genotypes. Since Drp1 oligomerization has been associated with Drp1 activation (Cho et al., 2014; X. Guo et al., 2013; P. P. Zhu et al., 2004), Drp1 tetrameric forms were also analysed. A trend to increase was observed in R6/1 cultures compared to WT cultures (Figure 30B).

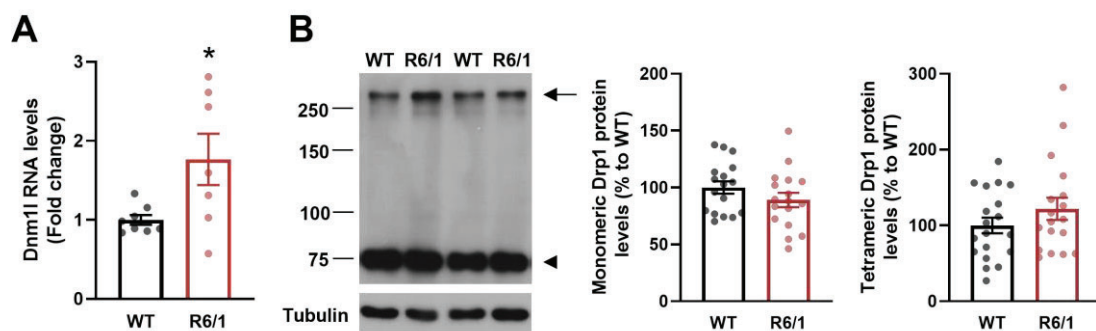


Figure 30. Increased Dnm1l RNA and Drp1 oligomeric protein levels in R6/1 striatal primary neurons. (A) mRNA levels of *Dnm1l*, the encoding gene for Drp1, were measured by quantitative RT-qPCR in striatal cultures from WT and R6/1 embryos. *Dnm1l* mRNA levels were normalized to 18S (Student t-test, $t=2.473$, $df=13$; $p=0.0280$). (B) Immunoblotting and densitometry quantification of monomeric (Student t-test, $t=1.297$, $df=32$; $p=0.2038$) and tetrameric (Mann-Whitney test, $A, B=330, 373, U=140$; $p=0.3583$) forms of Drp1 protein in total lysates obtained from WT and R6/1 striatal cultures. Tubulin was used as loading control. Arrow and arrowhead indicate oligomeric and monomeric Drp1 forms respectively. Molecular weight markers positions are indicated in kDa. Data represent mean \pm SEM. In A, $n=7-8$ mouse embryos; in B, $n=17-19$ mouse embryos. * $p<0.05$ vs WT.

1.5.2. Drp1 inhibition restores mitochondrial fragmentation and ER-mitochondrial contacts in R6/1 striatal neurons

Next, we wanted to investigate whether enhanced Drp1 activity was involved in the exacerbated mitochondrial fragmentation that we observed in HD neurons. With this aim, we treated R6/1 primary striatal neurons with 25 μ M Mdivi-1 for 1 h. Mdivi-1 (*mitochondrial division inhibitor*) is a well-established pharmacological inhibitor of Drp1, that impairs its self-assembly and hence, mitigates mitochondrial fission (Cassidy-Stone et al., 2008). Striatal neurons were first transfected with pDsRed2-mito in red, then treated with vehicle (DMSO) or Mdivi-1 and finally immunolabeled with MAP2 in green (Figure 31A). Mitochondrial network morphology was evaluated by confocal microscopy. As expected, when comparing WT and R6/1 treated with vehicle, R6/1 neurons replicated the mitochondrial morphology previously reported in section 1.1 with a higher number of mitochondria along with lower Aspect Ratio and Form Factor values. This excessive mitochondrial fragmentation in R6/1 cultures was restored after Mdivi-1 treatment, showing comparable values of number of mitochondria, length, and complexity to WT vehicle neurons (Figure 31B). Moreover, we observed that the donut-shaped mitochondria present in R6/1 vehicle disappeared with Mdivi-1 treatment (Figure 31A). This ring form in mitochondria has been associated with higher oxidative stress production (Ahmad et al., 2013). Overall, these findings point out that abnormalities in mitochondrial network morphology in R6/1 neurons are dependent on Drp1 activity.

RESULTS

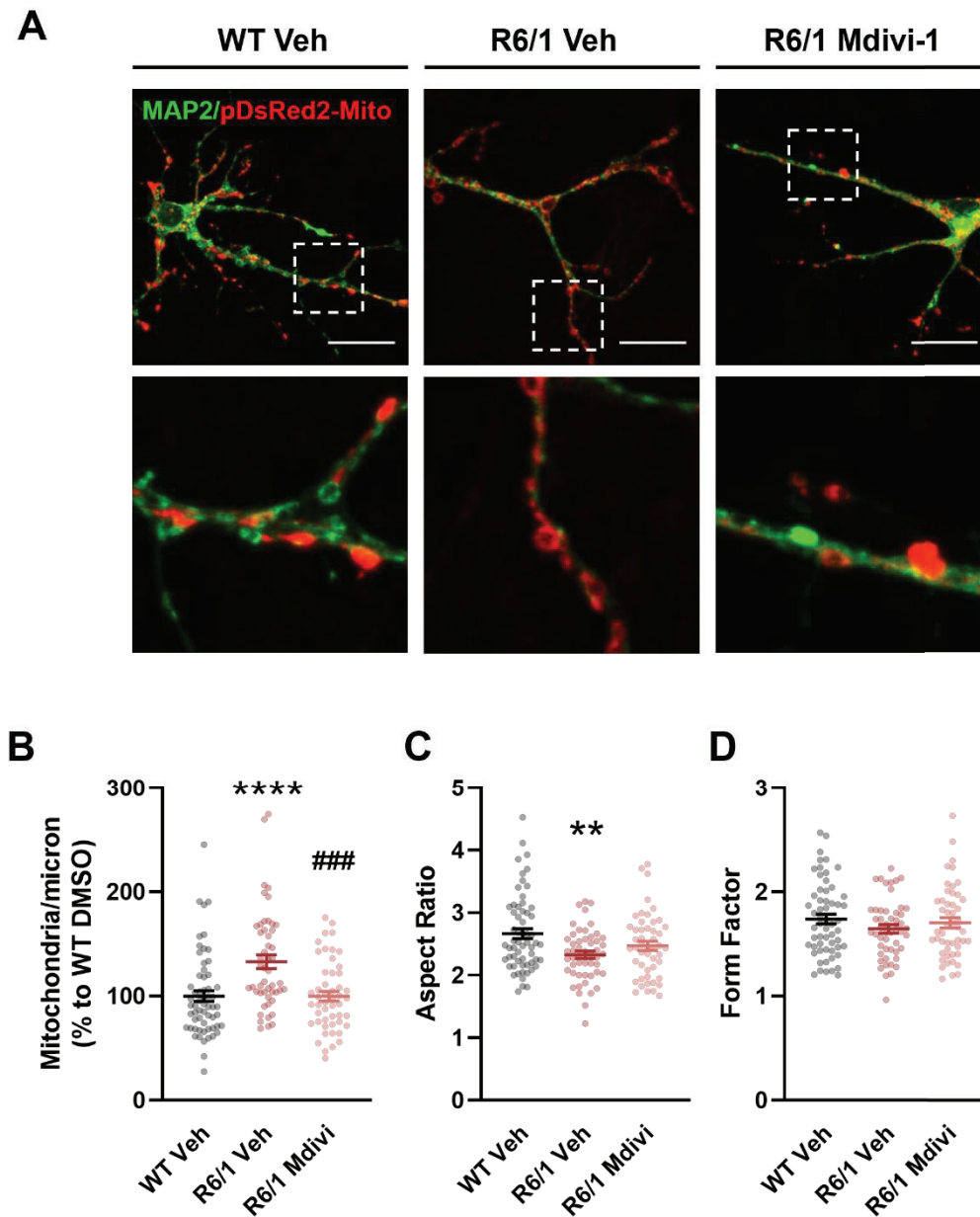


Figure 31. Excessive mitochondrial fragmentation in R6/1 striatal neurons is restored after Drp1 inhibition. (A) Confocal images of WT and R6/1 striatal primary neurons at DIV14 treated with vehicle (DMSO) or 25 μ M Mdivi-1. Neurons were transfected with pDsRed2-mito in red and immunolabeled with MAP2 in green. The white boxed areas are magnified at the lower panels. Scale bar, 20 μ m. Mdivi-1 treatment in R6/1 neurons restored mitochondrial morphological parameters (B) number of mitochondria per micron of neurite as percentage (one-way ANOVA, $F_{(2, 156)}=2.488$; $p<0.0001$), (C) Aspect Ratio (one-way ANOVA, $F_{(2, 156)}=5.753$; $p=0.0039$), and (D) Form Factor (one-way ANOVA, $F_{(2, 154)}=1.092$; $p=0.3380$). Data represent mean \pm SEM of 9-11 neurons 5-6 different embryos per genotype ($n=50-60$). Each point represents the mean of all mitochondria in each neuron. ** $p<0.01$, **** $p<0.0001$ vs WT Veh; ### $p<0.001$ vs R6/1 Veh.

1.6. Inhibition of Drp1 prevents alterations in MAMs and mitochondrial function

Given the effect of Drp1 inhibition on mitochondria morphology, we next hypothesised that increased Drp1-mediated mitochondrial fragmentation could be underlying the loss of ER-mitochondria contacts in R6/1 striatal neurons. To this purpose, primary striatal neurons were transfected with both GFP-Sec61 and pDsRed2-Mito plasmids to target ER in green and mitochondria in red respectively (Figure 32A) and overlapping of fluorescence was analysed by confocal microscopy. Quantification of colocalisation by Mander's coefficient revealed that Drp1 inhibition with Mdivi-1 restored ER-mitochondria juxtaposition in R6/1 neurons (Figure 32B). These results prove that increased Drp1 activity in R6/1 striatal neurons induces aberrant mitochondrial fragmentation that triggers the loss of ER-mitochondria contacts.

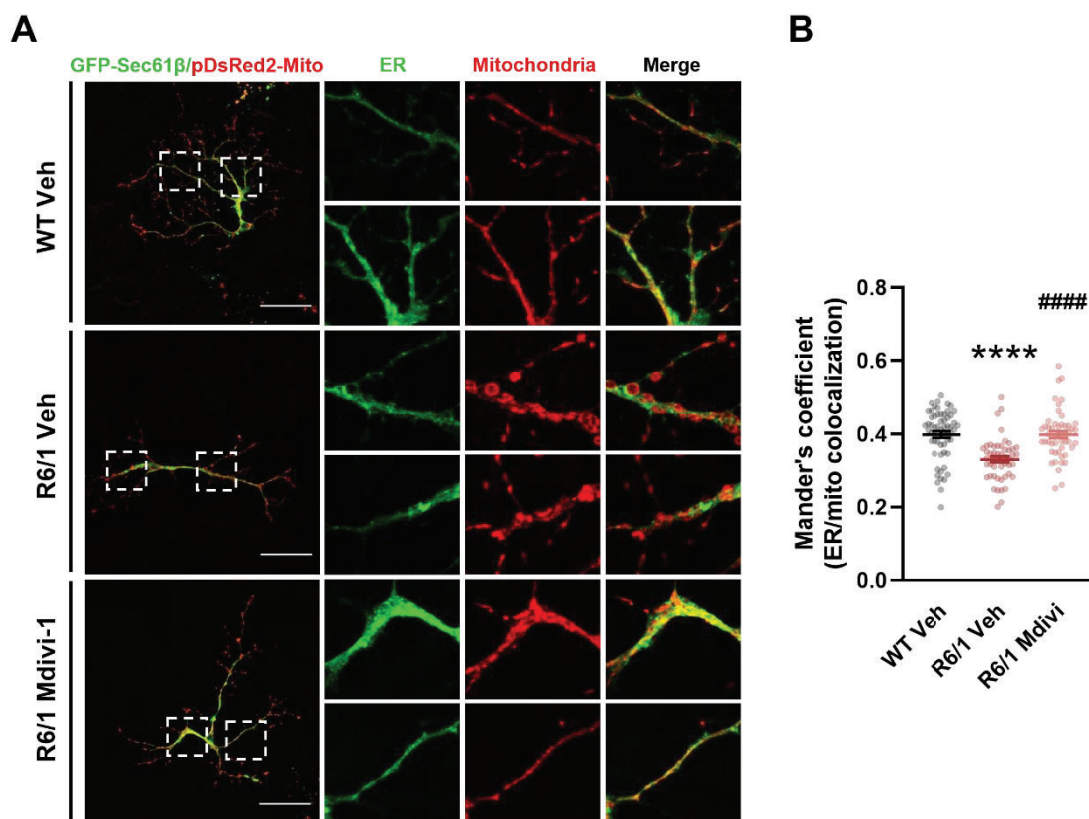


Figure 32. Drp1 inhibition recovers loss of ER-mitochondrial contact sites in R6/1 striatal neurons. (A) Confocal images of primary striatal cultures from WT and R6/1 embryos at DIV14 treated with vehicle (DMSO) or 25 μ M Mdivi-1. Neurons were transfected with GFP-Sec61- β in green and pDsRed2-mito in red to label ER and mitochondria respectively. Single and merged channels magnifications from the boxed area in white are shown in the right panels. Scale bar, 50 μ m. (B) Quantification of plasmids colocalisation by Mander's coefficient (one-way ANOVA, $F_{(2, 156)}=18.73$, $p<0.0001$). Data represent mean \pm SEM of 5-6 different embryos with 10 neurons per genotype ($n=50-60$). Each point represents a neuron. **** $p<0.0001$ vs WT Veh; ##### $p<0.0001$ vs R6/1 Veh.

RESULTS

1.6.1. Drp1 inhibition prevents disturbances in ROS production and calcium homeostasis

Next, we aimed to prove whether Drp1 inhibition could restore not only morphological parameters but also mitochondria function. Thus, striatal primary neurons were treated with vehicle (DMSO) or Mdivi-1 and then incubated with MitoSOX to detect levels of superoxide, the predominant mitochondrial ROS product. Intensity of MitoSOX dye was analysed by confocal microscopy and quantified (Figure 33A). Vehicle-treated R6/1 neurons showed a raise in MitoSOX intensity compared to WT vehicle neurons. On the contrary, R6/1 striatal cultures that received Mdivi-1 presented superoxide levels similar to WT vehicle and significantly lower than R6/1 vehicle (Figure 33B). This indicates that augmented mitochondrial fragmentation in R6/1 striatal cultures entails a higher oxidative stress.

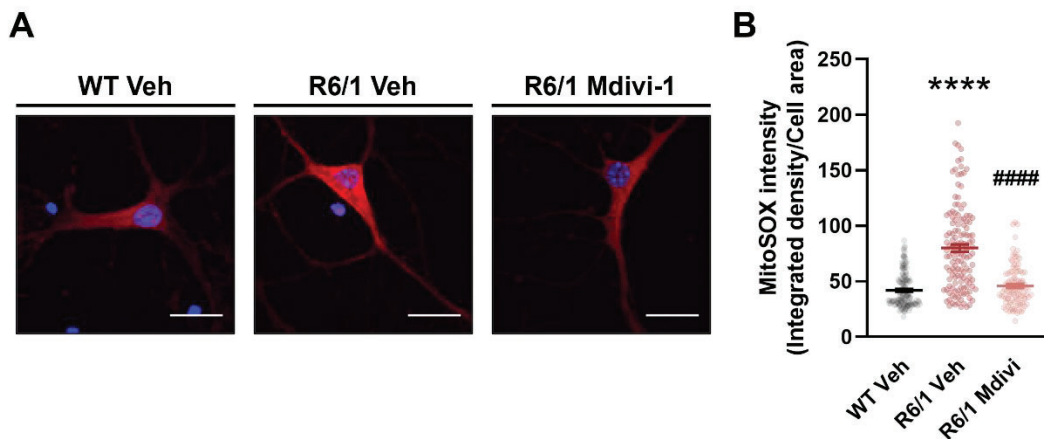


Figure 33. Increased mitochondrial ROS production in R6/1 striatal neurons is normalized after pharmacological Drp1 inhibition. (A) Confocal images of primary striatal neurons from WT and R6/1 at DIV14 after treatment with vehicle (DMSO) or 25 μ M Mdivi-1. Mitochondrial superoxide production was labelled with MitoSOX in red and nuclei appear in blue. Scale bar, 20 μ m. (B) Quantification of MitoSOX fluorescence intensity was measured as Integrated Density and relativized to cell area. Kruskal-Wallis test with Dunn's *post hoc* analysis, $p < 0.0001$. Data represent mean \pm SEM of 15-20 neurons from 7-10 different embryos per genotype ($n = 110-140$). **** $p < 0.0001$ vs WT Veh; ### $p < 0.001$ vs R6/1 Veh.

Finally, we assessed ER-mitochondrial Ca^{2+} transfer in WT and R6/1 striatal neuronal cultures following treatment with vehicle (DMSO) or Mdivi-1. Cells were loaded with Fluo4 and TMRM to monitor Ca_i^{2+} and $\Delta\psi_m$ and stimulated sequentially with thapsigargin and FCCP (Figure 34A). Mdivi-1 treatment did not induce changes in basal levels of Fluo4 or TMRM. However, Drp1 inhibition in R6/1 neurons prevented the increment in Ca_i^{2+} and mitochondrial depolarization after thapsigargin. Consequently, when FCCP was added, reduction of Ca_i^{2+} levels and lowering of $\Delta\psi_m$ was avoided in R6/1 neurons treated with Mdivi-1 (Figure 34B). Overall, these results highlight the implication of disrupted ER-mitochondria crosstalk in calcium mishandling in HD striatum.

RESULTS

2. CONTRIBUTION OF ASTROCYTIC MITOCHONDRIA TO STRIATAL VULNERABILITY IN HD

Following neurons, astrocytes are the most abundant cell population in the striatum. Although mitochondrial defects in striatal neurons in HD have been largely explored, less is known about the role and regulation of mitochondrial dynamics in astrocytes. In this second study, we first characterized the expression of several astrocyte markers in the striatum of a HD mouse model along the disease progression. Then, we tested whether metabolism and mitochondrial dynamics could also be dysregulated in HD astrocytes. Finally, we investigated the mechanisms mediating mitochondrial communication from astrocytes to neurons. Overall, we hypothesised that alterations in mitochondrial function in striatal astrocytes could contribute to the striatal vulnerability that occurs in HD.

2.1. Characterization of astrocyte population in R6/1 striatum

To date, several criteria have been proposed to classify different types of astrocytes. However, the expression of astrocyte markers can vary depending on the brain region and with age (Khakh & Deneen, 2019). We aimed to explore astrocyte population in the striatum and to study whether presence of mHtt could affect the expression of the different markers, and therefore the astrocyte population.

2.1.1. Protein levels of astrocyte markers in striatal tissue and primary cultures from R6/1 mice are not altered

Protein levels of ALDH1L1 (Figure 35A), GFAP (Figure 35B), S100 β (Figure 35C), and GLAST (Figure 35D) were evaluated in total lysates from striatum of WT and R6/1 mice by Western Blot. Several ages were tested to evaluate alterations throughout the disease, namely 8, 12, 20 and 30 weeks. As in the first study, these ages were chosen to evaluate pre-symptomatic, onset of cognitive deficits, motor deficits and late stages respectively. When comparing WT and R6/1, no significant differences were found in the levels of ALDH1L1, GFAP or S100 β . On the contrary, GLAST levels showed a significant lowering in R6/1 mice at 12 weeks of age with a tendency to decrease at 20 and 30 weeks of age, which is in line with previous published results (Estrada-Sánchez et al., 2009; Faideau et al., 2010), indicating a loss of GLAST at middle stages of HD.

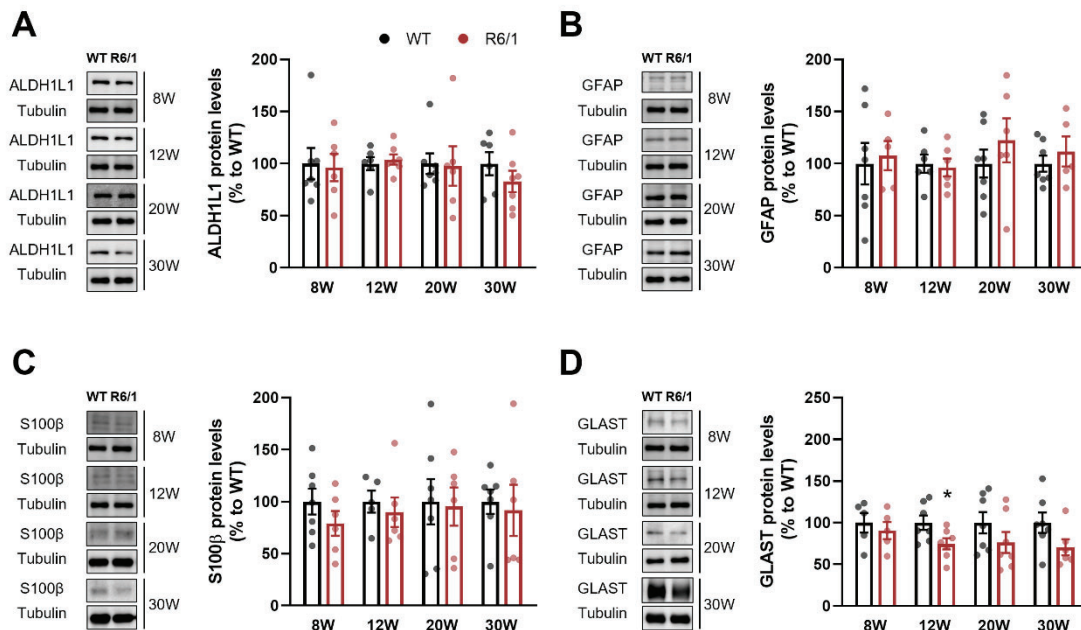


Figure 35. Astrocyte markers ALDH1L1, GFAP, S100 β , and GLAST are not altered in the striatum of R6/1 mice. Immunoblotting and densitometry quantification of protein levels of ALDH1L1 (A), GFAP (B), S100 β (C) and GLAST (D) in total lysates from WT (black) and R6/1 (red) mice. Different stages of the disease were tested, namely 8, 12, 20 and 30 weeks (W). Tubulin was used as loading control. Relative protein levels are expressed as percentage to WT mice at every age. Data represent mean \pm SEM, n=5-7 animals. * p<0.05 vs WT as determined by Student's t-test.

Then, a time course analysis of the same astrocyte markers was performed in striatal total lysates from WT (Figure 36A) and R6/1 (Figure 36B) mice. We observed that ALDH1L1 levels remained unchanged both in WT and R6/1 mice (Figure 36C), pointing at ALDH1L1 as a suitable astrocyte marker since it is unaffected by age or genotype. On the contrary, S100 β (Figure 36D) revealed an increment with the age, at 30 weeks in WT and 20 and 30 weeks of age in R6/1 mice. This indicates that maturation of astrocytes increases with aging regardless the genotype. Likewise, GFAP levels (Figure 36E) augmented at 20 and 30 weeks in the WT and at 30 weeks in the R6/1 mice, suggesting that aging triggers the astrocytes reactivity. Finally, GLAST showed no alterations with the age neither in WT nor in R6/1, reinforcing the idea that the diminution described above is due to the presence of mHtt (Figure 36F).

RESULTS

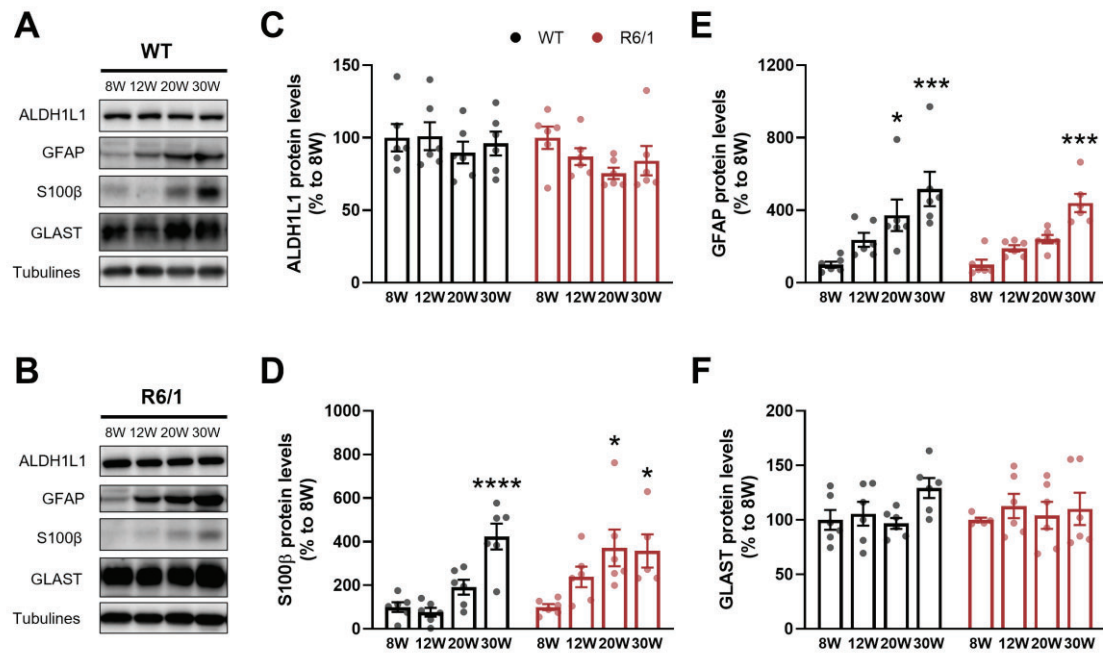


Figure 36. Time course of astrocyte markers **ALDH1L1**, **GFAP**, **S100β**, and **GLAST** in the striatum of **WT** and **R6/1** mice. Immunoblotting of proteins of interest in striatal total lysates of **WT** (**A**) and **R6/1** (**B**) mice. Densitometry quantification of protein levels of **ALDH1L1** (**C**), **S100β** (**D**), **GFAP** (**E**), and **GLAST** (**F**). For each genotype, 8, 12, 20 and 30 weeks of age were tested. Tubulin was used as loading control. Relative protein levels are expressed as percentage to 8W mice. Data represent mean \pm SEM, $n=5-7$ animals. * $p<0.05$ vs WT as determined by one-way ANOVA.

Moreover, we examined the protein levels of astrocyte markers in striatal primary astrocytes from **WT** and **R6/1** mice at different days *in vitro* (DIV). Neither **ALDH1L1** nor **GFAP** levels were altered between genotypes in **DIV14**, **DIV21** or **DIV28**. These results indicate that **R6/1** striatal astrocytic cultures do not present higher astrocyte reactivity at any of the *in vitro* stages compared to **WT** astrocytes.

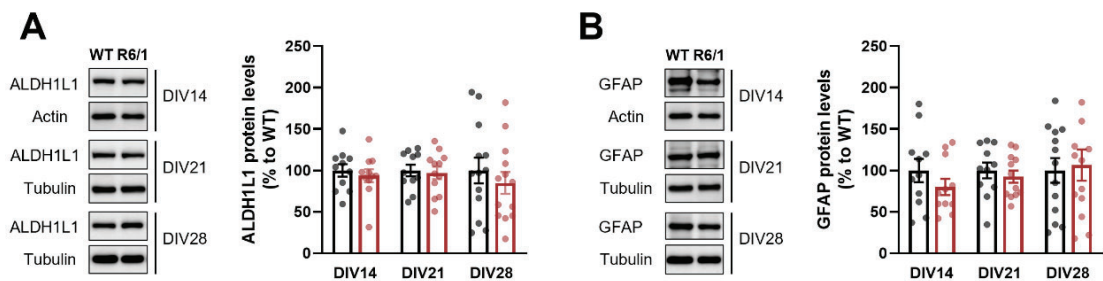


Figure 37. Levels of astrocyte markers **ALDH1L1** and **GFAP** in primary striatal astrocytes of **R6/1** mice. Immunoblotting and densitometry quantification of protein levels of **ALDH1L1** (**A**) and **GFAP** (**B**) in **WT** (black) and **R6/1** (red) primary striatal astrocytes. Cultures at different days *in vitro* (DIV) were tested, namely 14, 21, and 28. Tubulin was used as loading control. Relative protein levels are expressed as percentage to **WT** culture at every condition. Data represent mean \pm SEM, $n=11-13$ animals.

2.1.2. Distribution of astrocyte populations is not altered in the striatum of R6/1 mice

Though total levels of different astrocyte markers were not found different between genotypes and along the disease progression, we next aimed to analyse the distribution of the astrocyte populations in the striatum with age and disease. To this aim, the bulk of the striatal tissue was labelled combing the four different markers: ALDH1L1, GFAP, S100 β , and GLAST along with a cell viability dye, and fluorescence was analysed by flow cytometry. Number of positive cells were relativized to the total amount of live cells (Figure 38A). Results showed no changes in the number of positive cells for each of the evaluated markers between WT and R6/1 mice striatum (Figure 38B).

Overall, these results are in line with the outcome from biochemical analysis, indicating that striatum of R6/1 mice at late stages do not present major alterations in the percentage of different astrocyte populations.

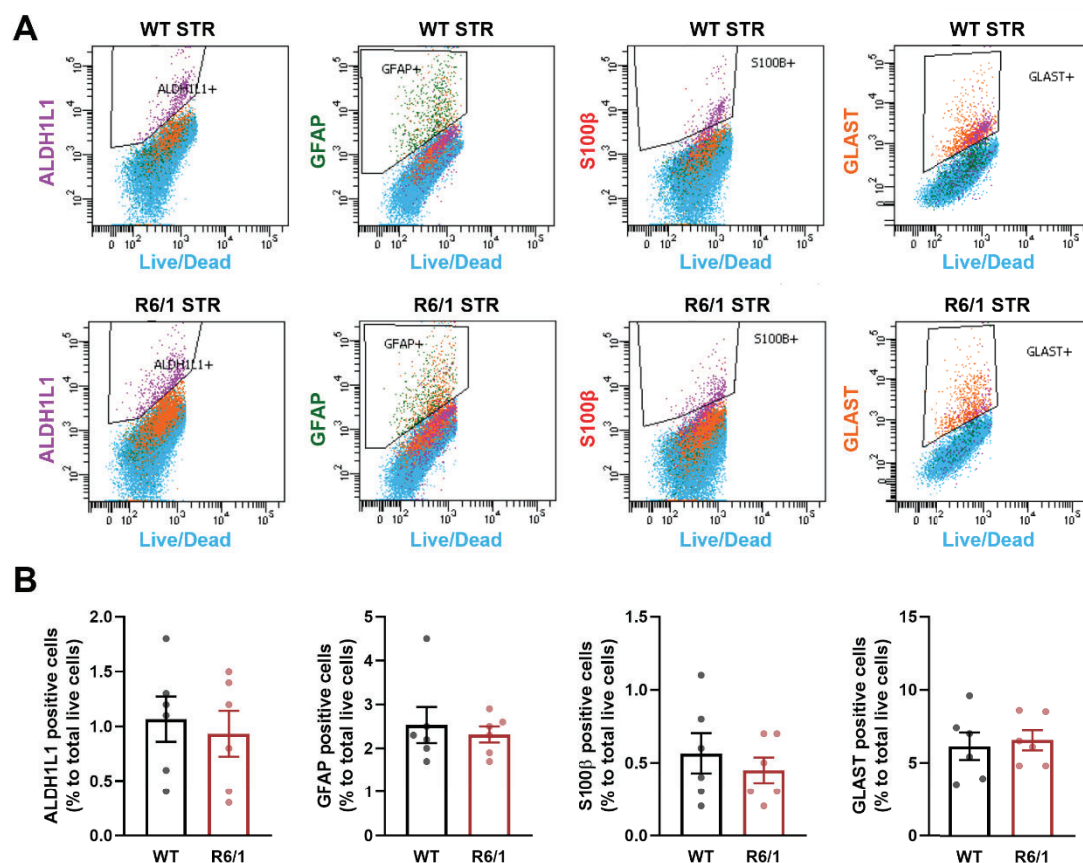


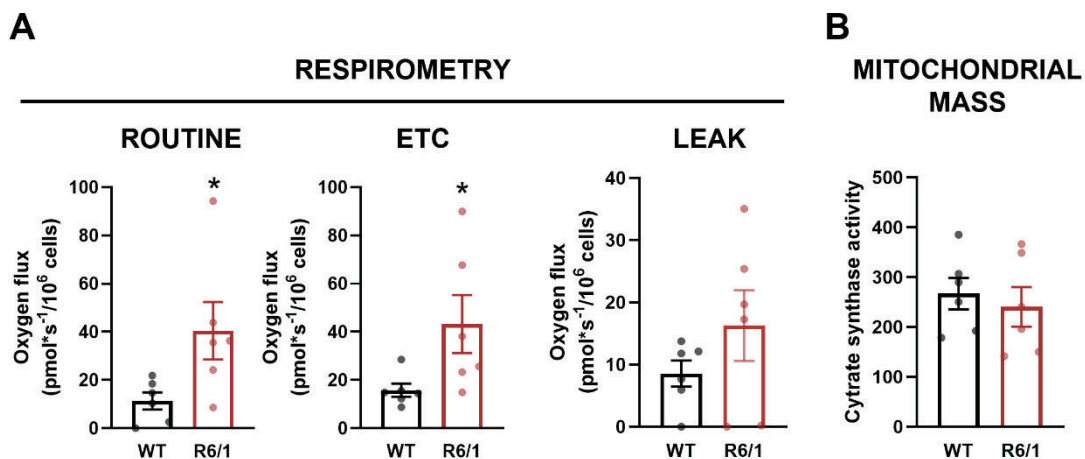
Figure 38. Astrocyte markers in striatum of WT and R6/1 mice at 20W. Striatum from 20W old WT and R6/1 mice was disaggregated and labelled simultaneously with ALDH1L1, GFAP, S100 β and GLAST. **(A)** Representative plots of the analysed fluorescence for each marker by flow cytometry. Black gates delimit the area of selected positive cells. **(B)** Quantification of number of positive cells was relativized to the total number of live cells. Data represent mean \pm SEM, each point represents an animal (n=6).

RESULTS

2.2. Oxidative and glycolytic metabolisms are increased in R6/1 striatal astrocytes

Despite no differences in astrocyte populations, we wondered whether striatal R6/1 astrocytes could display defects in the metabolism. To test this possibility, we first analysed mitochondrial respiration by measuring oxygen consumption with OROBOROS in WT and R6/1 primary striatal astrocytes. Oxygen consumption was normalized to number of cells on each assay. Results showed that R6/1 astrocytes presented an increased basal (routine) as well as increased maximal (ETC) respiration, indicating an excessive function of the oxidative phosphorylation (Figure 39A).

To corroborate that this hyperactivation in mitochondrial respiration was not due to more mitochondria population, we quantified mitochondrial mass by measuring citrate synthase activity. WT and R6/1 primary astrocytes displayed similar levels of enzymatic activity, suggesting no alterations in mitochondrial content (Figure 39B). Simultaneously, we measured metabolites in the medium of WT and R6/1 astrocytic cultures. While a slight although not significant decrease in glucose levels remained unchanged, lactate was higher in R6/1 compared to WT, accompanied by an acidification of the medium (Figure 39C). This outcome suggested an increment not only in mitochondrial respiration but also in glycolysis. However, this hyperactivation of metabolism did not increase the levels of oxidative stress measured by lipid peroxidation (Figure 39).



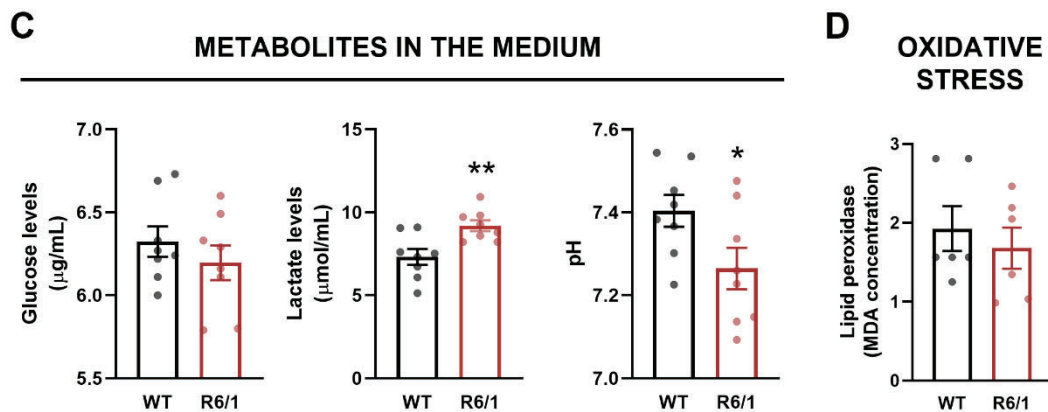


Figure 39. Aerobic metabolism and glycolysis are augmented in R6/1 striatal astrocytes. (A) Mitochondrial oxygen consumption was measured with OROBOROS in basal conditions (routine) and maximal respiration (ETC) after uncoupling with CCCP. To induce leak of protons, oligomycin was added to cells. (B) Enzymatic activity of citrate synthase was measured to determine mitochondrial mass. (C) Levels of glucose and lactate and pH was measured in the culture medium of primary astrocytes using EPOC microfluidic cards. (D) Oxidative stress was analysed by measuring concentration of malondialdehyde (MDA) as a readout of lipid peroxidase. Data represent mean \pm SEM, $n=6$ animals. * $p<0.05$, ** $p<0.01$ vs WT as determined by Student's t-test.

2.3. Mitochondria in adult R6/1 striatal astrocytes are not less functional

To better understand the mitochondrial defects underlying the hypermetabolism observed in HD astrocytes, we aimed to assess the mitochondrial functionality in R6/1 striatal astrocytes. To this end, striatal astrocytes were isolated from WT and R6/1 mice at 20 weeks of age (see the following section for details on astrocytes' isolation) and stained with MitoTracker dyes. Following the methodology used by Monteiro et al. (Monteiro et al., 2020), MitoTracker Green and MitoTracker Red were combined to label mitochondrial mass and functionality and were analysed by flow cytometry. While MitoTracker Green passively accumulates to the mitochondria, MitoTracker Red depends on the $\Delta\psi_m$. Hence, functional mitochondria were labelled with high levels in both dyes while dysfunctional ones only with MitoTracker Green due to the loss of $\Delta\psi_m$ (Figure 40A).

Among the bulk of cells analysed, up to 95% cells were positive for MitoTracker Green and similar levels were found between genotypes. This outcome indicates that WT and R6/1 astrocytes present similar mitochondrial mass, corroborating the previous results. Regarding MitoTracker Red, positive particles were categorised in functional or dysfunctional mitochondria according to high or low levels of fluorescence intensity.

RESULTS

Surprisingly, the pool of functional and dysfunctional mitochondria were unaltered comparing WT and R6/1 astrocytes (Figure 40B). These data suggest that mitochondrial alterations in HD astrocytes are not due to a loss of functional mitochondria.

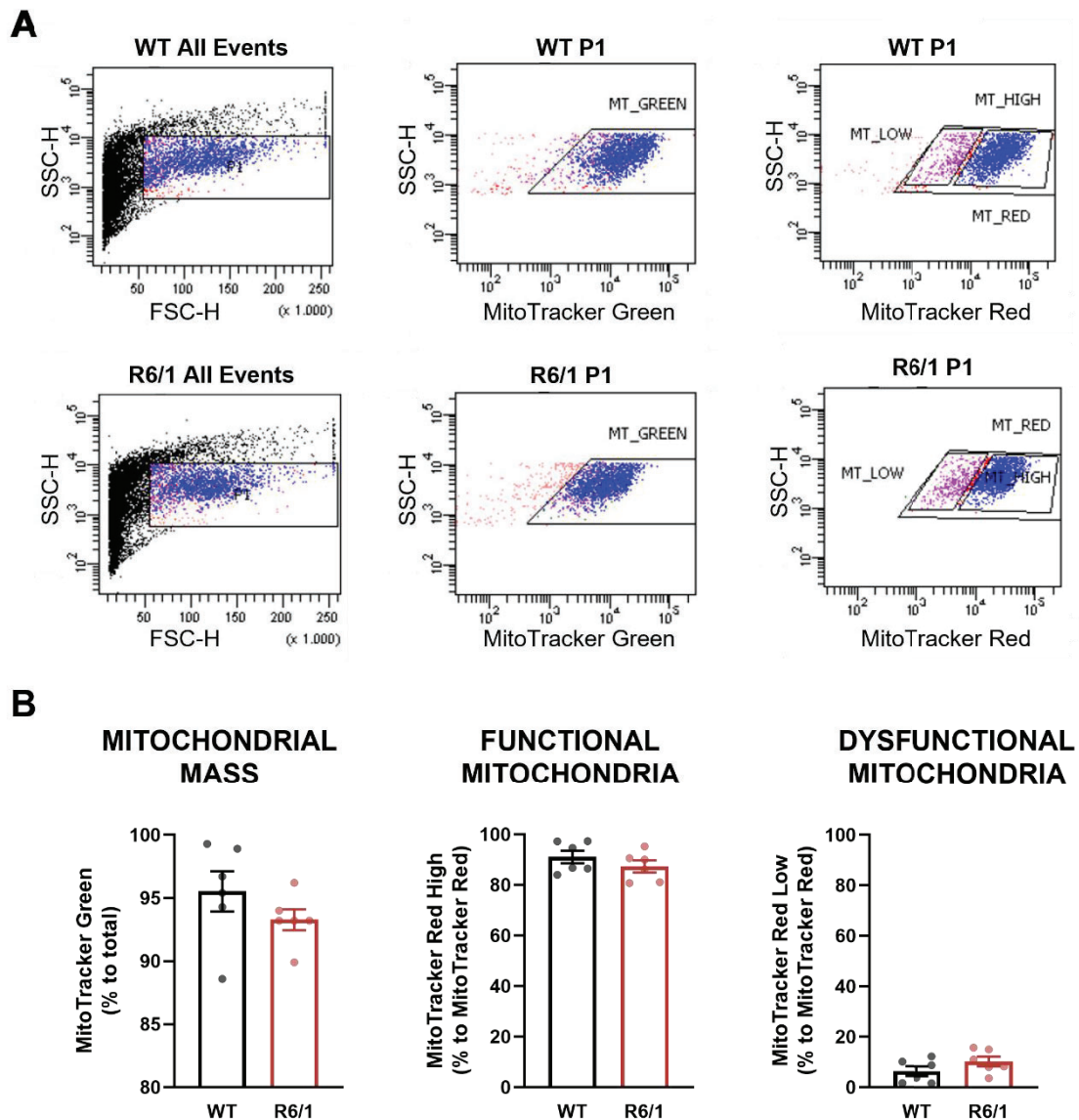


Figure 40. Evaluation of mitochondrial mass and functionality of mitochondria in striatal astrocytes of WT and R6/1 mice at 20W. Astrocytes were isolated from striatum of adult WT and R6/1 mice and mitochondria were stained with MitoTracker Green and MitoTracker Red. **(A)** Representative plots of the analysed fluorescence by flow cytometry of WT and R6/1 astrocytes. Black lines delimit the gates for particles with a size similar to mitochondria (P1), MitoTracker Green (middle panels) and MitoTracker Red Low and High (right panels). **(B)** Quantification of number of positive particles expressed as percentage to the parent population. Data represent mean \pm SEM. Each point represents an animal (n=6).

2.4. Mitochondrial dynamics are altered in R6/1 striatal astrocytes

Considering that mitochondria constantly remodel their morphology to rapidly adapt to changes in cell function, we wondered whether mitochondrial dynamics could be altered in R6/1 striatal astrocytes. We hypothesised that the enhanced metabolism in R6/1 astrocytes could trigger mitochondrial fission events in an attempt to dissipate the excessive energy.

2.4.1. Increased Drp1 and Cdk5 in adult R6/1 striatal astrocytes

In order to study mitochondria related proteins specifically in astrocytes, we first isolated astrocytes from the striatum of adult WT and R6/1 mice by ACSA-2+ magnetic labelling and separation (G. Kantzer et al., 2017). Notice that the ACSA-2 antigen is expressed specifically on astrocytes in a similar pattern to GLAST expression. First, we validated the isolation by Western Blot. GLAST protein was present in the positive ACSA-2 fraction but not in the negative fraction in both genotypes at different stages of the disease (8, 12 and 20 weeks of age). Conversely, actin was detected in all samples regardless the cell type (Figure 41). This points out that astrocytes were correctly isolated from the bulk of cells in the striatal tissue. We qualitatively noticed that protein levels of actin were not constant when comparing positive fractions of WT and R6/1 at the different ages. Henceforth, ALDH1L1 will be used as loading control in the Western Blot of isolated astrocytes. We have previously reported ALDH1L1 as the most constant astrocyte marker either between genotypes or along the disease (see section 2.1 in this chapter).

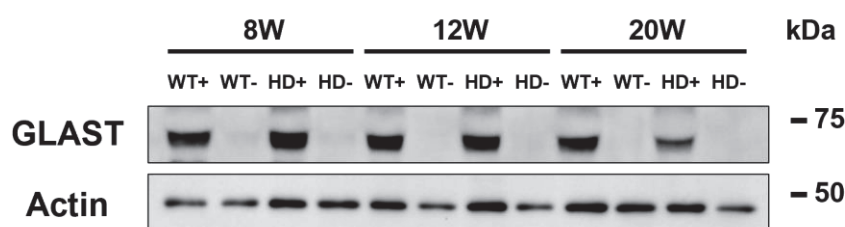


Figure 41. Validation of ACSA2+ isolation by Western Blot. Adult astrocytes were isolated by magnetic labelling of ACSA-2. Positive (+) and negative (-) ACSA-2 fractions were included from WT and R6/1 mice at 8, 12, and 20 weeks (W) of age. GLAST was blotted as a marker for astrocytes. Molecular weight markers positions are indicated in kDa.

RESULTS

First, we evaluated protein related to mitochondrial fission in striatal astrocytes isolated from adult WT and R6/1 animals. It has been described that Cdk5 phosphorylates Drp1 (Jahani-Asl et al., 2015), and can act as an upstream regulator of mitochondrial fission, driving to mitochondrial defects (Meuer et al., 2007; Rong et al., 2020). Therefore, we measured levels of genes encoding Drp1 (*Dnm1l*) and Cdk5 (*Cdk5r1*) by RT-qPCR and both genes were increased in R6/1 astrocytes from 20 weeks old mice (Figure 42A). Moreover, we tested protein levels at different stages of the disease. Although not significant, Drp1 showed a trend to augment in R6/1 at 12 and 20 weeks of age compared to WT animals. Regarding Cdk5, R6/1 astrocytes presented a rise at 12 weeks and a tendency at 20 weeks of age (Figure 42B). Together these findings suggest that mitochondrial fission is enhanced in striatal astrocytes in the presence of mHtt at middle and late stages of HD.

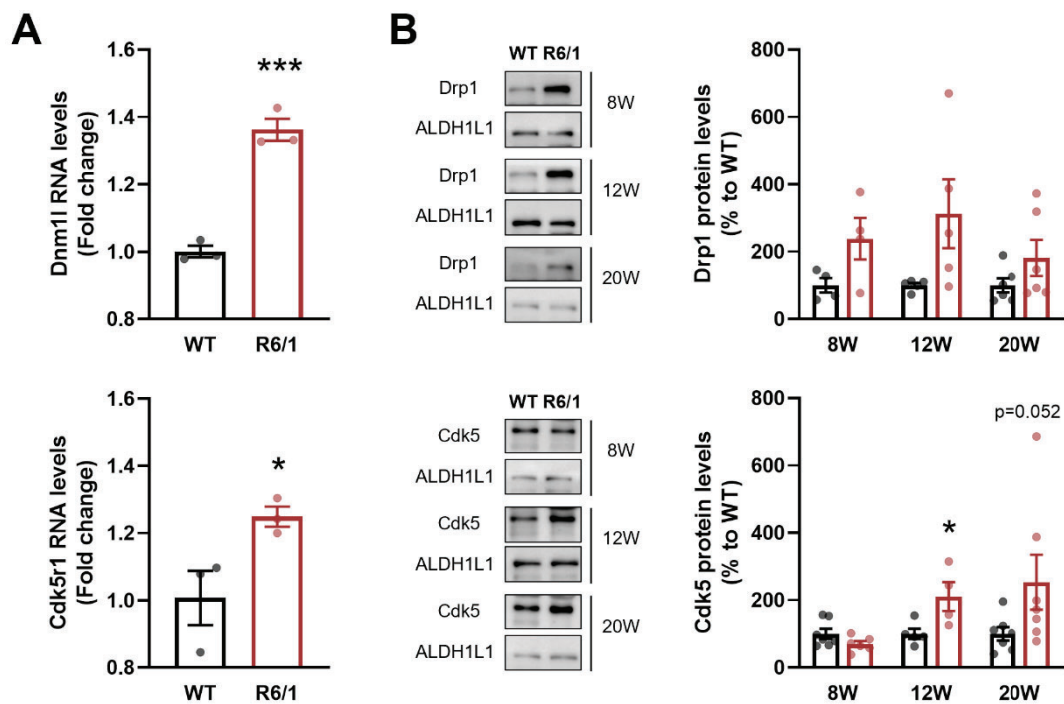


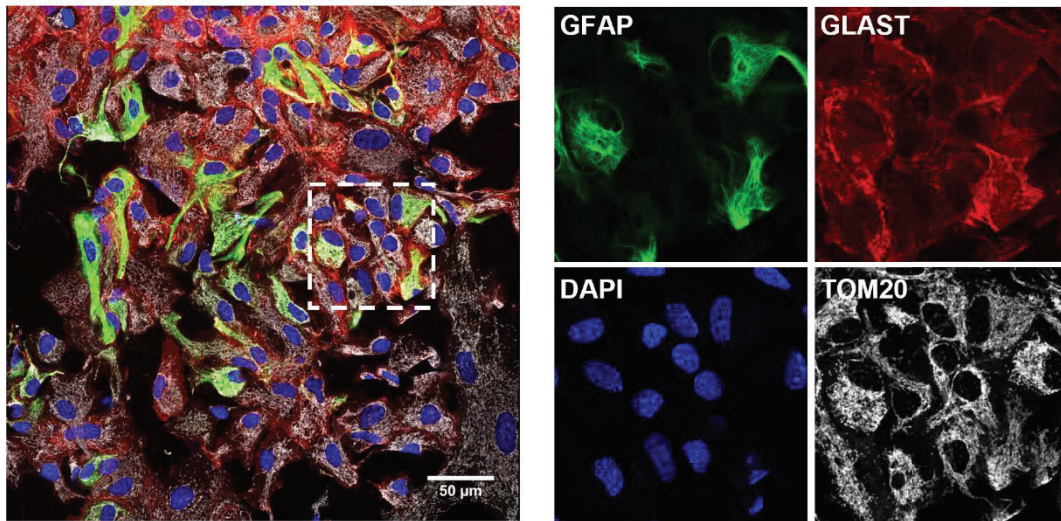
Figure 42. Levels of mRNA and protein of Drp1 and Cdk5 are increased in adult striatal astrocytes from R6/1 mice. Astrocyte were isolated from striatum of adult WT and R6/1 mice. **(A)** mRNA levels of *Dnm1l* (Student t-test, $t=9.815$, $df=4$; $p=0.0006$) and *Cdk5r1* (Student t-test, $t=2.810$, $df=4$; $p=0.0483$) were measured by quantitative RT-qPCR in isolated astrocytes from WT and R6/1 mice at 20W of age. mRNA levels were normalized to 18S and related to WT as fold change. **(B)** Immunoblotting and densitometry quantification of protein levels of Drp1 and Cdk5 in WT (black) and R6/1 (red) mice at different stages of the disease (W, weeks). ALDH1L1 was used as loading control. Relative protein levels are expressed as percentage to WT mice at every age. Data represent mean \pm SEM. Each point represents a pool of 2-3 animals. In **A**, $n=3$ (7-9 animals); in **B**, $n=4-6$ (12-18 animals). * $p<0.05$, *** $p<0.001$ vs WT.

2.4.2. Alterations in mitochondrial morphology are observed in specific HD striatal astrocyte population

To assess mitochondrial morphology in HD astrocytes, WT and R6/1 striatal astrocytic cultures at DIV14 were stained with TOM20, GLAST and GFAP to label mitochondria and two populations of astrocytes: GLAST as a general astrocytic marker and GFAP for those reactive astrocytes (Figure 43A). We aimed to evaluate whether mitochondrial morphology was differently affected in GFAP astrocytes. Thus, we analysed separately cells only positive for GLAST (GLAST+GFAP-) and those positive for GFAP (GFAP+). Morphometrical analysis by confocal microscopy revealed that GLAST astrocytes in R6/1 striatal cultures presented a higher cell area compared to WT. This hypertrophy could be interpreted as a sign of increased reactivity of the R6/1 astrocytes. However, when measuring number and area of mitochondria, as well as Aspect Ratio, no significant differences were detected between genotypes. Regarding GFAP positive astrocytes, both cell area and number of mitochondria were unchanged when comparing WT and R6/1 cultures. Nevertheless, R6/1 GFAP astrocytes showed lower mitochondrial area along with higher values of Aspect Ratio, indicating alterations in mitochondrial shape. Altogether, these results suggested that mitochondrial morphology is preferentially affected in GFAP+ astrocytes in R6/1 mice.

RESULTS

A



B

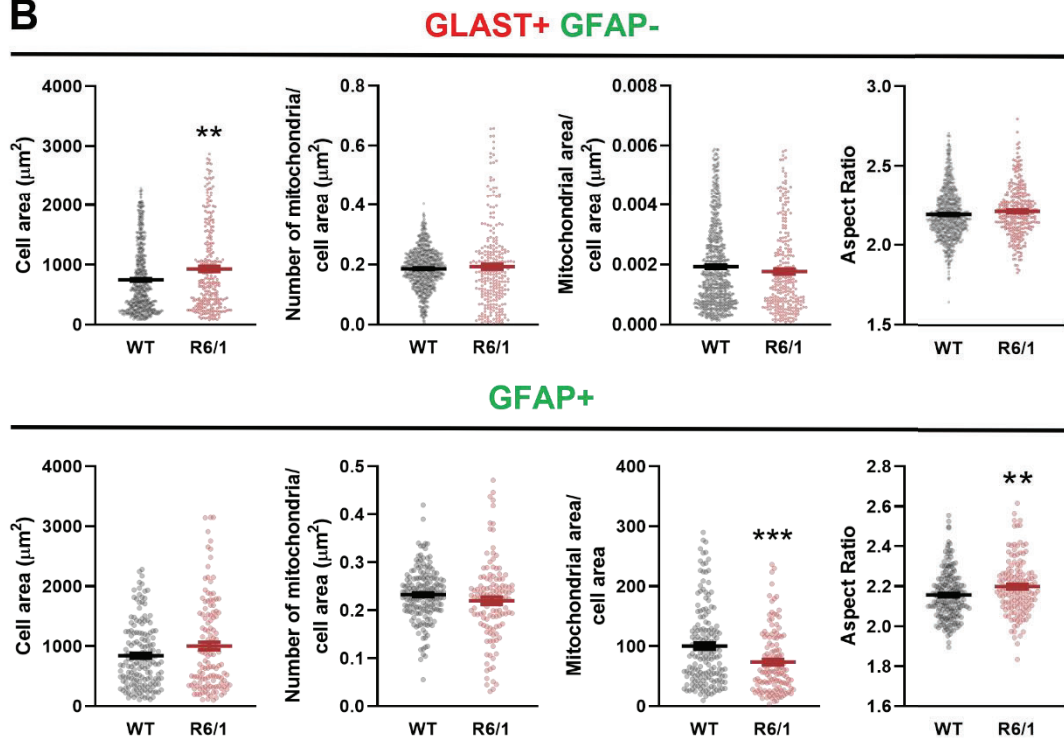


Figure 43. Mitochondrial morphology is altered differentially in R6/1 striatal primary astrocytes. (A) Confocal images of R6/1 striatal primary astrocytes at DIV14 immunolabeled with GFAP, GLAST and TOM20 in green, red and white respectively. Panels on the right show magnification of the boxed areas in white. Scale bar, 50 μm . (B) Quantification of cell area, number of mitochondria, mitochondrial area and Aspect Ratio for GLAST+GFAP- cells and GFAP+ cells. Data are means \pm SEM from 8 mosaics from 3-4 different animals per genotype. In GLAST+GFAP-, $n=698-314$; in GFAP+, $n=137-180$. In cell area and number of mitochondria, each point represents a single value for each cell. In Mitochondrial area and Aspect Ratio, each point represents the mean of all mitochondria in each astrocyte. ** $p<0.01$, *** $p<0.001$ vs WT.

2.5. Mitochondrial release from R6/1 astrocytes contributes to striatal neuronal vulnerability

One of the proposed mechanisms of neuroglia crosstalk is mediated by mitochondria. Transmitophagy, that is mitochondrial transfer between cells, have been described as a mechanism that occurs in a physiological context. However, some investigations reported a disruption in this process in pathological conditions as stroke injury or PD (Hayakawa et al., 2016; Lippert & Borlongan, 2019; Morales et al., 2020). Considering that we have demonstrated mitochondrial alterations in HD striatal neurons and astrocytes, we attempted to examine whether transmitophagy from astrocytes to neurons could also be altered in HD.

2.5.1. Characterization of extracellular astrocytic mitochondria

First, we aimed to study if striatal astrocytes in culture could release mitochondria in basal conditions. To test so, we cultured WT and R6/1 primary striatal cultures and media was collected at DIV14 and processed for electron microscopy analysis. Mitochondria were detected in media from both genotypes (Figure 44A) either as mito-particles (embedded in membranous structures) or free mitochondria as previously reported by Hayakawa et al. (Hayakawa et al., 2016) (Figure 44B).

RESULTS

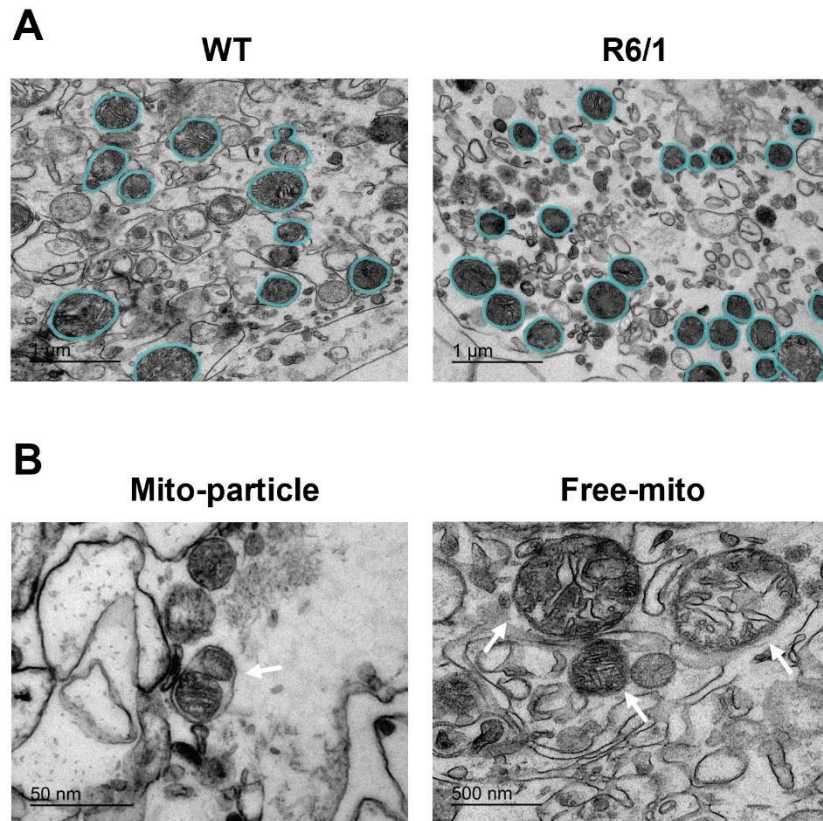


Figure 44. Mitochondria is present in the astrocyte conditioned media from WT and R6/1 striatal astrocytes. (A) Mitochondria were found in ACM from WT and R6/1 cultures. Blue lines delimit mitochondria. Scale bar, 1 micron. (B) Mitochondria were found inside vesicles (mito-particles) and as free mitochondria. White arrows indicate the structures of interest. Scale bars: left panel 50 nm, right panel 500 nm.

Since electron microscopy could not assess the functionality of released mitochondria, we combined MitoTracker dyes and flow cytometry to determine the percentage of functional mitochondria in the extracellular media. Striatal primary astrocytes from WT and R6/1 were incubated with MitoTracker Green and MitoTracker Red to simultaneously trace mitochondrial mass and functional mitochondria respectively. Fluorescence was measured in ACM from WT and R6/1 astrocytic cultures by flow cytometry as shown in Figure 45A. We counted particles positive for MitoTracker Red among MitoTracker Green gate, showing both genotypes about 97% of positive MitoTracker Red mitochondria. Likewise in adult astrocytes, we established two population within MitoTracker Red positive particles: high and low levels for functional and dysfunctional mitochondria respectively. We did not detected differences neither in high or low levels of MitoTracker Red comparing WT and R6/1 samples (Figure 45B). Altogether, these results suggested that ACM from both WT and R6/1 contained similar proportion of fully functional mitochondria.

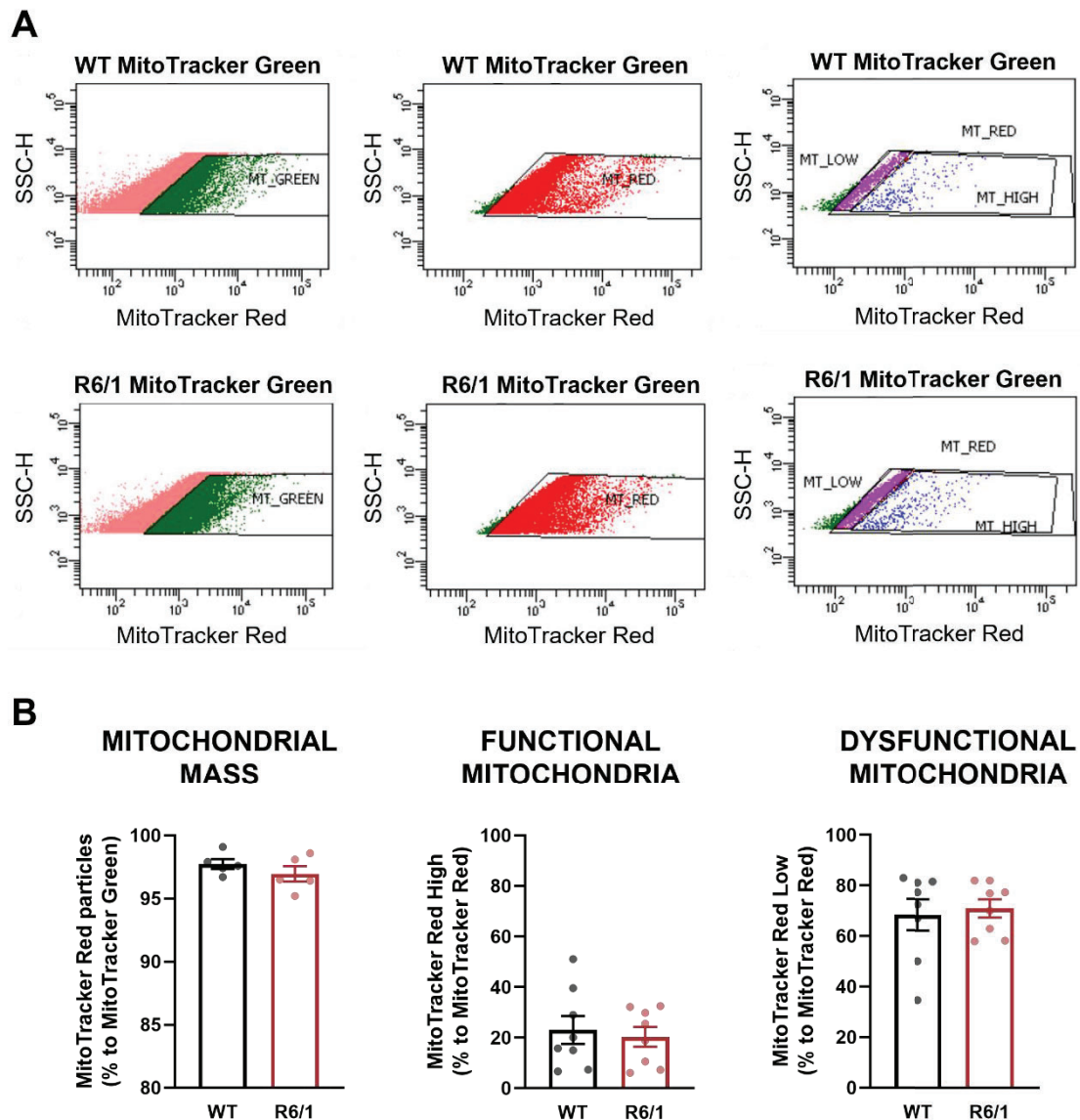


Figure 45. Mitochondria present in the ACM from WT and R6/1 primary striatal astrocytes are functional. ACM was stained with MitoTracker Green and MitoTracker Red. (A) Representative plots of the analysed fluorescence by flow cytometry of WT and R6/1 samples. Black lines delimit the gates for MitoTracker green (left panels), MitoTracker Red (middle panels) and MitoTracker Low and High (right panels). (B) Quantification of number of positive particles expressed as percentage to the parent population. Data represent mean \pm SEM. Each point represents the ACM of a single animal (n=6-8).

2.5.2. Mitochondria from R6/1 neurons induce toxic effects in striatal neurons

To explore the effect of astrocytic mitochondria in neurons, cultured WT and R6/1 striatal astrocytes were stained with MitoTracker Red to only label functional mitochondria. After 24h, astrocytic conditioned medium (ACM) was collected and transferred to WT striatal primary neurons at DIV15 for 24h (Figure 46A).

RESULTS

First, we analysed the uptake of released astrocytic mitochondria (red stained mitochondria) by WT neurons. Although MitoTracker Red is a specific dye for functional mitochondria, colocalisation of mitochondrial marker TOM20 with MitoTracker Red was performed to cross-check that red signal corresponded to mitochondria. Additionally, WT neurons were stained for MAP2. Confocal microscopy analysis revealed positive particles for MitoTracker Red in WT neurons incubated with either WT or R6/1 ACM, confirming that WT striatal neurons can acquire extracellular mitochondria from astrocytes, independently of the genotype of the original astrocyte (Figure 46B).

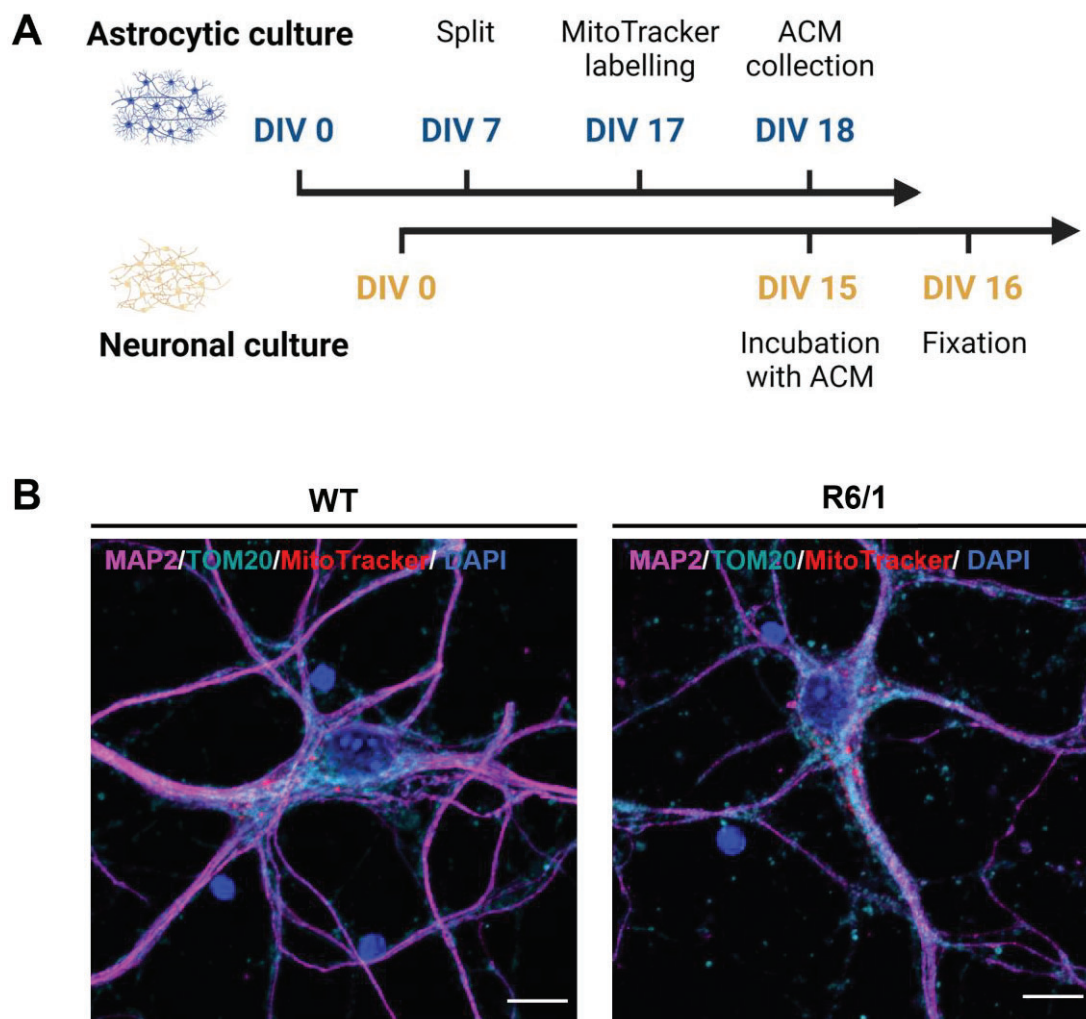


Figure 46. Extracellular mitochondria can be uptaken by striatal neurons. (A) Schematic representation of experimental design. Astrocytes were obtained from striatum of WT and R6/1 pups at postnatal day 2 and MitoTracker was incubated at DIV17. In parallel, WT striatal neurons were obtained from WT embryos at E18 and cultured until DIV16. ACM from WT or R6/1 cultures were transferred to WT neurons and incubated for 24h. Neurons were processed at DIV16 for further experiments. (B) WT neurons after ACM treatment were stained with MAP2 (magenta) and TOM20 (cyan) to immunolabel neuronal area and mitochondria respectively. MitoTracker Red indicates astrocytic mitochondria inside the neuron. Scale bar: 10 μ m.

RESULTS

Then, we tested oxidative stress in WT neurons after treatment with ACM from WT or R6/1 astrocytic cultures. CellROX was used as fluorescent indicator of ROS production mainly in nucleus and mitochondria. Intensity of CellROX was analysed with confocal microscopy and quantified. Striatal neurons with mitochondria from R6/1 astrocytes showed an increased in CellROX intensity compared to those with mitochondria from WT astrocytes (Figure 47A). This means that R6/1 mitochondria negatively affect the oxidative state of WT striatal neurons. Next, we evaluated the impact of astrocytic mitochondria in the WT neurons by quantification of neuronal branching in the same cultures. Neurons were labelled with MAP2 in green and Sholl analysis was performed (Figure 47B). Branching quantification revealed that neurons that received R6/1 ACM developed a smaller number of neurites than those with WT ACM (Figure 47B). These data point out a toxic effect of mitochondria from HD astrocytes on WT striatal neurons.

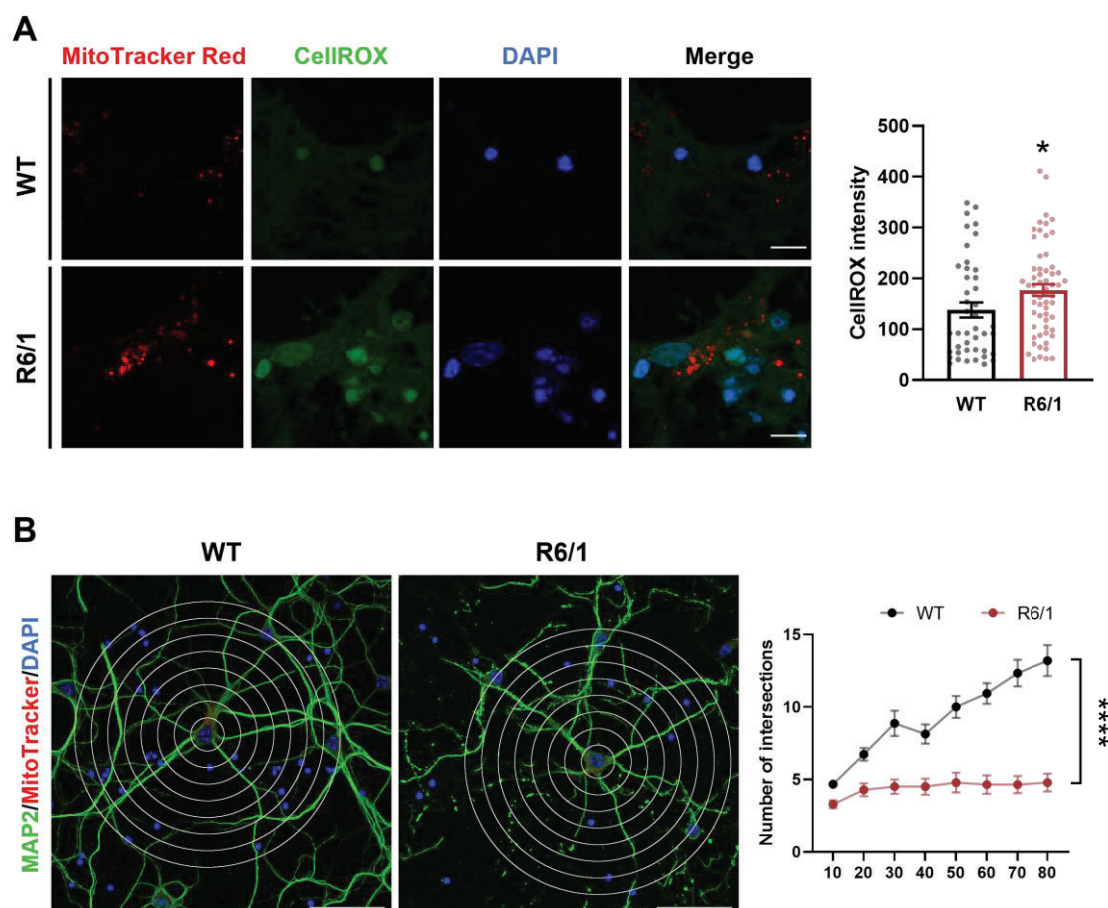


Figure 47. Mitochondria from R6/1 striatal astrocytes increase oxidative stress and hampers neuronal branching in WT striatal neurons. WT striatal neurons at DIV16 were treated with ACM of WT or R6/1 striatal astrocytes. Astrocytic mitochondria were labelled with MitoTracker Red and applied to WT neurons. **(A)** In the left panel, CellROX in green shows oxidative stress in WT neurons and nuclei appear in blue. Scale bar, 10 μ m. In the right panel, quantification of CellROX intensity measured in WT neurons and relativized to cell area. **(B)** In the left panel, neurons were immunostained with MAP2 in green and nuclei in blue and analysed by Sholl method (white concentric circles). Scale bar, 50 μ m. In the right panel, quantification of neuronal branching using Sholl analysis. * $p < 0.05$, **** $p < 0.0001$ vs WT.

RESULTS

2.5.3. Characterization of extracellular astrocytic mitochondria

Little is known about the molecular mechanisms underlying transmitophagy. However, CD38 has been described as a key factor in this process and ablation of CD38 was reported to decrease mitochondrial transfer from astrocyte to neurons (Hayakawa et al., 2016). We evaluated levels of CD38 in astrocytes isolated from adult WT and R6/1 mice by Western Blot. R6/1 showed a trend to increase at 12 weeks and a significant augmentation at 20 weeks compared to WT animals (Figure 48A). Likewise, CD38 protein levels in *post-mortem* caudate samples were increased in HD patients compared to control subjects (Figure 48B). This increment in CD38 could indicate alterations in the release of extracellular mitochondria from HD astrocytes.

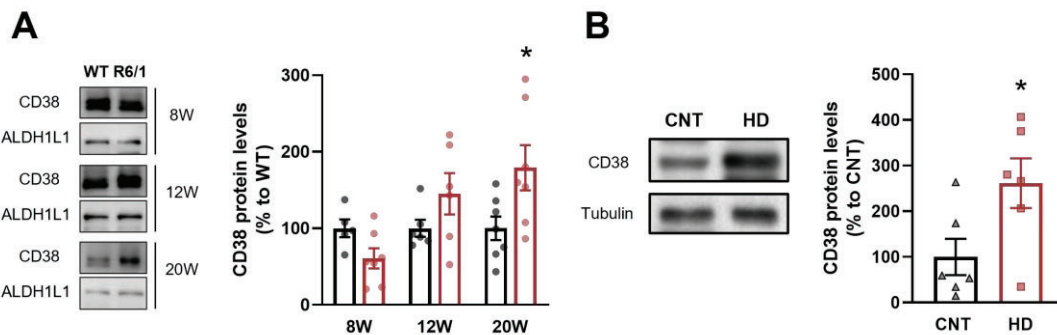


Figure 48. Levels of CD38 protein are increased in adult striatal astrocytes of R6/1 mice and in *post-mortem* caudate of HD patients. (A) Immunoblotting of CD38 protein levels in WT (black) and R6/1 (red) mice at different stages of the disease (W, weeks). ALDH1L1 was used as loading control. Relative protein levels are expressed as percentage to WT mice at every age. (B) Immunoblotting of CD38 protein levels in control subjects and HD patients. Tubulin was used as loading control. Relative protein levels are expressed as percentage to control subjects. Data represent mean \pm SEM. In A, each point represents a pool of 2-3 animals, n=4-6 (12-18 animals). In B, each point represents a human subject. * $p < 0.05$ vs WT.

3. ROLE OF PYK2 IN MITOCHONDRIA AND MAMs

Pyk2 is a non-tyrosine kinase enriched in hippocampal neurons. Several studies have identified Pyk2 as a key regulator of synaptic plasticity that, when compromised, may contribute to neuronal pathology in different neurodegenerative disorders, such as AD and HD. In neurons, Pyk2 is mostly present in the cytosol although upon activation, it can translocate to the nucleus and dendritic spines. Nonetheless, little is known about other Pyk2 subcellular localisations. In this third study, we aimed to evaluate whether Pyk2 localises in mitochondria and MAMs and its relevance in regulating mitochondrial morphology and function in physiological conditions. This knowledge would help to better understand the contribution of Pyk2 dysfunction in neurological disorders. To this end, Pyk2 knockout mice (Pyk2^{-/-}) were used for *in vivo* and *in vitro* studies as well as several mutant Pyk2 constructs to analyse the contribution of Pyk2 on mitochondrial dynamics and ER-contact sites in neurons.

3.1. Pyk2 is reduced in the striatum of HD patients

We analysed Pyk2 protein levels in *post-mortem* tissue from the putamen of control subjects and HD patients. HD patients showed a reduction about 40% compared to healthy individuals (Figure 49). Previous work of our group demonstrated that R6/1 mice presented a drop of Pyk2 protein levels in the hippocampus. Since Pyk2 is more enriched in hippocampal neurons than those in the striatum, following experiments to explore the involvement of Pyk2 in mitochondrial function were performed in the hippocampus.

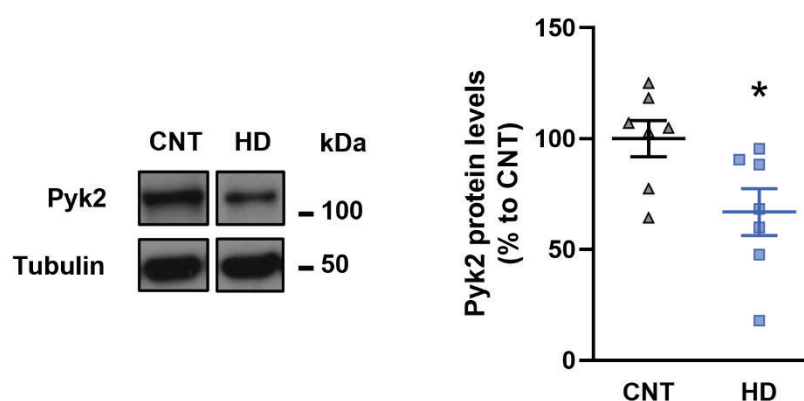


Figure 49. Protein levels of Pyk2 are reduced in the putamen of HD patients. Immunoblotting and densitometry quantification of Pyk2 (Student t-test, $t=2.484$, $df=12$; $p=0.0288$). Tubulin was used as loading control. Relative protein levels are expressed as percentage to control subjects. Data represent mean \pm SEM, $n=7$ subjects. * $p<0.05$, * $p<0.01$ vs CNT.

RESULTS

3.2. Pyk2 interacts with mitochondrial proteins in hippocampus

The physiological and molecular role of Pyk2 in the brain is not yet completely understood. We considered that the elucidation of the Pyk2 interactome could help to decipher its direct association with specific cellular processes in the brain. For that reason, Pyk2 was immunoprecipitated from hippocampus of Pyk2^{+/+} mice. Pyk2^{-/-} hippocampal material as well as IgG irrelevant antibody were included as negative controls to detect non-specific-associated proteins. First, hippocampal Pyk2 immunoprecipitation was confirmed using Western Blot (Figure 50A). Subsequent mass-spectrometry analysis was performed to identify Pyk2-associated proteins (Supplementary Table 1). Data were curated by excluding non-specific-associated proteins detected in both Pyk2^{-/-} and IgG immunoprecipitations. After restrictive curation, 52 proteins were considered as co-immunoprecipitating with Pyk2.

This Pyk2 interactome was functionally analysed using Metascape (Zhou et al., 2019). As shown in Figure 50C, multiple functional categories were significantly enriched (Supplementary Table 2). "NMDA receptor activation events" (LogP: -13,95) was represented by 34 Pyk2 associated-proteins (CALM3, CAMK2D, PRKAR2A, TUBA4A, TUBA1B, TUBB3, TUBB4A, TUBB4B, TBAL3, TCP1, GNB1, PRKCG, YWHAQ, DYNC1H1, HBA1, RPL8, RPL18, RPL23A, RPL27A, SOD2, PRDX5, ATP5F1C, SYT7, MBP, PPP3CB, UBA1, CYFIP2, ARHGAP26, ATP2B1, SRSF3, MAP1A, MAP1B, MAP4, KHDRBS1). Fifteen Pyk2 interactors were associated with "Synaptic plasticity regulation" (LogP = -8,84, MAP1A, MAP1B, PPP3CB, PRKCG, TNFR, SYT7, SYNGR1, CALM3, MAP4, TUBB3, CYFIP2, PLEC, PXN, GPI, SOD2) whereas 24 associated proteins were directly related with "calcium regulation" (LogP = -8,16, ATP2B1, CALM3, CAMK2D, GNB1, PRKAR2A, PRKCG, YWHAQ, PPP3CB, PFKL, PFKM, PXN, CTBP1, SYT7, ENO1, RAB3C, TNFR, SOD2, MAP1B, CYFIP2, TUBA4A, HBA1, PLEC, ATP5F1C, MBP). Interestingly, biofunctions such as "generation of precursor metabolites and energy" (LogP = -6,56, 17 Pyk2-associated proteins; ATP5F1C, ENO1, GPI, OXCT1, PFKL, PFKM, PLEC, SOD2, CAMK2D, PRKCG, CALM3, PRDX5, TUBA4A, DYNC1H1, SYNGR1, TUBB4B, CBR1) and "mitochondrial biogenesis" (LogP = -3,25, 6 Pyk2-associated proteins; ATP5F1C, CALM3, SOD2, PFKM, PLEC, CBR1) were also significantly over-represented in our Pyk2-interactome data. In summary, the results confirmed the main function of Pyk2 as a downstream regulator of NMDA receptor activity and synaptic plasticity, but they also highlighted a novel role of Pyk2 in the regulation of calcium homeostasis and mitochondrial function in neurons.

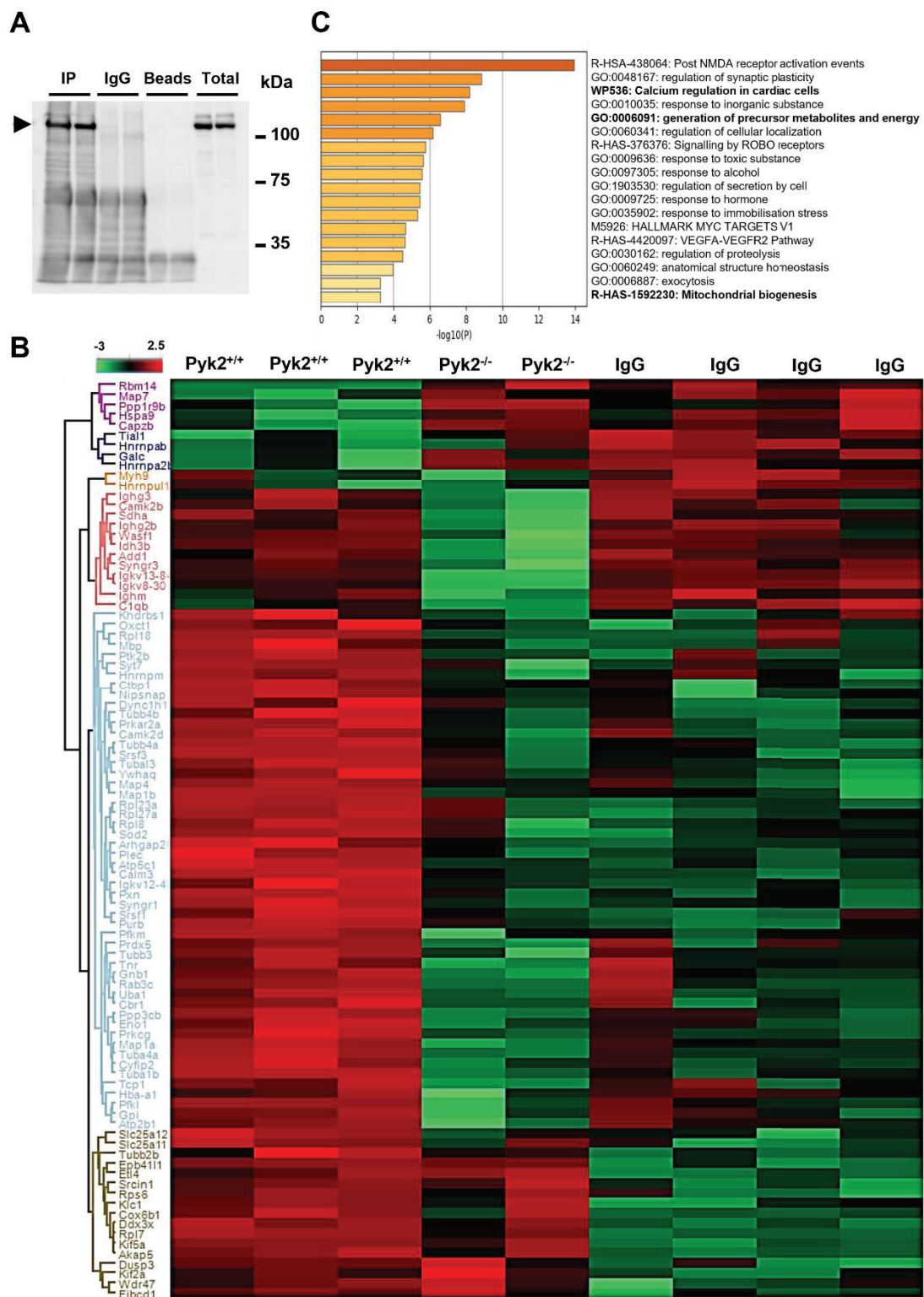


Figure 50. Molecular interactors of Pyk2 in mouse hippocampus. (A) Representative blotting of immunoprecipitation assay for Pyk2. Hippocampal tissue from adult Pyk2^{+/+} mice were used to obtain protein extracts. IgG antibodies and total lysates were added to the assay as a control of the assay and of the antibody immunoreactivity respectively. Black arrowhead indicates Pyk2 band. Molecular weight markers positions are indicated in kDa. (B) Heatmap representation showing both clustering and the intensity for the immunoprecipitated proteins in each biological condition. (C) Statistically enriched biofunctions from Pyk2 associated-proteins (from light blue cluster in B; see Supplementary Table 2 for details). In bold, gene ontology terms related to mitochondrial function.

RESULTS

3.3. Pyk2 is localised in mitochondria and MAMs

Since proteomic analysis pointed out the interaction of Pyk2 with proteins related to mitochondria and calcium signalling, we sought to study the role of Pyk2 in mitochondria. First, we performed a subcellular fractionation in hippocampal tissue of Pyk2^{+/+} mice to assess Pyk2 distribution within the cell (Figure 51). As expected, Pyk2 was detected in total, nuclear, and cytosolic fractions. Interestingly, Pyk2 was also present in isolated mitochondria. Mitochondrial fraction was validated by an enrichment of OXPHOS complex V (CoxV) compared to total lysate.

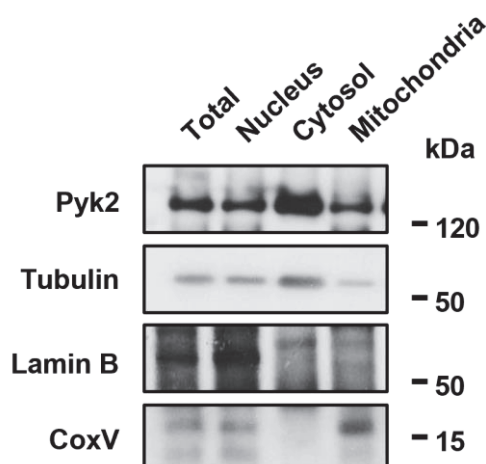


Figure 51. Pyk2 localisation at different subcellular fractions. Representative immunoblotting of Pyk2 in isolated nucleus, cytosol and mitochondria obtained from hippocampal tissue from Pyk2^{+/+} mice. Total lysate was included. Tubulin, Lamin B and CoxV were blotted to confirm the correct fractionation. Molecular weight markers positions are indicated in kDa.

To validate these findings, CA1 pyramidal neurons from Pyk2^{+/+} were processed for electron microscopy and Pyk2 was immunolabelled with gold particles. In line with the subcellular fractionation, Pyk2 positive particles were observed both in the nucleus and in the mitochondria (Figure 52A). Surprisingly, Pyk2 was detected not only inside mitochondria but also in their close contacts to ER (Figure 52A). To test method specificity of the immunogold staining procedure, the primary antibody was omitted. Under these conditions, no selective labelling was observed (Figure 52B).

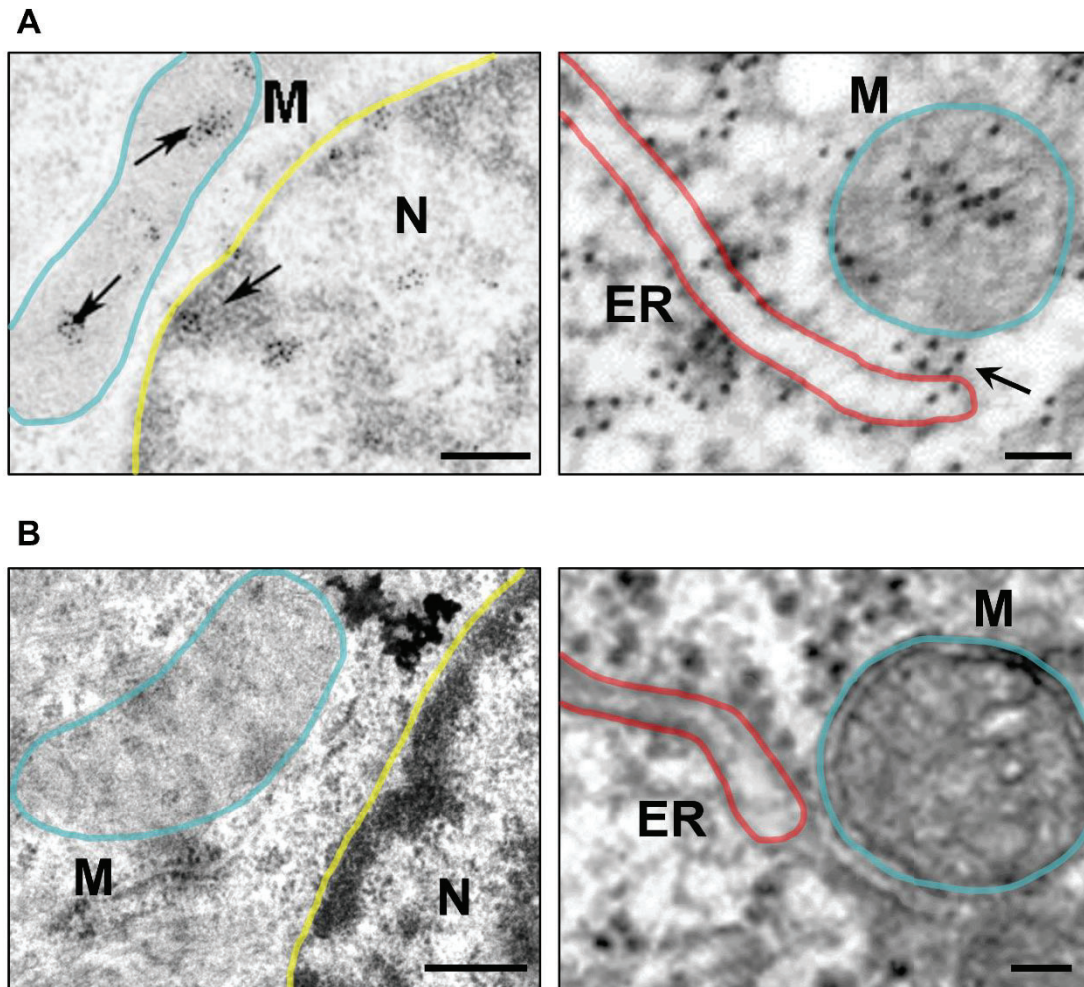


Figure 52. Pyk2 is present in mitochondria and MAMs. (A) Electron microscopy images of hippocampal neurons from *Pyk2*^{+/+} mice with Pyk2-immunogold labelling showing Pyk2 localisation inside the nucleus, the inner part of mitochondria (M), and in the ER-mitochondria contact sites. Black arrows point Pyk2 accumulation, blue lines delimit mitochondria, red lines the ER and yellow lines the nucleus. Scale bars: left panel 0.4 μm , right panel 0.06 μm . (B) Negative control without Pyk2 antibody in hippocampal sections of *Pyk2*^{+/+} mice. Scale bars: left panel 0.4 μm , right panel 0.06 μm .

RESULTS

3.4. ER-mitochondrial contact sites formation is regulated by Pyk2

Given the presence of Pyk2 in MAMs, we aimed to study the involvement of Pyk2 in the formation of contact sites between ER and mitochondria. First, we assessed levels of MAMs-resident proteins by Western blotting in hippocampal total lysates from Pyk2^{+/+} and Pyk2^{-/-} mice. Pyk2^{-/-} presented a reduction in IP3R3 levels (Figure 53B) and an increment in VDAC1 levels (Figure 53C). Thus, lack of Pyk2 induces changes in MAMs structural proteins.

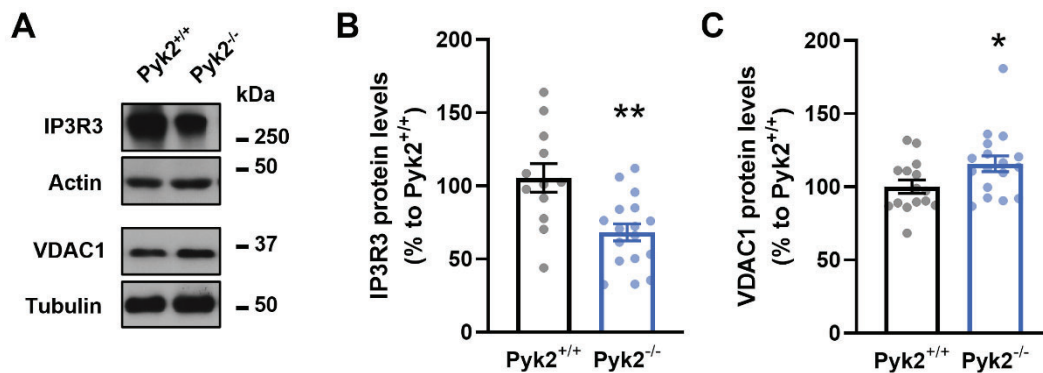


Figure 53. Levels of MAMs proteins IP3R3 and VDAC1 are altered in the hippocampus of Pyk2^{-/-} mice. (A) Representative immunoblotting of IP3R3 and VDAC1 in total lysate of hippocampus from Pyk2^{+/+} and Pyk2^{-/-} mice. (B) Densitometry quantification of IP3R3 (Student t-test, $t=3.457$, $df=27$; $p=0,0018$). Actin was used as loading control. (C) Densitometry quantification of VDAC1 (Mann-Whitney test, $A, B=189, 339$, $U=69$; $p=0,0270$). Tubulin was used as loading control. Molecular weight markers positions are indicated in kDa. Relative protein levels are expressed as percentage to Pyk2^{+/+}. Data represent mean \pm SEM, $n=12-19$ animals per group. * $p<0.05$, ** $p<0.01$ vs Pyk2^{+/+}.

To further study these organelles interaction, we examined ER-mitochondria contact sites both *in vivo* and *in vitro* in hippocampal Pyk2^{-/-} neurons. When hippocampal sections were analysed by electron microscopy, Pyk2^{-/-} neurons showed an increment in the number of MAMs compared to the Pyk2^{+/+} (Figure 54A). Similarly, ER-mitochondria contact sites were measured in hippocampal neuronal cultures using a proximity ligation assay (PLA). To this aim, IP3R3 and VDAC1 were targeted as probes for ER and mitochondria respectively. Number of MAMs, measured as interaction between targeted proteins, was augmented in Pyk2^{-/-} neurons (Figure 54B). Overall, these results suggest that Pyk2 regulates the establishment of ER-mitochondrial contact sites and absence of this protein results in a gain of contact sites.

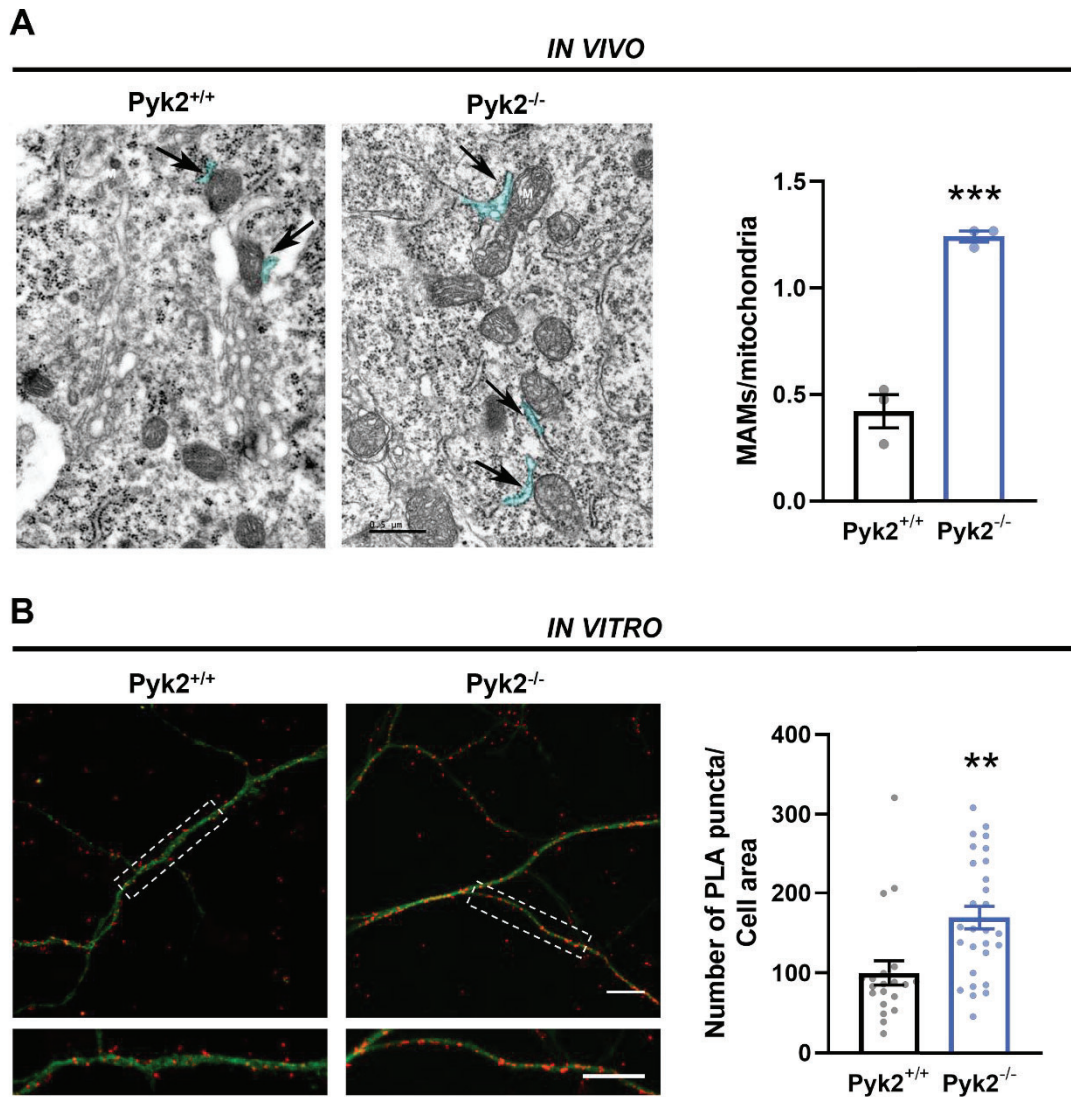


Figure 54. Absence of Pyk2 increases ER-mitochondria contact sites *in vivo* and *in vitro* hippocampal neurons. (A) In left panel, electron microscopy images of MAMs in hippocampal slices from $Pyk2^{+/+}$ and $Pyk2^{-/-}$. Black arrows indicate close ER-mitochondria contacts and blue areas delineate the counted MAM region. Scale bar, 0.5 μm . In right panel, quantification shows more MAMs per mitochondria in $Pyk2^{-/-}$ neurons (Student's t-test, $t=9.936$, $df=4$; $p=0.0006$). (B) In left panel, confocal images of VDAC/IP3R3 interaction by *proximity ligation assay* (PLA) in primary hippocampal neurons from $Pyk2^{+/+}$ and $Pyk2^{-/-}$. Interaction between targeted proteins appears in red and MAP2 in green. Scale, 10 μm . In right panel, quantification of ER-mitochondrial contact sites by PLA (Student's t-test, $t=3.307$, $df=46$; $p=0.0018$) also reveals an increment of MAMs in $Pyk2^{-/-}$ neurons. Number of PLA particles is relativized to cell area. Data represent mean \pm SEM. In **A**, 50 mitochondria from 6 different cells per genotype (3 animals per genotype) were analysed; in **B**, $n=20-28$ neurons per genotype from 3 different cultures. ** $p<0.01$, *** $p<0.001$ vs $Pyk2^{+/+}$.

RESULTS

3.5. Pyk2 is involved in ER-mitochondria calcium transfer in hippocampal neuronal cultures

MAMs are specialized regions that one of their main functions is Ca^{2+} regulation. Considering that the absence of Pyk2 exacerbates ER-mitochondrial contact sites, we aimed to explore its involvement in Ca^{2+} transfer between both organelles. Hence, we tested it with live cell imaging in primary hippocampal neurons from Pyk2^{+/+} and Pyk2^{-/-} cultures. Neurons were dyed with Fluo4 and TMRM to label Ca_i^{2+} and $\Delta\psi_m$ respectively (Figure 55A). In basal conditions, no differences in fluorescence intensity were found when comparing Pyk2^{+/+} and Pyk2^{-/-}. Then, thapsigargin (TG) was injected to inhibit SERCA activity and to deplete Ca^{2+} store in the ER. As expected, after the treatment, Pyk2^{+/+} cells increased Ca_i^{2+} levels and lowered $\Delta\psi_m$. On the contrary, in Pyk2^{-/-} neurons thapsigargin did not induce a significant increase in Ca_i^{2+} levels, either compared to Pyk2^{+/+} or to Pyk2^{-/-} in basal conditions (Figure 55B and Figure 55C). Consistent with these results, $\Delta\psi_m$ remained unchanged. Next, cells were treated with FCCP, an oxidative phosphorylation uncoupler, to induce maximal mitochondria depolarisation. Right after this stress, Ca_i^{2+} levels raised in Pyk2^{+/+} neurons (~180%) and to a lesser extent, in Pyk2^{-/-} cells (~70%). Accordingly, mitochondria depolarisation was observed in Pyk2^{+/+} neurons, manifested as a significant decrease in TMRM fluorescence (Figure 55B and Figure 55C). Since the mitochondrial calcium uptake strongly depends on the cytoplasmic calcium concentration (Szabadkai et al., 2003; Williams et al., 2013), less reduction in the $\Delta\psi_m$ of Pyk2^{-/-} neurons was detected. This effect could be attributable to the lower response to thapsigargin observed in Pyk2^{-/-} cells. Altogether this experiment demonstrates that ER depletion in the absence of Pyk2 leads to smaller cytoplasmic calcium elevation, which could be a sign of altered calcium capacity of ER in this condition.

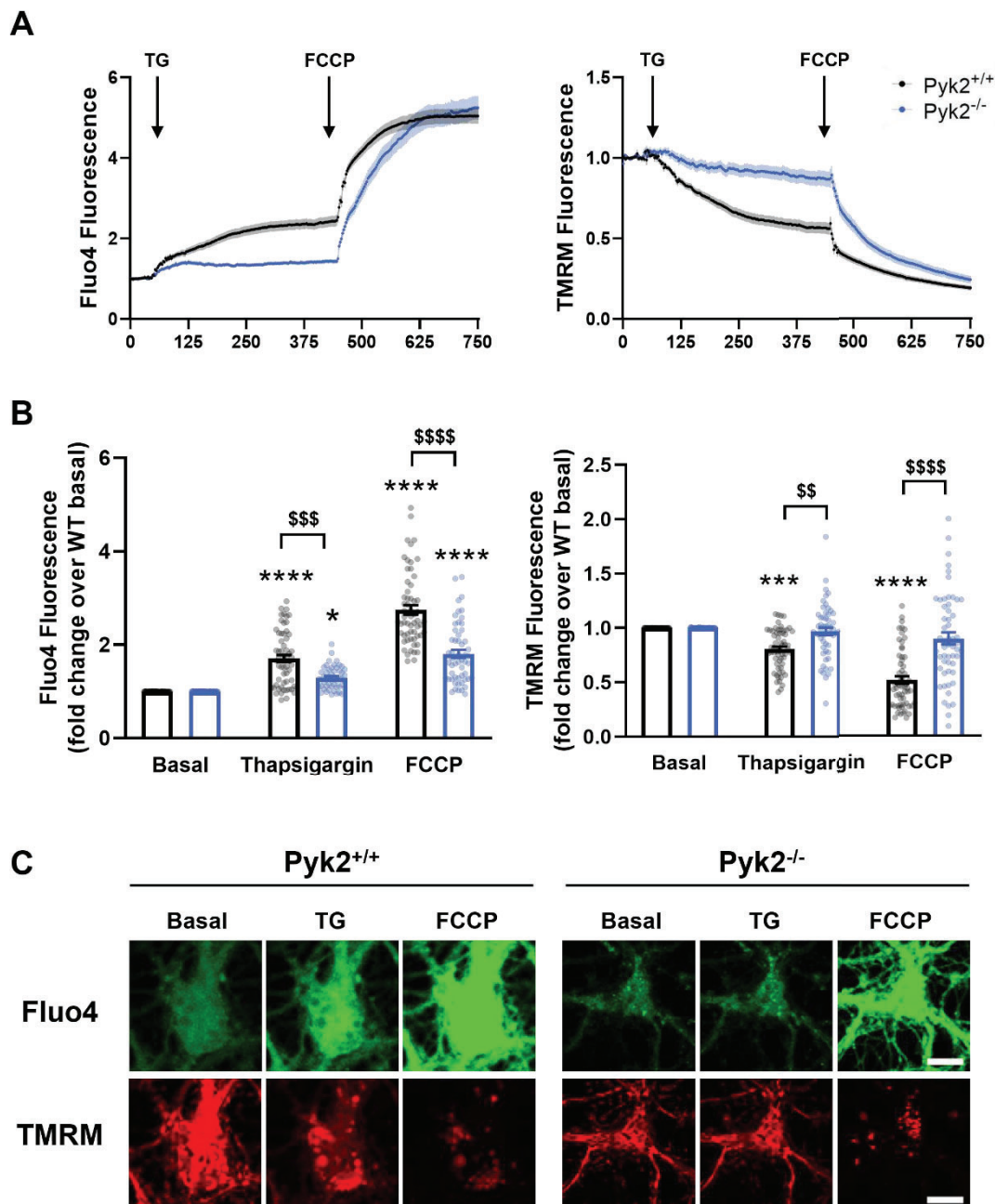


Figure 55. Lack of Pyk2 affects ER-mitochondrial calcium transfer in hippocampal neurons. Primary neurons from $Pyk2^{+/+}$ and $Pyk2^{-/-}$ mice were labelled with 5 μ M Fluo4 and 20 nM TMRM to trace intracellular calcium and mitochondrial membrane potential respectively. Cells were stimulated with thapsigargin (TG, 0.5 μ M) at 50 sec and with FCCP (2 μ M) at 450 sec. **(A)** Representative fluorescence traces of Fluo4 (left panel) and TMRM (right panel) from individual $Pyk2^{+/+}$ and $Pyk2^{-/-}$ neurons, in black and blue respectively, through the experiment. Black arrows point the addition of the treatment. **(B)** Quantification of fluorescence fold change of Fluo4 (upper panel) and TMRM (lower panel) before (basal) and after TG or FCCP treatment. Values are normalized to $Pyk2^{+/+}$ neurons in basal conditions. **(C)** Representative confocal images of Fluo4 (green) and TMRM (red) fluorescence in basal conditions and after TG and FCCP exposure. Scale bar, 10 μ m. Data represent mean \pm SEM. $n=55-62$ neurons per genotype from 4 different cultures. *** $p < 0.001$ vs basal $Pyk2^{+/+}$; \$\$\$\$ $p < 0.001$ vs $Pyk2^{+/+}$ at each condition as determined by two-way ANOVA.

RESULTS

3.6. Pyk2 regulates mitochondrial dynamics and morphology *in vivo* and *in vitro* hippocampal neurons

MAMs are highly implicated in the regulation of mitochondrial dynamics (Rowland & Voeltz, 2012b). As we have previously seen that lack of Pyk2 leads to defects in ER-mitochondria crosstalk, we wondered whether mitochondrial dynamics could also be affected. First, we evaluated levels of proteins involved in the fission and fusion events in total lysates of hippocampus Pyk2^{+/+} and Pyk2^{-/-} mice by Western Blotting. Pyk2^{-/-} mice presented increased TOM20 protein levels, indicating a higher mitochondrial mass. Moreover, Drp1 fission protein levels were also augmented in Pyk2^{-/-} (Figure 56A-C). On the other hand, levels of mitochondrial fusion proteins Opa1 and Mfn2 were not altered (Figure 56D-F) when comparing genotypes. Altogether, these findings suggest that lack of Pyk2 could induce aberrant mitochondrial fragmentation due to an increased mitochondrial fission but not decreased fusion.

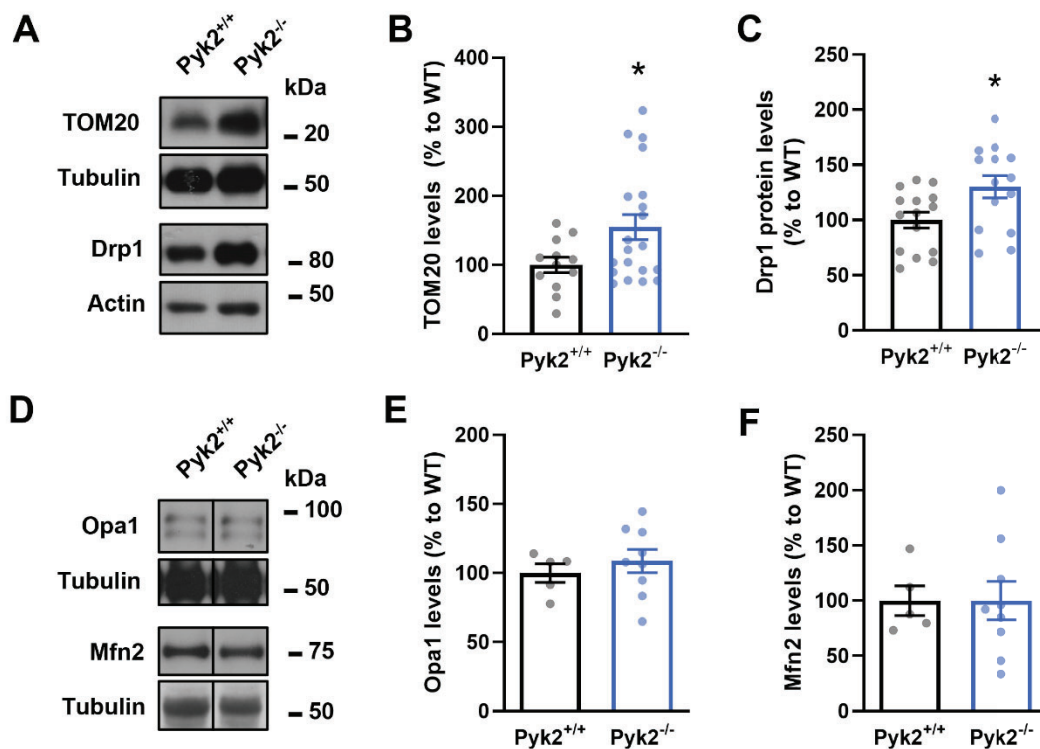


Figure 56. Levels of mitochondrial fission but not fusion are altered in hippocampus of Pyk2^{-/-} mice. Total lysates of hippocampus from Pyk2^{+/+} and Pyk2^{-/-} mice were analysed by Western Blotting. (A-C) Immunoblotting and its quantification of TOM20 (Student t-test, $t=2.175$, $df=30$; $p=0.0376$) and Drp1 (Student t-test, $t=2.455$, $df=27$; $p=0.0208$). (D-F) Immunoblotting and its quantification of Opa1 (Student t-test, $t=0.7007$, $df=12$; $p=0.4968$) and Mfn2 (Student t-test, $t=0.0009984$, $df=12$; $p=0.9992$). Actin or tubulin were used as loading control. Molecular weight markers positions are indicated in kDa. Relative protein levels are expressed as percentage to Pyk2^{+/+}. Data represent mean \pm SEM. In B and C, $n=12-20$; in E and F, $n=5-9$. * $p < 0.05$ vs Pyk2^{+/+}.

RESULTS

Next, we assessed mitochondrial morphology in CA1 pyramidal neurons from both $Pyk2^{+/+}$ and $Pyk2^{-/-}$ mice by electron microscopy (Figure 57A). $Pyk2^{-/-}$ neurons showed a rise in the number of mitochondria (Figure 57B), corroborating the previous increase in TOM20 protein levels (Figure 56A-B). In addition, morphometrical studies revealed a lowering both in Aspect Ratio (Figure 57C) and Form Factors (Figure 57D) of $Pyk2^{-/-}$ neurons, suggesting rounder and less branched mitochondria.

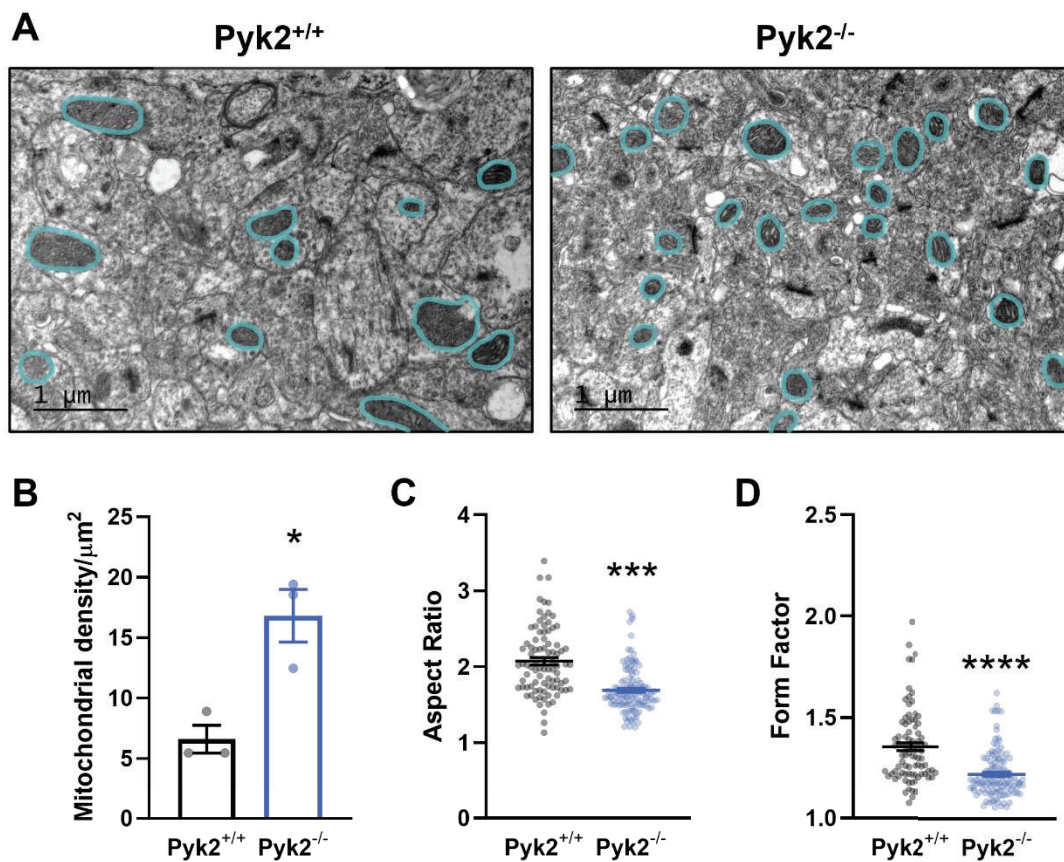


Figure 57. Increased mitochondrial fragmentation in hippocampal neurons of $Pyk2^{-/-}$ mice. (A) Electron microscopy images from hippocampal neurons from $Pyk2^{+/+}$ (left) and $Pyk2^{-/-}$ (right) mice. Blue lines delimit mitochondria. Scale bar, 1 micron. $Pyk2^{-/-}$ neurons showed higher (B) mitochondrial density (Student t-test, $t=4.136$, $df=4$; $p=0.0144$), less (C) Aspect Ratio (Mann-Whitney test, $A, B=11883, 9438, U=2298$; $p<0.0001$), and less (D) Form Factor (Mann-Whitney test, $A, B=11353, 9353, U=2332$; $p<0.0001$). Data represent mean \pm SEM from three different animals per genotype. * $p<0.05$, *** $p<0.001$, **** $p<0.0001$ vs $Pyk2^{+/+}$. In B, each point represents the mean of each animal ($n=3$). In C and D, each point represents each mitochondrion ($n=87-119$).

RESULTS

Moreover, we studied mitochondrial morphology in primary hippocampal neurons. Neuronal cultures were immunolabeled with TOM20 and MAP2 in green and red respectively morphometrical analysis were applied. In line with the *in vivo* experiments, *Pyk2*^{-/-} neurons presented excessive mitochondrial fragmentation as revealed by a higher number of mitochondria together with a reduction in length and branching, as indicated by lower values of Aspect Ratio and Form Factor (Figure 58). Overall, both our *in vivo* and *in vitro* models show that absence of *Pyk2* in neurons result in more mitochondria, with a less elongated and complex shape.

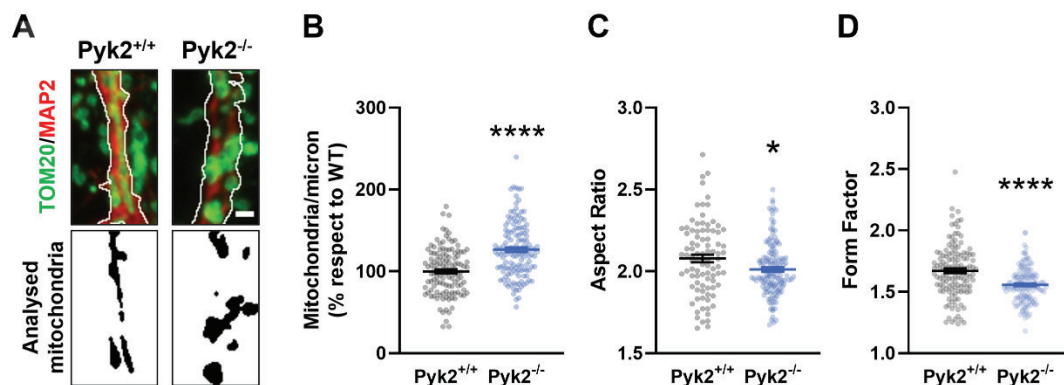


Figure 58. Mitochondrial morphology is altered in primary hippocampal *Pyk2*^{-/-} neurons. (A) Confocal images of primary hippocampal neurons from *Pyk2*^{+/+} and *Pyk2*^{-/-} embryos were immunolabeled with TOM20 in green and MAP2 in red (upper panel). White lines delimit the analysed region of the neurites. In the lower panel, correspondent binary image with the analysed mitochondria in black with white background. Scale bar, 1 μ m. *Pyk2*^{-/-} neurons presented increased (B) number of mitochondria per micron of neurite (Student t-test, $t=6.834$, $df=258$; $p<0.0001$), lower (C) Aspect Ratio (Mann-Whitney t-test, $A, B=11659, 14906, U=5036$; $p=0.0101$) and lower (D) Form Factor (Mann-Whitney t-test, $A, B=2056, 15748, U=5878$, $p<0.0001$). Data are means \pm SEM of 15-20 neurons from 8 different embryos per genotype ($n=128-140$). Each point represents the mean of all mitochondria in each neuron. * $p<0.05$, **** $p<0.0001$ vs *Pyk2*^{+/+}.

3.7. Nuclear translocation and location domains of *Pyk2* control dynamics of hippocampal mitochondria

To deepen the molecular mechanisms underlying mitochondrial regulation by *Pyk2*, we transfected hippocampal primary neurons with several truncated forms of GFP-*Pyk2*: DFAT, YF, and RST (Figure 59A). Mutated constructs were compared with GFP transfected cells both from *Pyk2*^{+/+} and *Pyk2*^{-/-} cultures. As expected, restoration of *Pyk2* levels in hippocampal *Pyk2*^{-/-} neurons recovered number of mitochondria (Figure 59B-C). Likewise, *Pyk2*^{-/-} neurons transduced with DFAT and YF constructs also rescued the

RESULTS

number of mitochondria. Interestingly, RRST construct was unable to recover this parameter showing the same phenotype as the one in *Pyk2*^{-/-} neurons only transfected with GFP (Figure 59B-C). These findings suggest that the corresponding motifs in the *Pyk2* protein (RR_{184,185}, and/or S₇₄₇-T₇₄₉) are directly involved in the role of *Pyk2* in mitochondria, for instance in the binding of specific partners, or that the effects of *Pyk2* on mitochondria indirectly demands the nuclear translocation of *Pyk2* that is prevented in the RRST mutant (C. Faure et al., 2007; Giralt et al., 2017).

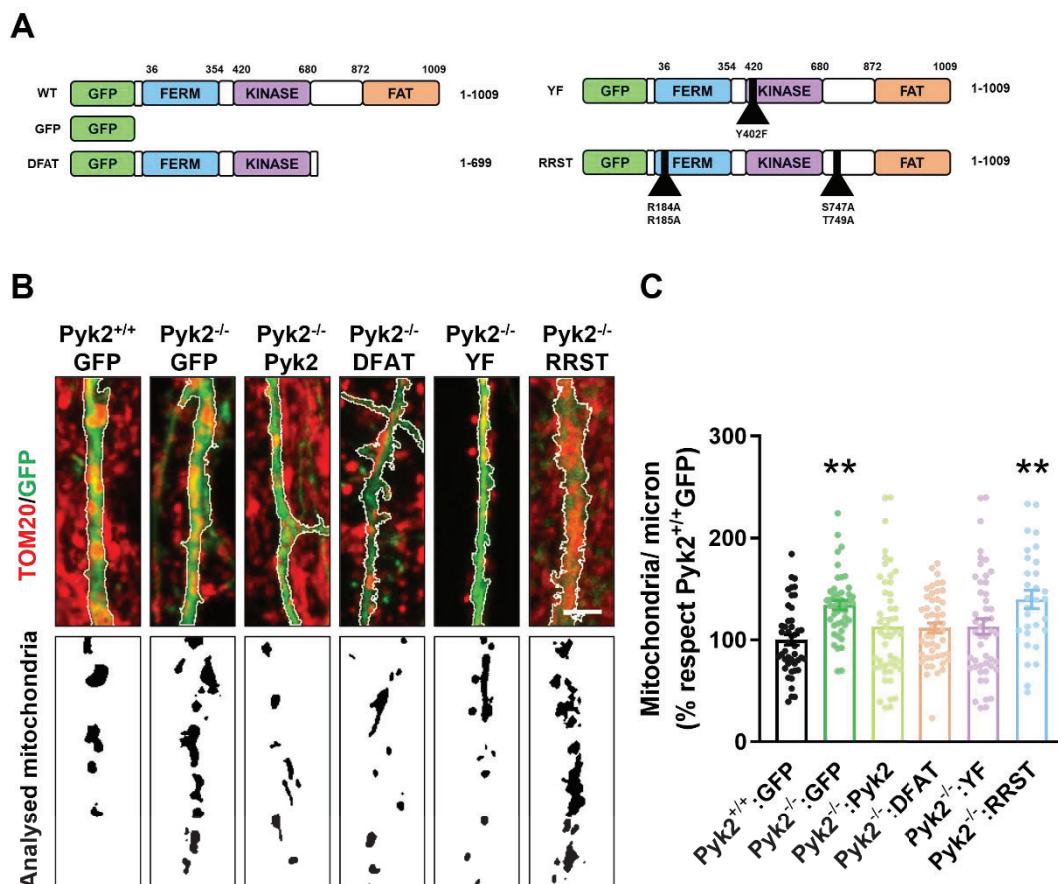


Figure 59. Mechanisms of *Pyk2*-dependent modulation of mitochondrial density. Primary hippocampal neurons from *Pyk2*^{+/+} and *Pyk2*^{-/-} mice were transfected with different constructs. (A) Schematic representation of the plasmids used: *Pyk2*, GFP, DFAT (*Pyk2* without the entire FAT domain), YF (*Pyk2* with a point mutation in the tyrosine 402 residue for an alanine) and RRST (with four-point mutations in the import/export nuclear domains called R_{184A}, R_{185A}, S_{747A} and T_{749A}). (B) Neurons were immunolabelled with TOM20 in red and GFP expressed by the plasmids appears in green (upper panel). Correspondent binary images of the analysed mitochondria in black with white background (lower panel). Scale bar, 3 μ m. (C) Quantification of number of mitochondrial in neurons transfected with the different constructs in A and B (one-way ANOVA, $F_{(5, 258)}=4.881$, $p=0.0003$). Tukey's multiple comparisons test was used as a *post hoc*. Data are means \pm SEM of 7-10 neurons from 4 different cultures per genotype ($n=30-40$). Each point represents the mean of all mitochondria in each neuron. ** $p<0.01$ vs *Pyk2*^{+/+}: GFP group.

RESULTS

In an attempt to assess this possible translocation of Pyk2 into the mitochondria, Pyk2^{+/+} hippocampal neurons were treated with 40 μ M glutamate for 15 min. Neurons were immunolabeled with Pyk2 and observed by electron microscopy to analyse particle distribution. Notably, after glutamate treatment, density of Pyk2 particles in mitochondria increased, supporting the idea of a translocation of Pyk2 into the mitochondria upon neuronal activation (Figure 60).

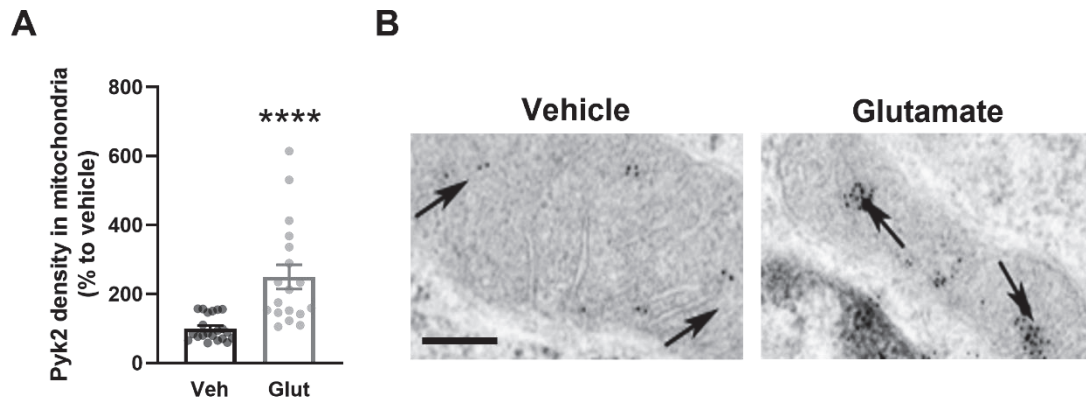


Figure 60. Pyk2 translocates to mitochondria upon neuronal activity. Neurons from primary hippocampal cultures of Pyk2^{+/+} mice were treated with vehicle or glutamate for 15 min. **(A)** Quantification of density of Pyk2 particles relative to vehicle group (Mann-Whitney test, A, B=271, 259, U=40; $p < 0.0001$). **(B)** Electron microscopy images showing Pyk2 presence inside the mitochondria. Black arrows indicate gold particles of Pyk2 antibody after vehicle (left) or glutamate (right) treatment. Scale bar, 0.1 μ m. Data represent mean \pm SEM from 7 different neuronal cultures (n=21-20 neurons per group). **** $p < 0.0001$ vs Veh.

DISCUSSION

The earliest description of mitochondria as intracellular structures was reported by Richard Altmann in 1890 (Altmann, 1890). They were first named as “bioblast” since they were perceived as “elementary organisms” living inside cells in control of vital functions. Later in 1898, Carl Benda coined the term mitochondrion composed by the Greek words “mitos” (threads) and “chondros” (granule) to describe the appearance of the organelles (Benda, 1898; Ernster & Schatz, 1981). This brief historical view highlights the relevance of mitochondrial morphology that recent research has supported showing how fundamental are mitochondrial dynamics to regulate these organelles’ shape and enable the proper distribution and function (Giacomello et al., 2020). In this Thesis, we aimed to deeply understand the mechanisms controlling mitochondrial dynamics and how the presence of mHtt disrupts these events, leading to detrimental consequences for striatal neural cells. In particular, we focused on the study of ER-mitochondria interactions, the transfer of extracellular mechanisms and the regulation of mitochondria by Pyk2.

1. ROLE OF MITOCHONDRIAL DYNAMICS AND MAMs IN HD STRIATAL NEURONAL VULNERABILITY

Mitochondrial dysfunction is a common phenomenon in many neurodegenerative diseases, including HD. In the current work, we proved that R6/1 striatal neurons displayed exacerbated mitochondrial fragmentation, meaning more mitochondria with less elongated and complex shape. Similarly, previous studies from our group and others in HD cellular and mouse models have shown rounder mitochondria as a result of increased mitochondrial fission events (Cherubini et al., 2015; X. Guo et al., 2013; Naia et al., 2021; Reddy, 2014). Additionally, mitochondria from *post-mortem* caudate are smaller at grades 2 and 4 of HD compared to control subjects (J. Kim et al., 2010). Nonetheless, these alterations were no further found in cortical or hippocampal R6/1 neurons, suggesting that are dependent on brain region. A possible explanation is that striatal mitochondria are more susceptible to mHtt toxicity due their intrinsic properties. Particularly, striatum from WT mice show higher OXPHOS activity and more mitochondrial mass than cortex or hippocampus (Pickrell et al., 2011), causing more affection to OXPHOS dysfunction in the striatum than other brain areas. In addition, mitochondria from striatal neurons are less motile and more prone to divide than their counterparts in the cortex (Guedes-Dias et al., 2015). Thus, striatal neurons may be especially vulnerable to mHtt toxicity because of the brain-dependent heterogeneity in mitochondrial functions.

DISCUSSION

Moreover, we reported for the first time a loss of ER-mitochondria contact sites in HD striatal neurons. Later research from Rego's group confirmed this finding in striatal neurons of the HD mouse model YAC128, showing less ER-mitochondria interaction sites as well as reduced organelles' colocalization. In addition, they showed the decreased expression of Sigma-1 receptor, a chaperone enriched in MAMs, that hampered the formation of ER-mitochondria contact sites in the presence of mHtt (Naia et al., 2021). Overall, we suggest that mitochondrial proneness to undergo fragmentation could lead to the disruption of MAMs in HD striatal neurons.

However, increased mitochondrial fission may not be the only mechanism involved in this loss of ER-mitochondria interaction. Hence, we hypothesised that reduction of MAMs anchoring proteins could affect communication between both organelles. MAMs are compartments enriched in specific proteins as Grp75, IP3R3 and Mfn2 that enable ER-mitochondria tethering and facilitate the calcium efflux in this hotspot. Our results showed a substantial decrease of Grp75, IP3R3 and Mfn2 in *post-mortem* putamen of HD patients. Moreover, these three proteins were also diminished at middle stages of the disease in two mouse models, the R6/1 and knock-in HdhQ111. Although it does not seem an early event, we suggest that reduction of MAMs proteins could be not only a consequence of striatal degeneration but also a contributor to the HD progression. Indeed, it has been described that mHtt directly binds IP3R1, another IP3R isoform present at the MAMs, and that blockage of this interaction *in vivo* in YAC128 mice can regulate abnormal calcium signalling, reducing MSN neuronal loss and rescuing deficits in motor coordination (Tang et al., 2004, 2009). In addition, Naia et al. recently showed a drop in IP3R3 expression in HD striatal neurons (Naia et al., 2021).

Conversely, the evaluation of these MAMs proteins in other brain regions affected in the HD as cortex and hippocampal revealed no alterations in protein levels neither in human samples nor murine models. As previously discussed, this contrast between brain areas may be caused by the differential susceptibility of striatal mitochondria. Since no comparative study on MAMs proteins in the brain is available, is hard to further discuss this outcome. Nevertheless, MAMs are tightly related to calcium homeostasis and it is known that HD striatal mitochondria are more sensitive to Ca²⁺ overload than their counterparts in the cortex (Brustovetsky et al., 2003). Hence, selective decrease of MAMs protein related to Ca²⁺ efflux may partially explain the sensitivity of MSN to degenerate in the presence of mHtt.

DISCUSSION

One of the limitations of our investigation is that biochemical studies were performed in total brain lysates and reduction of these proteins cannot be exclusively attributed to neurons. Moreover, although enriched in MAMs, these proteins are expressed in other subcellular compartments as cytosol, ER or mitochondria. To accurately study protein levels in these microdomains, we isolated MAMs fraction from mouse striatum (data not shown in this Thesis). Despite some tendency to diminished levels of Grp75, IP3R3, Mfn2 and Sigma-1 receptor in R6/1 striatum, we could not validate these results because of lack of a proper MAMs loading control. Thus, further research should address the identification and development of exclusive markers of the MAMs portion, that could improve the understanding of interaction between ER and mitochondria.

Considering the alterations observed in MAMs integrity, we supposed that disruption of ER-mitochondria coupling contributed to Ca^{2+} mishandling in HD striatum. Notably, our cultured HD neurons exhibited alterations in Ca^{2+} efflux between organelles, suggesting an impaired mitochondrial calcium uptake. In accordance, defective mitochondrial Ca^{2+} homeostasis has been previously described in HD striatum (Milakovic et al., 2006; Naia et al., 2017; Rosenstock et al., 2010). Additionally, a study in a PD model of *Drosophila* proved that disturbances in ER-mitochondria contacts interfered in mitochondrial calcium regulation, contributing to neurodegeneration (K. S. Lee et al., 2018).

Regarding the explanation for mitochondrial calcium mishandling in HD striatum, initial investigation only pointed out the higher mitochondrial sensitivity to Ca^{2+} loads (Brustovetsky et al., 2003; Choo et al., 2004; Milakovic et al., 2006). Indeed, mitochondria isolated from HD striatal cells and knock-in mice showed that mHtt reduced the Ca^{2+} threshold necessary to induce mPTP (Choo et al., 2004). Moreover, Panov et al. reported that isolated mitochondria from lymphoblasts from HD patients as well as from YAC mice brains displayed lower $\Delta\psi_m$ and less calcium capacity than those from healthy subjects or WT mice (Panov et al., 2002). Conversely, other authors proved that isolated brain mitochondria from HD transgenic mice displayed enhanced mitochondrial capacity of Ca^{2+} uptake (Oliveira et al., 2007; Pellman et al., 2015). These discrepancies might be due to the loss of interactions with other organelles as ER since all these experiments were performed in isolated mitochondria, losing the appropriate context. On the other side, our and other findings performed in intact neurons propose that mitochondrial Ca^{2+} mishandling could be attributed not only to disruption of intrinsic mitochondrial properties but also to MAMs formation (Jung et al., 2020; K. S. Lee et al., 2018).

DISCUSSION

Among all proteins involved in mitochondrial dynamics, Drp1 is one of the key factors in remodelling mitochondria shape and it has been widely studied. It has been reported in several HD cell and mouse models that Drp1 protein levels and activity are increased (Cherubini et al., 2015; Costa et al., 2010; Manczak & Hemachandra Reddy, 2015). Moreover, samples of *post-mortem* caudate from HD patients show increased Drp1 protein levels throughout the disease along with a reduction of Mfn1 at grade 3 and grade 4 of HD (J. Kim et al., 2010). Interestingly, striatum of grade 3 HD patients presented higher protein levels of Drp1 compared to cerebellum whereas in control patients, levels were similar between brain areas, indicating that HD striatum is especially susceptible to alterations in mitochondrial dynamics (Shirendeb et al., 2011).

Since mHtt can bind Drp1 and enhances its GTPase activity (Song et al., 2011), we hypothesised that excessive Drp1 activity could mediate the alterations in mitochondrial morphology and interactions with ER previously discussed. To test this, we treated R6/1 neurons with Mdivi-1 (*mitochondrial division inhibitor*), a well-known pharmacological Drp1 inhibitor (Cassidy-Stone et al., 2008) that reduces the number of mitochondria in WT cells (Manczak & Hemachandra Reddy, 2015). In our hands, inhibition of Drp1 in R6/1 neurons not only restored the excessive mitochondrial fragmentation but also prevented the loss of ER-mitochondria apposition. This outcome demonstrated that aberrant mitochondrial fission is mediating ER-mitochondria tethering.

Additionally, Mdivi-1 treatment in HD striatal cell line prevented from increased oxidative stress and less cell viability induced by mHtt (Manczak & Hemachandra Reddy, 2015). Likewise, we observed that mitochondrial oxidative stress derived from mHtt was restored in R6/1 primary neurons. These results are in line with other findings in primary neuronal cultures that showed how reduction of ROS after Mdivi-1 was partially due to the increment of the activity of antioxidant enzymes superoxide dismutase and catalase (J. M. Liu et al., 2015). Finally, Mdivi-1 treatment in our HD cultured neurons restored ER-mitochondria Ca^{2+} transfer, ameliorating the limited mitochondrial capacity of Ca^{2+} buffering. Accordingly, Mdivi-1 treatment in excitotoxicity neuronal models proved to protected against toxic activation of NMDA and restored mitochondrial Ca^{2+} homeostasis capacity (Ruiz et al., 2018). Hence, we pose that mitochondrial fragmentation in HD neurons contributes to the loss of ER-mitochondrial interaction and hampers Ca^{2+} efflux.

Besides cell cultures, Mdivi-1 has been used *in vivo* in mouse models of neurodegeneration. Intraperitoneal administration of Mdivi-1 proved to be neuroprotective in two different mouse models of PD, preventing motor function deficits, neurodegeneration and mitochondrial dysfunction and altered morphology in synaptic

terminals (Bido et al., 2017; Rappold et al., 2014). In turn, Mdivi-1 also showed protective effects in neurons from AD mice, both *in vitro* and *in vivo*, improving disruption of mitochondrial dynamics and cognitive deficits (W. Wang et al., 2017). To date, Mdivi-1 has not been tested in HD animals. However, R6/2 mice have been treated with another Drp1 inhibitor, P110-TAT with systemic subcutaneous administration. Treated HD mice displayed reduced neurological defects and improvement of mitochondria function along with amelioration of HD neuropathology, as loss of MSN and intracellular Htt aggregates (X. Guo et al., 2013). Altogether, pharmacological inhibition of Drp1 brings promising results for the treatment of neurodegenerative diseases, including HD. However, further research would be needed before proposing Mdivi-1 as a feasible therapeutic strategy such as toxicological profile, pharmacokinetics and chronic treatments.

Overall, in the first study of this Thesis we have proved that the presence of mHtt in striatal neurons increases the activity of Drp1, promoting mitochondria to undergo fragmentation. As a result of disturbances in the mitochondrial network, these organelles are misplaced and lose their contacts with the ER, hampering the correct transfer and homeostasis of calcium (Figure 61). Lastly, we propose that these mechanisms are specific altered in the striatum of HD, contributing to the selective vulnerability that occurs in this disease.

2. CONTRIBUTION OF ASTROCYTIC MITOCHONDRIA TO STRIATAL VULNERABILITY IN HD

Despite that major neuropathological feature in HD is the selective loss of MSN, mHtt also affects the function of other neural cells in the striatum. Indeed, astrocytes are the second most prevalent cell type in mouse striatum (Gokce et al., 2016) and many investigations have implicated the pathology of astrocytes as contributors to the preferential striatal neuronal degeneration that occurs in HD (Benraiss et al., 2016, 2021; Khakh et al., 2017; Osipovitch et al., 2019; Wilton & Stevens, 2020).

Growing evidence point out the striking heterogeneity in astrocyte population not only morphological but also molecular and functional (Chai et al., 2017; Escartin et al., 2021). Hence, recent efforts have focused on purified astrocytes from mouse brain and establishing specific expression patterns for different brain regions (Al-Dalahmah et al., 2020; Diaz-Castro et al., 2019; Duran et al., 2019). However, molecular signatures

DISCUSSION

extracted from single-cell RNA studies should be validated from a functional perspective in mouse models, such as combination of cell markers.

To this aim, we examined expression of several astrocyte markers in the striatum of WT and R6/1 mice: ALDH1L, GFAP, S100 β and GLAST. Of them, we propose ALDH1L1 as the most reliable marker for striatal astrocytes since it remained unchanged with aging in WT mice. In accordance with this, other authors also proposed ALDH1L1 as a pan-astrocytic marker homogeneously expressed in the brain that widely distributes within the cell (Mudannayake et al., 2016; Yongjie Yang et al., 2011), in contrast to GFAP, that only labels about 15% of the total cell area (Bushong et al., 2002). Moreover, neither protein levels nor distribution of ALDH1L1 were modified at any stage of the disease in R6/1 striatum, suggesting no major changes in the mass population of astrocytes.

Concerning S100 β , although it is not exclusively expressed in astrocytes (Matias et al., 2019; Sofroniew & Vinters, 2010), it is generally related as a marker for astrocyte maturation (Al-Dalahmah et al., 2020; Escartin et al., 2021). In our R6/1 mice, S100 β protein levels and expression remained unchanged compared to WT. Similarly, previous published analysis by immunofluorescence in the striatum of knock-in HD mice showed no differences in S100 β expression compared to WT mice (Brown et al., 2021), which might be interpreted as no alterations in astrocyte's maturation in the HD striatum.

Regarding GLAST, we confirmed a drop in protein levels at middle stages of HD in the striatum of R6/1 while at early and advance stages remained unchanged. These results corroborate previous findings showing decreased expression of GLAST in HD mouse brains only at middle but not at early stages (Estrada-Sánchez et al., 2009; Faideau et al., 2010). Similarly, the other astrocytic glutamate transporter GLT-1 displayed lowered expression and function in brain samples of mouse models and HD patients (Bradford et al., 2009; Estrada-Sánchez et al., 2009; Liévens et al., 2001; Shin et al., 2005). As a matter of fact, restoration of GLT-1 levels in symptomatic R6/2 mice ameliorated HD-related behavioural and motor deficits (B. R. Miller et al., 2008). Moreover, cultured R6/2 astrocytes conferred less protection to striatal neurons against glutamate toxicity than WT astrocytes (Shin et al., 2005). Consequently, the reduction of glutamate transporters directly impacts in the glutamate uptake by the astrocyte, which accumulates at the extracellular space and reduces neuroprotection against excitotoxicity, thus contributing to loss of striatal neurons in HD (Estrada-Sánchez et al., 2009).

Despite it has been the marker of choice for reactive astrocytes for many years, GFAP labels an heterogeneous population with region-dependent expression (Y. Lee et al., 2008; Saba et al., 2020; Sofroniew & Vinters, 2010; Walz & Lang, 1998). In the striatum,

DISCUSSION

GFAP is scarcely expressed and only in a limited number of astrocytes (Gokce et al., 2016; Khakh, 2019; Saba et al., 2020), highlighting that it is not a robust striatal marker for astrocytes and the identification of others may be needed. In *post-mortem* striatum of HD patients, astrogliosis manifested as an increment of astrocytes is detected as early as Vonsattel grade 1 (J. P. Vonsattel et al., 1985; J. P. G. Vonsattel & Marian, 1998). Contrary to these findings, not all HD genetic mice recapitulate this phenotype although dysfunction of astrocytes still occurs (Mangiarini et al., 1996; Tong et al., 2014). In line with this hypothesis, we did not report an increment in GFAP in striatal astrocytes of R6/1 mice. Similarly, striatum of R6/2 at symptomatic stages did not show changes in GFAP protein levels, number of cells, cell area or processes (Tong et al., 2014).

In contrast, generation of HD mouse models using lentiviral vectors (Htt171-82Q) reproduced a loss of MSN along with a progressive phenotype of reactive astrocytes with increased GFAP expression, similar to the observed in HD patients (Ben Haim et al., 2015; Faideau et al., 2010). However, in these studies they considered the number of positive cells for GFAP while mRNA or protein levels were not quantified. These same authors suggested that prevention of astrogliosis by inhibition of the JAK/STAT3 pathway in the striatum of HD mouse reduced the HD neuropathology as mHtt aggregates and neuronal death (Ben Haim et al., 2015). A possible explanation to this discrepancy might be the methodological approach of HD mouse model generation and which parameters are used to analyse reactive astrocytes.

Following the evaluation of signs of astrogliosis, we analysed the astrocyte's morphology in primary HD cultures. R6/1 astrocytes expressing GLAST showed larger cell area compared to WT indicating a hypertrophy, a distinct trait of reactive astrocytes (Escartin et al., 2021), while cells positive for GFAP did not. This could be due to the limited detection of GFAP labelling, that withhold engrossment of fine processes or soma of the HD cells. In sum, our results do corroborate astrogliosis although highlight that the rise of GFAP may not be the most reliable feature of astrocyte activation in HD striatum since it occurs in many but not necessary all reactive astrocytes.

To widen the analysis of astrogliosis, several parameters must be into consideration as morphology, proliferation, cell signalling and proteome (Escartin et al., 2021). Hence, current understanding of astrocytes is shifting towards different states of reactivity depending on the context rather than all-or-none phenomenon (Sofroniew & Vinters, 2010). All things considered, we and others propose that the most accurate approach to explore astrocytes' phenotype in the mouse striatum is a combined panel with several markers rather than focusing on a single protein.

DISCUSSION

While neurons mostly rely on mitochondrial oxidative phosphorylation (OXPHOS) for their metabolism, astrocytes preferentially present a more glycolytic profile (Bolaños, 2016; Supplie et al., 2017). Nonetheless, mitochondrial function in astrocytes can be affected either directly by pathogenic factors or as result of astrogliosis, leading to overworked mitochondria (Gollihue & Norris, 2020). When evaluating mitochondrial metabolism, we found an increment in mitochondrial respiration in HD astrocytes. We hypothesise that these mitochondrial hyperactivation could be triggered to meet energetic demands of hypertrophied R6/1 astrocytes. In contrast to our findings, primary cortical astrocytes of YAC128 mice showed impaired mitochondrial respiration, both basal and maximal capacity respiration (Ehrnhoefer et al., 2018). This inconsistency may be due to differences in the studied brain region.

Moreover, others authors have recently posed the evaluation of glucose, pyruvate, and lactate as functional signals of astrogliosis (Escartin et al., 2021; Lerchundi et al., 2020; Mächler et al., 2016). In our hands, cultured R6/1 astrocytes produced higher levels of lactate. Lactate is the result of glucose utilization by astrocytes during glycolytic metabolism, suggesting that a rise of lactate levels could be related to an increment in glycolysis. It is encouraging to compare these results with previous findings from magnetic resonance spectroscopy in the brain of HD symptomatic patients, that indicated a gain in lactate content, which authors of that study related to alterations in mitochondrial function and brain energy metabolism in HD (Martin et al., 2007). This raise in lactate production may also be seen as a signal of astrogliosis in the HD striatum.

In agreement with this idea, previous literature reported that augmentation of glycolytic enzymes such as aldolase C (ALDOC) could be potential markers for reactive astrocytes (Halford et al., 2017; Levine et al., 2016). Indeed, STAT3, a regulator of the switch between OXPHOS and glycolysis, has been described to increase expression of GFAP and ALDOC during response of reactive astrocytes (Levine et al., 2016). Moreover, STAT3 pathway is activated in striatal astrocytes of HD mice as well as in human putamen of HD patients (Abjean et al., 2022; Ben Haim et al., 2015), reinforcing the link between a boost in glycolysis and astrogliosis. In turn, modulation of STAT3 pathway in astrocytes ameliorated striatal atrophy, glutamate levels, mHtt aggregates in neurons and reactivity of astrocytes (Abjean et al., 2022; Ben Haim et al., 2015). Altogether, since astrocytic and neuronal metabolisms are interconnected, it is feasible to postulate that alterations in the metabolism of striatal astrocytes could impact in function and survival of MSN, contributing to the neuronal vulnerability of the striatum in HD.

DISCUSSION

The expected interpretation of the augmented mitochondrial metabolism in HD striatal astrocytes would be an increment in mitochondrial mass. However, measurement of mitochondrial mass and number using different approaches revealed no differences between WT and R6/1 astrocytes. Moreover, we evaluated mitochondrial functionality in isolated striatal astrocytes. The absence of loss of $\Delta\psi_m$ in R6/1 astrocytes broadly supports the idea that alterations in mitochondria are not due to a hypofunction. Similarly, primary astrocytes from YAC128 mice presented levels of $\Delta\psi_m$ comparable to WT animals (Ehrnhoefer et al., 2018). Because of dearth of results addressing mitochondrial functionality in HD striatal astrocytes is hard to further discuss this outcome. However, the combination of different techniques brings robust proofs that mitochondrial mass is not altered in the bulk of HD striatal astrocytes and reinforces the boost in mitochondrial respiration in R6/1 astrocytes.

Since changes in mitochondrial function may impact on their dynamics, we wondered whether mitochondrial fusion and fission events could be disrupted in R6/1 striatal astrocytes. In accordance with our previous findings in HD neurons (Cherubini et al., 2015), Drp1 and Cdk5 were augmented in astrocytes from adult R6/1 mice. This increment in proteins related to mitochondrial fission suggests a shift in mitochondrial dynamics towards fission that may be interpreted as a strategy to dissipate energy through the constant division of these organelles. Nevertheless, an issue that was not addressed in this study was whether mitophagy was also enhanced in HD astrocytes. It is likely that, as mitochondrial fission is enhanced but number and mass of mitochondria are not altered in the bulk of astrocytes, mechanisms for mitophagy would also be incremented. Further research should be undertaken to investigate this possibility.

Lastly, we evaluated mitochondrial morphology in astrocytic cultures using GLAST and GFAP as astrocyte markers. In those astrocytes only expressing GLAST, no alterations in mitochondrial area or branching were detected between genotypes. On the contrary, those R6/1 astrocytes also expressing GFAP showed less mitochondrial area along with increased branching. Similarly, altered ultrastructure of mitochondria was reported in astrocytes from brains of juvenile HD patients (Goebel et al., 1978; Oliveira, 2010). This similarity may be explained by the use of GFAP in the identification of astrocytes in *post-mortem* samples. Another possible explanation for this phenomenon is that those astrocytes expressing GFAP are in a higher reactivity state and mitochondrial morphology results disrupted.

Overall, we have demonstrated a boost in the metabolism along with alterations of proteins involved in mitochondrial fission. Together with the above-mentioned cell

DISCUSSION

hypertrophy, we propose the hyperactivation of mitochondrial respiration as well as the disruption of mitochondrial dynamics as new functional indicators of astrogliosis in HD striatum. Whether the role of astrogliosis in HD progression represents a gain of detrimental or protective functions remains a matter of discussion. It has been reported that both situations may occur simultaneously and that final impact will depend on the astrocyte subpopulations newly acquired or lost and their correspondent function (Escartin et al., 2021; Khakh & Sofroniew, 2014; Palpagama et al., 2019).

The last aim of this study was to evaluate whether mitochondria from HD astrocytes could be transferred to striatal neurons and what was the effect. Intercellular mitochondrial transfer has been described as a mechanism of tissue homeostasis and rescue of damaged cells both in health and disease (reviewed in (D. Liu et al., 2021; Shanmughapriya et al., 2020)). Particularly in the CNS, several studies have address the effect of transmitophagy under pathological situations as ischemic insult (Babenko et al., 2015; Hayakawa et al., 2016; Hayakawa, Chan, et al., 2018; Lippert & Borlongan, 2019; Morancho et al., 2015), AD (Joshi et al., 2019; Nitzan et al., 2019) or PD (Morales et al., 2020; Rostami et al., 2017; Valdinocci et al., 2019). It has been postulated that astrocytes could degrade neuronal damaged mitochondria and supply new functional mitochondria to the neuron as a neuroprotective strategy against toxic stimuli (M. V. Berridge et al., 2016). Following the research performed in other models of neurodegeneration, we aimed to address this transmitophagy in HD.

We detected extracellular mitochondria released by WT and R6/1 astrocytes in culture, similarly to previous research in *in vitro* models of other brain injuries (Hayakawa et al., 2016; Joshi et al., 2019). Moreover, nearly the entire pool of extracellular mitochondrial was functional, showing no differences between genotypes. Despite similar mitochondrial functionality, astrocytic mitochondria impacted differently in striatal neurons depending on the genotype. Neurons receiving mitochondria from HD astrocytes increased the oxidative stress levels as well as reduced the neurite branching. Altogether, these findings suggest that HD mitochondria from astrocytes present some intrinsic properties that trigger neuronal damage, which could in turn contribute to the selective vulnerability of MSN in HD. Nevertheless, since medium from cultured HD astrocyte may contain other soluble factors that could induce neurotoxicity, negative controls should be included in this experiment such as depletion of mitochondria from the medium as previously described (Joshi et al., 2019). Notably, an important issue for future research would be to challenge the mitochondrial transfer in HD in a more complex system as co-cultures or *in vivo* models and evaluate the transfer from astrocytes to neurons and vice versa.

DISCUSSION

One of the few molecular components identified in the transfer of extracellular mitochondria is CD38. In the brain, CD38 triggers mitochondrial release from astrocytes (Hayakawa et al., 2016) and it participates in neuro-glia communication (Bruzzone et al., 2004; Hattori et al., 2017). We described for the first time the involvement of CD38 in HD. Protein levels of CD38 were increased in striatal astrocytes of R6/1 mice and in *post-mortem* caudate of HD patients. To date, it has been hypothesised that CD38 may be boosted in several neurodegenerative disorders and that could be linked to the lowered levels of NAD, a substrate of CD38 metabolism, observed in models of AD, PD and HD (Guerreiro et al., 2020; Lautrup et al., 2019). In turn, depletion of CD38 in mice led to higher NAD levels (Barbosa et al., 2007) and enhancement of NAD proved to ameliorate the mitochondrial function and prevent from damage derived from oxidative stress (Lautrup et al., 2019). Thus, in future studies it would be of interest to modulate CD38 activity in HD astrocytes and evaluate whether its partial inhibition could benefit striatal neurons by preventing neurotoxicity.

On the other side, recent research proposed the interaction between ER and mitochondria as another mechanism involved in the transfer of extracellular mitochondria. It was demonstrated in primary osteocytes that mitochondrial transfer along the cell required the association to the ER and that Mfn2 inhibition impeded mitochondrial transfer (J. Gao et al., 2019). Moreover, a study in human astrocytes demonstrated that accumulated α -synuclein can be transferred to other astrocytes via TNT, one of the paths for mitochondrial transfer. This same investigation showed that α -synuclein accumulation induced ER swelling and altered mitochondrial dynamics, finally provoking autophagy disturbances (Rostami et al., 2017). Despite the evidence suggesting the importance of ER-mitochondrial interactions in transmitophagy, many questions remain to be elucidated and future research should address them.

Finally, mitochondrial transplantation has been postulated as a novel therapeutic approach for several diseases, including those related with the CNS (Hayakawa, Bruzzese, et al., 2018). Interestingly, mitochondrial transfer in the brain of AD mice reduced neuronal loss and gliosis in the hippocampus as well as ameliorated cognitive deficits (Nitzan et al., 2019). Similarly, microinjections to the affected brain area and intravenous administration of mitochondria in PD mouse models rescued neuronal functionality (J. C. Chang et al., 2016; Shi et al., 2017). These promising results open a potential clinical application for neurodegenerative diseases, including HD.

DISCUSSION

In summary, in the second study of this Thesis we have demonstrated that HD striatal astrocytes do not show main changes in the expression of astrocyte markers. However, we have shown other features of astrogliosis as cell hypertrophy and enhanced mitochondrial metabolism. Finally, HD astrocytes transfer mitochondria that trigger toxic effects in striatal neurons (Figure 61). Altogether, disturbances in mitochondrial function of HD astrocytes contribute to the striatal neuronal vulnerability that occurs in HD.

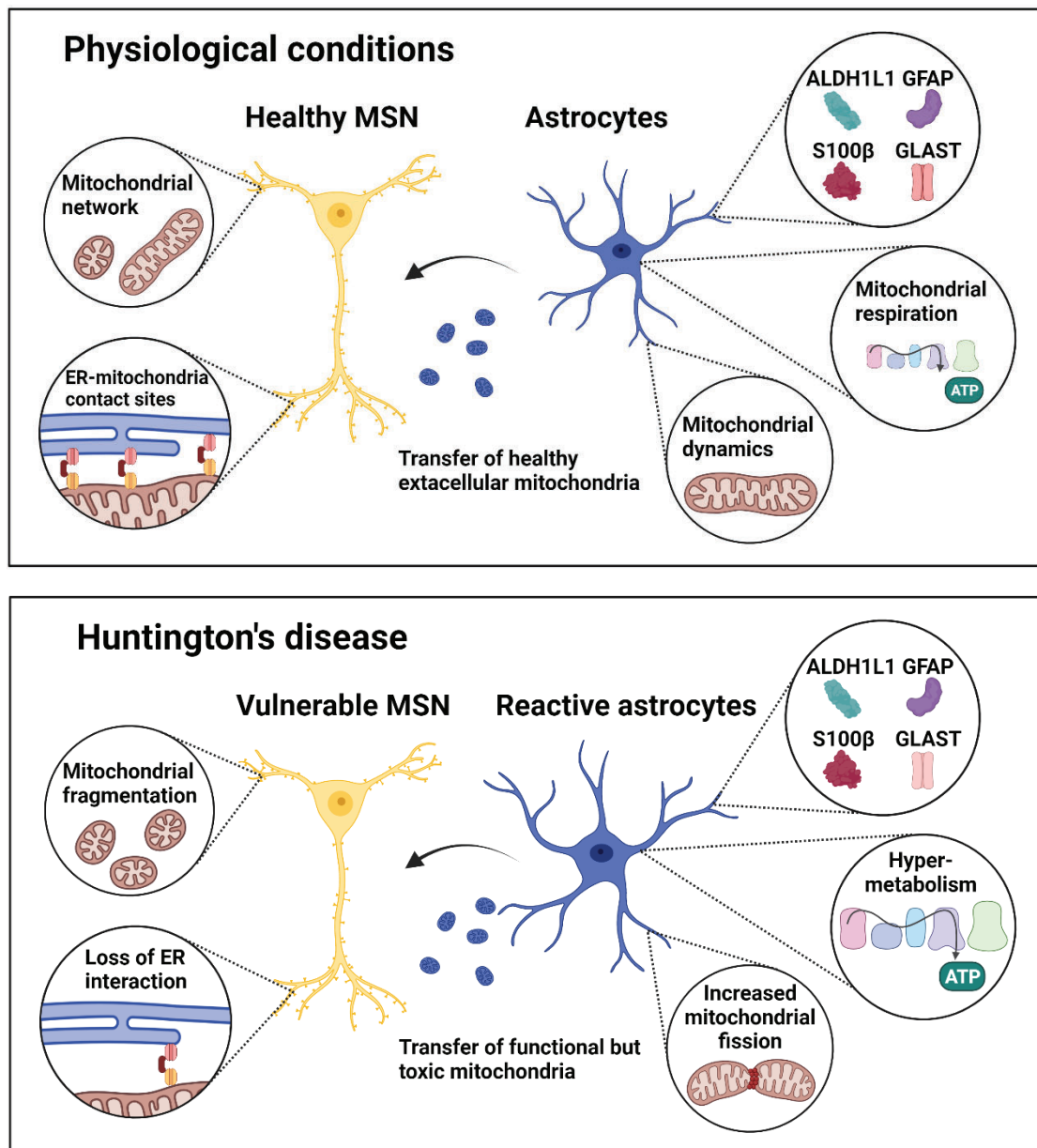


Figure 61. Mitochondrial function and dynamics are altered in neurons and astrocytes of HD striatum. In physiological conditions, mitochondrial function and dynamics are tightly regulated. In striatal astrocytes, the markers ALDH1L1, GFAP, S100 β and GLAST are expressed. Astrocytes communicate with neurons through the transfer of extracellular healthy mitochondria. In HD, neurons present exacerbated mitochondrial fragmentation along with a reduction in ER-mitochondria contact sites. Although HD astrocyte present similar expression of markers, cells are hypertrophic with an increment in mitochondrial respiration and mitochondrial fission. Finally, HD astrocytes transfer functional mitochondria that trigger toxic effects in striatal neurons.

3. ROLE OF PYK2 IN MITOCHONDRIA AND MAMs

Pyk2 is considered a scaffolding protein with abundant protein interactions (reviewed in (de Pins et al., 2021)) that has been largely involved in synaptic plasticity and, when its function is compromised, in several neurodegenerative diseases (Giralt et al., 2017; Kumar et al., 2021; Nakamura et al., 2002). Since Pyk2 interactome in hippocampus, the brain region with highest Pyk2 expression, was not studied in detail so far, we aimed to partially define it using immunoprecipitation coupled to mass-spectrometry. First, we found that most of the proteins associated with Pyk2 were directly implicated in NMDA function and synaptic plasticity, corroborating previous reports in neurons from mouse brain (Bartos et al., 2010; Girault, Costa, et al., 1999; Heidinger et al., 2002). Surprisingly, we also identified Pyk2 partners involved in calcium regulation and mitochondrial function.

To further elaborate on this discovery, we studied subcellular distribution of Pyk2 in hippocampal neurons of Pyk2^{+/+} mice. Not only did we confirm the presence of Pyk2 in the cytosol and the nucleus previously described (Camille Faure et al., 2013), but we also identified a novel localisation in mitochondria and their contact sites with the ER. Consistent with this outcome, other authors proved the interaction of Pyk2 with some chaperone proteins enriched in the MAMs as Grp75 and Grp78/BiP in glioblastoma cell lines (Vomaske et al., 2010). In contact sites between ER and mitochondria, Grp75 strengthens the IP3R3-VDAC1 complex whereas Grp78, together with SGR1, stabilises IP3R3 and boosts Ca²⁺ signalling (Hayashi & Su, 2007; Prasad et al., 2017). In line with these findings, we reported that the lack of Pyk2 triggers changes in IP3R3 and VDAC1 protein levels, along with an increment in ER-mitochondria juxtaposition in hippocampal neurons both in *in vivo* and in *in vitro* murine models. Altogether, we demonstrated that Pyk2 is an essential protein for the structural integrity of MAMs in a physiological context.

As discussed above, MAMs are highly involved in the maintenance of calcium homeostasis. Given the structural alterations in MAMs observed in Pyk2^{-/-} mice, we hypothesised that Pyk2 could be implicated in the calcium buffering regulated by ER and mitochondria. In our hands, the lack of Pyk2 in hippocampal neurons hampered the calcium buffering capacity of ER. In line with this outcome, previous research in endothelial cells reported that Pyk2 phosphorylates STIM1, a calcium sensor in the ER, thus modulating Ca²⁺ store depletion in the ER (Soni et al., 2017; Yazbeck et al., 2017). Moreover, Pyk2 depletion in murine macrophages promoted alterations in calcium signalling, showing a reduction in intracellular Ca²⁺ release and in IP3 production after chemokine stimulation (Okigaki et al., 2003). Although the methodology used in our work

DISCUSSION

did not trace specifically calcium from each subcellular compartment, we postulate that lack of Pyk2 promotes alterations in MAMs proteins along with ER-mitochondrial interaction, finally impacting on the Ca^{2+} exchange between organelles and thus, on its homeostasis.

However, little is known about how Pyk2 regulates the molecular mechanisms of mitochondrial calcium buffering. It has been posited that Pyk2 could interact with the mitochondrial calcium uniporter (MCU), modulating mitochondrial calcium uptake (O-Uchi et al., 2014; K. Zhang et al., 2018). Thus, in cardiomyocytes, adrenergic stimulation induces Pyk2 translocation from cytosol to mitochondrial matrix where it directly phosphorylates MCU, facilitating Ca^{2+} entry into the mitochondria (O-Uchi et al., 2014). Other studies in cardiac and neuroblastoma cells have shown that Ca^{2+} entry via TRPM2 activates Pyk2/MCU signalling and modulates mitochondrial function and cell survival (Hirschler-Laszkiewicz et al., 2018; B. A. Miller et al., 2019).

Besides calcium homeostasis, MAMs also modulate mitochondrial dynamics (De Brito & Scorrano, 2008; Friedman et al., 2011; Rowland & Voeltz, 2012a). Given the previous findings, we aimed to assess the mitochondrial dynamics and morphology in the absence of Pyk2. In hippocampus of Pyk2^{-/-} mice, fission protein Drp1 was enhanced while fusion proteins Mfn2 and Opa1 were not altered. Moreover, lack of Pyk2 induced an increment in the number of mitochondria along with a lowering in the elongation and the branching of these organelles, common features of an exacerbated mitochondrial fragmentation. This mitochondrial fragmentation could compromise neuronal function and viability since other studies have reported that ablation of fusion or fission proteins promotes an oxidative stress response, neuroinflammation and neuronal death in the hippocampus (Jiang et al., 2018; Oettinghaus et al., 2016; G. Park et al., 2021).

Despite we describe in this Thesis a new function of Pyk2 in mitochondrial dynamics, the underlying mechanism remains unclear. We aimed to understand how Pyk2 controls the changes in mitochondria density and shape. Firstly, we reported that Pyk2 translocated to the mitochondria upon activation in hippocampal neurons. Supporting this result, Pyk2 activation was shown to induce its own translocation to the mitochondria in cell lines and to trigger mitochondrial ROS production (O-Uchi et al., 2014). Additionally, stimulation of murine macrophages with chemokines prompted a redistribution of the subcellular localisation of Pyk2 (Okigaki et al., 2003). Altogether, these findings suggest that Pyk2 relocates within the cell depending on the cellular necessities.

Furthermore, we challenged different domains of Pyk2 to delimit the ones mostly involved in the regulation of mitochondrial biogenesis and, among the tested domains,

the RREST was the most significant. Mutations in nuclear transport and location motifs of Pyk2 did not revert number of mitochondria in hippocampal neurons, thus suggesting the relevance of Pyk2 domains of nuclear location and transport in mitochondrial dynamics. These findings could indicate two potential independent mechanisms: on the one hand, Pyk2 needs to translocate into the mitochondria and, once there, it regulates undetermined physiological molecular pathways. Indeed, the chaperone HSPA8, located in the MAMs, is responsible for protein imports into mitochondria (Stricher et al., 2013) and it has been described as a protein partner interacting with Pyk2 (Vomaske et al., 2010). On the other hand, Pyk2 nuclear import motifs are necessary to translocate Pyk2 to the nucleus as previously shown (Corvol et al., 2005; C. Faure et al., 2007) to regulate the transcription of genes (Hum et al., 2014) related with the function of the mitochondria. In agreement with this idea, it is well known that the mitochondria and the nucleus are coordinated in several physiological conditions (Pei & Wallace, 2018; Quirós et al., 2016). In this context, Pyk2 could be a molecular bridge of such a process. However, future investigations should address this possibility to decipher the concrete mechanism.

In sum, the third study of this Thesis has provided a deeper insight into the role of Pyk2 in mitochondrial function in neurons under physiological conditions. We propose Pyk2 as a key player in the modulation of mitochondrial dynamics and the regulation of ER-mitochondria contact sites (Figure 62).

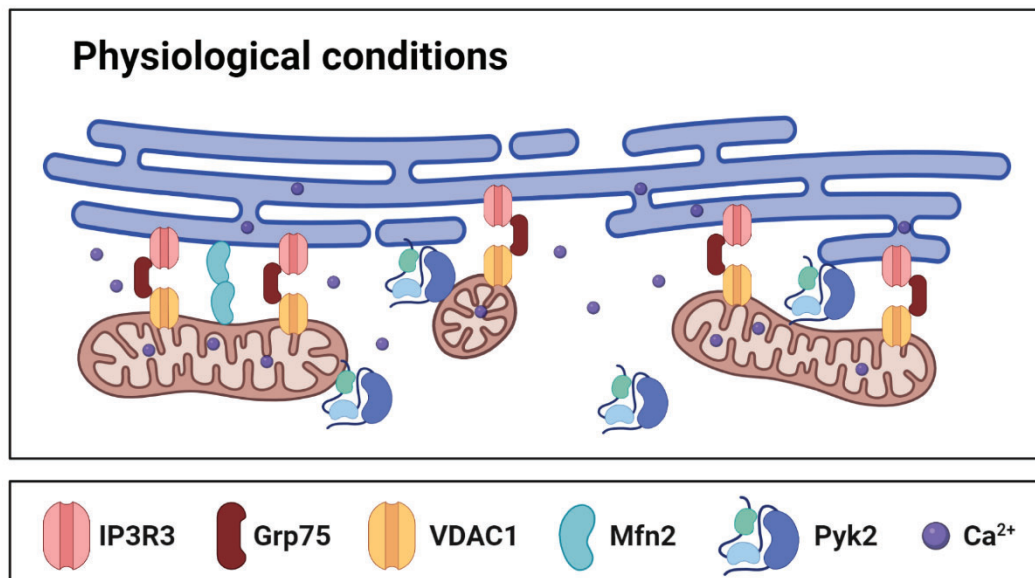


Figure 62. Pyk2 regulates MAMs and mitochondrial dynamics in neurons. Pyk2 is present inside mitochondria and in MAMs. When localised in these subcellular compartments, Pyk2 modulates mitochondrial morphology and the formation of ER-mitochondria contact sites.

DISCUSSION

As we have demonstrated in this Thesis, the disruption of the structural integrity of mitochondria and MAMs results in the mishandling of calcium. Since defects in calcium homeostasis is a common feature in neurodegenerative diseases, including HD, it is feasible to propose that dysregulation of mitochondrial dynamics regulated by Pyk2 may be involved in pathological mechanisms of HD. This hypothesis will be further discussed in the next section.

4. PYK2: A NEW PLAYER IN THE DISRUPTION OF MITOCHONDRIAL DYNAMICS AND MAMs IN HD?

Pyk2 has been previously implicated in the hippocampal impairments of neurodegenerative disorders as AD and HD (Giralt et al., 2017, 2018; Kilinc et al., 2020; Salazar et al., 2019). In line with these findings, we reported a lowering in Pyk2 protein levels in *post-mortem* putamen of HD patients. However, in this Thesis we did not address whether this reduction of Pyk2 could mediate the mitochondrial dysfunction observed in HD striatal neurons. In the following section, we will speculate about how Pyk2 regulation of mitochondrial dynamics and MAMs could be affected in the striatum of HD.

Mitochondria are considered a hub for integration of cellular signalling since dynamic remodelling of their morphology enables a rapid adaptative response to cellular or tissue demands. Post-translational modifications, as reversible phosphorylation, in mitochondrial proteins have been pointed out as a mechanism to achieve this immediate reshaping of the organelle (reviewed in (Giacomello et al., 2020; Lucero et al., 2019). Indeed, proteomic studies showed that up to 40% of the mitochondrial proteome is phosphorylated (Giorgianni et al., 2014; Kruse & Højlund, 2017; Padrão et al., 2013) and at least 30 kinases and phosphatases have been described to be related to mitochondria, either by translocation to the organelle or by having mitochondrial substrates (S. Lim et al., 2016; Lucero et al., 2019).

In particular, it has been widely studied the phosphorylation of Drp1, the main regulator of mitochondrial fission. On the one hand, phosphorylation at serine 585 and serine 616 by Cdk1/Cyclin B promotes fission (Taguchi et al., 2007). Similarly, Cdk5 also phosphorylates Drp1 at serine 616 (Cho et al., 2014; Jahani-Asl et al., 2015). Indeed, our group has previously described the involvement of Drp1 phosphorylation mediated by Cdk5 in HD striatal neurons. In this study, we showed how the presence of mHtt

DISCUSSION

enhanced Cdk5 activity, leading to increased Drp1 activity and resulting in an exacerbated mitochondrial fission (Cherubini et al., 2015). On the other hand, phosphorylation at serine 637 by PKA inhibits mitochondrial fission (Cereghetti et al., 2008; C. R. Chang & Blackstone, 2007; L. C. Gomes et al., 2011). In addition, dephosphorylation mediated by calcineurin regulates Drp1 translocation to mitochondria, leading to an enhancement of mitochondrial fission (Cereghetti et al., 2008). Additionally, Drp1 can also be phosphorylated by GSK-3, activating its GTPase activity and promoting mitochondrial fission (Yan et al., 2015). GSK-3 has been implicated in several neurodegenerative diseases, including HD (Rippin & Eldar-Finkelman, 2021). In fact, blockage of GSK-3 in HD cell and mouse models reduced the mHtt toxicity and ameliorated HD motor symptoms (Rippin et al., 2021).

Regarding Mfn2, phosphorylation by PINK1 promotes fission and Parkin-mediated mitophagy (Y. Chen & Dorn II, 2013). Similarly, phosphorylation mediated by JNK prevents mitochondrial fragmentation and promotes proteasomal degradation of Mfn2 (Leboucher et al., 2012). Furthermore, a recent work reported the phosphorylation of Mfn2 by several Src-family kinases (SFK), including Src. O-Uchi's group has studied the repercussion of Mfn2 phosphorylation by SFK in HEK2983T cells (P. Zhang et al., 2022). Interestingly, these authors found that activation of SFK promoted an increment in ER-mitochondria interactions, which facilitated the transport of Ca^{2+} from ER to mitochondria.

It is worth reminding that SFK phosphorylate Pyk2, promoting its activation, and that the regulation of these kinases is mutually dependent (reviewed in (de Pins et al., 2021)). Hence, it is plausible thinking that cellular modulation mediated by SFK may also be affected by Pyk2 regulation. All things considered, we hypothesise that dysregulation of Pyk2 under pathological conditions could mediate alterations in mitochondrial dynamics and interaction with ER in neurons. In this thesis we have demonstrated that HD striatal neurons present a loss of MAMs and disrupted calcium homeostasis along with a reduction of Pyk2 levels in HD patients. Conversely, Pyk2 is activated in the AD mouse model APP/PS1 mice (Salazar et al., 2019). The AD-related protein PS1 is enriched in MAMs and presenilin-mutant cells have shown an increment in ER-mitochondrial apposition (Area-Gomez et al., 2012). Regarding PD, Pyk2 has been reported to phosphorylate α -synuclein via SFK (Nakamura et al., 2002). It has been reported that α -synuclein localises in the MAMs (Guardia-Laguarta et al., 2014) and modulates the interactions between ER and mitochondria, since overexpression of α -synuclein enhanced ER-mitochondria contacts (Calì et al., 2012). Taken together, we propose Pyk2 as a scaffold protein that anchors ER and mitochondria, ensuring the correct

DISCUSSION

interaction between these organelles and preventing from mishandling of calcium. Hence, a feasible approach to test this possibility would be to overexpress Pyk2 in HD neurons and evaluate the formation of ER-mitochondria interactions, expecting a recovery in MAMs integrity and function.

On the other hand, we have also described the involvement of Pyk2 in calcium homeostasis, particularly in the calcium capacity of the ER. As mentioned above, Pyk2 phosphorylates STIM1 (Soni et al., 2017; Yazbeck et al., 2017), a calcium sensor in the luminal space of the ER. It has been reported that phosphorylation of STIM1 can both activate and inactivate the entry of Ca^{2+} to the ER (Pozo-Guisado & Martin-Romero, 2013). Several studies have implicated STIM1 and the related molecular pathway in the pathological mechanisms of HD (reviewed in (Czeredys, 2020)). In particular, the expression of the N-terminal fragment of mHtt increased the entry of Ca^{2+} to the ER in a STIM1-dependent manner. Moreover, the knockdown of STIM1 prevented from spine loss in YAC128 MSN (J. Wu et al., 2018). It could conceivably be hypothesised that the reduction of Pyk2 in HD neurons could mediate an aberrant entry of Ca^{2+} to the ER, causing an overload of calcium and leading to the observed disruption of Ca^{2+} transport between ER and mitochondria. Despite several questions remain unanswered at present, this hypothesis would open a new perspective of the role of Pyk2 in HD pathology.

Finally, it is reasonable to wonder how Pyk2 regulates mitochondrial alterations in astrocytes and its contribution to striatal degeneration in HD. However, little is known about Pyk2 in astrocytes. To date, the only study that addressed this topic described the importance of Pyk2 in astrocytes migration after a brain lesion (Giralt et al., 2016). Conversely, Src has been postulated to mediate astrocyte-to-neuron communication that activates neurite retraction (Maldonado et al., 2017). Nonetheless, there are still many unresolved questions before Pyk2 could be suggested as a player in the defective neuroglial transfer of mitochondria in HD.

In summary, in this Thesis we have provided compelling evidence on how alteration of cellular signalling impacts on the mitochondrial dynamics, modifying the organelle's function and morphology. We propose that modulation of mitochondrial dynamics, either by increased fission or by loosening of interaction with ER could contribute to the striatal vulnerability of HD (Figure 63).

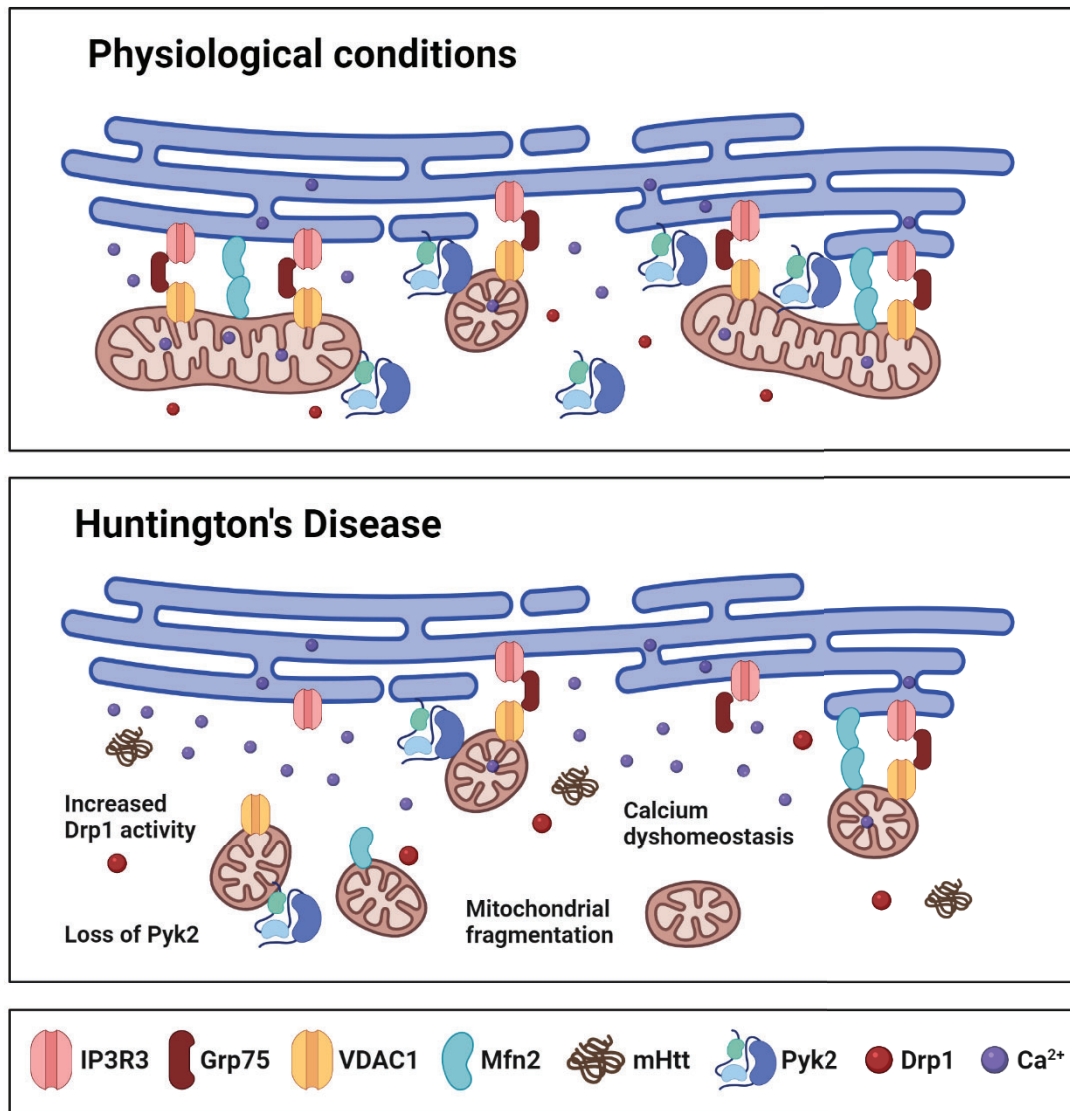


Figure 63. Mitochondrial morphology and MAMs are altered in striatal HD neurons. Schematic representation of the proposed model of mitochondrial fragmentation and its consequences in HD neurons. In physiological conditions, ER and mitochondria interact forming IP3R3-VDAC1 complexes, strengthened by Grp75 and Mfn2. In these microdomains, Ca²⁺ is transferred from the ER to the mitochondria, which buffers alterations in intracellular levels of Ca²⁺. Pyk2 localises both in mitochondria and MAMs, regulating their dynamics. In HD, mitochondrial fragmentation and a reduction in MAMs proteins induce the loss of ER-mitochondria contact sites, triggering defects in calcium homeostasis. Loss of Pyk2 in HD neurons could contribute to the mitochondrial dysfunction.

CONCLUSIONS

CONCLUSIONS

The main conclusions extracted from the results presented in this Thesis are the following:

1. Increased mitochondrial fragmentation leads to a loss of ER-mitochondrial contact sites in R6/1 striatal neurons.
2. MAMs proteins related to Ca^{2+} homeostasis Grp75, IP3R3 and Mfn2 are selectively reduced in the striatum of HD mouse models and putamen of HD patients.
3. Ca^{2+} homeostasis regulated by ER-mitochondria crosstalk is altered in R6/1 striatal neurons.
4. The pharmacological inhibition of Drp1 restores mitochondrial morphology and ER-mitochondria interaction, demonstrating that these alterations are associated to Drp1 aberrant activity.
5. Astrocyte markers ALDH1L1, GFAP, S100 β and GLAST are expressed in murine striatum and they are unaltered in R6/1 mice along the disease progression.
6. R6/1 striatal astrocytes show cell hypertrophy along with enhanced mitochondrial respiration, indicating an increment in astrogliosis.
7. Mitochondria released from R6/1 striatal astrocytes can be internalised by striatal neurons and trigger neuronal toxicity, that could contribute to the selective vulnerability of the striatum in HD.
8. Pyk2 is localised in mitochondria and MAMs in hippocampal neurons and it regulates the dynamics and function of these subcellular compartments.

REFERENCES

REFERENCES

- Abjean, L., Ben Haim, L., Riquelme-Perez, M., Gipchtein, P., Derbois, C., Palomares, M.-A., Petit, F., Herard, A.-S., Gaillard, M. C., Guillermier, M., Gaudin-Guérif, M., Aurégan, G., Sagar, N., Héry, C., Dufour, N., Robil, N., Kabani, M., Melki, R., De la Grange, P., ... Escartin, C. (2022). Reactive astrocytes promote proteostasis in Huntington's disease through the JAK2-STAT3 pathway. *Brain*, 5–6.
- Acuña, A. I., Esparza, M., Kramm, C., Beltrán, F. A., Parra, A. V., Cepeda, C., Toro, C. A., Vidal, R. L., Hetz, C., Concha, I. I., Brauchi, S., Levine, M. S., & Castro, M. A. (2013). A failure in energy metabolism and antioxidant uptake precede symptoms of Huntington's disease in mice. *Nature Communications*, 4(May), 1–13. <https://doi.org/10.1038/ncomms3917>
- Ahmad, T., Aggarwal, K., Pattnaik, B., Mukherjee, S., Sethi, T., Tiwari, B. K., Kumar, M., Micheal, A., Mabalirajan, U., Ghosh, B., Sinha Roy, S., & Agrawal, A. (2013). Computational classification of mitochondrial shapes reflects stress and redox state. *Cell Death and Disease*, 4(1), e461-10. <https://doi.org/10.1038/cddis.2012.213>
- Akimoto, N., Kamiyama, Y., Yamafuji, M., Fujita, K., Seike, T., Kido, M. A., Yokoyama, S., Higashida, H., & Noda, M. (2013). Immunohistochemistry of CD38 in Different Cell Types in the Hypothalamus and Pituitary of Male Mice. *Messenger*, 2(1), 54–61. <https://doi.org/10.1166/msr.2013.1021>
- Al-Dalahmah, O., Sosunov, A. A., Shaik, A., Ofori, K., Liu, Y., Vonsattel, J. P., Adorjan, I., Menon, V., & Goldman, J. E. (2020). Single-nucleus RNA-seq identifies Huntington disease astrocyte states. *Acta Neuropathologica Communications*, 8(1), 1–21. <https://doi.org/10.1186/s40478-020-0880-6>
- Alavi, M. V., Bette, S., Schimpf, S., Schuettauf, F., Schraermeyer, U., Wehrl, H. F., Ruttiger, L., Beck, S. C., Tonagel, F., Pichler, B. J., Knipper, M., Peters, T., Laufs, J., & Wissinger, B. (2007). A splice site mutation in the murine Opa1 gene features pathology of autosomal dominant optic atrophy. *Brain*, 130(4), 1029–1042. <https://doi.org/10.1093/brain/awm005>
- Ali, N. J., & Levine, M. S. (2006). Changes in expression of N-methyl-D-aspartate receptor subunits occur early in the R6/2 mouse model of Huntington's disease. *Developmental Neuroscience*, 28(3), 230–238. <https://doi.org/10.1159/000091921>
- Altmann, R. (1890). *Die Elementarorganismen und ihre Beziehungen zu den Zellen* (Veit (ed.)).
- Alvarez-Periel, E., Puigdemívol, M., Brito, V., Plattner, F., Bibb, J. A., Alberch, J., & Ginés, S. (2018). Cdk5 Contributes to Huntington's Disease Learning and Memory Deficits via Modulation of Brain Region-Specific Substrates. *Molecular Neurobiology*, 55(8), 6250–6268. <https://doi.org/10.1007/s12035-017-0828-4>
- Arcucci, A., Montagnani, S., & Gionti, E. (2006). Expression and intracellular localization of Pyk2 in normal and v-src transformed chicken epiphyseal chondrocytes. *Biochimie*, 88, 77–84. <https://doi.org/10.1016/j.biochi.2005.06.013>
- Area-Gomez, E., Del Carmen Lara Castillo, M., Tambini, M. D., Guardia-Laguarta, C., De Groof, A. J. C. C., Madra, M., Ikenouchi, J., Umeda, M., Bird, T. D., Sturley, S. L., & Schon, E. A. (2012). Upregulated function of mitochondria-associated ER membranes in Alzheimer disease. *The EMBO Journal*, 31(21), 4106–4123. <https://doi.org/10.1038/emboj.2012.202>
- Arrasate, M., Mitra, S., Schweitzer, E. S., Segal, M. R., & Finkbeiner, S. (2004). Inclusion body formation reduces levels of mutant huntingtin and the risk of neuronal death. *Nature*, 431(7010), 805–810. <https://doi.org/10.1038/nature02998>

REFERENCES

- Arzberger, T., Krampfl, K., Leimbgruber, S., & Weindl, A. (1997). Changes of NMDA receptor subunit (NR1, NR2B) and glutamate transporter (GLT1) mRNA expression in Huntington's disease-An in situ hybridization study. *Journal of Neuropathology and Experimental Neurology*, *54*(4), 440–454.
- Avraham, S., London, R., Fu, Y., Ota, S., Hiregowdara, D., Li, J., Jiang, S., Pasztor, L. M., White, R. A., Groopman, J. E., & Avraham, H. (1995). Identification and characterization of a novel related adhesion focal tyrosine kinase (RAFTK) from megakaryocytes and brain. *Journal of Biological Chemistry*, *270*(46), 27742–27751. <https://doi.org/10.1074/jbc.270.46.27742>
- Aziz, N. A., Anguelova, G. V., Marinus, J., Van Dijk, J. G., & Roos, R. A. C. (2010). Autonomic symptoms in patients and pre-manifest mutation carriers of Huntington's disease. *European Journal of Neurology*, *17*(8), 1068–1074. <https://doi.org/10.1111/j.1468-1331.2010.02973.x>
- Babenko, V. A., Silachev, D. N., Zorova, L. D., Pevzner, I. B., Khutorenko, A. A., Plotnikov, E. Y., Sukhikh, G. T., & Zorov, D. B. (2015). Improving the Post-Stroke Therapeutic Potency of Mesenchymal Multipotent Stromal Cells by Cocultivation With Cortical Neurons: The Role of Crosstalk Between Cells. *Stem Cells Translational Medicine*, *4*(9), 1011–1020. <https://doi.org/10.5966/sctm.2015-0010>
- Barbosa, M. T. P., Soares, S. M., Novak, C. M., Sinclair, D., Levine, J. A., Aksoy, P., & Chini, E. N. (2007). The enzyme CD38 (a NAD glycohydrolase, EC 3.2.2.5) is necessary for the development of diet-induced obesity. *The FASEB Journal*, *21*(13), 3629–3639. <https://doi.org/10.1096/fj.07-8290com>
- Bartos, J. A., Ulrich, J. D., Li, H., Beazely, M. A., Chen, Y., MacDonald, J. F., & Hell, J. W. (2010). Postsynaptic Clustering and Activation of Pyk2 by PSD-95. *Journal of Neuroscience*, *30*(2), 449–463. <https://doi.org/10.1523/JNEUROSCI.4992-08.2010>
- Bates, G. P., Dorsey, R., Gusella, J. F., Hayden, M. R., Kay, C., Leavitt, B. R., Nance, M., Ross, C. A., Scahill, R. I., Wetzel, R., Wild, E. J., & Tabrizi, S. J. (2015). Huntington disease. *Nature Reviews Disease Primers*, *1*(April), 1–21. <https://doi.org/10.1038/nrdp.2015.5>
- Batiuk, M. Y., Martirosyan, A., Wahis, J., de Vin, F., Marneffe, C., Kusserow, C., Koeppen, J., Viana, J. F., Oliveira, J. F., Voet, T., Ponting, C. P., Belgard, T. G., & Holt, M. G. (2020). Identification of region-specific astrocyte subtypes at single cell resolution. *Nature Communications*, *11*(1), 1–15. <https://doi.org/10.1038/s41467-019-14198-8>
- Beal, M. F., Brouillet, E., Jenkins, B. G., Ferrante, R. J., Kowall, N. W., Miller, J. M., Storey, E., Srivastava, R., Rosen, B. R., & Hyman, B. T. (1993). Neurochemical and histologic characterization of striatal excitotoxic lesions produced by the mitochondrial toxin 3-nitropropionic acid. *Journal of Neuroscience*, *13*(10), 4181–4192. <https://doi.org/10.1523/jneurosci.13-10-04181.1993>
- Beal, M. F., Ferrante, R. J., Swartz, K. J., & Kowall, N. W. (1991). Chronic quinolinic acid lesions in rats closely resemble Huntington's disease. *Journal of Neuroscience*, *11*(6), 1649–1659. <https://doi.org/10.1523/jneurosci.11-06-01649.1991>
- Beal, M. Flint. (2000). Energetics in the pathogenesis of neurodegenerative diseases. *Trends in Neurosciences*, *23*(7), 298–304. [https://doi.org/10.1016/S0166-2236\(00\)01584-8](https://doi.org/10.1016/S0166-2236(00)01584-8)
- Beal, M. Flint, Kowall, N. W., Ellison, D. W., Mazurek, M. F., Swartz, K. J., & Martin, J. B. (1986). Replication of the neurochemical characteristics of Huntington's disease by quinolinic acid. *Nature*, *321*(6066), 168–171. <https://doi.org/10.1038/321168a0>

REFERENCES

- Beecham, G. W., Hamilton, K., Naj, A. C., Martin, E. R., Huentelman, M., Myers, A. J., Corneveaux, J. J., Hardy, J., Vonsattel, J. P., Younkin, S. G., Bennett, D. A., De Jager, P. L., Larson, E. B., Crane, P. K., Kamboh, M. I., Kofler, J. K., Mash, D. C., Duque, L., Gilbert, J. R., ... Montine, T. J. (2014). Genome-Wide Association Meta-analysis of Neuropathologic Features of Alzheimer's Disease and Related Dementias. *PLoS Genetics*, *10*(9). <https://doi.org/10.1371/journal.pgen.1004606>
- Behrens, P. F., Franz, P., Woodman, B., Lindenberg, K. S., & Landwehrmeyer, G. B. (2002). Impaired glutamate transport and glutamate - Glutamine cycling: Downstream effects of the Huntington mutation. *Brain*, *125*(8), 1908–1922. <https://doi.org/10.1093/brain/awf180>
- Ben Haim, L., Ceyzériat, K., Carrilo-Sauvage, M. A., Aubry, F., Auregan, G., Guillermier, M., Ruiz, M., Petit, F., Houitte, D., Faivre, E., Vandesquille, M., Aron-Badin, R., Dhenain, M., Déglon, N., Hantraye, P., Brouillet, E., Bonvento, G., & Escartin, C. (2015). The JAK/STAT3 pathway is a common inducer of astrocyte reactivity in Alzheimer's and Huntington's diseases. *Journal of Neuroscience*, *35*(6), 2817–2829. <https://doi.org/10.1523/JNEUROSCI.3516-14.2015>
- Benda, C. (1898). Ueber die Spermatogenese der Vertebraten und höherer Evertbraten, II Theil: Die Histogenese der Spermien. *Arch Anat Physiol*, *73*, 393–398.
- Benraiss, A., Mariani, J. N., Osipovitch, M., Cornwell, A., Windrem, M. S., Villanueva, C. B., Chandler-Militello, D., & Goldman, S. A. (2021). Cell-intrinsic glial pathology is conserved across human and murine models of Huntington's disease. *Cell Reports*, *36*(1), 109308. <https://doi.org/10.1016/j.celrep.2021.109308>
- Benraiss, A., Wang, S., Herrlinger, S., Li, X., Chandler-Militello, D., Mauceri, J., Burm, H. B., Toner, M., Osipovitch, M., Jim Xu, Q., Ding, F., Wang, F., Kang, N., Kang, J., Curtin, P. C., Brunner, D., Windrem, M. S., Munoz-Sanjuan, I., Nedergaard, M., & Goldman, S. A. (2016). Human glia can both induce and rescue aspects of disease phenotype in Huntington disease. *Nature Communications*, *7*. <https://doi.org/10.1038/ncomms11758>
- Berridge, M. J., Lipp, P., & Bootman, M. D. (2000). The versatility and universality of calcium signalling. *Nature Reviews*, *1*(October), 11–21. <https://doi.org/https://doi.org/10.1038/35036035>
- Berridge, M. V., Schneider, R. T., & McConnell, M. J. (2016). Mitochondrial Transfer from Astrocytes to Neurons following Ischemic Insult: Guilt by Association? *Cell Metabolism*, *24*(3), 376–378. <https://doi.org/10.1016/j.cmet.2016.08.023>
- Bido, S., Soria, F. N., Fan, R. Z., Bezaud, E., & Tieu, K. (2017). Mitochondrial division inhibitor-1 is neuroprotective in the A53T- α -synuclein rat model of Parkinson's disease. *Scientific Reports*, *7*(1), 1–13. <https://doi.org/10.1038/s41598-017-07181-0>
- Bolaños, J. P. (2016). Bioenergetics and redox adaptations of astrocytes to neuronal activity. *Journal of Neurochemistry*, *139*, 115–125. <https://doi.org/10.1111/jnc.13486>
- Borlongan, C. V., Koutouzis, T. K., & Sanberg, P. R. (1997). 3-Nitropropionic acid animal model and Huntington's disease. *Neuroscience and Biobehavioral Reviews*, *21*(3), 289–293. [https://doi.org/10.1016/S0149-7634\(96\)00027-9](https://doi.org/10.1016/S0149-7634(96)00027-9)
- Borrell-Pagès, M., Zala, D., Humbert, S., & Saudou, F. (2006). Huntington's disease: From huntingtin function and dysfunction to therapeutic strategies. *Cellular and Molecular Life Sciences*, *63*(22), 2642–2660. <https://doi.org/10.1007/s00018-006->

REFERENCES

6242-0

- Boussicault, L., Hérard, A. S., Calingasan, N., Petit, F., Malgorn, C., Merienne, N., Jan, C., Gaillard, M. C., Lerchundi, R., Barros, L. F., Escartin, C., Delzescaux, T., Mariani, J., Hantraye, P., Beal, M. F., Brouillet, E., Véga, C., & Bonvento, G. (2014). Impaired brain energy metabolism in the BACHD mouse model of Huntington's disease: Critical role of astrocyte-neuron interactions. *Journal of Cerebral Blood Flow and Metabolism*, *34*(9), 1500–1510. <https://doi.org/10.1038/jcbfm.2014.110>
- Bradford, J., Shin, J.-Y. Y., Roberts, M., Wang, C.-E. E., Li, X.-J. J., & Li, S. (2009). Expression of mutant huntingtin in mouse brain astrocytes causes age-dependent neurological symptoms. *Proceedings of the National Academy of Sciences of the United States of America*, *106*(52), 22480–22485. <https://doi.org/10.1073/pnas.0911503106>
- Brown, T. G., Thayer, M., Zarate, N., & Gomez-Pastor, R. (2021). Striatal compartmentalization and clustering of different subtypes of astrocytes is altered in the zQ175 Huntington's disease mouse model. In *bioRxiv*. <https://doi.org/10.2493/jjspe.87.947>
- Browne, S. E., & Beal, M. F. (2004). The Energetics of Huntington's Disease. *Neurochemical Research*, *29*(3), 531–546.
- Browne, S. E., Bowling, A. C., MacGarvey, U., Baik, M. J., Berger, S. C., Muqit, M. M. K., Bird, E. D., & Beal, M. F. (1997). Oxidative damage and metabolic dysfunction in huntington's disease: Selective vulnerability of the basal ganglia. *Annals of Neurology*, *41*(5), 646–653. <https://doi.org/10.1002/ana.410410514>
- Brustovetsky, N., Brustovetsky, T., Purl, K. J., Capano, M., Crompton, M., & Dubinsky, J. M. (2003). Increased susceptibility of striatal mitochondria to calcium-induced permeability transition. *Journal of Neuroscience*, *23*(12), 4858–4867. <https://doi.org/10.1523/jneurosci.23-12-04858.2003>
- Bruzzone, S., Verderio, C., Schenk, U., Fedele, E., Zocchi, E., Matteolit, M., & De Flora, A. (2004). Glutamate-mediated overexpression of CD38 in astrocytes cultured with neurones. *Journal of Neurochemistry*, *89*(1), 264–272. <https://doi.org/10.1111/j.1471-4159.2003.02326.x>
- Bushong, E. A., Martone, M. E., Jones, Y. Z., & Ellisman, M. H. (2002). Protoplasmic astrocytes in CA1 stratum radiatum occupy separate anatomical domains. *Journal of Neuroscience*, *22*(1), 183–192. <https://doi.org/10.1523/jneurosci.22-01-00183.2002>
- Calì, T., Ottolini, D., Negro, A., & Brini, M. (2012). α -Synuclein Controls Mitochondrial Calcium Homeostasis by Enhancing Endoplasmic Reticulum-Mitochondria Interactions. *Journal of Biological Chemistry*, *287*(22), 17914–17929. <https://doi.org/10.1074/jbc.M111.302794>
- Calì, T., Ottolini, D., Negro, A., & Brini, M. (2013). Enhanced parkin levels favor ER-mitochondria crosstalk and guarantee Ca²⁺ transfer to sustain cell bioenergetics. *Biochimica et Biophysica Acta - Molecular Basis of Disease*, *1832*(4), 495–508. <https://doi.org/10.1016/j.bbadis.2013.01.004>
- Camacho-Pereira, J., Tarragó, M. G., Chini, C. C. S., Nin, V., Escande, C., Warner, G. M., Puranik, A. S., Schoon, R. A., Reid, J. M., Galina, A., & Chini, E. N. (2016). CD38 Dictates Age-Related NAD Decline and Mitochondrial Dysfunction through an SIRT3-Dependent Mechanism. *Cell Metabolism*, *23*(6), 1127–1139. <https://doi.org/10.1016/j.cmet.2016.05.006>

REFERENCES

- Cassidy-Stone, A., Chipuk, J. E., Ingerman, E., Song, C., Yoo, C., Kuwana, T., Kurth, M. J., Shaw, J. T., Hinshaw, J. E., Green, D. R., & Nunnari, J. (2008). Chemical Inhibition of the Mitochondrial Division Dynamin Reveals Its Role in Bax/Bak-Dependent Mitochondrial Outer Membrane Permeabilization. *Developmental Cell*, *14*(2), 193–204. <https://doi.org/10.1016/j.devcel.2007.11.019>
- Castaldo, P., Cataldi, M., Magi, S., Lariccia, V., Arcangeli, S., & Amoroso, S. (2009). Role of the mitochondrial sodium/calcium exchanger in neuronal physiology and in the pathogenesis of neurological diseases. *Progress in Neurobiology*, *87*(1), 58–79. <https://doi.org/10.1016/j.pneurobio.2008.09.017>
- Cazaubon, S., Chaverot, N., Romero, I. A., Girault, J. A., Adamson, P., Strosberg, A. D., & Couraud, P. O. (1997). Growth factor activity of endothelin-1 in primary astrocytes mediated by adhesion-dependent and -independent pathways. *Journal of Neuroscience*, *17*(16), 6203–6212. <https://doi.org/10.1523/jneurosci.17-16-06203.1997>
- Celardo, I., Costa, A. C., Lehmann, S., Jones, C., Wood, N., Mencacci, N. E., Mallucci, G. R., Loh, S. H. Y., & Martins, L. M. (2016). Mitofusin-mediated ER stress triggers neurodegeneration in pink1/parkin models of Parkinson's disease. *Cell Death and Disease*, *7*(6), e2271-7. <https://doi.org/10.1038/cddis.2016.173>
- Cepeda, C., Ariano, M. A., Calvert, C. R., Flores-Hernández, J., Chandler B, S. H., Leavitt, B. R., Hayden, M. R., & Levine, M. S. (2001). NMDA receptor function in mouse models of Huntington disease. *Journal of Neuroscience Research*, *66*(4), 525–539. <https://doi.org/10.1002/jnr.1244>
- Cereghetti, G. M., Stangherlin, A., Martins De Brito, O., Chang, C. R., Blackstone, C., Bernardi, P., & Scorrano, L. (2008). Dephosphorylation by calcineurin regulates translocation of Drp1 to mitochondria. *Proceedings of the National Academy of Sciences of the United States of America*, *105*(41), 15803–15808. <https://doi.org/10.1073/pnas.0808249105>
- Chai, H., Diaz-Castro, B., Shigetomi, E., Monte, E., Oceau, J. C., Yu, X., Cohn, W., Rajendran, P. S., Vondriska, T. M., Whitelegge, J. P., Coppola, G., & Khakh, B. S. (2017). Neural Circuit-Specialized Astrocytes: Transcriptomic, Proteomic, Morphological, and Functional Evidence. *Neuron*, *95*(3), 531-549.e9. <https://doi.org/10.1016/j.neuron.2017.06.029>
- Chan, D. C. (2006). Mitochondrial fusion and fission in mammals. *Annual Review of Cell and Developmental Biology*, *22*, 79–99. <https://doi.org/10.1146/annurev.cellbio.22.010305.104638>
- Chang, C. R., & Blackstone, C. (2007). Cyclic AMP-dependent protein kinase phosphorylation of Drp1 regulates its GTPase activity and mitochondrial morphology. *Journal of Biological Chemistry*, *282*(30), 21583–21587. <https://doi.org/10.1074/jbc.C700083200>
- Chang, C. Y., Liang, M. Z., & Chen, L. (2019). Current progress of mitochondrial transplantation that promotes neuronal regeneration. *Translational Neurodegeneration*, *8*(1), 1–12. <https://doi.org/10.1186/s40035-019-0158-8>
- Chang, J. C., Wu, S. L., Liu, K. H., Chen, Y. H., Chuang, C. Sen, Cheng, F. C., Su, H. L., Wei, Y. H., Kuo, S. J., & Liu, C. S. (2016). Allogeneic/xenogeneic transplantation of peptide-labeled mitochondria in Parkinson's disease: Restoration of mitochondria functions and attenuation of 6-hydroxydopamine-induced neurotoxicity. *Translational Research*, *170*, 40-56.e3. <https://doi.org/10.1016/j.trsl.2015.12.003>

REFERENCES

- Chaturvedi, R. K., Calingasan, N. Y., Yang, L., Hennessey, T., Johri, A., & Beal, M. F. (2010). Impairment of PGC-1 α expression, neuropathology and hepatic steatosis in a transgenic mouse model of Huntington's disease following chronic energy deprivation. *Human Molecular Genetics*, *19*(16), 3190–3205. <https://doi.org/10.1093/hmg/ddq229>
- Chaudhuri, R., Arora, H., & Seth, P. (2021). Mitochondrial calcium signaling in the brain and its modulation by neurotropic viruses. *Mitochondrion*, *59*(March), 8–16. <https://doi.org/10.1016/j.mito.2021.03.010>
- Chen, H., Chomyn, A., & Chan, D. C. (2005). Disruption of fusion results in mitochondrial heterogeneity and dysfunction. *Journal of Biological Chemistry*, *280*(28), 26185–26192. <https://doi.org/10.1074/jbc.M503062200>
- Chen, H., Detmer, S. A., Ewald, A. J., Griffin, E. E., Fraser, S. E., & Chan, D. C. (2003). Mitofusins Mfn1 and Mfn2 coordinately regulate mitochondrial fusion and are essential for embryonic development. *Journal of Cell Biology*, *160*(2), 189–200. <https://doi.org/10.1083/jcb.200211046>
- Chen, Y., & Dorn II, G. W. (2013). PINK1-Phosphorylated Mitofusin 2 Is a Parkin Receptor for Culling Damaged Mitochondria. *Science*, *340*(April), 471–476.
- Cheng, H. C., Qi, R. Z., Paudel, H., & Zhu, H. J. (2011). Regulation and function of protein kinases and phosphatases. *Enzyme Research*, *2011*(1), 7–9. <https://doi.org/10.4061/2011/794089>
- Cherubini, M., Puigdellívol, M., Alberch, J., & Ginés, S. (2015). Cdk5-mediated mitochondrial fission: A key player in dopaminergic toxicity in Huntington's disease. *Biochimica et Biophysica Acta - Molecular Basis of Disease*, *1852*(10), 2145–2160. <https://doi.org/10.1016/j.bbadis.2015.06.025>
- Cho, B., Kim, H., Cho, H. M., Kim, H. J., Jeong, J., Park, S. K., Hwang, E. M., Park, J. Y., Kim, W. R., & Sun, W. (2014). CDK5-dependent inhibitory phosphorylation of Drp1 during neuronal maturation. *Experimental and Molecular Medicine*, *46*(7), e105-10. <https://doi.org/10.1038/emm.2014.36>
- Choo, Y. S., Johnson, G. V. W., MacDonald, M., Detloff, P. J., & Lesort, M. (2004). Mutant huntingtin directly increases susceptibility of mitochondria to the calcium-induced permeability transition and cytochrome c release. *Human Molecular Genetics*, *13*(14), 1407–1420. <https://doi.org/10.1093/hmg/ddh162>
- Chou, S. H. Y., Lan, J., Esposito, E., Ning, M. M., Balaj, L., Ji, X., Lo, E. H., & Hayakawa, K. (2017). Extracellular Mitochondria in Cerebrospinal Fluid and Neurological Recovery after Subarachnoid Hemorrhage. *Stroke*, *48*(8), 2231–2237. <https://doi.org/10.1161/STROKEAHA.117.017758>
- Contreras, L., Drago, I., Zampese, E., & Pozzan, T. (2010). Mitochondria: The calcium connection. *Biochimica et Biophysica Acta - Bioenergetics*, *1797*(6–7), 607–618. <https://doi.org/10.1016/j.bbabi.2010.05.005>
- Cooper, J. K., Schilling, G., Peters, M. F., Herring, W. J., Sharp, A. H., Kaminsky, Z., Masone, J., Khan, F. A., Delanoy, M., Borchelt, D. R., Dawson, V. L., Dawson, T. M., & Ross, C. A. (1998). Truncated N-terminal fragments of huntingtin with expanded glutamine repeats form nuclear and cytoplasmic aggregates in cell culture. *Human Molecular Genetics*, *7*(5), 783–790. <https://doi.org/10.1093/hmg/7.5.783>
- Corvol, J.-C., Valjent, E., Toutant, M., Enslin, H., Irinopoulou, T., Lev, S., Hervé, D., & Girault, J.-A. (2005). Depolarization Activates ERK and Proline-rich Tyrosine Kinase

REFERENCES

- 2 (PYK2) Independently in Different Cellular Compartments in Hippocampal Slices. *Journal of Biological Chemistry*, 280(1), 660–668. <https://doi.org/10.1074/jbc.M411312200>
- Costa, V., Giacomello, M., Hudec, R., Lopreiato, R., Ermak, G., Lim, D., Malorni, W., Davies, K. J. A., Carafoli, E., & Scorrano, L. (2010). Mitochondrial fission and cristae disruption increase the response of cell models of Huntington's disease to apoptotic stimuli. *EMBO Molecular Medicine*, 2(12), 490–503. <https://doi.org/10.1002/emmm.201000102>
- Cox, Jürgen, & Mann, M. (2008). MaxQuant enables high peptide identification rates, individualized p.p.b.-range mass accuracies and proteome-wide protein quantification. *Nature Biotechnology*, 26(12), 1367–1372. <https://doi.org/10.1038/nbt.1511>
- Cox, Jürgen, Neuhauser, N., Michalski, A., Scheltema, R. A., Olsen, J. V., & Mann, M. (2011). Andromeda: A Peptide Search Engine Integrated into the MaxQuant Environment. *Journal of Proteome Research*, 10(4), 1794–1805. <https://doi.org/10.1021/pr101065j>
- Cronin, T., Rosser, A., & Massey, T. (2019). Clinical Presentation and Features of Juvenile-Onset Huntington's Disease: A Systematic Review. *Journal of Huntington's Disease*, 8(2), 171–179. <https://doi.org/10.3233/JHD-180339>
- Csordás, G., Renken, C., Várnai, P., Walter, L., Weaver, D., Buttle, K. F., Balla, T., Mannella, C. A., & Hajnóczky, G. (2006). Structural and functional features and significance of the physical linkage between ER and mitochondria. *Journal of Cell Biology*, 174(7), 915–921. <https://doi.org/10.1083/jcb.200604016>
- Cui, L., Jeong, H., Borovecki, F., Parkhurst, C. N., Tanese, N., & Krainc, D. (2006). Transcriptional Repression of PGC-1 α by Mutant Huntingtin Leads to Mitochondrial Dysfunction and Neurodegeneration. *Cell*, 127(1), 59–69. <https://doi.org/10.1016/j.cell.2006.09.015>
- Czeredys, M. (2020). Dysregulation of Neuronal Calcium Signaling via Store-Operated Channels in Huntington's Disease. *Frontiers in Cell and Developmental Biology*, 8(December). <https://doi.org/10.3389/fcell.2020.611735>
- Davis, C. H. O., Kim, K. Y., Bushong, E. A., Mills, E. A., Boassa, D., Shih, T., Kinebuchi, M., Phan, S., Zhou, Y., Bihlmeyer, N. A., Nguyen, J. V., Jin, Y., Ellisman, M. H., & Marsh-Armstrong, N. (2014). Transcellular degradation of axonal mitochondria. *Proceedings of the National Academy of Sciences of the United States of America*, 111(26), 9633–9638. <https://doi.org/10.1073/pnas.1404651111>
- De Brito, O. M., & Scorrano, L. (2008). Mitofusin 2 tethers endoplasmic reticulum to mitochondria. *Nature*, 456(7222), 605–610. <https://doi.org/10.1038/nature07534>
- De Jager, P. L., Srivastava, G., Lunnon, K., Burgess, J., Schalkwyk, L. C., Yu, L., Eaton, M. L., Keenan, B. T., Ernst, J., McCabe, C., Tang, A., Raj, T., Replogle, J., Brodeur, W., Gabriel, S., Chai, H. S., Younkin, C., Younkin, S. G., Zou, F., ... Bennett, D. A. (2014). Alzheimer's disease: Early alterations in brain DNA methylation at ANK1, BIN1, RHBDF2 and other loci. *Nature Neuroscience*, 17(9), 1156–1163. <https://doi.org/10.1038/nn.3786>
- de Pins, B., Mendes, T., Giralt, A., & Girault, J.-A. A. (2021). The Non-receptor Tyrosine Kinase Pyk2 in Brain Function and Neurological and Psychiatric Diseases. *Frontiers in Synaptic Neuroscience*, 13(October), 1–27. <https://doi.org/10.3389/fnsyn.2021.749001>

REFERENCES

- Deng, Y. P., Albin, R. L., Penney, J. B., Young, A. B., Anderson, K. D., & Reiner, A. (2004). Differential loss of striatal projection systems in Huntington's disease: A quantitative immunohistochemical study. *Journal of Chemical Neuroanatomy*, 27(3), 143–164. <https://doi.org/10.1016/j.jchemneu.2004.02.005>
- Diaz-Castro, B., Gangwani, M. R., Yu, X., Coppola, G., & Khakh, B. S. (2019). Astrocyte molecular signatures in Huntington's disease. *Science Translational Medicine*, 11(514), 1–13. <https://doi.org/10.1126/scitranslmed.aaw8546>
- Dikic, I., Dikic, I., & Schlessinger, J. (1998). Identification of a new Pyk2 isoform implicated in chemokine and antigen receptor signaling. *Journal of Biological Chemistry*, 273(23), 14301–14308. <https://doi.org/10.1074/jbc.273.23.14301>
- Dikic, I., Tokiwa, G., Lev, S., Courtneidge, S. A., & Schlessinger, J. (1996). A role for Pyk2 and Src in linking G-protein-coupled receptors with MAP kinase activation. *Letter to Nature*, 383(6), 547–550.
- Dimmer, K. S., Scorrano, L., Kim, J., Moody, J. P., Edgerly, C. K., Bordiuk, O. L., Cormier, K., Beal, M. F., Ferrante, R. J., Li, G. W. D., Scorrano, L., Dimmer, K. S., & Scorrano, L. (2011). *(De) constructing Mitochondria : What For?* 6, 233–241.
- Dourlen, P., Fernandez-Gomez, F. J., Dupont, C., Grenier-Boley, B., Bellenguez, C., Obriot, H., Caillierez, R., Sottejeau, Y., Chapuis, J., Bretteville, A., Abdelfettah, F., Delay, C., Malmanche, N., Soininen, H., Hiltunen, M., Galas, M. C., Amouyel, P., Sergeant, N., Buée, L., ... Dermaut, B. (2017). Functional screening of Alzheimer risk loci identifies PTK2B as an in vivo modulator and early marker of Tau pathology. *Molecular Psychiatry*, 22(6), 874–883. <https://doi.org/10.1038/mp.2016.59>
- Du, F., Yu, Q., Yan, S., Hu, G., Lue, L. F., Walker, D. G., Wu, L., Yan, S. F., Tieu, K., & Yan, S. S. (2017). PINK1 signalling rescues amyloid pathology and mitochondrial dysfunction in Alzheimer's disease. *Brain*, 140(12), 3233–3251. <https://doi.org/10.1093/brain/awx258>
- Dubé, L., Smith, A. D., & Bolam, J. P. (1988). Identification of synaptic terminals of thalamic or cortical origin in contact with distinct medium-size spiny neurons in the rat neostriatum. *Journal of Comparative Neurology*, 267(4), 455–471. <https://doi.org/10.1002/cne.902670402>
- Dunty, J. M., & Schaller, M. D. (2002). The N termini of focal adhesion kinase family members regulate substrate phosphorylation, localization, and cell morphology. *Journal of Biological Chemistry*, 277(47), 45644–45654. <https://doi.org/10.1074/jbc.M201779200>
- Duran, R. C. D., Wang, C. Y., Zheng, H., Deneen, B., & Wu, J. Q. (2019). Brain region-specific gene signatures revealed by distinct astrocyte subpopulations unveil links to glioma and neurodegenerative diseases. *ENeuro*, 6(2). <https://doi.org/10.1523/ENEURO.0288-18.2019>
- Duyao, M., Ambrose, C., Myers, R., Novelletto, A., Persichetti, F., Frontali, M., Folstein, S., Ross, C., Franz, M., Abbott, M., Gray, J., Conneally, P., Young, A., Penney, J., Hollingsworth, Z., Shoulson, I., Lazzarini, A., Falek, A., Koroshetz, W., ... Macdonald, M. (1993). Trinucleotide repeat length instability and age of onset in Huntington's disease. *Nature Genetics*, 4(4), 387–392. <https://doi.org/10.1038/ng0893-387>
- Duyao, M. P., Auerbach, A. B., Ryan, A., Persichetti, F., Barnes, G. T., Mcneil, S. M., Ge, P., Vonsattel, J.-P., Gusella, J. F., Joyner, A. L., & MacDonald, M. E. (1995). Inactivation of the Mouse Huntington's Disease Gene Homolog Hdh. *Science*, 269(5222), 407–410. <https://doi.org/10.1126/science.7618107>

REFERENCES

- Ehrnhoefer, D. E., Southwell, A. L., Sivasubramanian, M., Qiu, X., Villanueva, E. B., Xie, Y., Walth, S., Anderson, L., Fazeli, A., Casal, L., Felczak, B., Tsang, M., & Hayden, M. R. (2018). HACE1 is essential for astrocyte mitochondrial function and influences Huntington disease phenotypes in vivo. *Human Molecular Genetics*, *27*(2), 239–253. <https://doi.org/10.1093/hmg/ddx394>
- English, K., Shepherd, A., Uzor, N. E., Trinh, R., Kavelaars, A., & Heijnen, C. J. (2020). Astrocytes rescue neuronal health after cisplatin treatment through mitochondrial transfer. *Acta Neuropathologica Communications*, *8*(1), 1–14. <https://doi.org/10.1186/s40478-020-00897-7>
- Ernster, L., & Schatz, G. (1981). Mitochondria: A historical review. *Journal of Cell Biology*, *91*(3 II), 227–237. <https://doi.org/10.1083/jcb.91.3.227s>
- Escartin, C., Galea, E., Lakatos, A., O’Callaghan, J. P., Petzold, G. C., Serrano-Pozo, A., Steinhäuser, C., Volterra, A., Carmignoto, G., Agarwal, A., Allen, N. J., Araque, A., Barbeito, L., Barzilai, A., Bergles, D. E., Bonvento, G., Butt, A. M., Chen, W. T., Cohen-Salmon, M., ... Verkhratsky, A. (2021). Reactive astrocyte nomenclature, definitions, and future directions. *Nature Neuroscience*, *24*(3), 312–325. <https://doi.org/10.1038/s41593-020-00783-4>
- Esteras, N., & Abramov, A. Y. (2020). Mitochondrial Calcium Deregulation in the Mechanism of Beta-Amyloid and Tau Pathology. *Cells*, *9*(9), 1711. <https://doi.org/10.3390/cells9092135>
- Estrada-Sánchez, A. M., Montiel, T., Segovia, J., & Massieu, L. (2009). Glutamate toxicity in the striatum of the R6/2 Huntington’s disease transgenic mice is age-dependent and correlates with decreased levels of glutamate transporters. *Neurobiology of Disease*, *34*(1), 78–86. <https://doi.org/10.1016/j.nbd.2008.12.017>
- Estrada-Sánchez, A. M., & Rebec, G. V. (2012). Corticostriatal dysfunction and glutamate transporter 1 (GLT1) in Huntington’s disease: Interactions between neurons and astrocytes. *Basal Ganglia*, *2*(2), 57–66. <https://doi.org/10.1016/j.baga.2012.04.029>
- Estrada Sánchez, A. M., Mejía-Toiber, J., & Massieu, L. (2008). Excitotoxic Neuronal Death and the Pathogenesis of Huntington’s Disease. *Archives of Medical Research*, *39*(3), 265–276. <https://doi.org/10.1016/j.arcmed.2007.11.011>
- Eysert, F., Kinoshita, P. F., Mary, A., Vaillant-Beuchot, L., Checler, F., & Chami, M. (2020). Molecular dysfunctions of mitochondria-associated membranes (MAMs) in Alzheimer’s disease. *International Journal of Molecular Sciences*, *21*(24), 9123. <https://doi.org/10.3390/ijms21249521>
- Faideau, M., Kim, J., Cormier, K., Gilmore, R., Welch, M., Auregan, G., Dufour, N., Guillermier, M., Brouillet, E., Hantraye, P., DéGlon, N., Ferrante, R. J., & Bonvento, G. (2010). In vivo expression of polyglutamine-expanded huntingtin by mouse striatal astrocytes impairs glutamate transport: A correlation with Huntington’s disease subjects. *Human Molecular Genetics*, *19*(15), 3053–3067. <https://doi.org/10.1093/hmg/ddq212>
- Faure, C., Corvol, J.-C., Toutant, M., Valjent, E., Hvalby, O., Jensen, V., El Messari, S., Corsi, J.-M., Kadare, G., & Girault, J.-A. (2007). Calcineurin is essential for depolarization-induced nuclear translocation and tyrosine phosphorylation of PYK2 in neurons. *Journal of Cell Science*, *120*(17), 3034–3044. <https://doi.org/10.1242/jcs.009613>

REFERENCES

- Faure, Camille, Ramos, M., & Girault, J. A. (2013). Pyk2 cytonuclear localization: Mechanisms and regulation by serine dephosphorylation. *Cellular and Molecular Life Sciences*, *70*(1), 137–152. <https://doi.org/10.1007/s00018-012-1075-5>
- Ferreiro, E., Oliveira, C. R., & Pereira, C. M. F. (2008). The release of calcium from the endoplasmic reticulum induced by amyloid-beta and prion peptides activates the mitochondrial apoptotic pathway. *Neurobiology of Disease*, *30*(3), 331–342. <https://doi.org/10.1016/j.nbd.2008.02.003>
- Filadi, R., Greotti, E., Turacchio, G., Luini, A., Pozzan, T., & Pizzo, P. (2016). Presenilin 2 Modulates Endoplasmic Reticulum-Mitochondria Coupling by Tuning the Antagonistic Effect of Mitofusin 2. *Cell Reports*, *15*(10), 2226–2238. <https://doi.org/10.1016/j.celrep.2016.05.013>
- Fowler, P. C., Byrne, D. J., Blackstone, C., & O'sullivan, N. C. (2020). Loss of the mitochondrial fission GTPase Drp1 contributes to neurodegeneration in a drosophila model of hereditary spastic paraplegia. *Brain Sciences*, *10*(9), 1–18. <https://doi.org/10.3390/brainsci10090646>
- Franco-Iborra, S., Plaza-Zabala, A., Montpeyo, M., Sebastian, D., Vila, M., & Martinez-Vicente, M. (2021). Mutant HTT (huntingtin) impairs mitophagy in a cellular model of Huntington disease. *Autophagy*, *17*(3), 672–689. <https://doi.org/10.1080/15548627.2020.1728096>
- Frezza, C., Cipolat, S., Martins de Brito, O., Micaroni, M., Beznoussenko, G. V., Rudka, T., Bartoli, D., Polishuck, R. S., Danial, N. N., De Strooper, B., & Scorrano, L. (2006). OPA1 Controls Apoptotic Cristae Remodeling Independently from Mitochondrial Fusion. *Cell*, *126*(1), 177–189. <https://doi.org/10.1016/j.cell.2006.06.025>
- Friedman, J. R., Lackner, L. L., West, M., DiBenedetto, J. R., Nunnari, J., & Voeltz, G. K. (2011). ER tubules mark sites of mitochondrial division. *Science*, *334*(6054), 358–362. <https://doi.org/10.1126/science.1207385>
- G. Kantzer, C., Boutin, C., Herzig, I. D., Wittwer, C., Reiß, S., Tiveron, M. C., Drewes, J., Rockel, T. D., Ohlig, S., Ninkovic, J., Cremer, H., Pennartz, S., Jungblut, M., & Bosio, A. (2017). Anti-ACSA-2 defines a novel monoclonal antibody for prospective isolation of living neonatal and adult astrocytes. *GLIA*, *65*(6), 990–1004. <https://doi.org/10.1002/glia.23140>
- Gandhi, S., Wood-Kaczmar, A., Yao, Z., Plun-Favreau, H., Deas, E., Klupsch, K., Downward, J., Latchman, D. S., Tabrizi, S. J., Wood, N. W., Duchen, M. R., & Abramov, A. Y. (2009). PINK1-Associated Parkinson's Disease Is Caused by Neuronal Vulnerability to Calcium-Induced Cell Death. *Molecular Cell*, *33*(5), 627–638. <https://doi.org/10.1016/j.molcel.2009.02.013>
- Gao, J., Qin, A., Liu, D., Ruan, R., Wang, Q., Yuan, J., Sum Cheng, T., Filipovska, A., Papadimitriou, J. M., Dai, K., Jiang, Q., Gao, X., Feng, J. Q., Takayanagi, H., Zhang, C., Zheng, M. H., Cheng, T. S., Filipovska, A., Papadimitriou, J. M., ... Zheng, M. H. (2019). Endoplasmic reticulum mediates mitochondrial transfer within the osteocyte dendritic network. *Science Advances*, *5*(11), 1–13. <https://doi.org/10.1126/sciadv.aaw7215>
- Gao, P., Yan, Z., & Zhu, Z. (2020). Mitochondria-Associated Endoplasmic Reticulum Membranes in Cardiovascular Diseases. *Frontiers in Cell and Developmental Biology*, *8*(November), 1–17. <https://doi.org/10.3389/fcell.2020.604240>
- Gerfen, C. R. (1988). Synaptic organization of the striatum. *Journal of Electron Microscopy Technique*, *10*(3), 265–281. <https://doi.org/10.1002/jemt.1060100305>

REFERENCES

- Gerfen, C. R., Engber, T. M., Mahan, L. C., Susel, Z., Chase, T. N., Monsma, F. J., & Sibley, D. R. (1990). D1 and D2 dopamine receptor-regulated gene expression of striatonigral and striatopallidal neurons. *Science*, *250*(1986), 1429–1432. <http://dx.doi.org/10.1126/science.2147780>
- Giacomello, M., Pyakurel, A., Glytsou, C., & Scorrano, L. (2020). The cell biology of mitochondrial membrane dynamics. *Nature Reviews Molecular Cell Biology*, *21*(4), 204–224. <https://doi.org/10.1038/s41580-020-0210-7>
- Giorgi, C., Marchi, S., & Pinton, P. (2018). The machineries, regulation and cellular functions of mitochondrial calcium. *Nature Reviews Molecular Cell Biology*, *19*(11), 713–730. <https://doi.org/10.1038/s41580-018-0052-8>
- Giorgianni, F., Usman Khan, M., Weber, K. T., Gerling, I. C., & Beranova-Giorgianni, S. (2014). Phosphoproteome mapping of cardiomyocyte mitochondria in a rat model of heart failure. *Molecular and Cellular Biochemistry*, *389*(1–2), 159–167. <https://doi.org/10.1007/s11010-013-1937-7>
- Giralt, A., Brito, V., Chevy, Q., Simonnet, C., Otsu, Y., Cifuentes-Díaz, C., De Pins, B., Coura, R., Alberch, J., Ginés, S., Poncer, J.-C. C., & Girault, J.-A. A. (2017). Pyk2 modulates hippocampal excitatory synapses and contributes to cognitive deficits in a Huntington's disease model. *Nature Communications*, *8*(May), 15592. <https://doi.org/10.1038/ncomms15592>
- Giralt, A., Coura, R., & Girault, J.-A. (2016). Pyk2 is essential for astrocytes mobility following brain lesion. *Glia*, *64*(4), 620–634. <https://doi.org/10.1002/glia.22952>
- Giralt, A., de Pins, B., Cifuentes-Díaz, C., López-Molina, L., Farah, A. T. A. T., Tible, M., Deramecourt, V., Arold, S. T. S. T., Ginés, S., Hugon, J., & Girault, J. A. J.-A. (2018). PTK2B/Pyk2 overexpression improves a mouse model of Alzheimer's disease. *Experimental Neurology*, *307*(January), 62–73. <https://doi.org/10.1016/j.expneurol.2018.05.020>
- Giralt, A., Saavedra, A., Alberch, J., & Pérez-Navarro, E. (2012). Cognitive dysfunction in Huntington's disease: Humans, mouse models and molecular mechanisms. *Journal of Huntington's Disease*, *1*(2), 155–173. <https://doi.org/10.3233/JHD-120023>
- Girault, J. A., Costa, A., Derkinderen, P., Studler, J. M., & Toutant, M. (1999). FAK and PYK2/CAK β in the nervous system: A link between neuronal activity, plasticity and survival? *Trends in Neurosciences*, *22*(6), 257–263. [https://doi.org/10.1016/S0166-2236\(98\)01358-7](https://doi.org/10.1016/S0166-2236(98)01358-7)
- Girault, J. A., Labesse, G., Mornon, J. P., & Callebaut, I. (1999). The N-termini of FAK and JAKs contain divergent band 4.1 domains. *Trends in Biochemical Sciences*, *24*(2), 54–57. [https://doi.org/10.1016/S0968-0004\(98\)01331-0](https://doi.org/10.1016/S0968-0004(98)01331-0)
- Goebel, H. H., Heipertz, R., Scholz, W., Iqba, K., & Tellez-Nagel, I. (1978). Juvenile Huntington chorea: clinical, ultrastructural, and biochemical studies. *Neurology*, *28*(1), 23–31.
- Gokce, O., Stanley, G. M., Treutlein, B., Neff, N. F., Camp, J. G., Malenka, R. C., Rothwell, P. E., Fuccillo, M. V., Südhof, T. C., & Quake, S. R. (2016). Cellular Taxonomy of the Mouse Striatum as Revealed by Single-Cell RNA-Seq. *Cell Reports*, *16*(4), 1126–1137. <https://doi.org/10.1016/j.celrep.2016.06.059>
- Gollihue, J. L., & Norris, C. M. (2020). Astrocyte mitochondria: Central players and potential therapeutic targets for neurodegenerative diseases and injury. *Ageing Research Reviews*, *59*(January), 101039. <https://doi.org/10.1016/j.arr.2020.101039>

REFERENCES

- Gomes, D. A., Thompson, M., Souto, N. C., Goes, T. S., Goes, A. M., Rodrigues, M. A., Gomez, M. V., Nathanson, M. H., & Leite, M. F. (2005). The type III inositol 1,4,5-trisphosphate receptor preferentially transmits apoptotic Ca²⁺ signals into mitochondria. *Journal of Biological Chemistry*, *280*(49), 40892–40900. <https://doi.org/10.1074/jbc.M506623200>
- Gomes, L. C., Benedetto, G. Di, & Scorrano, L. (2011). During autophagy mitochondria elongate, are spared from degradation and sustain cell viability. *Nature Cell Biology*, *13*(5), 589–598. <https://doi.org/10.1038/ncb2220>
- González-Casacuberta, I., Juárez-Flores, D. L., Ezquerra, M., Fucho, R., Catalán-García, M., Guitart-Mampel, M., Tobías, E., García-Ruiz, C., Fernández-Checa, J. C., Tolosa, E., Martí, M. J., Grau, J. M., Fernández-Santiago, R., Cardellach, F., Morén, C., & Garrabou, G. (2019). Mitochondrial and autophagic alterations in skin fibroblasts from Parkinson disease patients with Parkin mutations. *Aging*, *11*(11), 3750–3767. <https://doi.org/10.18632/aging.102014>
- Gottlieb, R. A., & Bernstein, D. (2016). Mitochondrial remodeling: Rearranging, recycling, and reprogramming. In *Cell Calcium* (Vol. 60, Issue 2, pp. 88–101). Elsevier Ltd. <https://doi.org/10.1016/j.ceca.2016.04.006>
- Gray, M., Shirasaki, D. I., Cepeda, C., André, V. M., Wilburn, B., Lu, X. H., Tao, J., Yamazaki, I., Li, S. H., Sun, Y. E., Li, X. J., Levine, M. S., & Yang, X. W. (2008). Full-length human mutant huntingtin with a stable polyglutamine repeat can elicit progressive and selective neuropathogenesis in BACHD mice. *Journal of Neuroscience*, *28*(24), 6182–6195. <https://doi.org/10.1523/JNEUROSCI.0857-08.2008>
- Gu, M., Gash, M. T., Mann, V. M., Javoy-Agid, F., Cooper, J. M., & Schapira, A. H. V. (1996). Mitochondrial defect in Huntington's disease caudate nucleus. *Annals of Neurology*, *39*(3), 385–389. <https://doi.org/10.1002/ana.410390317>
- Guardia-Laguarta, C., Area-Gomez, E., Rüb, C., Liu, Y., Magrané, J., Becker, D., Voos, W., Schon, E. A., & Przedborski, S. (2014). α -synuclein is localized to mitochondria-associated ER membranes. *Journal of Neuroscience*, *34*(1), 249–259. <https://doi.org/10.1523/JNEUROSCI.2507-13.2014>
- Guedes-Dias, P., de Proença, J., Soares, T. R., Leitão-Rocha, A., Pinho, B. R., Duchén, M. R., & Oliveira, J. M. A. (2015). HDAC6 inhibition induces mitochondrial fusion, autophagic flux and reduces diffuse mutant huntingtin in striatal neurons. *Biochimica et Biophysica Acta - Molecular Basis of Disease*, *1852*(11), 2484–2493. <https://doi.org/10.1016/j.bbadis.2015.08.012>
- Guedes-Dias, P., Pinho, B. R., Soares, T. R., de Proença, J., Duchén, M. R., & Oliveira, J. M. A. (2016). Mitochondrial dynamics and quality control in Huntington's disease. *Neurobiology of Disease*, *90*, 51–57. <https://doi.org/10.1016/j.nbd.2015.09.008>
- Guerreiro, S., Privat, A. L., Bressac, L., & Toulorge, D. (2020). CD38 in Neurodegeneration and Neuroinflammation. *Cells*, *9*(2). <https://doi.org/10.3390/cells9020471>
- Gunawardena, S., Her, L. S., Brusch, R. G., Laymon, R. A., Niesman, I. R., Gordesky-Gold, B., Sintasath, L., Bonini, N. M., & Goldstein, L. S. B. (2003). Disruption of axonal transport by loss of huntingtin or expression of pathogenic polyQ proteins in *Drosophila*. *Neuron*, *40*(1), 25–40. [https://doi.org/10.1016/S0896-6273\(03\)00594-4](https://doi.org/10.1016/S0896-6273(03)00594-4)
- Guo, X., Disatnik, M. H., Monbureau, M., Shamloo, M., Mochly-Rosen, D., & Qi, X. (2013). Inhibition of mitochondrial fragmentation diminishes Huntington's disease-associated neurodegeneration. *Journal of Clinical Investigation*, *123*(12), 5371–

REFERENCES

5388. <https://doi.org/10.1172/JCI70911>
- Guo, Z., Rudow, G., Pletnikova, O., Codispoti, K. E., Orr, B. A., Crain, B. J., Duan, W., Margolis, R. L., Rosenblatt, A., Ross, C. A., & Troncoso, J. C. (2012). Striatal neuronal loss correlates with clinical motor impairment in Huntington's disease. *Movement Disorders*, 27(11), 1379–1386. <https://doi.org/10.1002/mds.25159>
- Gusella, J. F., Wexler, N. S., Conneally, P. M., Naylor, S. L., Anderson, M. A., Tanzi, R. E., Watkins, P. C., Ottina, K., Wallace, M. R., Sakaguchi, A. Y., Young, A. B., Shoulson, I., Bonilla, E., & Martin, J. B. (1983). A polymorphic DNA marker genetically linked to Huntington's disease. *Nature*, 306(5940), 234–238. <https://doi.org/10.1038/306234a0>
- Hachem, S., Aguirre, A., Vives, V., Marks, A., Gallo, V., & Legraverend, C. (2005). Spatial and temporal expression of S100B in cells of oligodendrocyte lineage. *Glia*, 51(2), 81–97. <https://doi.org/10.1002/glia.20184>
- Hackam, A. S., Singaraja, R., Zhang, T., Gan, L., & Hayden, M. R. (1999). In vitro evidence for both the nucleus and cytoplasm as subcellular sites of pathogenesis in Huntington's disease. *Human Molecular Genetics*, 8(1), 25–33. <https://doi.org/10.1093/hmg/8.1.25>
- Halford, J., Shen, S., Itamura, K., Levine, J., Chong, A. C., Czerwieniec, G., Glenn, T. C., Hovda, D. A., Vespa, P., Bullock, R., Dietrich, W. D., Mondello, S., Loo, J. A., & Wanner, I. B. (2017). New astroglial injury-defined biomarkers for neurotrauma assessment. *Journal of Cerebral Blood Flow and Metabolism*, 37(10), 3278–3299. <https://doi.org/10.1177/0271678X17724681>
- Han, H., Tan, J., Wang, R., Wan, H., He, Y., Yan, X., Guo, J., Gao, Q., Li, J., Shang, S., Chen, F., Tian, R., Liu, W., Liao, L., Tang, B., & Zhang, Z. (2020). PINK 1 phosphorylates Drp1 S616 to regulate mitophagy-independent mitochondrial dynamics. *EMBO Reports*, 21(8), 1–17. <https://doi.org/10.15252/embr.201948686>
- Harrington, D. L., Liu, D., Smith, M. M., Mills, J. A., Long, J. D., Aylward, E. H., & Paulsen, J. S. (2014). Neuroanatomical correlates of cognitive functioning in prodromal Huntington disease. *Brain and Behavior*, 4(1), 29–40. <https://doi.org/10.1002/brb3.185>
- Hattori, T., Kaji, M., Ishii, H., Jureepon, R., Takarada-Iemata, M., Minh Ta, H., Manh Le, T., Konno, A., Hirai, H., Shiraishi, Y., Ozaki, N., Yamamoto, Y., Okamoto, H., Yokoyama, S., Higashida, H., Kitao, Y., & Hori, O. (2017). CD38 positively regulates postnatal development of astrocytes cell-autonomously and oligodendrocytes non-cell-autonomously. *GLIA*, 65(6), 974–989. <https://doi.org/10.1002/glia.23139>
- Hayakawa, K., Bruzzese, M., Chou, S. H. Y., Ning, M. M., Ji, X., & Lo, E. H. (2018). Extracellular mitochondria for therapy and diagnosis in acute central nervous system injury. *JAMA Neurology*, 75(1), 119–122. <https://doi.org/10.1001/jamaneurol.2017.3475>
- Hayakawa, K., Chan, S. J., Mandeville, E. T., Park, J. H., Bruzzese, M., Montaner, J., Arai, K., Rosell, A., & Lo, E. H. (2018). Protective Effects of Endothelial Progenitor Cell-Derived Extracellular Mitochondria in Brain Endothelium. *Stem Cells*, 36(9), 1404–1410. <https://doi.org/10.1002/stem.2856>
- Hayakawa, K., Esposito, E., Wang, X., Terasaki, Y., Liu, Y., Xing, C., Ji, X., & Lo, E. H. (2016). Transfer of mitochondria from astrocytes to neurons after stroke. *Nature*, 535(7613), 551–555. <https://doi.org/10.1038/nature19805>

REFERENCES

- Hayashi, T., & Su, T.-P. (2007). Sigma-1 Receptor Chaperones at the ER- Mitochondrion Interface Regulate Ca²⁺ Signaling and Cell Survival. *Cell*, *131*(3), 596–610. <https://doi.org/10.1016/j.cell.2007.08.036>
- Hedskog, L., Pinho, C. M., Filadi, R., Ronnback, A., Hertwig, L., Wiehager, B., Larssen, P., Gellhaar, S., Sandebring, A., Westerlund, M., Graff, C., Winblad, B., Galter, D., Behbahani, H., Pizzo, P., Glaser, E., Ankarcona, M., Rönnbäck, A., Hertwig, L., ... Ankarcona, M. (2013). Modulation of the endoplasmic reticulum-mitochondria interface in Alzheimer's disease and related models. *Proceedings of the National Academy of Sciences*, *110*(19), 7916–7921. <https://doi.org/10.1073/pnas.1300677110>
- Hees, J. T. (2019). Calcium Dysregulation and Mitochondrial Dysfunction Form A Vicious Cycle in Parkinson's Disease. *American Journal of Biomedical Science & Research*, *5*(3), 246–249. <https://doi.org/10.34297/ajbsr.2019.05.000920>
- Heidinger, V., Manzerra, P., Wang, X. Q., Strasser, U., Yu, S. P., Choi, D. W., & Behrens, M. M. (2002). Metabotropic glutamate receptor 1-induced upregulation of NMDA receptor current: Mediation through the Pyk2/Src-family kinase pathway in cortical neurons. *Journal of Neuroscience*, *22*(13), 5452–5461. <https://doi.org/10.1523/jneurosci.22-13-05452.2002>
- Hirschler-Laszkiwicz, I., Chen, S. J., Bao, L., Wang, J., Zhang, X. Q., Shanmughapriya, S., Keefer, K., Madesh, M., Cheung, J. Y., & Miller, B. A. (2018). The human ion channel TRPM2 modulates neuroblastoma cell survival and mitochondrial function through Pyk2, CREB, and MCU activation. *American Journal of Physiology - Cell Physiology*, *315*(4), C571–C586. <https://doi.org/10.1152/ajpcell.00098.2018>
- Hodgson, J. G., Agopyan, N., Gutekunst, C. A., Leavitt, B. R., Lepiane, F., Singaraja, R., Smith, D. J., Bissada, N., McCutcheon, K., Nasir, J., Jamot, L., Xiao-Jiang, L., Stevens, M. E., Rosemond, E., Roder, J. C., Phillips, A. G., Rubin, E. M., Hersch, S. M., & Hayden, M. R. (1999). A YAC mouse model for Huntington's disease with full-length mutant huntingtin, cytoplasmic toxicity, and selective striatal neurodegeneration. *Neuron*, *23*(1), 181–192. [https://doi.org/10.1016/S0896-6273\(00\)80764-3](https://doi.org/10.1016/S0896-6273(00)80764-3)
- Hsin, H., Kim, M. J., Wang, C.-F., & Sheng, M. (2010). Proline-Rich Tyrosine Kinase 2 Regulates Hippocampal Long-Term Depression. *Journal of Neuroscience*, *30*(36), 11983–11993. <https://doi.org/10.1523/JNEUROSCI.1029-10.2010>
- Huang, P. J., Kuo, C. C., Lee, H. C., Shen, C. I., Cheng, F. C., Wu, S. F., Chang, J. C., Pan, H. C., Lin, S. Z., Liu, C. S., & Su, H. L. (2016). Transferring xenogenic mitochondria provides neural protection against ischemic stress in ischemic rat brains. *Cell Transplantation*, *25*(5), 913–927. <https://doi.org/10.3727/096368915X689785>
- Hum, J. M., Day, R. N., Bidwell, J. P., Wang, Y., & Pavalko, F. M. (2014). Mechanical Loading in Osteocytes Induces Formation of a Src/Pyk2/MBD2 Complex That Suppresses Anabolic Gene Expression. *PLoS ONE*, *9*(5), e97942. <https://doi.org/10.1371/journal.pone.0097942>
- Huntington, G. (2003). On Chorea. In *J Neuropsychiatry Clin Neurosci* (Vol. 15, Issue 1).
- Husi, H., Ward, M. A., Choudhary, J. S., Blackstock, W. P., & Grant, S. G. N. (2000). Proteomic analysis of NMDA receptor-adhesion protein signaling complexes. *Nature Neuroscience*, *3*(7), 661–669. <https://doi.org/10.1038/76615>
- Ishihara, N., Nomura, M., Jofuku, A., Kato, H., Suzuki, S. O., Masuda, K., Otera, H., Nakanishi, Y., Nonaka, I., Goto, Y. I., Taguchi, N., Morinaga, H., Maeda, M.,

REFERENCES

- Takayanagi, R., Yokota, S., & Mihara, K. (2009). Mitochondrial fission factor Drp1 is essential for embryonic development and synapse formation in mice. *Nature Cell Biology*, 11(8), 958–966. <https://doi.org/10.1038/ncb1907>
- Ivankovic-Dikic, I., Grönroos, E., Blaukat, A., Barth, B. U., & Dikic, I. (2000). Pyk2 and FAK regulate neurite outgrowth induced by growth factors and integrins. *Nature Cell Biology*, 2(9), 574–581. <https://doi.org/10.1038/35023515>
- Jackson, J. G., O'Donnell, J. C., Takano, H., Coulter, D. A., & Robinson, M. B. (2014). Neuronal activity and glutamate uptake decrease mitochondrial mobility in astrocytes and position mitochondria near glutamate transporters. *Journal of Neuroscience*, 34(5), 1613–1624. <https://doi.org/10.1523/JNEUROSCI.3510-13.2014>
- Jackson, J. G., & Robinson, M. B. (2018). Regulation of mitochondrial dynamics in astrocytes: Mechanisms, consequences, and unknowns. *Glia*, 66(6), 1213–1234. <https://doi.org/10.1002/glia.23252>
- Jahani-Asl, A., Huang, E., Irrcher, I., Rashidian, J., Ishihara, N., Lagace, D. C., Slack, R. S., & Park, D. S. (2015). CDK5 phosphorylates DRP1 and drives mitochondrial defects in NMDA-induced neuronal death. *Human Molecular Genetics*, 24(16), 4573–4583. <https://doi.org/10.1093/hmg/ddv188>
- Jansen, A. H. P., van Hal, M., op den Kelder, I. C., Meier, R. T., de Ruiter, A. A., Schut, M. H., Smith, D. L., Grit, C., Brouwer, N., Kamphuis, W., Boddeke, H. W. G. M., den Dunnen, W. F. A., van Roon, W. M. C., Bates, G. P., Hol, E. M., & Reits, E. A. (2017). Frequency of nuclear mutant huntingtin inclusion formation in neurons and glia is cell-type-specific. *Glia*, 65(1), 50–61. <https://doi.org/10.1002/glia.23050>
- Jiang, S., Nandy, P., Wang, W., Ma, X., Hsia, J., Wang, C., Wang, Z., Niu, M., Siedlak, S. L., Torres, S., Fujioka, H., Xu, Y., Lee, H., Perry, G., Liu, J., & Zhu, X. (2018). Mfn2 ablation causes an oxidative stress response and eventual neuronal death in the hippocampus and cortex. *Molecular Neurodegeneration*, 13(1), 5. <https://doi.org/10.1186/s13024-018-0238-8>
- Joshi, A. U., Minhas, P. S., Liddelow, S. A., Haileselassie, B., Andreasson, K. I., Dorn, G. W., & Mochly-Rosen, D. (2019). Fragmented mitochondria released from microglia trigger A1 astrocytic response and propagate inflammatory neurodegeneration. *Nature Neuroscience*, 22(10), 1635–1648. <https://doi.org/10.1038/s41593-019-0486-0>
- Jung, H., Kim, S. Y., Canbakis Cecen, F. S., Cho, Y., & Kwon, S. K. (2020). Dysfunction of Mitochondrial Ca²⁺ Regulatory Machineries in Brain Aging and Neurodegenerative Diseases. *Frontiers in Cell and Developmental Biology*, 8(December), 1–11. <https://doi.org/10.3389/fcell.2020.599792>
- Khakh, B. S. (2019). Astrocyte–Neuron Interactions in the Striatum: Insights on Identity, Form, and Function. *Trends in Neurosciences*, 42(9), 617–630. <https://doi.org/10.1016/j.tins.2019.06.003>
- Khakh, B. S., Beaumont, V., Cachope, R., Munoz-Sanjuan, I., Goldman, S. A., & Grantyn, R. (2017). Unravelling and Exploiting Astrocyte Dysfunction in Huntington's Disease. *Trends in Neurosciences*, 40(7), 422–437. <https://doi.org/10.1016/j.tins.2017.05.002>
- Khakh, B. S., & Deneen, B. (2019). The Emerging Nature of Astrocyte Diversity. *Annual Review of Neuroscience*, 42, 187–207. <https://doi.org/10.1146/annurev-neuro-070918-050443>

REFERENCES

- Khakh, B. S., & Sofroniew, M. V. (2014). Astrocytes and Huntington's disease. *ACS Chemical Neuroscience*, *5*(7), 494–496. <https://doi.org/10.1021/cn500100r>
- Khakh, B. S., & Sofroniew, M. V. (2015). Diversity of astrocyte functions and phenotypes in neural circuits. *Nature Neuroscience*, *18*(7), 942–952. <https://doi.org/10.1038/nn.4043>
- Kilinc, D., Vreulx, A.-C., Mendes, T., Flaig, A., Marques-Coelho, D., Verschoore, M., Demiautte, F., Amouyel, P., Eysert, F., Dourlen, P., Chapuis, J., Costa, M. R., Malmanche, N., Checler, F., & Lambert, J.-C. (2020). Pyk2 overexpression in postsynaptic neurons blocks amyloid β 1–42-induced synaptotoxicity in microfluidic co-cultures. *Brain Communications*, *2*(2). <https://doi.org/10.1093/braincomms/fcaa139>
- Kim, E. H., Thu, D. C. V., Tippett, L. J., Oorschot, D. E., Hogg, V. M., Roxburgh, R., Synek, B. J., Waldvogel, H. J., & Faull, R. L. M. (2014). Cortical interneuron loss and symptom heterogeneity in Huntington disease. *Annals of Neurology*, *75*(5), 717–727. <https://doi.org/10.1002/ana.24162>
- Kim, J., Moody, J. P., Edgerly, C. K., Bordiuk, O. L., Cormier, K., Smith, K., Flint Beal, M., & Ferrante, R. J. (2010). Mitochondrial loss, dysfunction and altered dynamics in Huntington's disease. *Human Molecular Genetics*, *19*(20), 3919–3935. <https://doi.org/10.1093/hmg/ddq306>
- Köhler, C., Dinekov, M., & Götz, J. (2013). Active glycogen synthase kinase-3 and tau pathology-related tyrosine phosphorylation in pR5 human tau transgenic mice. *Neurobiology of Aging*, *34*(5), 1369–1379. <https://doi.org/10.1016/j.neurobiolaging.2012.11.010>
- Kohno, T., Matsuda, E., Sasaki, H., & Sasaki, T. (2008). Protein-tyrosine kinase CAK β /PYK2 is activated by binding Ca²⁺/calmodulin to FERM F2 α 2 helix and thus forming its dimer. *Biochemical Journal*, *410*(3), 513–523. <https://doi.org/10.1042/BJ20070665>
- Kotrasová, V., Keresztesová, B., Ondrovičová, G., Bauer, J. A., Havalová, H., Pevala, V., Kutejová, E., & Kunová, N. (2021). Mitochondrial kinases and the role of mitochondrial protein phosphorylation in health and disease. *Life*, *11*(2), 1–37. <https://doi.org/10.3390/life11020082>
- Kruse, R., & Højlund, K. (2017). Mitochondrial phosphoproteomics of mammalian tissues. *Mitochondrion*, *33*, 45–57. <https://doi.org/10.1016/j.mito.2016.08.004>
- Kühlbrandt, W. (2015). Structure and function of mitochondrial membrane protein complexes. *BMC Biology*, *13*(1), 1–11. <https://doi.org/10.1186/s12915-015-0201-x>
- Kumar, R., Tiwari, V., & Dey, S. (2021). Role of proline-rich tyrosine kinase 2 (Pyk2) in the pathogenesis of Alzheimer's disease. *European Journal of Neuroscience*, July 2021, 1–11. <https://doi.org/10.1111/ejn.15569>
- Kurup, P. K., Xu, J., Videira, R. A., Ononenyi, C., Baltazar, G., Lombroso, P. J., & Nairn, A. C. (2015). STEP61 is a substrate of the E3 ligase parkin and is upregulated in Parkinson's disease. *Proceedings of the National Academy of Sciences of the United States of America*, *112*(4), 1202–1207. <https://doi.org/10.1073/pnas.1417423112>
- Kurup, P., Zhang, Y., Xu, J., Venkitaramani, D. V., Haroutunian, V., Greengard, P., Nairn, A. C., & Lombroso, P. J. (2010). A β -mediated NMDA receptor endocytosis in alzheimer's disease involves ubiquitination of the tyrosine phosphatase STEP61. *Journal of Neuroscience*, *30*(17), 5948–5957.

REFERENCES

- <https://doi.org/10.1523/JNEUROSCI.0157-10.2010>
- Lackner, L. L., & Nunnari, J. (2010). Small Molecule Inhibitors of Mitochondrial Division: Tools that Translate Basic Biological Research into Medicine. *Chemistry and Biology*, 17(6), 578–583. <https://doi.org/10.1016/j.chembiol.2010.05.016>
- Lambert, J. C., Ibrahim-Verbaas, C. A., Harold, D., Naj, A. C., Sims, R., Bellenguez, C., Jun, G., DeStefano, A. L., Bis, J. C., Beecham, G. W., Grenier-Boley, B., Russo, G., Thornton-Wells, T. A., Jones, N., Smith, A. V., Chouraki, V., Thomas, C., Ikram, M. A., Zelenika, D., ... Seshadri, S. (2013). Meta-analysis of 74,046 individuals identifies 11 new susceptibility loci for Alzheimer's disease. *Nature Genetics*, 45(12), 1452–1458. <https://doi.org/10.1038/ng.2802>
- Lautrup, S., Sinclair, D. A., Mattson, M. P., & Fang, E. F. (2019). NAD⁺ in Brain Aging and Neurodegenerative Disorders. *Cell Metabolism*, 30(4), 630–655. <https://doi.org/10.1016/j.cmet.2019.09.001>
- Leboucher, G. P., Tsai, Y. C., Yang, M., Shaw, K. C., Zhou, M., Veenstra, T. D., Glickman, M. H., & Weissman, A. M. (2012). Stress-Induced Phosphorylation and Proteasomal Degradation of Mitofusin 2 Facilitates Mitochondrial Fragmentation and Apoptosis. *Molecular Cell*, 47(4), 547–557. <https://doi.org/10.1016/j.molcel.2012.05.041>
- Lee, K. S., Huh, S., Lee, S., Wu, Z., Kim, A. K., Kang, H. Y., & Lu, B. (2018). Altered ER-mitochondria contact impacts mitochondria calcium homeostasis and contributes to neurodegeneration in vivo in disease models. *Proceedings of the National Academy of Sciences of the United States of America*, 115(38), E8844–E8853. <https://doi.org/10.1073/pnas.1721136115>
- Lee, S., Salazar, S. V., Cox, T. O., & Strittmatter, S. M. (2019). Pyk2 Signaling through Graf1 and RhoA GTPase Is Required for Amyloid- β Oligomer-Triggered Synapse Loss. *Neurobiology of Disease*, 39(10), 1910–1929. <https://doi.org/10.1523/JNEUROSCI.2983-18.2018>
- Lee, W. C. M., Yoshihara, M., & Littleton, J. T. (2004). Cytoplasmic aggregates trap polyglutamine-containing proteins and block axonal transport in a Drosophila model of Huntington's disease. *Proceedings of the National Academy of Sciences of the United States of America*, 101(9), 3224–3229. <https://doi.org/10.1073/pnas.0400243101>
- Lee, Y., Messing, A., Su, M., & Brenner, M. (2008). GFAP promoter elements required for region-specific and astrocyte-specific expression. *Glia*, 56(5), 481–493. <https://doi.org/10.1002/glia.20622>
- Lerchundi, R., Huang, N., & Rose, C. R. (2020). Quantitative Imaging of Changes in Astrocytic and Neuronal Adenosine Triphosphate Using Two Different Variants of ATeam. *Frontiers in Cellular Neuroscience*, 14(April), 1–13. <https://doi.org/10.3389/fncel.2020.00080>
- Lev, S., Moreno, H., Martinez, R., Canoll, P., Peles, E., Musacchio, J. M., Plowman, G. D., Rudy, B., & Schlessinger, J. (1995). Protein tyrosine kinase PYK2 involved in Ca²⁺-induced regulation of ion channel and MAP kinase functions. *Nature*, 376(6543), 737–745. <https://doi.org/10.1038/376737a0>
- Levine, J., Kwon, E., Paez, P., Yan, W., Czerwieniec, G., Loo, J. A., Sofroniew, M. V., & Wanner, I. B. (2016). Traumatically injured astrocytes release a proteomic signature modulated by STAT3-dependent cell survival. *Glia*, 64(5), 668–694. <https://doi.org/10.1002/glia.22953>

REFERENCES

- Li, X., Dy, R. C., Cance, W. G., Graves, L. M., & Earp, H. S. (1999). Interactions between two cytoskeleton-associated tyrosine kinases: Calcium-dependent tyrosine kinase and focal adhesion tyrosine kinase. *Journal of Biological Chemistry*, *274*(13), 8917–8924. <https://doi.org/10.1074/jbc.274.13.8917>
- Liesa, M., & Shirihai, O. S. (2013). Mitochondrial dynamics in the regulation of nutrient utilization and energy expenditure. *Cell Metabolism*, *17*(4), 491–506. <https://doi.org/10.1016/j.cmet.2013.03.002>
- Liévens, J. C., Woodman, B., Mahal, A., Spasic-Bosovic, O., Samuel, D., Kerkerian-Le Goff, L., & Bates, G. P. (2001). Impaired glutamate uptake in the R6 Huntington's disease transgenic mice. *Neurobiology of Disease*, *8*(5), 807–821. <https://doi.org/10.1006/nbdi.2001.0430>
- Lim, D., Fedrizzi, L., Tartari, M., Zuccato, C., Cattaneo, E., Brini, M., & Carafoli, E. (2008). Calcium homeostasis and mitochondrial dysfunction in striatal neurons of Huntington disease. *Journal of Biological Chemistry*, *283*(9), 5780–5789. <https://doi.org/10.1074/jbc.M704704200>
- Lim, S., Smith, K. R., Lim, S. T. S., Tian, R., Lu, J., & Tan, M. (2016). Regulation of mitochondrial functions by protein phosphorylation and dephosphorylation. *Cell and Bioscience*, *6*(1), 1–15. <https://doi.org/10.1186/s13578-016-0089-3>
- Lipinski, C. A., & Loftus, J. C. (2010). The Pyk2 FERM domain: a Novel Therapeutic Target Christopher. *Expert Opinion on Therapeutic Targets*, *14*(1), 95–108. <https://doi.org/10.1517/14728220903473194>.The
- Lipinski, C. A., Tran, N. L., Dooley, A., Pang, Y. P., Rohl, C., Kloss, J., Yang, Z., McDonough, W., Craig, D., Berens, M. E., & Loftus, J. C. (2006). Critical role of the FERM domain in Pyk2 stimulated glioma cell migration. *Biochemical and Biophysical Research Communications*, *349*(3), 939–947. <https://doi.org/10.1016/j.bbrc.2006.08.134>
- Lippert, T., & Borlongan, C. V. (2019). Prophylactic treatment of hyperbaric oxygen treatment mitigates inflammatory response via mitochondria transfer. *CNS Neuroscience and Therapeutics*, *25*(8), 815–823. <https://doi.org/10.1111/cns.13124>
- Liu, D., Gao, Y., Liu, J., Huang, Y., Yin, J., Feng, Y., Shi, L., Meloni, B. P., Zhang, C., Zheng, M., & Gao, J. (2021). Intercellular mitochondrial transfer as a means of tissue revitalization. *Signal Transduction and Targeted Therapy*, *6*(1). <https://doi.org/10.1038/s41392-020-00440-z>
- Liu, F. T., Chen, Y., Yang, Y. J., Yang, L., Yu, M., Zhao, J., Wu, J. J., Huang, F., Liu, W., Ding, Z. T., & Wang, J. (2015). Involvement of mortalin/GRP75/mthsp70 in the mitochondrial impairments induced by A53T mutant α -synuclein. *Brain Research*, *1604*, 52–61. <https://doi.org/10.1016/j.brainres.2015.01.050>
- Liu, J. M., Yi, Z., Liu, S. Z., Chang, J. H., Dang, X. B., Li, Q. Y., & Zhang, Y. L. (2015). The mitochondrial division inhibitor mdivi-1 attenuates spinal cord ischemia-reperfusion injury both in vitro and in vivo: Involvement of BK channels. *Brain Research*, *1619*, 155–165. <https://doi.org/10.1016/j.brainres.2015.03.033>
- Lloret, A., Dragileva, E., Teed, A., Espinola, J., Fossale, E., Gillis, T., Lopez, E., Myers, R. H., MacDonald, M. E., & Wheeler, V. C. (2006). Genetic background modifies nuclear mutant huntingtin accumulation and HD CAG repeat instability in Huntington's disease knock-in mice. *Human Molecular Genetics*, *15*(12), 2015–2024. <https://doi.org/10.1093/hmg/ddl125>

REFERENCES

- Lombroso, P. J., Nairn, A. C., Ogren, M., & Kurup, P. (2016). Molecular underpinnings of neurodegenerative disorders: Striatal-enriched protein tyrosine phosphatase signaling and synaptic plasticity. *F1000Research*, 5. <https://doi.org/10.12688/f1000research.8571.1>
- Lu, L., Zhang, C., Cai, Q., Lu, Q., Duan, C., Zhu, Y., & Yang, H. (2013). Voltage-dependent anion channel involved in the α -synuclein-induced dopaminergic neuron toxicity in rats. *Acta Biochimica et Biophysica Sinica*, 45(3), 170–178. <https://doi.org/10.1093/abbs/gms114>
- Lucero, M., Suarez, A. E., & Chambers, J. W. (2019). Phosphoregulation on mitochondria: Integration of cell and organelle responses. *CNS Neuroscience and Therapeutics*, 25(7), 837–858. <https://doi.org/10.1111/cns.13141>
- Mächler, P., Wyss, M. T., Elsayed, M., Stobart, J., Gutierrez, R., Von Faber-Castell, A., Kaelin, V., Zuend, M., San Martín, A., Romero-Gómez, I., Baeza-Lehnert, F., Lengacher, S., Schneider, B. L., Aebischer, P., Magistretti, P. J., Barros, L. F., & Weber, B. (2016). In Vivo Evidence for a Lactate Gradient from Astrocytes to Neurons. *Cell Metabolism*, 23(1), 94–102. <https://doi.org/10.1016/j.cmet.2015.10.010>
- Maldonado, H., Calderon, C., Burgos-Bravo, F., Kobler, O., Zuschratter, W., Ramirez, O., Härtel, S., Schneider, P., Quest, A. F. G., Herrera-Molina, R., & Leyton, L. (2017). Astrocyte-to-neuron communication through integrin-engaged Thy-1/CBP/Csk/Src complex triggers neurite retraction via the RhoA/ROCK pathway. *Biochimica et Biophysica Acta - Molecular Cell Research*, 1864(2), 243–254. <https://doi.org/10.1016/j.bbamcr.2016.11.006>
- Manczak, M., Calkins, M. J., & Reddy, P. H. (2011). Impaired mitochondrial dynamics and abnormal interaction of amyloid beta with mitochondrial protein Drp1 in neurons from patients with Alzheimer's disease: Implications for neuronal damage. *Human Molecular Genetics*, 20(13), 2495–2509. <https://doi.org/10.1093/hmg/ddr139>
- Manczak, M., & Hemachandra Reddy, P. (2015). Mitochondrial division inhibitor 1 protects against mutant huntingtin-induced abnormal mitochondrial dynamics and neuronal damage in Huntington's disease. *Human Molecular Genetics*, 24(25), 7308–7325. <https://doi.org/10.1093/hmg/ddv429>
- Mangiarini, L., Sathasivam, K., Seller, M., Cozens, B., Harper, A., Hetherington, C., Lawton, M., Trotter, Y., Lehrach, H., Davies, S. W., & Bates, G. P. (1996). *Exon 1 of the HD Gene with an Expanded CAG Repeat Is Sufficient to Cause a Progressive Neurological Phenotype in Transgenic Mice*. 87, 493–506. http://ac.els-cdn.com/S0092867400813690/1-s2.0-S0092867400813690-main.pdf?_tid=7db7695e-7afe-11e7-94f8-0000aacb35d&acdnat=1502062090_1e45eb383db00141a08e5daa67072892
- Margulis, L. (1967). On the origin of mitosing cells. *Journal of Theoretical Biology*, 14(3), 255–274. <http://www.ncbi.nlm.nih.gov/pubmed/11541390>
- Martin, W. R. W., Wieler, M., & Hanstock, C. C. (2007). Is brain lactate increased in Huntington's disease? *Journal of the Neurological Sciences*, 263(1–2), 70–74. <https://doi.org/10.1016/j.jns.2007.05.035>
- Mastrolia, V., al Massadi, O., de Pins, B., & Girault, J.-A. (2021). Pyk2 in dorsal hippocampus plays a selective role in spatial memory and synaptic plasticity. *Scientific Reports*, 11(1), 16357. <https://doi.org/10.1038/s41598-021-95813-x>
- Matias, I., Morgado, J., & Gomes, F. C. A. (2019). Astrocyte Heterogeneity: Impact to Brain Aging and Disease. *Frontiers in Aging Neuroscience*, 11(March), 1–18.

REFERENCES

- <https://doi.org/10.3389/fnagi.2019.00059>
- McColgan, P., & Tabrizi, S. J. (2018). Huntington's disease: a clinical review. *European Journal of Neurology*, 25(1), 24–34. <https://doi.org/10.1111/ene.13413>
- McColgan, Peter, Razi, A., Gregory, S., Seunarine, K. K., Durr, A., A.C. Roos, R., Leavitt, B. R., Scahill, R. I., Clark, C. A., Langbehn, D. R., Rees, G., & Tabrizi, S. J. (2017). Structural and functional brain network correlates of depressive symptoms in premanifest Huntington's disease. *Human Brain Mapping*, 38(6), 2819–2829. <https://doi.org/10.1002/hbm.23527>
- Medja, F., Allouche, S., Frachon, P., Jardel, C., Malgat, M., de Camaret, B. M., Slama, A., Lunardi, J., Mazat, J. P., & Lombès, A. (2009). Development and implementation of standardized respiratory chain spectrophotometric assays for clinical diagnosis. *Mitochondrion*, 9(5), 331–339. <https://doi.org/10.1016/j.mito.2009.05.001>
- Mehrabi, N. F., Waldvogel, H. J., Tippett, L. J., Hogg, V. M., Synek, B. J., & Faull, R. L. M. (2016). Symptom heterogeneity in Huntington's disease correlates with neuronal degeneration in the cerebral cortex. *Neurobiology of Disease*, 96, 67–74. <https://doi.org/10.1016/j.nbd.2016.08.015>
- Menalled, L. B., Sison, J. D., Dragatsis, I., Zeitlin, S., & Chesselet, M. F. (2003). Time course of early motor and neuropathological anomalies in a knock-in mouse model of Huntington's disease with 140 CAG repeats. *Journal of Comparative Neurology*, 465(1), 11–26. <https://doi.org/10.1002/cne.10776>
- Menalled, L., Lutz, C., Ramboz, S., Brunner, D., Lager, B., Noble, S., Park, L., & Howland, D. (2014). A Field Guide to Working with Mouse Models of Huntington's Disease. *The Jackson Laboratory*, 1–44. <http://www.sciencedirect.com/science/article/pii/S0165614700018848>
- Mészáros, L. G., Bak, J., & Chu, A. (1993). Cyclic ADP-ribose as an endogenous regulator of the non-skeletal type ryanodine receptor Ca²⁺ channel. *Nature*, 364(6432), 76–79. <https://doi.org/10.1038/364076a0>
- Meuer, K., Suppanz, I. E., Lingor, P., Planchamp, V., Göricke, B., Fichtner, L., Braus, G. H., Dietz, G. P. H., Jakobs, S., Bähr, M., & Weishaupt, J. H. (2007). Cyclin-dependent kinase 5 is an upstream regulator of mitochondrial fission during neuronal apoptosis. *Cell Death and Differentiation*, 14(4), 651–661. <https://doi.org/10.1038/sj.cdd.4402087>
- Milakovic, T., Quintanilla, R. A., & Johnson, G. V. W. (2006). Mutant Huntingtin expression induces mitochondrial calcium handling defects in clonal striatal cells: Functional consequences. *Journal of Biological Chemistry*, 281(46), 34785–34795. <https://doi.org/10.1074/jbc.M603845200>
- Miller, B. A., Wang, J. F., Song, J., Zhang, X. Q., Hirschler-Laszkiwicz, I., Shanmughapriya, S., Tomar, D., Rajan, S., Feldman, A. M., Madesh, M., Sheu, S. S., & Cheung, J. Y. (2019). Trpm2 enhances physiological bioenergetics and protects against pathological oxidative cardiac injury: Role of Pyk2 phosphorylation. *Journal of Cellular Physiology*, 234(9), 15048–15060. <https://doi.org/10.1002/jcp.28146>
- Miller, B. R., Dorner, J. L., Shou, M., Sari, Y., Barton, S. J., Sengelaub, D. R., Kennedy, R. T., & Rebec, G. V. (2008). Up-regulation of GLUT1 expression increases glutamate uptake and attenuates the Huntington's disease phenotype in the R6/2 mouse. *Neuroscience*, 153(1), 329–337. <https://doi.org/10.1016/j.neuroscience.2008.02.004>

REFERENCES

- Milnerwood, A. J., Gladding, C. M., Pouladi, M. A., Kaufman, A. M., Hines, R. M., Boyd, J. D., Ko, R. W. Y., Vasuta, O. C., Graham, R. K., Hayden, M. R., Murphy, T. H., & Raymond, L. A. (2010). Early Increase in Extrasynaptic NMDA Receptor Signaling and Expression Contributes to Phenotype Onset in Huntington's Disease Mice. *Neuron*, *65*(2), 178–190. <https://doi.org/10.1016/j.neuron.2010.01.008>
- Møllersen, L., Rowe, A. D., Larsen, E., Rognes, T., & Klungland, A. (2010). Continuous and periodic expansion of CAG repeats in huntington's disease R6/1 mice. *PLoS Genetics*, *6*(12), 1–11. <https://doi.org/10.1371/journal.pgen.1001242>
- Montalban, E., Al-Massadi, O., Sancho-Balsells, A., Brito, V., de Pins, B., Alberch, J., Ginés, S., Girault, J.-A., & Giral, A. (2019). Pyk2 in the amygdala modulates chronic stress sequelae via PSD-95-related micro-structural changes. *Translational Psychiatry*, *9*(3). <https://doi.org/10.1038/s41398-018-0352-y>
- Monteiro, L. de B., Davanzo, G. G., de Aguiar, C. F., & Moraes-Vieira, P. M. M. (2020). Using flow cytometry for mitochondrial assays. *MethodsX*, *7*. <https://doi.org/10.1016/j.mex.2020.100938>
- Morales, I., Sanchez, A., Puertas-Avendaño, R., Rodriguez-Sabate, C., Perez-Barreto, A., & Rodriguez, M. (2020). Neuroglial transmitophagy and Parkinson's disease. *Glia*, *68*(11), 2277–2299. <https://doi.org/10.1002/glia.23839>
- Morancho, A., Ma, F., Barceló, V., Giral, D., Montaner, J., & Rosell, A. (2015). Impaired vascular remodeling after endothelial progenitor cell transplantation in MMP9-deficient mice suffering cortical cerebral ischemia. *Journal of Cerebral Blood Flow and Metabolism*, *35*(10), 1547–1551. <https://doi.org/10.1038/jcbfm.2015.180>
- Morigaki, R., & Goto, S. (2017). Striatal vulnerability in huntington's disease: Neuroprotection versus neurotoxicity. *Brain Sciences*, *7*(6), 02–25. <https://doi.org/10.3390/brainsci7060063>
- Morton, A. J., Glynn, D., Leavens, W., Zheng, Z., Faull, R. L. M., Skepper, J. N., & Wight, J. M. (2009). Paradoxical delay in the onset of disease caused by super-long CAG repeat expansions in R6/2 mice. *Neurobiology of Disease*, *33*(3), 331–341. <https://doi.org/10.1016/j.nbd.2008.11.015>
- Mudannayake, J. M., Mouravlev, A., Fong, D. M., & Young, D. (2016). Transcriptional activity of novel ALDH1L1 promoters in the rat brain following AAV vector-mediated gene transfer. *Molecular Therapy - Methods and Clinical Development*, *3*(October), 16075. <https://doi.org/10.1038/mtm.2016.75>
- Naia, L., Ferreira, I. L., Ferreira, E., & Rego, A. C. (2017). Mitochondrial Ca²⁺ handling in Huntington's and Alzheimer's diseases – Role of ER-mitochondria crosstalk. *Biochemical and Biophysical Research Communications*, *483*(4), 1069–1077. <https://doi.org/10.1016/j.bbrc.2016.07.122>
- Naia, L., Ly, P., Mota, S. I., Lopes, C., Maranga, C., Coelho, P., Gershoni-Emek, N., Ankarcona, M., Geva, M., Hayden, M. R., & Rego, A. C. (2021). The Sigma-1 Receptor Mediates Pridopidine Rescue of Mitochondrial Function in Huntington Disease Models. *Neurotherapeutics*, *18*(2), 1017–1038. <https://doi.org/10.1007/s13311-021-01022-9>
- Nakamura, T., Yamashita, H., Nagano, Y., Takahashi, T., Avraham, S., Avraham, H., Matsumoto, M., & Nakamura, S. (2002). Activation of Pyk2/RAFTK induces tyrosine phosphorylation of α -synuclein via Src-family kinases. *FEBS Letters*, *521*(1–3), 190–194. [https://doi.org/10.1016/S0014-5793\(02\)02861-2](https://doi.org/10.1016/S0014-5793(02)02861-2)
- Nana, A. L., Kim, E. H., Thu, D. C. V., Oorschot, D. E., Tippett, L. J., Hogg, V. M., Synek,

REFERENCES

- B. J., Roxburgh, R., Waldvogel, H. J., & Faull, R. L. M. (2014). Widespread heterogeneous neuronal loss across the cerebral cortex in Huntington's disease. *Journal of Huntington's Disease*, 3(1), 45–64. <https://doi.org/10.3233/JHD-140092>
- Nitzan, K., Benhamron, S., Valitsky, M., Kesner, E. E., Lichtenstein, M., Ben-Zvi, A., Ella, E., Segalstein, Y., Saada, A., Lorberboum-Galski, H., & Rosenmann, H. (2019). Mitochondrial Transfer Ameliorates Cognitive Deficits, Neuronal Loss, and Gliosis in Alzheimer's Disease Mice. *Journal of Alzheimer's Disease : JAD*, 72(2), 587–604. <https://doi.org/10.3233/JAD-190853>
- O-Uchi, J., Jhun, B. S., Xu, S., Hurst, S., Raffaello, A., Liu, X., Yi, B., Zhang, H., Gross, P., Mishra, J., Ainbinder, A., Kettlewell, S., Smith, G. L., Dirksen, R. T., Wang, W., Rizzuto, R., & Sheu, S. S. (2014). Adrenergic signaling regulates mitochondrial Ca²⁺ uptake through Pyk2-dependent tyrosine phosphorylation of the mitochondrial Ca²⁺ uniporter. *Antioxidants and Redox Signaling*, 21(6), 863–879. <https://doi.org/10.1089/ars.2013.5394>
- Oettinghaus, B., Schulz, J. M., Restelli, L. M., Licci, M., Savoia, C., Schmidt, A., Schmitt, K., Grimm, A., Morè, L., Hench, J., Tolnay, M., Eckert, A., D'Adamo, P., Franken, P., Ishihara, N., Mihara, K., Bischofberger, J., Scorrano, L., & Frank, S. (2016). Synaptic dysfunction, memory deficits and hippocampal atrophy due to ablation of mitochondrial fission in adult forebrain neurons. *Cell Death & Differentiation*, 23(1), 18–28. <https://doi.org/10.1038/cdd.2015.39>
- Okamoto, S. I., Pouladi, M. A., Talantova, M., Yao, D., Xia, P., Ehrnhoefer, D. E., Zaidi, R., Clemente, A., Kaul, M., Graham, R. K., Zhang, D., Vincent Chen, H. S., Tong, G., Hayden, M. R., & Lipton, S. A. (2009). Balance between synaptic versus extrasynaptic NMDA receptor activity influences inclusions and neurotoxicity of mutant huntingtin. *Nature Medicine*, 15(12), 1407–1413. <https://doi.org/10.1038/nm.2056>
- Okigaki, M., Davis, C., Falascat, M., Harroch, S., Felsenfeld, D. P., Sheetz, M. P., & Schlessinger, J. (2003). Pyk2 regulates multiple signaling events crucial for macrophage morphology and migration. *Proceedings of the National Academy of Sciences of the United States of America*, 100(19), 10740–10745. <https://doi.org/10.1073/pnas.1834348100>
- Okun, M. S., & Thommi, N. (2004). Americo Negrette (1924 to 2003): Diagnosing Huntington disease in Venezuela. *Neurology*, 63(2), 340–343. <https://doi.org/10.1212/01.WNL.0000129827.16522.78>
- Oliveira, J. M. A. (2010). Mitochondrial bioenergetics and dynamics in Huntington's disease: Tripartite synapses and selective striatal degeneration. In *Journal of Bioenergetics and Biomembranes* (Vol. 42, Issue 3, pp. 227–234). <https://doi.org/10.1007/s10863-010-9287-6>
- Oliveira, J. M. A., & Gonçalves, J. (2009). In situ mitochondrial Ca²⁺ buffering differences of intact neurons and astrocytes from cortex and striatum. *Journal of Biological Chemistry*, 284(8), 5010–5020. <https://doi.org/10.1074/jbc.M807459200>
- Oliveira, J. M. A., Jekabsons, M. B., Chen, S., Lin, A., Rego, A. C., Gonçalves, J., Ellerby, L. M., & Nicholls, D. G. (2007). Mitochondrial dysfunction in Huntington's disease: The bioenergetics of isolated and in situ mitochondria from transgenic mice. *Journal of Neurochemistry*, 101(1), 241–249. <https://doi.org/10.1111/j.1471-4159.2006.04361.x>
- Ordóñez, D. G., Lee, M. K., & Feany, M. B. (2018). α -synuclein Induces Mitochondrial Dysfunction through Spectrin and the Actin Cytoskeleton. *Neuron*, 97(1), 108–124.e6. <https://doi.org/10.1016/j.neuron.2017.11.036>

REFERENCES

- Osipovitch, M., Asenjo Martinez, A., Mariani, J. N., Cornwell, A., Dhaliwal, S., Zou, L., Chandler-Militello, D., Wang, S., Li, X., Benraiss, S. J., Agate, R., Lampp, A., Benraiss, A., Windrem, M. S., & Goldman, S. A. (2019). Human ESC-Derived Chimeric Mouse Models of Huntington's Disease Reveal Cell-Intrinsic Defects in Glial Progenitor Cell Differentiation. *Cell Stem Cell*, 24(1), 107-122.e7. <https://doi.org/10.1016/j.stem.2018.11.010>
- Ossovskaya, V., Lim, S. T., Ota, N., Schlaepfer, D. D., & Ilic, D. (2008). FAK nuclear export signal sequences. *FEBS Letters*, 582(16), 2402–2406. <https://doi.org/10.1016/j.febslet.2008.06.004>
- Padrão, A. I., Vitorino, R., Duarte, J. A., Ferreira, R., & Amado, F. (2013). Unraveling the phosphoproteome dynamics in mammal mitochondria from a network perspective. *Journal of Proteome Research*, 12(10), 4257–4267. <https://doi.org/10.1021/pr4003917>
- Paillusson, S., Gomez-Suaga, P., Stoica, R., Little, D., Gissen, P., Devine, M. J., Noble, W., Hanger, D. P., & Miller, C. C. J. (2017). α -Synuclein binds to the ER-mitochondria tethering protein VAPB to disrupt Ca²⁺ homeostasis and mitochondrial ATP production. *Acta Neuropathologica*, 134(1), 129–149. <https://doi.org/10.1007/s00401-017-1704-z>
- Pajarillo, E., Rizor, A., Lee, J., Aschner, M., & Lee, E. (2019). The role of astrocytic glutamate transporters GLT-1 and GLAST in neurological disorders: Potential targets for neurotherapeutics. *Neuropharmacology*, 161(December 2018), 107559. <https://doi.org/10.1016/j.neuropharm.2019.03.002>
- Palpagama, T. H., Waldvogel, H. J., Faull, R. L. M., & Kwakowsky, A. (2019). The Role of Microglia and Astrocytes in Huntington's Disease. *Frontiers in Molecular Neuroscience*, 12(October), 1–15. <https://doi.org/10.3389/fnmol.2019.00258>
- Panov, A. V., Gutekunst, C. A., Leavitt, B. R., Hayden, M. R., Burke, J. R., Strittmatter, W. J., & Greenamyre, J. T. (2002). Early mitochondrial calcium defects in Huntington's disease are a direct effect of polyglutamines. *Nature Neuroscience*, 5(8), 731–736. <https://doi.org/10.1038/nn884>
- Park, G., Lee, J. Y., Han, H. M., An, H. S., Jin, Z., Jeong, E. A., Kim, K. E., Shin, H. J., Lee, J., Kang, D., Kim, H. J., Bae, Y. C., & Roh, G. S. (2021). Ablation of dynamin-related protein 1 promotes diabetes-induced synaptic injury in the hippocampus. *Cell Death & Disease*, 12(5), 445. <https://doi.org/10.1038/s41419-021-03723-7>
- Park, S. Y., Avraham, H. K., & Avraham, S. (2004). RAFTK/Pyk2 activation is mediated by trans-acting autophosphorylation in a Src-independent manner. *Journal of Biological Chemistry*, 279(32), 33315–33322. <https://doi.org/10.1074/jbc.M313527200>
- Paulsen, J. S. (2005). Depression and Stages of Huntington's Disease. *Journal of Neuropsychiatry*, 17(4), 496–502. <https://doi.org/10.1176/appi.neuropsych.17.4.496>
- Paulsen, Jane S., Miller, A. C., Hayes, T., & Shaw, E. (2017). Cognitive and behavioural changes in Huntington disease before diagnosis. *Handbook of Clinical Neurology*, 144, 69–91.
- Pei, L., & Wallace, D. C. (2018). Mitochondrial Etiology of Neuropsychiatric Disorders. In *Biological Psychiatry* (Vol. 83, Issue 9, pp. 722–730). <https://doi.org/10.1016/j.biopsych.2017.11.018>

REFERENCES

- Pellman, J. J., Hamilton, J., Brustovetsky, T., & Brustovetsky, N. (2015). Ca²⁺ handling in isolated brain mitochondria and cultured neurons derived from the YAC128 mouse model of Huntington's disease. *Journal of Neurochemistry*, *134*(4), 652–667. <https://doi.org/10.1111/jnc.13165>
- Pickrell, A. M., Fukui, H., Wang, X., Pinto, M., & Moraes, C. T. (2011). The striatum is highly susceptible to mitochondrial oxidative phosphorylation dysfunctions. *Journal of Neuroscience*, *31*(27), 9895–9904. <https://doi.org/10.1523/JNEUROSCI.6223-10.2011>
- Pozo-Guisado, E., & Martin-Romero, F. J. (2013). The regulation of STIM1 by phosphorylation. *Communicative and Integrative Biology*, *6*(6). <https://doi.org/10.4161/cib.26283>
- Prasad, M., Pawlak, K. J., Burak, W. E., Perry, E. E., Marshall, B., Whittal, R. M., & Bose, H. S. (2017). Mitochondrial metabolic regulation by GRP78. *Science Advances*, *3*(2), e1602038. <https://doi.org/10.1126/sciadv.1602038>
- Quirós, P. M., Mottis, A., & Auwerx, J. (2016). Mitonuclear communication in homeostasis and stress. *Nature Reviews Molecular Cell Biology*, *17*(4), 213–226. <https://doi.org/10.1038/nrm.2016.23>
- Raffaello, A., Mammucari, C., Gherardi, G., & Rizzuto, R. (2016). Calcium at the Center of Cell Signaling: Interplay between Endoplasmic Reticulum, Mitochondria, and Lysosomes. *Trends in Biochemical Sciences*, *41*(12), 1035–1049. <https://doi.org/10.1016/j.tibs.2016.09.001>
- Raponi, E., Agenes, F., Delphin, C., Assard, N., Baudier, J., Legraverend, C., & Deloulme, J.-C. (2007). S100B Expression Defines a State in Which GFAP-Expressing Cells Lose Their Neural Stem Cell Potential and Acquire a More Mature Developmental Stage. *Glia*, *55*, 165–177. <https://doi.org/10.1002/glia>
- Rappold, P. M., Cui, M., Grima, J. C., Fan, R. Z., De Mesy-Bentley, K. L., Chen, L., Zhuang, X., Bowers, W. J., & Tieu, K. (2014). Drp1 inhibition attenuates neurotoxicity and dopamine release deficits in vivo. *Nature Communications*, *5*. <https://doi.org/10.1038/ncomms6244>
- Reddy, P. H. (2014). Increased mitochondrial fission and neuronal dysfunction in Huntington's disease: Implications for molecular inhibitors of excessive mitochondrial fission. *Drug Discovery Today*, *19*(7), 951–955. <https://doi.org/10.1016/j.drudis.2014.03.020>
- Reddy, P. H., & Shirendeb, U. P. (2012). Mutant huntingtin, abnormal mitochondrial dynamics, defective axonal transport of mitochondria, and selective synaptic degeneration in Huntington's disease. *Biochimica et Biophysica Acta - Molecular Basis of Disease*, *1822*(2), 101–110. <https://doi.org/10.1016/j.bbadis.2011.10.016>
- Reiner, A., Albin, R. L., Anderson, K. D., D'Amato, C. J., Penney, J. B., & Young, A. B. (1988). Differential loss of striatal projection neurons in Huntington disease. *Proceedings of the National Academy of Sciences of the United States of America*, *85*(15), 5733–5737. <https://doi.org/10.1073/pnas.85.15.5733>
- Richfield, E. K., Maguire-Zeiss, K. A., Cox, C., Gilmore, J., & Voorn, P. (1995). Reduced expression of preproenkephalin in striatal neurons from huntington's disease patients. *Annals of Neurology*, *37*(3), 335–343. <https://doi.org/10.1002/ana.410370309>
- Riguet, N., Mahul-Mellier, A. L., Maharjan, N., Burtscher, J., Croisier, M., Knott, G., Hastings, J., Patin, A., Reiterer, V., Farhan, H., Nasarov, S., & Lashuel, H. A.

REFERENCES

- (2021). Nuclear and cytoplasmic huntingtin inclusions exhibit distinct biochemical composition, interactome and ultrastructural properties. *Nature Communications*, 12(1), 1–27. <https://doi.org/10.1038/s41467-021-26684-z>
- Rippin, I., Bonder, K., Joseph, S., Sarsor, A., Vaks, L., & Eldar-Finkelman, H. (2021). Inhibition of GSK-3 ameliorates the pathogenesis of Huntington's disease. *Neurobiology of Disease*, 154, 105336. <https://doi.org/10.1016/j.nbd.2021.105336>
- Rippin, I., & Eldar-Finkelman, H. (2021). Mechanisms and therapeutic implications of GSK-3 in treating neurodegeneration. *Cells*, 10(2), 1–22. <https://doi.org/10.3390/cells10020262>
- Rizzuto, R., Brini, M., Murgia, M., & Pozzan, T. (1993). Microdomains with high Ca²⁺ close to IP₃-sensitive channels that are sensed by neighboring mitochondria. *Science*, 262(5134), 744–747. <https://doi.org/10.1126/science.8235595>
- Rizzuto, R., Pinton, P., Carrington, W., Fay, F. S., Fogarty, K. E., Lifshitz, L. M., Tuft, R. A., & Pozzan, T. (1998). Close contacts with the endoplasmic reticulum as determinants of mitochondrial Ca²⁺ responses. *Science*, 280(5370), 1763–1766. <https://doi.org/10.1126/science.280.5370.1763>
- Rodríguez-Arribas, M., Yakhine-Diop, S. M. S., Pedro, J. M. B. S., Gómez-Suaga, P., Gómez-Sánchez, R., Martínez-Chacón, G., Fuentes, J. M., González-Polo, R. A., & Niso-Santano, M. (2017). Mitochondria-Associated Membranes (MAMs): Overview and Its Role in Parkinson's Disease. *Molecular Neurobiology*, 54(8), 6287–6303. <https://doi.org/10.1007/s12035-016-0140-8>
- Rolón-Reyes, K., Kucheryavykh, Y. V., Cubano, L. A., Inyushin, M., Skatchkov, S. N., Eaton, M. J., Harrison, J. K., & Kucheryavykh, L. Y. (2015). Microglia activate migration of glioma cells through a Pyk2 intracellular pathway. *PLoS ONE*, 10(6), 1–18. <https://doi.org/10.1371/journal.pone.0131059>
- Rong, R., Xia, X., Peng, H., Li, H., You, M., Liang, Z., Yao, F., Yao, X., Xiong, K., Huang, J., Zhou, R., & Ji, D. (2020). Cdk5-mediated Drp1 phosphorylation drives mitochondrial defects and neuronal apoptosis in radiation-induced optic neuropathy. *Cell Death and Disease*, 11(9). <https://doi.org/10.1038/s41419-020-02922-y>
- Roos, R. A. (2010). Huntington's disease: a clinical review. *Orphanet Journal of Rare Diseases*, 5(40), 1–8.
- Rosenstock, T. R., Bertoncini, C. R. A. A., Teles, A. V., Hirata, H., Fernandes, M. J. S. S., & Smaili, S. S. (2010). Glutamate-induced alterations in Ca²⁺ signaling are modulated by mitochondrial Ca²⁺ handling capacity in brain slices of R6/1 transgenic mice. *European Journal of Neuroscience*, 32(1), 60–70. <https://doi.org/10.1111/j.1460-9568.2010.07268.x>
- Ross, C. A. (1997). Intranuclear neuronal inclusions: A common pathogenic mechanism for glutamine-repeat neurodegenerative diseases? *Neuron*, 19(6), 1147–1150. [https://doi.org/10.1016/S0896-6273\(00\)80405-5](https://doi.org/10.1016/S0896-6273(00)80405-5)
- Ross, C. A., & Tabrizi, S. J. (2011). Huntington's disease: From molecular pathogenesis to clinical treatment. *The Lancet Neurology*, 10(1), 83–98. [https://doi.org/10.1016/S1474-4422\(10\)70245-3](https://doi.org/10.1016/S1474-4422(10)70245-3)
- Rostami, J., Holmqvist, S., Lindström, V., Sigvardson, J., Westermark, G. T., Ingelsson, M., Bergström, J., Roybon, L., & Erlandsson, A. (2017). Human astrocytes transfer aggregated alpha-synuclein via tunneling nanotubes. *Journal of Neuroscience*, 37(49), 11835–11853. <https://doi.org/10.1523/JNEUROSCI.0983-17.2017>

REFERENCES

- Rotblat, B., Southwell, A. L., Ehrnhoefer, D. E., Skotte, N. H., Metzler, M., Franciosi, S., Leprivier, G., Somasekharan, S. P., Barokas, A., Deng, Y., Tang, T., Mathers, J., Cetinbas, N., Dugaard, M., Kwok, B., Li, L., Carnie, C. J., Fink, D., Nitsch, R., ... Sorensen, P. H. (2014). HACE1 reduces oxidative stress and mutant Huntingtin toxicity by promoting the NRF2 response. *Proceedings of the National Academy of Sciences of the United States of America*, *111*(8), 3032–3037. <https://doi.org/10.1073/pnas.1314421111>
- Rowland, A. A., & Voeltz, G. K. (2012a). Endoplasmic reticulum-mitochondria contacts: Function of the junction. *Nature Reviews Molecular Cell Biology*, *13*(10), 607–615. <https://doi.org/10.1038/nrm3440>
- Rowland, A. A., & Voeltz, G. K. (2012b). Endoplasmic reticulum–mitochondria contacts: function of the junction. *Nature Reviews Molecular Cell Biology*, *13*(10), 607–615. <https://doi.org/10.1038/nrm3440>
- Rozzi, S. J., Avdoshina, V., Fields, J. A., & Mocchetti, I. (2018). Human immunodeficiency virus Tat impairs mitochondrial fission in neurons. *Cell Death Discovery*, *4*(1). <https://doi.org/10.1038/s41420-017-0013-6>
- Ruiz, A., Alberdi, E., & Matute, C. (2018). Mitochondrial division inhibitor 1 (Mdivi-1) protects neurons against excitotoxicity through the modulation of mitochondrial function and intracellular Ca²⁺ signaling. *Frontiers in Molecular Neuroscience*, *11*(January), 1–16. <https://doi.org/10.3389/fnmol.2018.00003>
- Rusiñol, A. E., Cui, Z., Chen, M. H., & Vance, J. E. (1994). A unique mitochondria-associated membrane fraction from rat liver has a high capacity for lipid synthesis and contains pre-Golgi secretory proteins including nascent lipoproteins. *Journal of Biological Chemistry*, *269*(44), 27494–27502. [https://doi.org/10.1016/s0021-9258\(18\)47012-3](https://doi.org/10.1016/s0021-9258(18)47012-3)
- Rustom, A., Saffrich, R., Markovic, I., Walther, P., & Gerdes, H. H. (2004). Nanotubular Highways for Intercellular Organelle Transport. *Science*, *303*(5660), 1007–1010. <https://doi.org/10.1126/science.1093133>
- Saba, J., López Couselo, F., Turati, J., Carniglia, L., Durand, D., De Laurentiis, A., Lasaga, M., & Caruso, C. (2020). Astrocytes from cortex and striatum show differential responses to mitochondrial toxin and BDNF: Implications for protection of striatal neurons expressing mutant huntingtin. *Journal of Neuroinflammation*, *17*(1), 1–15. <https://doi.org/10.1186/s12974-020-01965-4>
- Salazar, S. V., Cox, T. O., Lee, S., Brody, A. H., Chyung, A. S., Haas, L. T., & Strittmatter, S. M. (2019). Alzheimer’s Disease Risk Factor Pyk2 Mediates Amyloid- β -Induced Synaptic Dysfunction and Loss. *The Journal of Neuroscience*, *39*(4), 758–772. <https://doi.org/10.1523/JNEUROSCI.1873-18.2018>
- Sanz-Blasco, S., Valero, R. A., Rodríguez-Crespo, I., Villalobos, C., & Núñez, L. (2008). Mitochondrial Ca²⁺ overload underlies A β oligomers neurotoxicity providing an unexpected mechanism of neuroprotection by NSAIDs. *PLoS ONE*, *3*(7). <https://doi.org/10.1371/journal.pone.0002718>
- Sasaki, H., Nagura, K., Ishino, M., Tobioka, H., Kotani, K., & Sasaki, T. (1995). Cloning and characterization of cell adhesion kinase β , a novel protein-tyrosine kinase of the focal adhesion kinase subfamily. *Journal of Biological Chemistry*, *270*(36), 21206–21219. <https://doi.org/10.1074/jbc.270.36.21206>
- Saudou, F., & Humbert, S. (2016). The Biology of Huntingtin. *Neuron*, *89*(5), 910–926. <https://doi.org/10.1016/j.neuron.2016.02.003>

REFERENCES

- Sayas, L., Ariaens, A., Ponsioen, B., & Moolenaar, W. (2006). GSK-3 Is Activated by the Tyrosine Kinase Pyk2 during LPA1-mediated Neurite Retraction. *Molecular Biology of the Cell*, 17(April), 1834–1844. <https://doi.org/10.1091/mbc.E05>
- Schilling, G., Becher, M. W., Sharp, A. H., Jinnah, H. A., Duan, K., Kotzuk, J. A., Slunt, H. H., Ratovitski, T., Cooper, J. K., Jenkins, N. A., Copeland, N. G., Price, D. L., Ross, C. A., & Borchelt, D. R. (1999). Intranuclear inclusions and neuritic aggregates in transgenic mice expressing a mutant N-terminal fragment of huntingtin. *Human Molecular Genetics*, 8(3), 397–407. <https://doi.org/10.1093/hmg/8.3.397>
- Scorrano, L. (2013). Keeping mitochondria in shape: A matter of life and death. *European Journal of Clinical Investigation*, 43(8), 886–893. <https://doi.org/10.1111/eci.12135>
- Seabold, G. K., Burette, A., Lim, I. A., Weinberg, R. J., & Hell, J. W. (2003). Interaction of the tyrosine kinase Pyk2 with the N-methyl-D-aspartate receptor complex via the Src homology 3 domains of PSD-95 and SAP102. *Journal of Biological Chemistry*, 278(17), 15040–15048. <https://doi.org/10.1074/jbc.M212825200>
- Sena, L. A., & Chandel, N. S. (2012). Physiological roles of mitochondrial reactive oxygen species. *Molecular Cell*, 48(2), 158–167. <https://doi.org/10.1016/j.molcel.2012.09.025>
- Seong, I. S., Ivanova, E., Lee, J. M., Choo, Y. S., Fossale, E., Anderson, M. A., Gusella, J. F., Laramie, J. M., Myers, R. H., Lesort, M., & MacDonald, M. E. (2005). HD CAG repeat implicates a dominant property of huntingtin in mitochondrial energy metabolism. *Human Molecular Genetics*, 14(19), 2871–2880. <https://doi.org/10.1093/hmg/ddi319>
- Shanmughapriya, S., Langford, D., & Natarajaseenivasan, K. (2020). Inter and Intracellular mitochondrial trafficking in health and disease. *Ageing Research Reviews*, 62(July), 101128. <https://doi.org/10.1016/j.arr.2020.101128>
- Sharp, A. H., Nucifora, F. C., Blondel, O., Sheppard, C. A., Zhang, C., Snyder, S. H., Russell, J. T., Ryugo, D. K., & Ross, C. A. (1999). Differential cellular expression of isoforms of inositol 1,4,5- triphosphate receptors in neurons and glia in brain. *Journal of Comparative Neurology*, 406(2), 207–220. [https://doi.org/10.1002/\(SICI\)1096-9861\(19990405\)406:2<207::AID-CNE6>3.0.CO;2-7](https://doi.org/10.1002/(SICI)1096-9861(19990405)406:2<207::AID-CNE6>3.0.CO;2-7)
- Shevchenko, A., Tomas, H., Havliš, J., Olsen, J. V., & Mann, M. (2007). In-gel digestion for mass spectrometric characterization of proteins and proteomes. *Nature Protocols*, 1(6), 2856–2860. <https://doi.org/10.1038/nprot.2006.468>
- Shi, X., Zhao, M., Fu, C., & Fu, A. (2017). Intravenous administration of mitochondria for treating experimental Parkinson's disease. *Mitochondrion*, 34, 91–100. <https://doi.org/10.1016/j.mito.2017.02.005>
- Shin, J. Y., Fang, Z. H., Yu, Z. X., Wang, C. E., Li, S. H., & Li, X. J. (2005). Expression of mutant huntingtin in glial cells contributes to neuronal excitotoxicity. *Journal of Cell Biology*, 171(6), 1001–1012. <https://doi.org/10.1083/jcb.200508072>
- Shirendeb, U., Reddy, A. P., Manczak, M., Calkins, M. J., Mao, P., Tagle, D. A., Reddy, H. P., & Reddy, P. H. (2011). Abnormal mitochondrial dynamics, mitochondrial loss and mutant huntingtin oligomers in Huntington's disease: Implications for selective neuronal damage. *Human Molecular Genetics*, 20(7), 1438–1455. <https://doi.org/10.1093/hmg/ddr024>

REFERENCES

- Shoshan-Barmatz, V., & Ben-Hail, D. (2012). VDAC, a multi-functional mitochondrial protein as a pharmacological target. *Mitochondrion*, 12(1), 24–34. <https://doi.org/10.1016/j.mito.2011.04.001>
- Slow, E. J., van Raamsdonk, J., Rogers, D., Coleman, S. H., Graham, R. K., Deng, Y., Oh, R., Bissada, N., Hossain, S. M., Yang, Y. Z., Li, X. J., Simpson, E. M., Gutekunst, C. A., Leavitt, B. R., & Hayden, M. R. (2003). Selective striatal neuronal loss in a YAC128 mouse model of Huntington disease. *Human Molecular Genetics*, 12(13), 1555–1567. <https://doi.org/10.1093/hmg/ddg169>
- Sofroniew, M. V., & Vinters, H. V. (2010). Astrocytes: Biology and pathology. *Acta Neuropathologica*, 119(1), 7–35. <https://doi.org/10.1007/s00401-009-0619-8>
- Song, W., Chen, J., Petrilli, A., Liot, G., Klinglmayr, E., Zhou, Y., Poquiz, P., Tjong, J., Pouladi, M. A., Hayden, M. R., Masliah, E., Ellisman, M., Rouiller, I., Schwarzenbacher, R., Bossy, B., Perkins, G., & Bossy-Wetzler, E. (2011). Mutant huntingtin binds the mitochondrial fission GTPase dynamin-related protein-1 and increases its enzymatic activity. *Nature Medicine*, 17(3), 377–383. <https://doi.org/10.1038/nm.2313>
- Soni, D., Regmi, S. C., Wang, D. M., Debroy, A., Zhao, Y. Y., Vogel, S. M., Malik, A. B., & Tiruppathi, C. (2017). Pyk2 phosphorylation of VE-PTP downstream of STIM1-induced Ca²⁺ entry regulates disassembly of adherens junctions. *American Journal of Physiology - Lung Cellular and Molecular Physiology*, 312(6), L1003–L1017. <https://doi.org/10.1152/ajplung.00008.2017>
- Spees, J. L., Olson, S. D., Whitney, M. J., & Prockop, D. J. (2006). Mitochondrial transfer between cells can rescue aerobic respiration. *Proceedings of the National Academy of Sciences of the United States of America*, 103(5), 1283–1288. <https://doi.org/10.1073/pnas.0510511103>
- Stephen, T. L., Higgs, N. F., Sheehan, D. F., Awabdh, S. Al, López-Doménech, G., Arancibia-Carcamo, I. L., & Kittler, J. T. (2015). Miro1 regulates activity-driven positioning of mitochondria within astrocytic processes apposed to synapses to regulate intracellular calcium signaling. *Journal of Neuroscience*, 35(48), 15996–16011. <https://doi.org/10.1523/JNEUROSCI.2068-15.2015>
- Stricher, F., Macri, C., Ruff, M., & Muller, S. (2013). HSPA8/HSC70 chaperone protein. *Autophagy*, 9(12), 1937–1954. <https://doi.org/10.4161/auto.26448>
- Supplie, L. M., Düking, T., Campbell, G., Diaz, F., Moraes, C. T., Götz, M., Hamprecht, B., Boretius, S., Mahad, D., & Nave, K. A. (2017). Respiration-deficient astrocytes survive as glycolytic cells in vivo. *Journal of Neuroscience*, 37(16), 4231–4242. <https://doi.org/10.1523/JNEUROSCI.0756-16.2017>
- Szabadkai, G., Simoni, A. M., & Rizzuto, R. (2003). Mitochondrial Ca²⁺ uptake requires sustained Ca²⁺ release from the endoplasmic reticulum. *Journal of Biological Chemistry*, 278(17), 15153–15161. <https://doi.org/10.1074/jbc.M300180200>
- Taanman, J. W. (1999). The mitochondrial genome: Structure, transcription, translation and replication. *Biochimica et Biophysica Acta - Bioenergetics*, 1410(2), 103–123. [https://doi.org/10.1016/S0005-2728\(98\)00161-3](https://doi.org/10.1016/S0005-2728(98)00161-3)
- Tabrizi, S. J., Flower, M. D., Ross, C. A., & Wild, E. J. (2020). Huntington disease: new insights into molecular pathogenesis and therapeutic opportunities. *Nature Reviews Neurology*, 16(10), 529–546. <https://doi.org/10.1038/s41582-020-0389-4>
- Taguchi, N., Ishihara, N., Jofuku, A., Oka, T., & Mihara, K. (2007). Mitotic phosphorylation of dynamin-related GTPase Drp1 participates in mitochondrial

REFERENCES

- fission. *Journal of Biological Chemistry*, 282(15), 11521–11529. <https://doi.org/10.1074/jbc.M607279200>
- Tang, T. S., Guo, C., Wang, H., Chen, X., & Bezprozvanny, I. (2009). Neuroprotective effects of inositol 1,4,5-trisphosphate receptor C-terminal fragment in a Huntington's disease mouse model. *Journal of Neuroscience*, 29(5), 1257–1266. <https://doi.org/10.1523/JNEUROSCI.4411-08.2009>
- Tang, T. S., Tu, H., Chan, E. Y. W., Maximov, A., Wang, Z., Wellington, C. L., Hayden, M. R., & Bezprozvanny, I. (2003). Huntingtin and huntingtin-associated protein 1 influence neuronal calcium signaling mediated by inositol-(1,4,5) triphosphate receptor type 1. *Neuron*, 39(2), 227–239. [https://doi.org/10.1016/S0896-6273\(03\)00366-0](https://doi.org/10.1016/S0896-6273(03)00366-0)
- Tang, T. S., Tu, H., Orban, P. C., Chan, E. Y. W., Hayden, M. R., & Bezprozvanny, I. (2004). HAP1 facilitates effects of mutant huntingtin on inositol 1,4,5-trisphosphate-induced Ca²⁺ release in primary culture of striatal medium spiny neurons. *European Journal of Neuroscience*, 20(7), 1779–1787. <https://doi.org/10.1111/j.1460-9568.2004.03633.x>
- The Huntington's Disease Collaborative. (1993). A Novel Gene Containing a Trinucleotide Repeat That Is Expanded and Unstable on Huntington's Disease Chromosomes. *Cell*, 72, 971–983.
- Tian, D., Litvak, V., & Lev, S. (2000). Cerebral ischemia and seizures induce tyrosine phosphorylation of PYK2 in neurons and microglial cells. *Journal of Neuroscience*, 20(17), 6478–6487. <https://doi.org/10.1523/jneurosci.20-17-06478.2000>
- Tong, X., Ao, Y., Faas, G. C., Nwaobi, S. E., Xu, J., Hausteiner, M. D., Anderson, M. A., Mody, I., Olsen, M. L., Sofroniew, M. V., & Khakh, B. S. (2014). Astrocyte Kir4.1 ion channel deficits contribute to neuronal dysfunction in Huntington's disease model mice. *Nature Neuroscience*, 17(5), 694–703. <https://doi.org/10.1038/nn.3691>
- Trushina, E., Dyer, R. B., Badger, J. D., Ure, D., Eide, L., Tran, D. D., Vrieze, B. T., Legendre-Guillemin, V., McPherson, P. S., Mandavilli, B. S., Van Houten, B., Zeitlin, S., McNiven, M., Aebersold, R., Hayden, M., Parisi, J. E., Seeberg, E., Dragatsis, I., Doyle, K., ... McMurray, C. T. (2004). Mutant Huntingtin Impairs Axonal Trafficking in Mammalian Neurons In Vivo and In Vitro. *Molecular and Cellular Biology*, 24(18), 8195–8209. <https://doi.org/10.1128/mcb.24.18.8195-8209.2004>
- Tyanova, S., Temu, T., Sinitcyn, P., Carlson, A., Hein, M. Y., Geiger, T., Mann, M., & Cox, J. (2016). The Perseus computational platform for comprehensive analysis of (prote)omics data. In *Nature Methods* (Vol. 13, Issue 9, pp. 731–740). <https://doi.org/10.1038/nmeth.3901>
- Valdinocci, D., Simões, R. F., Kovarova, J., Cunha-Oliveira, T., Neuzil, J., & Pountney, D. L. (2019). Intracellular and Intercellular Mitochondrial Dynamics in Parkinson's Disease. *Frontiers in Neuroscience*, 13(September), 1–8. <https://doi.org/10.3389/fnins.2019.00930>
- Van Duijn, E., Kingma, E. M., & Van Der Mast, R. C. (2007). Psychopathology in verified Huntington's disease gene carriers. *Journal of Neuropsychiatry and Clinical Neurosciences*, 19(4), 441–448. <https://doi.org/10.1176/jnp.2007.19.4.441>
- Vomaske, J., Varnum, S., Melnychuk, R., Smith, P., Pasa-Tolic, L., Shutthanandan, J. I., & Streblow, D. N. (2010). HCMV pUS28 initiates pro-migratory signaling via activation of Pyk2 kinase. *Herpesviridae*, 1(1), 2. <https://doi.org/10.1186/2042-4280-1-2>

REFERENCES

- Vonsattel, J. P. G., & Marian, D. (1998). Huntington Disease. *Journal of Neuropathology and Experimental Neurology*, 57(5), 369–384.
- Vonsattel, J. P., Myers, R. H., Stevens, T. J., Ferrante, R. J., Bird, E. D., & Richardson, E. P. J. (1985). Neuropathological classification of Huntington's disease. *Journal of Neuropathology and Experimental Neurology*, 44(6), 559–577. <https://doi.org/10.1097/00005072-198511000-00003>
- Walz, W., & Lang, M. K. (1998). Immunocytochemical evidence for a distinct GFAP-negative subpopulation of astrocytes in the adult rat hippocampus. *Neuroscience Letters*, 257(3), 127–130. [https://doi.org/10.1016/S0304-3940\(98\)00813-1](https://doi.org/10.1016/S0304-3940(98)00813-1)
- Wang, W., Yin, J., Ma, X., Zhao, F., Siedlak, S. L., Wang, Z., Torres, S., Fujioka, H., Xu, Y., Perry, G., & Zhu, X. (2017). Inhibition of mitochondrial fragmentation protects against Alzheimer's disease in rodent model. *Human Molecular Genetics*, 26(21), 4118–4131. <https://doi.org/10.1093/hmg/ddx299>
- Wang, X., Yan, M. H., Fujioka, H., Liu, J., Wilson-delfosse, A., Chen, S. G., Perry, G., Casadesus, G., & Zhu, X. (2012). LRRK2 regulates mitochondrial dynamics and function through direct interaction with DLP1. *Human Molecular Genetics*, 21(9), 1931–1944. <https://doi.org/10.1093/hmg/dds003>
- Wang, Y., Xu, E., Musich, P. R., & Lin, F. (2019). Mitochondrial dysfunction in neurodegenerative diseases and the potential countermeasure. *CNS Neuroscience and Therapeutics*, 25(7), 816–824. <https://doi.org/10.1111/cns.13116>
- Watanabe, S., Ilieva, H., Tamada, H., Nomura, H., Komine, O., Endo, F., Jin, S., Mancias, P., Kiyama, H., & Yamanaka, K. (2016). Mitochondria-associated membrane collapse is a common pathomechanism in SIGMAR 1 - and SOD 1 - linked ALS. *EMBO Molecular Medicine*, 8(12), 1421–1437. <https://doi.org/10.15252/emmm.201606403>
- Wegmann, S., Biernat, J., & Mandelkow, E. (2021). A current view on Tau protein phosphorylation in Alzheimer's disease. *Current Opinion in Neurobiology*, 69, 131–138. <https://doi.org/10.1016/j.conb.2021.03.003>
- Wetzel, H. H., Gehl, C. R., Dellefave-Castillo, L., Schiffman, J. F., Shannon, K. M., & Paulsen, J. S. (2011). Suicidal ideation in Huntington disease: The role of comorbidity. *Psychiatry Research*, 188(3), 372–376. <https://doi.org/10.1016/j.psychres.2011.05.006>
- Weydt, P., Pineda, V. V., Torrence, A. E., Libby, R. T., Satterfield, T. F., Lazarowski, E. R. R., Gilbert, M. L., Morton, G. J., Bammler, T. K., Strand, A. D., Cui, L., Beyer, R. P., Easley, C. N., Smith, A. C., Krainc, D., Luquet, S., Sweet, I. R. R., Schwartz, M. W., & La Spada, A. R. (2006). Thermoregulatory and metabolic defects in Huntington's disease transgenic mice implicate PGC-1 α in Huntington's disease neurodegeneration. *Cell Metabolism*, 4(5), 349–362. <https://doi.org/10.1016/j.cmet.2006.10.004>
- Wheeler, V. C., Auerbach, W., White, J. K., Srinidhi, J., Auerbach, A., Ryan, A., Duyao, M. P., Vrbanac, V., Weaver, M., Gusella, J. F., Joyner, A. L., & MacDonald, M. E. (1999). Length-dependent gametic CAG repeat instability in the Huntington's disease knock-in mouse. *Human Molecular Genetics*, 8(1), 115–122. <https://doi.org/10.1093/hmg/8.1.115>
- Wheeler, V. C., White, J. K., Gutekunst, C. A., Vrbanac, V., Weaver, M., Li, X. J., Li, S. H., Yi, H., Vonsattel, J. P., Gusella, J. F., Hersch, S., Auerbach, W., Joyner, A. L., & MacDonald, M. E. (2000). Long glutamine tracts cause nuclear localization of a novel form of huntingtin in medium spiny striatal neurons in Hdh(Q92) and

REFERENCES

- Hdh(Q111) knock-in mice. *Human Molecular Genetics*, 9(4), 503–513. <https://doi.org/10.1093/hmg/9.4.503>
- White, J. K., Auerbach, W., Duyao, M. P., Vonsattel, J.-P., Gusella, J. F., Joyner, A. L., & MacDonald, M. E. (1997). Huntingtin is required for neurogenesis and is not impaired by the Huntington's disease CAG expansion. *Nature Genetics*, 17, 404–410. <https://doi.org/10.1038/ng1297-404>
- Williams, G. S. B., Boyman, L., Chikando, A. C., Khairallah, R. J., & Lederer, W. J. (2013). Mitochondrial calcium uptake. *Proceedings of the National Academy of Sciences of the United States of America*, 110(26), 10479–10486. <https://doi.org/10.1073/pnas.1300410110>
- Wilton, D. K., & Stevens, B. (2020). The contribution of glial cells to Huntington's disease pathogenesis. *Neurobiology of Disease*, 143(May), 104963. <https://doi.org/10.1016/j.nbd.2020.104963>
- Wood, T. E., Barry, J., Yang, Z., Cepeda, C., Levine, M. S., & Gray, M. (2019). Mutant huntingtin reduction in astrocytes slows disease progression in the BACHD conditional Huntington's disease mouse model. *Human Molecular Genetics*, 28(3), 487–500. <https://doi.org/10.1093/hmg/ddy363>
- Wu, J., Ryskamp, D., Birnbaumer, L., & Bezprozvanny, I. (2018). Inhibition of TRPC1-Dependent Store-Operated Calcium Entry Improves Synaptic Stability and Motor Performance in a Mouse Model of Huntington's Disease. *Journal of Huntington's Disease*, 7(1), 35–50. <https://doi.org/10.3233/JHD-170266>
- Wu, S. S., Jácamo, R. O., Vong, S. K., & Rozengurt, E. (2006). Differential regulation of Pyk2 phosphorylation at Tyr-402 and Tyr-580 in intestinal epithelial cells: Roles of calcium, Src, Rho kinase, and the cytoskeleton. *Cellular Signalling*, 18(11), 1932–1940. <https://doi.org/10.1016/j.cellsig.2006.02.013>
- Xu, J., Chatterjee, M., Baguley, T. D., Brouillette, J., Kurup, P., Ghosh, D., Kanyo, J., Zhang, Y., Seyb, K., Ononenyi, C., Foscue, E., Anderson, G. M., Gresack, J., Cuny, G. D., Glicksman, M. A., Greengard, P., Lam, T. T., Tautz, L., Nairn, A. C., ... Lombroso, P. J. (2014). Inhibitor of the tyrosine phosphatase step reverses cognitive deficits in a mouse model of alzheimer' s disease. *PLoS Biology*, 12(8), 1–17. <https://doi.org/10.1371/journal.pbio.1001923>
- Xu, J., Kurup, P., Bartos, J. A., Patriarchi, T., Hell, J. W., & Lombroso, P. J. (2012). Striatal-enriched protein-tyrosine phosphatase (STEP) regulates Pyk2 kinase activity. *Journal of Biological Chemistry*, 287(25), 20942–20956. <https://doi.org/10.1074/jbc.M112.368654>
- Yamada, M., Mizuguchi, M., Otsuka, N., Ikeda, K., & Takahashi, H. (1997). Ultrastructural localization of CD38 immunoreactivity in rat brain. *Brain Research*, 756(1–2), 52–60. [https://doi.org/10.1016/S0006-8993\(97\)00117-0](https://doi.org/10.1016/S0006-8993(97)00117-0)
- Yan, J., Liu, X. H., Han, M. Z., Wang, Y. M., Sun, X. L., Yu, N., Li, T., Su, B., & Chen, Z. Y. (2015). Blockage of GSK3 β -mediated Drp1 phosphorylation provides neuroprotection in neuronal and mouse models of Alzheimer's disease. *Neurobiology of Aging*, 36(1), 211–227. <https://doi.org/10.1016/j.neurobiolaging.2014.08.005>
- Yang, D., Ying, J., Wang, X., Zhao, T., Yoon, S., Fang, Y., Zheng, Q., Liu, X., Yu, W., & Hua, F. (2021). Mitochondrial Dynamics: A Key Role in Neurodegeneration and a Potential Target for Neurodegenerative Disease. *Frontiers in Neuroscience*, 15(April). <https://doi.org/10.3389/fnins.2021.654785>

REFERENCES

- Yang, Yongjie, Vidensky, S., Jin, L., Jie, C., Lorenzini, I., Frankl, M., & Rothstein, J. D. (2011). Molecular comparison of GLT1+ and ALDH1L1+ astrocytes in vivo in astroglial reporter mice. *Glia*, *59*(2), 200–207. <https://doi.org/10.1002/glia.21089>
- Yang, Yufeng, Gehrke, S., Imai, Y., Huang, Z., Ouyang, Y., Wang, J. W., Yang, L., Beal, M. F., Vogel, H., & Lu, B. (2006). Mitochondrial pathology and muscle and dopaminergic neuron degeneration caused by inactivation of *Drosophila* Pink1 is rescued by Parkin. *Proceedings of the National Academy of Sciences of the United States of America*, *103*(28), 10793–10798. <https://doi.org/10.1073/pnas.0602493103>
- Yazbeck, P., Tauseef, M., Kruse, K., Amin, M. R., Sheikh, R., Feske, S., Komarova, Y., & Mehta, D. (2017). STIM1 Phosphorylation at Y361 Recruits Orai1 to STIM1 Puncta and Induces Ca²⁺ Entry. *Scientific Reports*, *7*(December 2016), 1–11. <https://doi.org/10.1038/srep42758>
- Young, A. B., Greenamyre, J. T., Hollingsworth, Z., Albin, R., D'Amato, C., Shoulson, I., & Penney, J. B. (1988). NMDA receptor losses in putamen from patients with Huntington's disease. *Science*, *241*(4868), 981–983. <https://doi.org/10.1126/science.2841762>
- Yu, H., Li, X., Marchetto, G. S., Dy, R., Hunter, D., Calvo, B., Dawson, T. L., Wilm, M., Andereg, R. J., Graves, L. M., & Shelton Earp, H. (1996). Activation of a novel calcium-dependent protein-tyrosine kinase. Correlation with c-Jun N-terminal kinase but not mitogen-activated protein kinase activation. *Journal of Biological Chemistry*, *271*(47), 29993–29998. <https://doi.org/10.1074/jbc.271.47.29993>
- Yu, X. M., Askalan, R., Keil, G. J., & Salter, M. W. (1997). NMDA channel regulation by channel-associated protein tyrosine kinase Src. *Science*, *275*(5300), 674–678. <https://doi.org/10.1126/science.275.5300.674>
- Yu, Z. X., Li, S. H., Evans, J., Pillarisetti, A., Li, H., & Li, X. J. (2003). Mutant huntingtin causes context-dependent neurodegeneration in mice with Huntington's disease. *Journal of Neuroscience*, *23*(6), 2193–2202. <https://doi.org/10.1523/jneurosci.23-06-02193.2003>
- Zeitlin, S., Liu, J. P., Chapman, D. L., Papaioannou, V. E., & Efstratiadis, A. (1995). Increased apoptosis and early embryonic lethality in mice nullizygous for the Huntington's disease gene homologue. *Nature Genetics*, *11*(2), 155–163. <https://doi.org/10.1038/ng1095-155>
- Zhang, H., Li, Q., Graham, R. K., Slow, E., Hayden, M. R., & Bezprozvanny, I. (2008). Full length mutant huntingtin is required for altered Ca²⁺ signaling and apoptosis of striatal neurons in the YAC mouse model of Huntington's disease. *Neurobiology of Disease*, *31*(1), 80–88. <https://doi.org/10.1016/j.nbd.2008.03.010>
- Zhang, K., Yan, J., Wang, L., Tian, X., Zhang, T., Guo, L., Li, B., Wang, W., & Liu, X. (2018). The Pyk2/MCU pathway in the rat middle cerebral artery occlusion model of ischemic stroke. *Neuroscience Research*, *131*, 52–62. <https://doi.org/10.1016/j.neures.2017.09.002>
- Zhang, P., Ford, K., Sung, J. S., Moeller, J., Suzuki, Y., Polina, I., Tachibana, T., Kusakari, Y., Cypress, M. W., Chaput, I., Drenkova, K., Landherr, M., Stephanie, M. A., Mishra, J., Mende, U., Jhun, B. S., & O-Uchi, J. (2022). *Tyrosine phosphorylation of mitofusin 2 regulates endoplasmic reticulum- mitochondria tethering*. <https://doi.org/10.1101/2022.02.21.481295>
- Zhang, Zengli, Ma, Z., Zou, W., Guo, H., Liu, M., Ma, Y., & Zhang, L. (2019). The Appropriate Marker for Astrocytes: Comparing the Distribution and Expression of

REFERENCES

- Three Astrocytic Markers in Different Mouse Cerebral Regions. *BioMed Research International*, 2019. <https://doi.org/10.1155/2019/9605265>
- Zhang, Zhao, Zhang, Y., Mou, Z., Chu, S., Chen, X., He, W., Guo, X., Yuan, Y., Takahashi, M., & Chen, N. (2014). Tyrosine 402 phosphorylation of Pyk2 is involved in ionomycin-induced neurotransmitter release. *PLoS ONE*, 9(4), 1–12. <https://doi.org/10.1371/journal.pone.0094574>
- Zhao, C., Du, C. P., Peng, Y., Xu, Z., Sun, C. C., Liu, Y., & Hou, X. Y. (2015). The Upregulation of NR2A-Containing N-Methyl-d-Aspartate Receptor Function by Tyrosine Phosphorylation of Postsynaptic Density 95 Via Facilitating Src/Proline-Rich Tyrosine Kinase 2 Activation. *Molecular Neurobiology*, 51(2), 500–511. <https://doi.org/10.1007/s12035-014-8796-4>
- Zhao, F., Wang, W., Wang, C., Siedlak, S. L., Fujioka, H., Tang, B., & Zhu, X. (2017). Mfn2 protects dopaminergic neurons exposed to paraquat both in vitro and in vivo: Implications for idiopathic Parkinson's disease. *Biochimica et Biophysica Acta - Molecular Basis of Disease*, 1863(6), 1359–1370. <https://doi.org/10.1016/j.bbadis.2017.02.016>
- Zhao, T., Hong, Y., Li, S., & Li, X. J. (2016). Compartment-dependent degradation of mutant huntingtin accounts for its preferential accumulation in neuronal processes. *Journal of Neuroscience*, 36(32), 8317–8328. <https://doi.org/10.1523/JNEUROSCI.0806-16.2016>
- Zhou, Y., Zhou, B., Pache, L., Chang, M., Khodabakhshi, A. H., Tanaseichuk, O., Benner, C., & Chanda, S. K. (2019). Metascape provides a biologist-oriented resource for the analysis of systems-level datasets. *Nature Communications*, 10(1), 1523. <https://doi.org/10.1038/s41467-019-09234-6>
- Zhu, P. P., Patterson, A., Stadler, J., Seeburg, D. P., Sheng, M., & Blackstone, C. (2004). Intra- and intermolecular domain interactions of the C-terminal GTPase effector domain of the multimeric dynamin-like GTPase Drp1. *Journal of Biological Chemistry*, 279(34), 35967–35974. <https://doi.org/10.1074/jbc.M404105200>
- Zhu, X. H., Lu, M., Lee, B. Y., Ugurbil, K., & Chen, W. (2015). In vivo NAD assay reveals the intracellular NAD contents and redox state in healthy human brain and their age dependences. *Proceedings of the National Academy of Sciences of the United States of America*, 112(9), 2876–2881. <https://doi.org/10.1073/pnas.1417921112>
- Zhu, X. H., Qiao, H., Du, F., Xiong, Q., Liu, X., Zhang, X., Ugurbil, K., & Chen, W. (2012). Quantitative imaging of energy expenditure in human brain. *NeuroImage*, 60(4), 2107–2117. <https://doi.org/10.1016/j.neuroimage.2012.02.013>
- Zhu, X., Perry, G., Moreira, P. I., Aliev, G., Cash, A. D., Hirai, K., & Smith, M. A. (2006). Mitochondrial abnormalities and oxidative imbalance in Alzheimer disease. *Journal of Alzheimer's Disease*, 9(2), 147–153. <https://doi.org/10.3233/JAD-2006-9207>
- Zorzano, A., & Claret, M. (2015). Implications of mitochondrial dynamics on neurodegeneration and on hypothalamic dysfunction. *Frontiers in Aging Neuroscience*, 7(JUN), 1–17. <https://doi.org/10.3389/fnagi.2015.00101>

ANNEX

Gene names	UniProt	Protein names	Cluster	Peptides	Unique peptides	Sequence coverage [%]	Mol. weight [kDa]	Score	LQ Intensity IP_Py2_WT-1_1A	LQ Intensity IP_Py2_WT-1_1B	LQ Intensity IP_Py2_WT-1_1C	LQ Intensity IP_Py2_WT-1_1D	LQ Intensity IP_Py2_WT-1_1E	LQ Intensity IgG_WT-1_2A	LQ Intensity IgG_WT-2_2B	LQ Intensity IgG_WT-1_2A	LQ Intensity IgG_WT-2_2B	LQ Intensity IgG_WT-1_2A	LQ Intensity IgG_WT-2_2B	Log ANOVA-p value
Syng1	O55200	Syntaxin-11	Cluster-85	2	2	10.3	25.652	28.014	1.05942452	1.33434223	1.21496903	0.46026566	-1.067281485	-0.604983177	-0.387978107	-0.225789562	-1.062466741	-0.387978107	-0.225789562	3.179869147
Srsf1	H7B095	Serine/arginine-rich splicing factor 1	Cluster-85	5	5	19	28.329	14.167	0.66048836	1.443397999	1.36619017	-0.13320598	-0.678180754	-0.96183147	-1.138958812	-0.895962119	-0.339660406	-1.138958812	-0.895962119	1.876031526
Purb	O33295	Transcriptional activator protein Pur-beta	Cluster-85	4	4	24.1	33.901	124.45	1.03806001	1.304038405	1.213808179	0.193873465	-0.558042109	-0.811507881	-1.199670034	-1.061544538	-0.184761226	-1.199670034	-1.061544538	2.833911948
Pfkfb	P47857	ATP-dependent 6-phosphofructokinase, muscle type	Cluster-85	17	14	28.2	85.268	45.488	1.187491775	1.20996058	0.943689388	-1.809704138	-1.213985011	-0.05121889	-0.909971535	-0.252684951	-0.110577777	-0.909971535	-0.252684951	1.957008895
Pfkfb	P94029	Peroxisome-5, mitochondrial	Cluster-85	7	7	40	21.897	26.15	0.657047906	0.94660151	1.049766302	-1.1112437844	-1.341407776	0.962062716	-1.109375238	-0.39609207	-0.456923663	-1.109375238	-0.39609207	1.456218841
Tubb3	Q9ERD7	Tubulin beta-3 chain	Cluster-85	19	16	56.9	50.418	84.786	0.771216393	1.28969121	1.063341737	-0.64810586	-1.841167927	0.565268874	-0.368072866	-0.412911147	-0.419305251	-0.368072866	-0.412911147	1.619632634
Gnb1	Q88Y19	Tenascin-R	Cluster-85	16	16	15.7	149.59	42.838	0.491286395	1.273930192	0.698327329	-1.468004495	-1.235755086	1.267889142	-0.406413674	-0.276038259	-0.406413674	-0.276038259	-0.406413674	1.619632634
Ttr	P62874	Transthyretin	Cluster-85	5	5	29.7	37.377	95.061	0.661554933	0.897311866	1.26755508	-1.445288491	-1.419310212	1.070236325	-0.203525052	-0.561208844	-0.203525052	-0.561208844	-0.203525052	1.786142107
Rab3c	P62823	Ras-related protein Rab-3C	Cluster-85	5	3	26.9	25.872	7.9401	0.795871079	0.99007953	1.13738203	-1.049088478	-1.092524758	1.180619478	-0.405275106	-0.792415857	-0.405275106	-0.792415857	-0.405275106	1.421333066
Ubr1	Q02053	Ubiquitin-like modifier-activating enzyme 1	Cluster-85	15	15	19.4	117.81	215.4	0.531692188	1.66823053	1.297390446	-0.850709736	-1.0483495	0.991650581	-0.810470939	-0.601334333	-0.810470939	-0.601334333	-0.810470939	1.443030491
Cbr1	P48758	Carbonyl reductase [NADPH]	Cluster-85	7	6	27.1	30.641	10.788	0.714371414	0.9056108	1.536537051	-0.811460316	-1.06332612	0.865942557	-0.400312364	-0.806390405	-0.400312364	-0.806390405	-0.400312364	1.849002883
Ppp3cb	E0C728	Protein phosphatase 3B	Cluster-85	9	4	17.9	59.074	7.1641	0.957675982	1.453489236	1.36729757	-1.247909004	-1.06332612	0.214618757	-0.547698137	-0.547698137	-0.547698137	-0.547698137	-0.547698137	2.836001022
Erc1	P63318	Alpha-enolase	Cluster-85	15	10	54.1	47.14	323.31	0.648783264	1.453489236	1.36729757	-1.247909004	-1.06332612	0.214618757	-0.547698137	-0.547698137	-0.547698137	-0.547698137	-0.547698137	2.836001022
Pkb2	Q30Y86	Protein kinase C gamma type	Cluster-85	28	26	52.2	78.357	323.31	0.934007401	1.595902801	1.278509736	-0.755576491	-0.94340086	0.190466821	-0.635562692	-0.324570924	-0.635562692	-0.324570924	-0.635562692	1.959486105
Mab1a	P63868	Microtubule-associated protein 1A	Cluster-85	47	46	25.6	300.14	261.8	0.83666501	1.359864776	0.981121302	-1.450986382	-1.156390667	0.35373677	-0.568568996	-0.586793767	-0.568568996	-0.586793767	-0.568568996	3.244154329
Tuba4a	P53206	Tubulin alpha-4A chain	Cluster-85	18	4	55.1	49.924	323.31	1.136400819	1.460204771	1.057849066	-1.024636017	-1.164994478	0.733696024	-0.586588849	-0.454330614	-0.586588849	-0.454330614	-0.586588849	2.511022685
Cyfp2	P52133	Cytoplasmic FMR1-interacting protein 2	Cluster-85	20	15	18.1	145.66	35.545	1.202333331	1.517075419	0.886357665	-1.26721251	-0.602938684	0.276964664	-0.854819179	-0.478254169	-0.854819179	-0.478254169	-0.854819179	1.952536889
Tuba1b	P52133	Tubulin alpha-1B chain	Cluster-85	19	0	61.9	50.151	1.924241	1.25734146	1.288004518	-1.183642626	-1.220865011	0.282933874	-0.945069134	-0.315273397	-0.361307854	-0.315273397	-0.361307854	-0.315273397	3.495253851
Tcp1	P11983	T-complex protein 1 subunit alpha	Cluster-85	12	12	22.8	60.448	66.012	0.785947025	0.60947824	1.328752279	-1.408149512	-1.220865011	0.282933874	-0.945069134	-0.315273397	-0.361307854	-0.315273397	-0.361307854	1.925653851
Hba-a1	Q91988	Alpha globin 1	Cluster-85	12	12	27.6	15.112	50.509	0.307917684	0.89590108	1.150575042	-2.350935552	-0.539356053	0.326133225	-0.543119669	-0.966308951	-0.543119669	-0.966308951	-0.543119669	1.607634402
Pki	P12382	ATP-dependent 6-phosphofructokinase, liver type	Cluster-85	16	11	24.6	85.359	45.927	1.037558556	1.02840519	0.989590108	-1.789859891	-0.72134632	0.690596685	-0.090304472	-0.467789561	-0.090304472	-0.467789561	-0.090304472	1.06039777
Ghi	P07945	Glucose-6-phosphate isomerase	Cluster-85	11	11	24.6	62.766	52.877	0.738573611	1.168223143	1.168223143	-1.78714326	-0.601141512	0.739312291	-0.354577869	-0.324265897	-0.354577869	-0.324265897	-0.354577869	1.407760725
Atfbz1	G5E829	Plasma membrane calcium-transporting ATPase 1	Cluster-85	24	13	26.5	134.75	315.38	0.610843718	0.90731883	1.041956604	-1.967147708	-1.004652977	0.777069032	-0.047188959	-0.070763506	-0.047188959	-0.070763506	-0.047188959	2.314453864
Sic25a11	Q88H59	Calcium-binding mitochondrial carrier protein Anlrbt	Cluster-86	24	21	46.4	74.569	158.72	1.64669466	1.09764495	0.998228014	-0.86945863	-0.031704068	-0.318279833	-0.405862093	-1.5629493	-0.438207924	-0.405862093	-1.5629493	2.123271117
Tubz2b	Q9CWF2	Mitochondrial 2-oxoglutarate/malate carrier protein	Cluster-86	9	9	36	34.155	72.088	1.09070448	0.86749724	0.841815472	-0.653796673	-0.738191843	0.121599838	-1.359952688	-1.242344022	-1.359952688	-1.242344022	-1.359952688	1.523848127
Epp4111	B9PW14	Tubulin beta-2B chain	Cluster-86	21	1	66.7	49.953	323.31	-0.099783264	1.873931766	1.258619666	0.009514122	0.175450608	-1.088115573	-0.478016764	-1.035903454	-0.478016764	-1.035903454	-0.478016764	1.670712554
Eh4	D3Z781	Enhancer trap locus 4	Cluster-86	32	32	29.4	146.61	213.25	0.711774771	0.711774771	0.380470896	0.678470731	-1.297570357	-0.457310855	-1.308625817	-1.019037366	-0.457310855	-1.019037366	-0.457310855	3.623807854
Scn1l	AA05718D00	SRC kinase signaling inhibitor 1	Cluster-86	48	0	50.4	131.62	323.31	0.477886468	0.793378485	0.95257527	-0.336900026	0.314333773	-0.519193033	-1.268940091	-0.626813054	-1.268940091	-0.626813054	-1.268940091	3.292616059
Rps6	PE2754	40S ribosomal protein S6	Cluster-86	5	5	25.7	28.68	142.28	0.465165108	1.058290839	0.91118669	-0.203851819	1.076590896	0.314567149	-1.159861565	-0.976967573	-1.159861565	-0.976967573	-1.159861565	1.426944652
Ric1	Q5UE59	Kinesin light chain	Cluster-86	13	4	27.3	61.629	21.85	0.73823869	1.016190052	0.894814432	-0.330008388	1.247111917	-1.395039678	-1.41262114	-0.46294266	-1.395039678	-1.41262114	-0.46294266	1.450368374
Cox6b1	P56991	Cytochrome c oxidase subunit VIb isoform 1	Cluster-86	4	4	52.3	10.071	6.8739	0.645204246	1.337618709	0.926314771	-0.661864579	1.211086035	-0.989183247	-0.856904566	-0.904003441	-0.856904566	-0.904003441	-0.856904566	1.781608884
Ddx3k	Q6Z167	ATP-dependent RNA helicase DDX3K	Cluster-86	24	4	4	73.011	20.401	1.236119406	0.795731723	1.054509997	-0.201680967	0.931335211	-0.828780285	-0.678106643	-1.16170311	-0.828780285	-0.678106643	-1.16170311	2.827360316
Rpl7	P14148	60S ribosomal protein L7	Cluster-86	4	4	14.8	31.419	6.9637	1.159740806	1.04506278	1.048632666	-0.103648966	0.931335211	-0.828780285	-0.678106643	-1.16170311	-0.828780285	-0.678106643	-1.16170311	3.820603327
Kif5a	P33175	Kinesin heavy chain isoform 5A	Cluster-86	36	26	43.6	117.02	190.51	0.86456068	0.92095739	0.948632666	-0.224400729	1.083981514	-0.885488713	-1.162689866	-0.853472748	-1.162689866	-0.853472748	-1.162689866	3.429102504
Alap5	D3YV60	Ala-ketide protein phosphatase 5	Cluster-86	19	19	50.2	79.396	189.51	0.731567144	0.956281012	0.956281012	-0.224400729	1.083981514	-0.885488713	-1.162689866	-0.853472748	-1.162689866	-0.853472748	-1.162689866	3.623807854
Drap3	H3B418	Dual specificity protein phosphatase	Cluster-86	2	2	20	15.273	15.273	0.65957147	0.745830118	0.745830118	-1.418964744	-0.107208548	-0.957658447	-0.286751866	-1.271432658	-0.957658447	-0.286751866	-1.271432658	1.435091977
Kif23	F8VQ42	Kinesin-like protein phosphatase	Cluster-86	7	7	10.3	75.908	10.794	0.248823708	0.731717807	0.311681679	1.55947249	0.935605544	-0.746466309	-1.171603799	-1.19840254	-0.746466309	-1.171603799	-1.19840254	0.299315537
Wdr47	Q8C9F6	WD repeat-containing protein 47	Cluster-86	5	5	6.0	102.31	83.506	0.181305362	0.691859353	0.94960328	1.347952843	0.225197718	-1.188062146	-0.840510388	-0.869061761	-0.840510388	-0.869061761	-0.840510388	1.809532029
Fibcd1	A2AN25	Fibronectin C domain-containing protein 1	Cluster-86	5	5	13.5	50.601	92.207	0.591188192	0.905272786	0.659883618	-1.456288934	-0.055496028	-1.166701424	-0.373333616	-0.39118977	-0.373333616	-0.39118977	-0.373333616	1.849509579

Supplementary Table 2. Functional mapping of Pyk2-associated proteins obtained by Metascope. The analysis was performed with various ontology sources, including KEGG Pathway, GO Biological Process, Reactome Gene Sets, Canonical Pathways, CORUM and WikiPathways. All genes in the genome were used as the enrichment background. Terms with a p-value < 0.01, a minimum count of 3, and an enrichment factor (ratio between the observed counts and the counts expected by chance) > 1.5 were grouped into clusters based on their membership similarities. To represent each cluster, the most statistically significant term was chosen.

GroupID	Category	Term	Description	LogP	Log(q-value)	InTerm_nList	Genes	Symbols
1_Summary	Reactome Gene Sets	R-HSA-438064	Post NMDA receptor activation events	-13.9513	-9.940	9/80	808,817,5576,7277,10376,10381,10382,10383,79861,6950,2782,5582,10971,1778,3039,6132,6141,6147,6157,6648,25824,509,9066,4155,5532,7317,26999,2,185,230,92,490,6428,4,130,41,31,4,134,10657	CALM3,CAMK2D,PRKAR2A,TUBA4A,TUBA1B,TUBB3,TUBB4A,TUBB4B,TUBB4C,TCP1,GNB1,PRKCG,YWHAQ,DYNC1H1,HBAL1,RPL18,RPL23A,RPL27A,SOD2,PRDX5,ATP5F1C,SYT7,MBP,PPP3CB,UBA1,CYFIP2,PTK2B,ARHGAP26,ATP2B1,SRSF3,MAP1A,MAP1B,MAP4,KHDRBS1
1_Member	Reactome Gene Sets	R-HSA-438064	Post NMDA receptor activation events	-13.9513	-9.940	9/80	808,817,5576,7277,10376,10381,10382,10383,79861	CALM3,CAMK2D,PRKAR2A,TUBA4A,TUBA1B,TUBB3,TUBB4A,TUBB4B,TUBB4C
1_Member	Reactome Gene Sets	R-HSA-389960	Formation of tubulin folding intermediates by CCT/TtrC	-13.9229	-9.940	7/25	6950,7277,10376,10381,10382,10383,79861	TCP1,TUBA4A,TUBA1B,TUBB3,TUBB4A,TUBB4B,TUBAL3
1_Member	Reactome Gene Sets	R-HSA-9619483	Activation of AMPK downstream of NMDARs	-13.4137	-9.756	7/29	808,7277,10376,10381,10382,10383,79861	CALM3,TUBA4A,TUBA1B,TUBB3,TUBB4A,TUBB4B,TUBAL3
1_Member	Reactome Gene Sets	R-HSA-112314	Neurotransmitter receptors and postsynaptic signal transmission	-13.395	-9.756	11/205	808,817,2,782,5576,5582,7277,10376,10381,10382,10383,79861	CALM3,CAMK2D,GNB1,PRKAR2A,PRKCG,TUBA4A,TUBA1B,TUBB3,TUBB4A,TUBAL3
1_Member	Reactome Gene Sets	R-HSA-442755	Activation of NMDA receptors and postsynaptic events	-13.3406	-9.756	9/93	808,817,5576,7277,10376,10381,10382,10383,79861	CALM3,CAMK2D,PRKAR2A,TUBA4A,TUBA1B,TUBB3,TUBB4A,TUBB4B,TUBB4C,TUBAL3
1_Member	Reactome Gene Sets	R-HSA-389958	Cooperation of Prefoldin and Trif/CCT in actin and tubulin folding	-13.0816	-9.643	7/32	6950,7277,10376,10381,10382,10383,79861	TCP1,TUBA4A,TUBA1B,TUBB3,TUBB4A,TUBB4B,TUBAL3
1_Member	Reactome Gene Sets	R-HSA-5626467	RHO GTPases activate IQGAPs	-13.0816	-9.643	7/32	808,7277,10376,10381,10382,10383,79861	CALM3,TUBA4A,TUBA1B,TUBB3,TUBB4A,TUBB4B,TUBAL3
1_Member	Reactome Gene Sets	R-HSA-190840	Microtubule-dependent trafficking of connexons from Golgi to the plasma membrane	-12.5059	-9.125	6/18	7277,10376,10381,10382,10383,79861	TUBA4A,TUBA1B,TUBB3,TUBB4A,TUBB4B,TUBAL3
1_Member	Reactome Gene Sets	R-HSA-1445148	Translocation of SLC2A4 (GLUT4) to the plasma membrane	-12.3886	-9.059	8/72	808,7277,10376,10381,10382,10383,79861	CALM3,TUBA4A,TUBA1B,TUBB3,TUBB4A,TUBB4B,TUBAL3
1_Member	Reactome Gene Sets	R-HSA-190872	Transport of connexons to the plasma membrane	-12.3417	-9.058	6/19	7277,10376,10381,10382,10383,79861	TUBA4A,TUBA1B,TUBB3,TUBB4A,TUBB4B,TUBAL3
1_Member	Reactome Gene Sets	R-HSA-9609736	Assembly and cell surface presentation of NMDA receptors	-12.2618	-9.019	7/41	817,7277,10376,10381,10382,10383,79861	CAMK2D,TUBA4A,TUBA1B,TUBB3,TUBB4A,TUBB4B,TUBAL3
1_Member	Reactome Gene Sets	R-HSA-9646399	Aggrephagy	-12.1066	-8.915	7/43	1778,7277,10376,10381,10382,10383,79861	DYNC1H1,TUBA4A,TUBA1B,TUBB3,TUBB4A,TUBB4B,TUBAL3
1_Member	Reactome Gene Sets	R-HSA-112315	Transmission across Chemical Synapses	-12.0849	-8.915	11/270	808,817,2,782,5576,5582,7277,10376,10381,10382,10383,79861	CALM3,CAMK2D,GNB1,PRKAR2A,PRKCG,TUBA4A,TUBA1B,TUBB3,TUBB4A,TUBB4B,TUBAL3
1_Member	Reactome Gene Sets	R-HSA-2262752	Cellular responses to stress	-11.9355	-8.798	15/757	817,1778,3039,6132,6141,6147,6157,6648,8,7277,10376,10381,10382,10383,25824,79861	CAMK2D,DYNC1H1,HBAL1,RPL18,RPL23A,RPL27A,SOD2,TUBA4A,TUBA1B,TUBB3,TUBB4A,TUBB4B,PRDX5,TUBAL3
1_Member	Reactome Gene Sets	R-HSA-389977	Post-chaperonin tubulin folding pathway	-11.904	-8.796	6/22	7277,10376,10381,10382,10383,79861	TUBA4A,TUBA1B,TUBB3,TUBB4A,TUBB4B,TUBAL3
1_Member	Reactome Gene Sets	R-HSA-8953897	Cellular responses to stimuli	-11.822	-8.742	15/771	817,1778,3039,6132,6141,6147,6157,6648,8,7277,10376,10381,10382,10383,25824,79861	CAMK2D,DYNC1H1,HBAL1,RPL18,RPL23A,RPL27A,SOD2,TUBA4A,TUBA1B,TUBB3,TUBB4A,TUBB4B,PRDX5,TUBAL3
1_Member	Reactome Gene Sets	R-HSA-1852241	Organelle biogenesis and maintenance	-11.6515	-8.598	11/296	509,808,1778,6648,6950,7277,10376,10381,10382,10383,79861	ATP5F1C,CALM3,DYNC1H1,SOD2,TCP1,TUBA4A,TUBA1B,TUBB3,TUBB4A,TUBB4B,TUBAL3
1_Member	Reactome Gene Sets	R-HSA-6811436	COPI-independent Golgi-to-ER retrograde traffic	-11.5556	-8.543	7/51	1778,7277,10376,10381,10382,10383,79861	DYNC1H1,TUBA4A,TUBA1B,TUBB3,TUBB4A,TUBB4B,TUBAL3
1_Member	Reactome Gene Sets	R-HSA-390466	Chaperonin-mediated protein folding	-11.5477	-8.543	8/91	2782,6950,7277,10376,10381,10382,10383,79861	GNB1,TCP1,TUBA4A,TUBA1B,TUBB3,TUBB4A,TUBB4B,TUBAL3

1_Member	Reactome Gene Sets	R-HSA-112316	Neuronal System	03/2004	808,817,2782,5576,5582,7277,9066,10376,10381,10382,10383,79861	-8,502	12/410	CALM3,CAMK2D,GNB1,PRKAR2A,PRKCG,TUBA4A,SYT7,TUBA1B,TUBB3,TUBB4A,TUBB4B,TUBAL3
1_Member	Reactome Gene Sets	R-HSA-391251	Protein folding		2782,6950,7277,10376,10381,10382,10383,79861	-8,392	8/97	GNB1,TCPI1,TUBA4A,TUBA1B,TUBB3,TUBB4A,TUBB4B,TUBAL3
1_Member	Reactome Gene Sets	R-HSA-3371497	HSP90 chaperone cycle for steroid hormone receptors (SHR) in the presence of ligand		83,79861	-8,392	7/55	DYNCL1H1,TUBA4A,TUBA1B,TUBB3,TUBB4A,TUBB4B,TUBAL3
1_Member	WikiPathways	WP2272	Pathogenic Escherichia coli infection		861	-8,392	7/55	TUBA4A,TUBA1B,TUBB3,TUBB4A,YWHAQ,TUBAL3
1_Member	Reactome Gene Sets	R-HSA-9675108	Nervous system development		4155,5532,5576,6132,6141,6147,6157,7277,10376,10381,10382,10383,79861	-8,112	13/577	MBP,PPP3CB,PRKAR2A,RPL8,RPL18,RPL23A,RPL27A,TUBA4A,TUBA1B,TUBB3,TUBB4A,TUBB4B,TUBAL3
1_Member	Reactome Gene Sets	R-HSA-9668328	Sealing of the nuclear envelope (NE) by ESCRT-III		7277,10376,10381,10382,10383,79861	-8,029	6/31	TUBA4A,TUBA1B,TUBB3,TUBB4A,TUBB4B,TUBAL3
1_Member	KEGG Pathway	hsa05022	Pathways of neurodegeneration - multiple diseases		509,808,817,5532,5582,7277,7317,10376,10381,10382,10383,79861	-7,863	12/476	ATP5F1C,CALM3,CAMK2D,PPP3CB,PRKCG,TUBA4A,UBA1,TUBA1B,TUBB3,TUBB4A,TUBB4B,TUBAL3
1_Member	KEGG Pathway	hsa05012	Parkinson disease		509,808,817,7277,7317,10376,10381,10382,10383,79861	-7,805	10/266	ATP5F1C,CALM3,CAMK2D,TUBA4A,UBA1,TUBA1B,TUBB3,TUBB4A,TUBB4B,TUBAL3
1_Member	WikiPathways	WP2359	Parkin-ubiquitin proteasomal system pathway		7277,7317,10376,10381,10382,10383,79861	-7,714	7/70	TUBA4A,UBA1,TUBA1B,TUBB3,TUBB4A,TUBB4B,TUBAL3
1_Member	Reactome Gene Sets	R-HSA-190861	Gap junction assembly		7277,10376,10381,10382,10383,79861	-7,674	6/36	TUBA4A,TUBA1B,TUBB3,TUBB4A,TUBB4B,TUBAL3
1_Member	Reactome Gene Sets	R-HSA-9663891	Selective autophagy		1778,7277,10376,10381,10382,10383,79861	-7,288	7/81	DYNCL1H1,TUBA4A,TUBA1B,TUBB3,TUBB4A,TUBB4B,TUBAL3
1_Member	Reactome Gene Sets	R-HSA-8955332	Carboxyterminal post-translational modifications of tubulin		7277,10376,10381,10382,10383,79861	-7,276	6/42	TUBA4A,TUBA1B,TUBB3,TUBB4A,TUBB4B,TUBAL3
1_Member	Reactome Gene Sets	R-HSA-422475	Axon guidance		5532,5576,6132,6141,6147,6157,7277,10376,10381,10382,10383,79861	-7,212	12/552	PPP3CB,PRKAR2A,RPL8,RPL18,RPL23A,RPL27A,TUBA4A,TUBA1B,TUBB3,TUBB4A,TUBB4B,TUBAL3
1_Member	KEGG Pathway	hsa04540	Gap junction		5582,7277,10376,10381,10382,10383,79861	-7,072	7/88	PRKCG,TUBA4A,TUBA1B,TUBB3,TUBB4A,TUBB4B,TUBAL3
1_Member	Reactome Gene Sets	R-HSA-195258	RHO GTPase Effectors		808,1778,7277,10376,10381,10382,10383,79861	-7,032	10/327	CALM3,DYNCL1H1,TUBA4A,TUBA1B,TUBB3,TUBB4A,TUBB4B,YWHAQ,CYFIP2,TUBAL3
1_Member	Reactome Gene Sets	R-HSA-190828	Gap junction trafficking		7277,10376,10381,10382,10383,79861	-7,032	6/47	TUBA4A,TUBA1B,TUBB3,TUBB4A,TUBB4B,TUBAL3
1_Member	Reactome Gene Sets	R-HSA-437239	Recycling pathway of L1		7277,10376,10381,10382,10383,79861	-7,032	6/47	TUBA4A,TUBA1B,TUBB3,TUBB4A,TUBB4B,TUBAL3
1_Member	Reactome Gene Sets	R-HSA-157858	Gap junction trafficking and regulation		7277,10376,10381,10382,10383,79861	-6,931	6/49	TUBA4A,TUBA1B,TUBB3,TUBB4A,TUBB4B,TUBAL3
1_Member	Reactome Gene Sets	R-HSA-380320	Recruitment of NuMA to mitotic centrosomes		1778,7277,10376,10381,10382,10383,79861	-6,929	7/94	DYNCL1H1,TUBA4A,TUBA1B,TUBB3,TUBB4A,TUBB4B,TUBAL3
1_Member	Reactome Gene Sets	R-HSA-6807878	COP-mediated anterograde transport		1778,7277,10376,10381,10382,10383,79861	-6,719	7/101	DYNCL1H1,TUBA4A,TUBA1B,TUBB3,TUBB4A,TUBB4B,TUBAL3
1_Member	Reactome Gene Sets	R-HSA-983189	Kinesins		7277,10376,10381,10382,10383,79861	-6,462	6/59	TUBA4A,TUBA1B,TUBB3,TUBB4A,TUBB4B,TUBAL3
1_Member	Reactome Gene Sets	R-HSA-389957	Prefoldin mediated transfer of substrate to CCT/TTC		6950,7277,10381,10382,10383,79861	-6,300	5/28	TCPI1,TUBA4A,TUBB3,TUBB4A,TUBB4B
1_Member	Reactome Gene Sets	R-HSA-9648025	EML4 and NUDC in mitotic spindle formation		1778,7277,10376,10381,10382,10383,79861	-6,300	7/117	DYNCL1H1,TUBA4A,TUBA1B,TUBB3,TUBB4A,TUBB4B,TUBAL3
1_Member	Reactome Gene Sets	R-HSA-2132295	MHC class II antigen presentation		1778,7277,10376,10381,10382,10383,79861	-6,167	7/123	DYNCL1H1,TUBA4A,TUBA1B,TUBB3,TUBB4A,TUBB4B,TUBAL3
1_Member	Reactome Gene Sets	R-HSA-5617833	Cilium Assembly		1778,6950,7277,10376,10381,10382,10383,79861	-6,150	8/201	DYNCL1H1,TCPI1,TUBA4A,TUBA1B,TUBB3,TUBB4A,TUBB4B,TUBAL3
1_Member	Reactome Gene Sets	R-HSA-194315	Signaling by Rho GTPases		808,1778,2185,7277,10376,10381,10382,10383,10971,23092,26999,79861	-6,150	12/707	CALM3,DYNCL1H1,PTK2B,TUBA4A,TUBA1B,TUBB3,TUBB4A,TUBB4B,YWHAQ,ARHGAP26,CYFIP2,TUBAL3
1_Member	Reactome Gene Sets	R-HSA-2500257	Resolution of Sister Chromatid Cohesion		1778,7277,10376,10381,10382,10383,79861	-6,123	7/126	DYNCL1H1,TUBA4A,TUBA1B,TUBB3,TUBB4A,TUBB4B,TUBAL3
1_Member	Reactome Gene Sets	R-HSA-9716542	Signaling by Rho GTPases, Micro GTPases and RHOBTB3		808,1778,2185,7277,10376,10381,10382,10383,10971,23092,26999,79861	-6,059	12/723	CALM3,DYNCL1H1,PTK2B,TUBA4A,TUBA1B,TUBB3,TUBB4A,TUBB4B,YWHAQ,ARHGAP26,CYFIP2,TUBAL3

1_Member	Reactome Gene Sets	R-HSA-8856688	Golgi-to-ER retrograde transport	-8,56983	-5,976 7/133	1778,7277,10376,10381,10382,10383,79861	DYNC1H1,TUBA4A,TUBA1B,TUBB3,TUBB4A,TUBB4B,TUBAL3
1_Member	Reactome Gene Sets	R-HSA-9609690	HCMV Early Events	-8,52451	-5,940 7/135	1778,7277,10376,10381,10382,10383,79861	DYNC1H1,TUBA4A,TUBA1B,TUBB3,TUBB4A,TUBB4B,TUBAL3
1_Member	Reactome Gene Sets	R-HSA-2995410	Nuclear Envelope (NE) Reassembly	-8,50226	-5,934 6/75	7277,10376,10381,10382,10383,79861	TUBA4A,TUBA1B,TUBB3,TUBB4A,TUBB4B,TUBAL3
1_Member	Reactome Gene Sets	R-HSA-1632852	Macroautophagy	-8,50212	-5,934 7/136	1778,7277,10376,10381,10382,10383,79861	DYNC1H1,TUBA4A,TUBA1B,TUBB3,TUBB4A,TUBB4B,TUBAL3
1_Member	Reactome Gene Sets	R-HSA-8852276	The role of GTSE1 in G2/M progression after G2 checkpoint	-8,43243	-5,873 6/77	7277,10376,10381,10382,10383,79861	TUBA4A,TUBA1B,TUBB3,TUBB4A,TUBB4B,TUBAL3
1_Member	Reactome Gene Sets	R-HSA-5663220	RHO GTPases Activate Formins	-8,41424	-5,863 7/140	1778,7277,10376,10381,10382,10383,79861	DYNC1H1,TUBA4A,TUBA1B,TUBB3,TUBB4A,TUBB4B,TUBAL3
1_Member	Reactome Gene Sets	R-HSA-109582	Hemostasis	-8,24184	-5,698 11/621	490,808,2782,5576,5582,7277,10376,10381,10382,10383,79861	ATP2B1,CALM3,GNB1,PRKAR2A,PRKCG,TUBA4A,TUBA1B,TUBB3,TUBB4A,TUBB4B,TUBAL3
1_Member	Reactome Gene Sets	R-HSA-9612973	Autophagy	-8,1855	-5,650 7/151	1778,7277,10376,10381,10382,10383,79861	DYNC1H1,TUBA4A,TUBA1B,TUBB3,TUBB4A,TUBB4B,TUBAL3
1_Member	KEGG Pathway	hsa04145	Phagosome	-8,16558	-5,645 7/152	1778,7277,10376,10381,10382,10383,79861	DYNC1H1,TUBA4A,TUBA1B,TUBB3,TUBB4A,TUBB4B,TUBAL3
1_Member	Reactome Gene Sets	R-HSA-199977	ER to Golgi Anterograde Transport	-8,12615	-5,613 7/154	1778,7277,10376,10381,10382,10383,79861	DYNC1H1,TUBA4A,TUBA1B,TUBB3,TUBB4A,TUBB4B,TUBAL3
1_Member	KEGG Pathway	hsa05132	Salmonella infection	-8,04944	-5,544 8/249	1778,7277,10376,10381,10382,10383,79861	DYNC1H1,TUBA4A,TUBA1B,TUBB3,TUBB4A,TUBB4B,TUBAL3
1_Member	KEGG Pathway	hsa05014	Amyotrophic lateral sclerosis	-8,02481	-5,526 9/364	509,5532,6428,7277,10376,10381,10382,10383,79861	ATP5F1C,PPP3CB,SRSF3,TUBA4A,TUBA1B,TUBB3,TUBB4A,TUBB4B,TUBAL3
1_Member	Reactome Gene Sets	R-HSA-9609646	HCMV Infection	-8,011	-5,520 7/160	1778,7277,10376,10381,10382,10383,79861	DYNC1H1,TUBA4A,TUBA1B,TUBB3,TUBB4A,TUBB4B,TUBAL3
1_Member	Reactome Gene Sets	R-HSA-983231	Factors involved in megakaryocyte development and platelet production	-7,86432	-5,393 7/168	5576,7277,10376,10381,10382,10383,79861	PRKAR2A,TUBA4A,TUBA1B,TUBB3,TUBB4A,TUBB4B,TUBAL3
1_Member	GO Biological Processes	GO:0000226	microtubule cytoskeleton organization	-7,83935	-5,375 10/521	10382,10383,79861	DYNC1H1,MAP1A,MAP1B,MAP4,TUBA4A,TUBA1B,TUBB3,TUBB4A,TUBB4B,TUBAL3
1_Member	KEGG Pathway	hsa05010	Alzheimer disease	-7,82441	-5,367 9/384	509,808,5532,7277,10376,10381,10382,10383,79861	ATP5F1C,CALM3,PPP3CB,TUBA4A,TUBA1B,TUBB3,TUBB4A,TUBB4B,TUBAL3
1_Member	WikiPathways	WP5124	Alzheimer's disease	-7,81351	-5,362 8/267	808,5532,7277,10376,10381,10382,10383,79861	CALM3,PPP3CB,TUBA4A,TUBA1B,TUBB3,TUBB4A,TUBB4B,TUBAL3
1_Member	Reactome Gene Sets	R-HSA-6811434	COP1-dependent Golgi-to-ER retrograde traffic	-7,77013	-5,325 6/99	7277,10376,10381,10382,10383,79861	TUBA4A,TUBA1B,TUBB3,TUBB4A,TUBB4B,TUBAL3
1_Member	KEGG Pathway	hsa05020	Prion disease	-7,73859	-5,300 8/273	509,5532,7277,10376,10381,10382,10383,79861	ATP5F1C,PPP3CB,TUBA4A,TUBA1B,TUBB3,TUBB4A,TUBB4B,TUBAL3
1_Member	Reactome Gene Sets	R-HSA-948021	Transport to the Golgi and subsequent modification	-7,5756	-5,143 7/185	1778,7277,10376,10381,10382,10383,79861	DYNC1H1,TUBA4A,TUBA1B,TUBB3,TUBB4A,TUBB4B,TUBAL3
1_Member	Reactome Gene Sets	R-HSA-2467813	Separation of Sister Chromatids	-7,48031	-5,057 7/191	1778,7277,10376,10381,10382,10383,79861	DYNC1H1,TUBA4A,TUBA1B,TUBB3,TUBB4A,TUBB4B,TUBAL3
1_Member	Reactome Gene Sets	R-HSA-5620924	Intraflagellar transport	-7,47759	-5,057 5/54	7277,10376,10381,10382,10383	TUBA4A,TUBA1B,TUBB3,TUBB4A,TUBB4B
1_Member	Reactome Gene Sets	R-HSA-5610787	Hedgehog 'off' state	-7,4248	-5,012 6/113	5576,7277,10376,10381,10382,10383,79861	PRKAR2A,TUBA4A,TUBA1B,TUBB3,TUBB4A,TUBB4B
1_Member	Reactome Gene Sets	R-HSA-69275	G2/M Transition	-7,40328	-5,006 7/196	1778,7277,10376,10381,10382,10383,79861	DYNC1H1,TUBA4A,TUBA1B,TUBB3,TUBB4A,TUBB4B,TUBAL3
1_Member	KEGG Pathway	hsa05130	Pathogenic Escherichia coli infection	-7,38812	-4,996 7/197	7277,10376,10381,10382,10383,26999,79861	TUBA4A,TUBA1B,TUBB3,TUBB4A,TUBB4B,CYFIP2,TUBAL3
1_Member	Reactome Gene Sets	R-HSA-453274	Mitotic G2-G2/M phases	-7,37305	-4,987 7/198	1778,7277,10376,10381,10382,10383,79861	DYNC1H1,TUBA4A,TUBA1B,TUBB3,TUBB4A,TUBB4B,TUBAL3
1_Member	KEGG Pathway	hsa05016	Huntington disease	-7,35545	-4,975 8/306	509,6648,7277,10376,10381,10382,10383,79861	ATP5F1C,SOD2,TUBA4A,TUBA1B,TUBB3,TUBB4A,TUBB4B,TUBAL3

1_Member	GO:000278	mitotic cell cycle	-7,34595	-4,971	10/588	3,79861	808,1778,4134,7277,10376,10381,10382,10383,10657,79861	CALM3,DYNCH1,MAP4,TUBA4A,TUBA1B,TUBB3,TUBB4A,TUBB4B,KH
1_Member	R-HSA-6811442	Intra-Golgi and retrograde Golgi-to-ER traffic	-7,31353	-4,944	7/202	861	1778,7277,10376,10381,10382,10383,79	DYNCH1H1,TUBA4A,TUBA1B,TUBB3,TUBB4A,TUBB4B,TUBAL3
1_Member	R-HSA-373760	LICAM interactions	-7,29031	-4,926	6/119	861	7277,10376,10381,10382,10383,79861	TUBA4A,TUBA1B,TUBB3,TUBB4A,TUBB4B,TUBAL3
1_Member	R-HSA-68877	Mitotic Prometaphase	-7,28424	-4,925	7/204	861	1778,7277,10376,10381,10382,10383,79	DYNCH1H1,TUBA4A,TUBA1B,TUBB3,TUBB4A,TUBB4B,TUBAL3
1_Member	WP2059	Alzheimer's disease and miRNA effects	-7,03359	-4,679	8/337	3,79861	808,553,7277,10376,10381,10382,1038	CALM3,PPP3CB,TUBA4A,TUBA1B,TUBB3,TUBB4A,TUBB4B,TUBAL3
1_Member	R-HSA-68882	Mitotic Anaphase	-6,85284	-4,504	7/236	861	1778,7277,10376,10381,10382,10383,79	DYNCH1H1,TUBA4A,TUBA1B,TUBB3,TUBB4A,TUBB4B,TUBAL3
1_Member	R-HSA-2555396	Mitotic Meta phase and Anaphase	-6,84037	-4,496	7/237	861	1778,7277,10376,10381,10382,10383,79	DYNCH1H1,TUBA4A,TUBA1B,TUBB3,TUBB4A,TUBB4B,TUBAL3
1_Member	R-HSA-5653656	Vesicle-mediated transport	-6,80147	-4,462	10/673	10383,10971,79861	808,1778,3039,7277,10376,10381,10382,10383,10971,79861	CALM3,DYNCH1H1,HBA1,TUBA4A,TUBA1B,TUBB3,TUBB4A,TUBB4B,YW
1_Member	R-HSA-5358351	Signaling by Hedgehog	-6,70979	-4,375	6/149	1778,4130,4131,4134,7277,10376,10381,	PRKAR2A,TUBA4A,TUBA1B,TUBB3,TUBB4A,TUBB4B	
1_Member	GO:0007017	microtubule-based process	-6,30185	-3,996	10/763	10382,10383,79861	1778,4130,4131,4134,7277,10376,10381,10382,10383,79861	DYNCH1H1,MAP1A,MAP1B,MAP4,TUBA4A,TUBA1B,TUBB3,TUBB4A,TUB
1_Member	R-HSA-1280218	Adaptive Immune System	-6,30185	-3,996	10/763	808,1778,5532,7277,7317,10376,10381,1	CALM3,DYNCH1H1,PPP3CB,TUBA4A,TUBA1B,TUBB3,TUBB4A,TUB	
1_Member	R-HSA-446203	Asparagine N-linked glycosylation	-6,11207	-3,841	7/304	1778,7277,10376,10381,10382,10383,79	808,1778,7277,10376,10381,10382,10383,79	DYNCH1H1,TUBA4A,TUBA1B,TUBB3,TUBB4A,TUBB4B,TUBAL3
1_Member	R-HSA-199991	Membrane Trafficking	-5,98545	-3,731	9/634	3,10971,79861	808,1778,7277,10376,10381,10382,1038	CALM3,DYNCH1H1,TUBA4A,TUBA1B,TUBB3,TUBB4A,TUBB4B,YWHAQ,T
1_Member	R-HSA-380259	Loss of Nlp from mitotic centrosomes	-5,21595	-3,072	4/70	1778,7277,10382,10383	1778,7277,10382,10383	DYNCH1H1,TUBA4A,TUBB4A,TUBB4B
1_Member	R-HSA-380284	Organization of the centrosome	-5,21595	-3,072	4/70	1778,7277,10382,10383	1778,7277,10382,10383	DYNCH1H1,TUBA4A,TUBB4A,TUBB4B
1_Member	R-HSA-68886	M Phase	-5,19899	-3,058	7/418	861	1778,7277,10376,10381,10382,10383,79	DYNCH1H1,TUBA4A,TUBA1B,TUBB3,TUBB4A,TUBB4B,TUBAL3
1_Member	R-HSA-8854518	AURKA Activation by TPX2	-5,14309	-3,009	4/73	1778,7277,10382,10383	1778,7277,10382,10383	DYNCH1H1,TUBA4A,TUBB4A,TUBB4B
1_Member	R-HSA-380270	Recruitment of mitotic centrosome proteins and complexes	-4,94194	-2,830	4/82	1778,7277,10382,10383	1778,7277,10382,10383	DYNCH1H1,TUBA4A,TUBB4A,TUBB4B
1_Member	R-HSA-380287	Centrosome maturation	-4,94194	-2,830	4/82	1778,7277,10382,10383	1778,7277,10382,10383	DYNCH1H1,TUBA4A,TUBB4A,TUBB4B
1_Member	R-HSA-2565942	Regulation of PLK1 Activity at G2/M Transition	-4,82028	-2,724	4/88	1778,7277,10382,10383	1778,7277,10382,10383	DYNCH1H1,TUBA4A,TUBB4A,TUBB4B
1_Member	R-HSA-1640170	Cell Cycle	-4,71606	-2,660	8/691	1778,7277,10376,10381,10382,10383,10	971,79861	DYNCH1H1,TUBA4A,TUBA1B,TUBB3,TUBB4A,TUBB4B,YWHAQ,TUBAL3
1_Member	R-HSA-5620912	Anchoring of the basal body to the plasma membrane	-4,6356	-2,595	4/98	1778,7277,10382,10383	1778,7277,10382,10383	DYNCH1H1,TUBA4A,TUBB4A,TUBB4B
1_Member	R-HSA-69278	Cell Cycle, Mitotic	-4,38327	-2,383	7/560	861	1778,7277,10376,10381,10382,10383,79	DYNCH1H1,TUBA4A,TUBA1B,TUBB3,TUBB4A,TUBB4B,TUBAL3
1_Member	hsa04210	Apoptosis	-2,79952	-1,060	3/136	7277,10376,79861	7277,10376,79861	TUBA4A,TUBA1B,TUBAL3
1_Member	hsa04530	Tight Junction	-2,53153	-0,832	3/169	7277,10376,79861	7277,10376,79861	TUBA4A,TUBA1B,TUBAL3
2_Summary	GO:0048167	regulation of synaptic plasticity	-8,84781	-6,198	8/197	2185,4130,4131,5532,5582,7143,9066,91	45,808,4134,10381,26999,5339,5829,282	PTK2B,MAP1A,MAP1B,PPP3CB,PRKCG,TNRC18,SYNGR1,CALM3,MAP4
2_Member	GO:0048167	regulation of synaptic plasticity	-8,84781	-6,198	8/197	1,6648	2185,4130,4131,5532,5582,7143,9066,91	TUBB3,CYFIP2,PLEC,PXN,GPI,SOD2
2_Member	GO:0050804	modulation of chemical synaptic transmission	-7,42025	-5,012	9/428	808,2185,4130,4131,5532,5582,7143,906	6,9145	PTK2B,MAP1A,MAP1B,PPP3CB,PRKCG,TNRC18,SYNGR1

2_Member	GO:Biological Processes	GO:0099177	regulation of trans-synaptic signaling	-7.41159	-5.009 9/429	808,2185,4130,4131,5532,5582,7143,906 6,9145	CALM3,PTK2B,MAP1A,MAP1B,PPP3CB,PRKCG,TNR,SYT7,SYNGR1
2_Member	GO:Biological Processes	GO:0031175	neuron projection development	-4.96049	-2.841 8/639	2185,4130,4131,4134,5532,7143,10381,2 6999	PTK2B,MAP1A,MAP1B,MAP4,PPP3CB,TNR,TUBB3,CYFIP2
2_Member	GO:Biological Processes	GO:0032990	cell part morphogenesis	-4.79855	-2.719 7/482	4130,4131,5339,5532,7143,10381,26999	MAP1A,MAP1B,PLEC,PPP3CB,TNR,TUBB3,CYFIP2
2_Member	GO:Biological Processes	GO:0000902	cell morphogenesis	-4.79825	-2.719 8/673	4130,4131,5339,5532,7143,10381,2 6999	MAP1A,MAP1B,PLEC,PPP3CB,TNR,TUBB3,CYFIP2
2_Member	GO:Biological Processes	GO:0032989	cellular component morphogenesis	-4.32037	-2.336 7/573	4130,4131,5339,5532,7143,10381,26999	MAP1A,MAP1B,PLEC,PPP3CB,TNR,TUBB3,CYFIP2
2_Member	GO:Biological Processes	GO:0007611	learning or memory	-4.08098	-2.115 5/264	2821,4130,5532,5582,7143	GPI,MAP1A,PPP3CB,PRKCG,TNR
2_Member	GO:Biological Processes	GO:0048842	neuron projection morphogenesis	-3.9408	-1.991 6/455	4130,4131,5532,7143,10381,26999	MAP1A,MAP1B,PPP3CB,TNR,TUBB3,CYFIP2
2_Member	GO:Biological Processes	GO:0120039	plasma membrane bounded cell projection morphogenesis	-3.92009	-1.977 6/459	4130,4131,5532,7143,10381,26999	MAP1A,MAP1B,PPP3CB,TNR,TUBB3,CYFIP2
2_Member	GO:Biological Processes	GO:0048858	cell projection morphogenesis	-3.89958	-1.960 6/463	4130,4131,5532,7143,10381,26999	MAP1A,MAP1B,PPP3CB,TNR,TUBB3,CYFIP2
2_Member	GO:Biological Processes	GO:0050890	cognition	-3.78121	-1.864 5/306	2821,4130,5532,5582,7143	GPI,MAP1A,PPP3CB,PRKCG,TNR
2_Member	GO:Biological Processes	GO:1990138	neuron projection extension	-3.69642	-1.796 3/67	4131,5532,26999	MAP1B,PPP3CB,CYFIP2
2_Member	GO:Biological Processes	GO:0000904	cell morphogenesis involved in differentiation	-3.61818	-1.728 6/522	4130,4131,5532,5829,7143,10381	MAP1A,MAP1B,PPP3CB,TNR,TUBB3
2_Member	GO:Biological Processes	GO:0007409	axonogenesis	-3.55797	-1.676 5/342	4130,4131,5532,7143,10381	MAP1A,MAP1B,PPP3CB,TNR,TUBB3
2_Member	GO:Biological Processes	GO:0007610	axon development	-3.44299	-1.581 6/563	2821,4130,5532,5582,6648,7143	GPI,MAP1A,PPP3CB,PRKCG,SOD2,TNR
2_Member	GO:Biological Processes	GO:0061564	developmental cell growth	-3.34878	-1.508 5/380	4130,4131,5532,7143,10381	MAP1A,MAP1B,PPP3CB,TNR,TUBB3
2_Member	GO:Biological Processes	GO:0048588	cell growth	-3.27705	-1.451 3/93	4131,5532,26999	MAP1B,PPP3CB,CYFIP2
2_Member	GO:Biological Processes	GO:0016049	cell morphogenesis involved in neuron differentiation	-3.25006	-1.429 3/95	4131,5532,26999	MAP1B,PPP3CB,CYFIP2
2_Member	GO:Biological Processes	GO:0048667	developmental growth involved in morphogenesis	-2.97671	-1.384 5/411	4130,4131,5532,7143,10381	MAP1A,MAP1B,PPP3CB,TNR,TUBB3
2_Member	GO:Biological Processes	GO:0060560	learning	-2.72006	-0.991 3/145	4130,5532,7143	MAP1A,PPP3CB,TNR
2_Member	GO:Biological Processes	GO:0048589	developmental growth	-2.45826	-0.767 4/369	4131,5339,5532,26999	MAP1B,PLEC,PPP3CB,CYFIP2
2_Member	GO:Biological Processes	GO:0040007	growth	-2.44499	-0.763 4/371	4131,5339,5532,26999	MAP1B,PLEC,PPP3CB,CYFIP2
2_Member	GO:Biological Processes	GO:0007626	locomotory behavior	-2.41466	-0.737 3/186	5532,6648,7143	PPP3CB,SOD2,TNR
3_Summary	WikiPathways	WP536	Calcium regulation in cardiac cells	-8.16558	-5.645 7/152	490,808,817,2782,5576,5582,10971,5582, 5211,5213,2185,5829,1487,9066,2023,11 5827,7143,6648,4131,26999,7277,3039,5 339,509,4155	ATP2B1,CALM3,CAMK2D,GNB1,PRKAR2A,PRKCG, YWHAQ,PPP3CB,PFKL, PFKM,PTK2B,PKX,CTBP1,SYT7,ENO1,RA83C, TNR,SOD2,MAP1B,CYFIP2, TUBA4A,HBA1,PLEC,ATP5F1C,MBP
3_Member	WikiPathways	WP536	Calcium regulation in cardiac cells	-8.16558	-5.645 7/152	490,808,817,2782,5576,5582,10971	ATP2B1,CALM3,CAMK2D,GNB1,PRKAR2A,PRKCG, YWHAQ
3_Member	Reactome Gene Sets	R-HSA-111885	Opioid Signalling	-7.96254	-5.478 6/92	808,817,2782,5532,5576,5582	CALM3,CAMK2D,GNB1,PPP3CB,PRKAR2A,PRKCG
3_Member	WikiPathways	WP289	Myometrial relaxation and contraction pathways	-6.55941	-4.235 6/158	808,817,2782,5576,5582,10971	CALM3,CAMK2D,GNB1,PRKAR2A,PRKCG,YWHAQ
3_Member	Reactome Gene Sets	R-HSA-111933	Calmodulin induced events	-6.3406	-4.025 4/37	808,817,5576,5582	CALM3,CAMK2D,PRKAR2A,PRKCG
3_Member	Reactome Gene Sets	R-HSA-111997	CaM pathway	-6.3406	-4.025 4/37	808,817,5576,5582	CALM3,CAMK2D,PRKAR2A,PRKCG
3_Member	Reactome Gene Sets	R-HSA-111996	Ca-dependent events	-6.24638	-3.949 4/39	808,817,5576,5582	CALM3,CAMK2D,PRKAR2A,PRKCG
3_Member	Reactome Gene Sets	R-HSA-1489509	DAG and IP3 signaling	-6.07233	-3.806 4/43	808,817,5576,5582	CALM3,CAMK2D,PRKAR2A,PRKCG
3_Member	KEGG Pathway	hsa04922	Glucagon signaling pathway	-5.98077	-3.730 5/107	808,817,5211,5213,5532	CALM3,CAMK2D,PFKL,PFKM,PPP3CB
3_Member	KEGG Pathway	hsa05170	Human immunodeficiency virus 1 infection	-5.8126	-3.582 6/12	808,2185,2782,5532,5582,5829	CALM3,PTK2B,GNB1,PPP3CB,PRKCG,PKX
3_Member	Reactome Gene Sets	R-HSA-112043	PLC beta mediated events	-5.77024	-3.543 4/51	808,817,5576,5582	CALM3,CAMK2D,PRKAR2A,PRKCG
3_Member	KEGG Pathway	hsa05163	Human cytomegalovirus infection	-5.66293	-3.405 6/225	808,2185,2782,5532,5582,5829	CALM3,PTK2B,GNB1,PPP3CB,PRKCG,PKX
3_Member	Reactome Gene Sets	R-HSA-112040	G-protein mediated events	-5.6057	-3.401 4/56	808,817,5576,5582	CALM3,CAMK2D,PRKAR2A,PRKCG
3_Member	KEGG Pathway	hsa04728	Dopaminergic synapse	-5.5302	-3.340 5/132	808,817,2782,5532,5582	CALM3,CAMK2D,GNB1,PPP3CB,PRKCG
3_Member	KEGG Pathway	hsa04020	Calcium signaling pathway	-5.50124	-3.314 6/240	490,808,817,2185,5532,5582	ATP2B1,CALM3,CAMK2D,PTK2B,PPP3CB,PRKCG
3_Member	KEGG Pathway	hsa04720	Long-term potentiation	-5.29215	-3.135 4/67	808,817,5532,5582	CALM3,CAMK2D,PPP3CB,PRKCG
3_Member	KEGG Pathway	hsa05031	Amphetamine addiction	-5.24036	-3.088 4/69	808,817,5532,5582	CALM3,CAMK2D,PPP3CB,PRKCG
3_Member	Reactome Gene Sets	R-HSA-180024	DARPP-32 events	-4.94055	-2.830 3/26	808,5532,5576	CALM3,PPP3CB,PRKAR2A
3_Member	Reactome Gene Sets	R-HSA-418594	G alpha (i) signalling events	-4.8045	-2.719 6/318	808,817,2782,5532,5576,5582	CALM3,CAMK2D,GNB1,PPP3CB,PRKAR2A,PRKCG

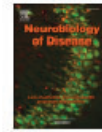
Gene	GO Biological Processes	Reactome Gene Sets	KEGG Pathway	Biological Process	Impact	Score	Pathway	Gene
5_Member	GO:0005975	Reactome Gene Sets		carbohydrate metabolic process	-2,11608	-0,485 4/462	2023,2821,5211,5213	ENO1,GPI,PFKL,PFKM
6_Summary	GO:0060341	GO Biological Processes		regulation of cellular localization	-6,17462	-3,886 -10/788	808,817,1778,2185,4130,4131,5019,5532,6950,10657,10382,10376,4134,115827	CALM3,CAMK2D,DYNC1H1,PTK2B,MAP1A,MAP1B,OXCT1,PPP3CB,TCF1,KHDRBS1,TUBB4A,TUBA1B,MAP4,RAB3C
6_Member	GO:0060341	GO Biological Processes		regulation of cellular localization	-6,17462	-3,886 -10/788	808,817,1778,2185,4130,4131,5019,5532,6950,10657	CALM3,CAMK2D,DYNC1H1,PTK2B,MAP1A,MAP1B,OXCT1,PPP3CB,TCF1,KHDRBS1
6_Member	GO:0070507	GO Biological Processes		regulation of microtubule cytoskeleton organization	-3,89262	-1,955 4/152	1778,4130,4131,10382	DYNC1H1,MAP1A,MAP1B,TUBB4A
6_Member	GO:0030705	GO Biological Processes		cytoskeleton-dependent intracellular transport	-3,53942	-1,662 4/188	1778,4130,4131,10376	DYNC1H1,MAP1A,MAP1B,TUBA1B
6_Member	GO:0031110	GO Biological Processes		regulation of microtubule polymerization or depolymerization	-3,34729	-1,508 3/88	4130,4131,10382	MAP1A,MAP1B,TUBB4A
6_Member	GO:0032886	GO Biological Processes		regulation of microtubule-based process	-3,08063	-1,287 4/249	1778,4130,4131,10382	DYNC1H1,MAP1A,MAP1B,TUBB4A
6_Member	GO:0010970	GO Biological Processes		transport along microtubule	-2,69473	-0,973 3/148	1778,4130,4131	DYNC1H1,MAP1A,MAP1B
6_Member	GO:0007018	GO Biological Processes		microtubule-based movement	-2,50951	-0,812 4/357	1778,4130,4131,4134	DYNC1H1,MAP1A,MAP1B,MAP4
6_Member	GO:0099111	GO Biological Processes		microtubule-based transport	-2,39524	-0,721 3/189	1778,4130,4131	DYNC1H1,MAP1A,MAP1B
6_Member	GO:0051640	GO Biological Processes		organelle localization	-2,09043	-0,461 4/470	1778,4131,4134,115827	DYNC1H1,MAP1B,MAP4,RAB3C
7_Summary	R-HSA-376176	Reactome Gene Sets		Signaling by ROBO receptors	-5,74234	-3,519 6/218	5332,5576,6132,6141,6147,6157,5582,4670,6426,6428,6648	PPP3CB,PRKAR2A,RPL18,RPL23A,PRKCG,HNRNPM1,SRSF1,SRSF3,SOD2
7_Member	R-HSA-376176	Reactome Gene Sets		Signaling by ROBO receptors	-5,74234	-3,519 6/218	5332,5576,6132,6141,6147,6157	PPP3CB,PRKAR2A,RPL18,RPL23A,RPL27A
7_Member	R-HSA-156902	Reactome Gene Sets		Peptide chain elongation	-4,80085	-2,719 4/89	6132,6141,6147,6157	RPL8,RPL18,RPL23A,RPL27A
7_Member	R-HSA-192823	Reactome Gene Sets		Viral mRNA Translation	-4,80085	-2,719 4/89	6132,6141,6147,6157	RPL8,RPL18,RPL23A,RPL27A
7_Member	WP477	WikiPathways		Cytoplasmic ribosomal proteins	-4,78164	-2,705 4/90	6132,6141,6147,6157	RPL8,RPL18,RPL23A,RPL27A
7_Member	R-HSA-156842	Reactome Gene Sets		Eukaryotic Translation Elongation	-4,72534	-2,667 4/93	6132,6141,6147,6157	RPL8,RPL18,RPL23A,RPL27A
7_Member	R-HSA-2408557	Reactome Gene Sets		Selenocysteine synthesis	-4,72534	-2,667 4/93	6132,6141,6147,6157	RPL8,RPL18,RPL23A,RPL27A
7_Member	R-HSA-72764	Reactome Gene Sets		Eukaryotic Translation Termination	-4,72534	-2,667 4/93	6132,6141,6147,6157	RPL8,RPL18,RPL23A,RPL27A
7_Member	R-HSA-975956	Reactome Gene Sets		Nonsense Mediated Decay (NMD) independent of the Exon Junction Complex (EJC)	-4,68885	-2,638 4/95	6132,6141,6147,6157	RPL8,RPL18,RPL23A,RPL27A
7_Member	R-HSA-72689	Reactome Gene Sets		Formation of a pool of free 40S subunits	-4,58403	-2,553 4/101	6132,6141,6147,6157	RPL8,RPL18,RPL23A,RPL27A
7_Member	R-HSA-9633012	Reactome Gene Sets		Response of EIF2AK4 (GCN2) to amino acid deficiency	-4,58403	-2,553 4/101	6132,6141,6147,6157	RPL8,RPL18,RPL23A,RPL27A
7_Member	R-HSA-156827	Reactome Gene Sets		L13a-mediated translational silencing of cytoplasmic expression	-4,42304	-2,409 4/111	6132,6141,6147,6157	RPL8,RPL18,RPL23A,RPL27A
7_Member	GO:0002181	GO Biological Processes		SRP-dependent co-translational protein targeting to membrane	-4,40779	-2,400 4/112	6132,6141,6147,6157	RPL8,RPL18,RPL23A,RPL27A
7_Member	R-HSA-1799339	Reactome Gene Sets		GTP hydrolysis and joining of the 60S ribosomal subunit	-4,40779	-2,400 4/112	6132,6141,6147,6157	RPL8,RPL18,RPL23A,RPL27A
7_Member	R-HSA-927802	Reactome Gene Sets		Nonsense-Mediated Decay (NMD) enhanced by the Exon Junction Complex (EJC)	-4,36287	-2,369 4/115	6132,6141,6147,6157	RPL8,RPL18,RPL23A,RPL27A
7_Member	R-HSA-975957	Reactome Gene Sets		Nonsense Mediated Decay (NMD)	-4,36287	-2,369 4/115	6132,6141,6147,6157	RPL8,RPL18,RPL23A,RPL27A
7_Member	hs05171	KEGG Pathway		Coronavirus disease - COVID-19	-4,34625	-2,357 5/232	5582,6132,6141,6147,6157	PRKCG,RPL8,RPL18,RPL23A,RPL27A
7_Member	R-HSA-2408522	Reactome Gene Sets		Selenoamino acid metabolism	-4,31916	-2,336 4/118	6132,6141,6147,6157	RPL8,RPL18,RPL23A,RPL27A
7_Member	R-HSA-72613	Reactome Gene Sets		Eukaryotic Translation Initiation	-4,30485	-2,326 4/119	6132,6141,6147,6157	RPL8,RPL18,RPL23A,RPL27A
7_Member	R-HSA-72737	Reactome Gene Sets		Cap-dependent Translation Initiation	-4,30485	-2,326 4/119	6132,6141,6147,6157	RPL8,RPL18,RPL23A,RPL27A
7_Member	R-HSA-168273	Reactome Gene Sets		Influenza Viral RNA Transcription and Replication	-4,09169	-2,124 4/135	6132,6141,6147,6157	RPL8,RPL18,RPL23A,RPL27A
7_Member	R-HSA-8953854	Reactome Gene Sets		Metabolism of RNA	-3,8846	-1,949 7/673	4670,6132,6141,6147,6157,6426,6428	HNRNPM1,RPL8,RPL18,RPL23A,RPL27A,SRSF1,SRSF3
7_Member	R-HSA-168255	Reactome Gene Sets		Influenza Infection	-3,8492	-1,923 4/156	6132,6141,6147,6157	RPL8,RPL18,RPL23A,RPL27A
7_Member	R-HSA-9711097	Reactome Gene Sets		Cellular response to starvation	-3,82794	-1,904 4/158	6132,6141,6147,6157	RPL8,RPL18,RPL23A,RPL27A
7_Member	hs03010	KEGG Pathway		Ribosome	-3,69631	-1,796 4/171	6132,6141,6147,6157	RPL8,RPL18,RPL23A,RPL27A
7_Member	R-HSA-9010553	Reactome Gene Sets		Regulation of expression of SLTs and ROBOs	-3,57493	-1,691 4/184	6132,6141,6147,6157	RPL8,RPL18,RPL23A,RPL27A
7_Member	R-HSA-6791226	Reactome Gene Sets		Major pathway of rRNA processing in the nucleolus and cytosol	-3,57493	-1,691 4/184	6132,6141,6147,6157	RPL8,RPL18,RPL23A,RPL27A
7_Member	R-HSA-9000970	Reactome Gene Sets		rRNA processing in the nucleolus and cytosol	-3,57493	-1,691 4/184	6132,6141,6147,6157	RPL8,RPL18,RPL23A,RPL27A

7_Member	Reactome Gene Sets	R-HSA-8868773	rRNA processing in the nucleus and cytosol	-3.48764	6132,6141,6147,6157	RPL8,RPL18,RPL23A,RPL27A
7_Member	Reactome Gene Sets	R-HSA-72312	rRNA processing	-1.553 4/204	6132,6141,6147,6157	RPL8,RPL18,RPL23A,RPL27A
7_Member	GO Biological Processes	GO:0006518	peptide metabolic process	-2.85842	6132,6141,6147,6157,6648	RPL8,RPL18,RPL23A,RPL27A,SOD2
7_Member	Reactome Gene Sets	R-HSA-72766	Translation	-1.086 4/291	6132,6141,6147,6157	RPL8,RPL18,RPL23A,RPL27A
7_Member	GO Biological Processes	GO:0006412	translation	-2.62278	6132,6141,6147,6157	RPL8,RPL18,RPL23A,RPL27A
7_Member	GO Biological Processes	GO:0043043	peptide biosynthetic process	-0.913 4/332	6132,6141,6147,6157	RPL8,RPL18,RPL23A,RPL27A
7_Member	Reactome Gene Sets	R-HSA-71291	Metabolism of amino acids and derivatives	-2.50083	6132,6141,6147,6157	RPL8,RPL18,RPL23A,RPL27A
7_Member	GO Biological Processes	GO:0043604	amide biosynthetic process	-2.43746	6132,6141,6147,6157	RPL8,RPL18,RPL23A,RPL27A
7_Member	GO Biological Processes	GO:0043603	cellular amide metabolic process	-2.07778	6132,6141,6147,6157	RPL8,RPL18,RPL23A,RPL27A
8_Summary	GO Biological Processes	GO:0009636	response to toxic substance	-2.06941	6132,6141,6147,6157,6648	RPL8,RPL18,RPL23A,RPL27A,SOD2
8_Member	GO Biological Processes	GO:0009636	response to toxic substance	-5.61871	3039,4131,4155,5582,6648,25824,2185,5 829,4670,1487,5339	HBA1,MAP1B,MBP,PRKCG,SOD2,PRDX5, EC
8_Member	GO Biological Processes	GO:0009636	response to toxic substance	-5.61871	3039,4131,4155,5582,6648,25824	HBA1,MAP1B,MBP,PRKCG,SOD2,PRDX5
8_Member	GO Biological Processes	GO:000302	response to reactive oxygen species	-4.98191	2185,3039,5829,6648,25824	PTK2B,HBA1,PKN,SOD2,PRDX5
8_Member	GO Biological Processes	GO:0006979	response to oxidative stress	-4.46872	2185,3039,4670,5829,6648,25824	PTK2B,HBA1,HNRNP,PKN,SOD2,PRDX5
8_Member	GO Biological Processes	GO:0042743	hydrogen peroxide metabolic process	-4.40144	3039,6648,25824	HBA1,SOD2,PRDX5
8_Member	GO Biological Processes	GO:0098869	cellular oxidant detoxification	-3.3187	3039,6648,25824	HBA1,SOD2,PRDX5
8_Member	WikiPathways	WP15	Selenium micronutrient network	-3.29078	3039,6648,25824	HBA1,SOD2,PRDX5
8_Member	GO Biological Processes	GO:0072593	reactive oxygen species metabolic process	-3.21067	3039,6648,25824	HBA1,SOD2,PRDX5
8_Member	Hallmark Gene Sets	M5949	HALLMARK PEROXISOME	-3.13556	1487,6648,25824	CTBP1,SOD2,PRDX5
8_Member	GO Biological Processes	GO:1990748	cellular detoxification	-3.12349	3039,6648,25824	HBA1,SOD2,PRDX5
8_Member	GO Biological Processes	GO:0042542	response to hydrogen peroxide	-3.11153	2185,3039,6648	PTK2B,HBA1,SOD2
8_Member	GO Biological Processes	GO:0097237	cellular response to toxic substance	-3.03105	3039,6648,25824	HBA1,SOD2,PRDX5
8_Member	GO Biological Processes	GO:0062197	cellular response to chemical stress	-3.01719	5339,5829,6648,25824	PLEC,PKN,SOD2,PRDX5
8_Member	GO Biological Processes	GO:0034614	cellular response to reactive oxygen species	-2.98738	5829,6648,25824	PKN,SOD2,PRDX5
8_Member	GO Biological Processes	GO:0098754	detoxification	-2.89665	3039,6648,25824	HBA1,SOD2,PRDX5
8_Member	Reactome Gene Sets	R-HSA-9711123	Cellular response to chemical stress	-2.59865	3039,6648,25824	HBA1,SOD2,PRDX5
8_Member	GO Biological Processes	GO:0034599	cellular response to oxidative stress	-2.22318	5829,6648,25824	PKN,SOD2,PRDX5
9_Summary	GO Biological Processes	GO:0097305	response to alcohol	-5.56459	490,808,2185,2782,5019,6648,4131,5339, 817,9066,5829	ATP2B1,CALM3,PTK2B,GNB1,OXCT1,SOD2, PKN
9_Member	GO Biological Processes	GO:0097305	response to alcohol	-5.56459	490,808,2185,2782,5019,6648	ATP2B1,CALM3,PTK2B,GNB1,OXCT1,SOD2
9_Member	GO Biological Processes	GO:0007584	response to nutrient	-3.99489	490,4131,5019,6648	ATP2B1,MAP1B,OXCT1,SOD2
9_Member	GO Biological Processes	GO:0033273	response to vitamin	-3.53449	490,4131,6648	ATP2B1,MAP1B,SOD2
9_Member	GO Biological Processes	GO:0097306	cellular response to alcohol	-3.3187	490,2782,6648	ATP2B1,GNB1,SOD2
9_Member	GO Biological Processes	GO:0031667	response to nutrient levels	-3.07509	490,4131,5019,5339,6648	ATP2B1,MAP1B,OXCT1,PLEC,SOD2
9_Member	GO Biological Processes	GO:0009991	response to extracellular stimulus	-2.93442	490,4131,5019,5339,6648	ATP2B1,MAP1B,OXCT1,PLEC,SOD2
9_Member	GO Biological Processes	GO:0008015	blood circulation	-2.33416	490,817,5339,6648	ATP2B1,CAMK2D,PLEC,SOD2
9_Member	GO Biological Processes	GO:0009611	response to wounding	-2.22411	4131,5339,6648,9066	MAP1B,PLEC,SOD2,SYT7
9_Member	GO Biological Processes	GO:0032870	cellular response to hormone stimulus	-2.09043	490,2782,4131,5829	ATP2B1,GNB1,MAP1B,PKN
9_Member	GO Biological Processes	GO:0003013	circulatory system process	-2.02245	490,817,5339,6648	ATP2B1,CAMK2D,PLEC,SOD2
9_Member	GO Biological Processes	GO:0003018	vascular process in circulatory system	-2.00064	490,5339,6648	ATP2B1,PLEC,SOD2
10_Summary	GO Biological Processes	GO:1903530	regulation of secretion by cell	-5.4412	808,5019,5211,5213,5532,5582,9066,115 827,6950,4130	CALM3,OXCT1,PFKL,PFKM,PPP3CB,PRKCG, SYT7,RAB3C,TCP1,MAP1A
10_Member	GO Biological Processes	GO:1903530	regulation of secretion by cell	-5.4412	808,5019,5211,5213,5532,5582,9066,115 827	CALM3,OXCT1,PFKL,PFKM,PPP3CB,PRKCG, SYT7,RAB3C
10_Member	GO Biological Processes	GO:0050796	regulation of insulin secretion	-5.30132	5019,5211,5213,5532,9066	OXCT1,PFKL,PFKM,PPP3CB,SYT7
10_Member	GO Biological Processes	GO:0051046	regulation of secretion	-5.12747	808,5019,5211,5213,5532,5582,9066,115 827	CALM3,OXCT1,PFKL,PFKM,PPP3CB,PRKCG, SYT7,RAB3C
10_Member	GO Biological Processes	GO:0090276	regulation of peptide hormone secretion	-4.90946	5019,5211,5213,5532,9066	OXCT1,PFKL,PFKM,PPP3CB,SYT7
10_Member	GO Biological Processes	GO:0002791	regulation of peptide secretion	-4.8742	5019,5211,5213,5532,9066	OXCT1,PFKL,PFKM,PPP3CB,SYT7
10_Member	GO Biological Processes	GO:0090087	regulation of peptide transport	-4.83955	5019,5211,5213,5532,9066	OXCT1,PFKL,PFKM,PPP3CB,SYT7

10_Member	GO:0046883	GO Biological Processes	regulation of hormone secretion	-4,35516	5/231	5019,5211,5213,5532,9066	OXCT1,PKL,PKM,PPP3CB,SYT7
10_Member	GO:0050708	GO Biological Processes	regulation of protein secretion	-4,17619	5/252	5019,5211,5213,5532,9066	OXCT1,PKL,PKM,PPP3CB,SYT7
10_Member	GO:0032024	GO Biological Processes	positive regulation of insulin secretion	-3,69642	3/67	5019,5213,5532	OXCT1,PKM,PPP3CB
10_Member	GO:0070201	GO Biological Processes	regulation of establishment of protein localization	-3,62712	6/520	5019,5211,5213,5532,6950,9066	OXCT1,PKL,PKM,PPP3CB,TCP1,SYT7
10_Member	GO:0090277	GO Biological Processes	positive regulation of peptide hormone secretion	-3,30466	3/91	5019,5213,5532	OXCT1,PKM,PPP3CB
10_Member	GO:0002793	GO Biological Processes	positive regulation of peptide secretion	-3,27705	3/93	5019,5213,5532	OXCT1,PKM,PPP3CB
10_Member	GO:1903829	GO Biological Processes	positive regulation of protein localization	-3,03556	5/446	4130,5019,5213,5532,6950	MAP1A,OXCT1,PKM,PPP3CB,TCP1
10_Member	GO:0046887	GO Biological Processes	positive regulation of hormone secretion	-2,95497	3/122	5019,5213,5532	OXCT1,PKM,PPP3CB
10_Member	GO:1903532	GO Biological Processes	positive regulation of secretion by cell	-2,92689	4/274	5019,5213,5532,9066	OXCT1,PKM,PPP3CB,SYT7
10_Member	GO:0050714	GO Biological Processes	positive regulation of protein secretion	-2,875	3/128	5019,5213,5532	OXCT1,PKM,PPP3CB
10_Member	GO:0051223	GO Biological Processes	regulation of protein transport	-2,83512	5/495	5019,5211,5213,5532,9066	OXCT1,PKL,PKM,PPP3CB,SYT7
10_Member	GO:0010817	GO Biological Processes	regulation of hormone levels	-2,83127	5/496	5019,5211,5213,5532,9066	OXCT1,PKL,PKM,PPP3CB,SYT7
10_Member	GO:0051047	GO Biological Processes	positive regulation of secretion	-2,78253	4/300	5019,5213,5532,9066	OXCT1,PKM,PPP3CB,SYT7
10_Member	GO:1904951	GO Biological Processes	positive regulation of establishment of protein localization	-2,73576	4/309	5019,5213,5532,6950	OXCT1,PKM,PPP3CB,TCP1
11_Summary	GO:0009725	GO Biological Processes	response to hormone	-5,4264	9/742	490,808,2185,2782,2821,4131,4155,5019,5829,10971,5582,7143	ATP2B1,CALM3,PTK2B,GNB1,GPI,MAP1B,MBP,OXCT1,PKN,YWHAQ,PRKCG,TNR
11_Member	GO:0009725	GO Biological Processes	response to hormone	-5,4264	9/742	490,808,2185,2782,2821,4131,4155,5019,5829	ATP2B1,CALM3,PTK2B,GNB1,GPI,MAP1B,MBP,OXCT1,PKN
11_Member	GO:1901654	GO Biological Processes	response to ketone	-4,77204	5/189	490,808,2782,2821,4155	ATP2B1,CALM3,GNB1,GPI,MBP
11_Member	GO:0021762	GO Biological Processes	substantia nigra development	-4,24291	3/44	808,4155,10971	CALM3,MBP,YWHAQ
11_Member	GO:0048857	GO Biological Processes	neural nucleus development	-1,843	3/64	808,4155,10971	CALM3,MBP,YWHAQ
11_Member	GO:0030901	GO Biological Processes	midbrain development	-3,39146	3/85	808,4155,10971	CALM3,MBP,YWHAQ
11_Member	R-HSA-418346	Reactome Gene Sets	Platelet homeostasis	-3,34729	3/88	490,808,2782	ATP2B1,CALM3,GNB1
11_Member	hsa04970	KEGG Pathway	Salivary secretion	-3,27705	3/93	490,808,5582	ATP2B1,CALM3,PRKCG
11_Member	GO:0048545	GO Biological Processes	response to steroid hormone	-2,93861	4/272	490,808,2821,4155	ATP2B1,CALM3,GPI,MBP
11_Member	GO:0007420	GO Biological Processes	brain development	-2,82009	6/742	490,808,4155,5019,7143,10971	ATP2B1,CALM3,MBP,OXCT1,TNR,YWHAQ
11_Member	GO:0060322	GO Biological Processes	head development	-2,69111	6/787	490,808,4155,5019,7143,10971	ATP2B1,CALM3,MBP,OXCT1,TNR,YWHAQ
12_Summary	GO:0035902	GO Biological Processes	response to immobilization stress	-5,29561	3/20	2185,2821,6648,5582,7143,873,4131,5211,1817,5019,5829,10971,2023,4130,6950	PTK2B,GPI,SOD2,PRKCG,TNR,CBR1,MAP1B,PKL,CAMK2D,OXCT1,PKN,YWHAQ,ENO1,MAP1A,TCPI
12_Member	GO:0035902	GO Biological Processes	response to immobilization stress	-5,29561	3/20	2185,2821,6648	PTK2B,GPI,SOD2
12_Member	GO:0043524	GO Biological Processes	negative regulation of neuron apoptotic process	-3,97159	4/145	2185,2821,5582,6648	PTK2B,GPI,PRKCG,SOD2
12_Member	GO:0060291	GO Biological Processes	long-term synaptic potentiation	-3,92833	3/56	2185,5582,7143	PTK2B,PRKCG,TNR
12_Member	GO:2000379	GO Biological Processes	positive regulation of reactive oxygen species metabolic process	-3,62181	3/71	873,2185,6648	CBR1,PTK2B,SOD2
12_Member	GO:0009743	GO Biological Processes	response to carbohydrate	-3,60211	4/181	2185,4131,5211,6648	PTK2B,MAP1B,PKL,SOD2
12_Member	GO:0010660	GO Biological Processes	regulation of muscle cell apoptotic process	-3,45298	3/81	817,2185,6648	CAMK2D,PTK2B,SOD2
12_Member	GO:0043523	GO Biological Processes	regulation of neuron apoptotic process	-3,38111	4/207	2185,2821,5582,6648	PTK2B,GPI,PRKCG,SOD2
12_Member	GO:1901215	GO Biological Processes	negative regulation of neuron death	-1,519	4/209	2185,2821,5582,6648	PTK2B,GPI,PRKCG,SOD2
12_Member	GO:0009410	GO Biological Processes	response to xenobiotic stimulus	-3,24291	5/401	873,2185,4131,5019,6648	CBR1,PTK2B,MAP1B,OXCT1,SOD2
12_Member	GO:0043279	GO Biological Processes	response to alkaloid	-3,22366	4/97	2185,2821,5582	PTK2B,GPI,PRKCG
12_Member	hsa04670	KEGG Pathway	Leukocyte transendothelial migration	-3,01998	3/114	2185,5582,5829	PTK2B,PRKCG,PKN
12_Member	GO:0045471	GO Biological Processes	response to ethanol	-2,96614	3/119	2185,5019,6648	PTK2B,OXCT1,SOD2
12_Member	GO:0050806	GO Biological Processes	positive regulation of synaptic transmission	-1,019	3/141	2185,5582,7143	PTK2B,PRKCG,TNR
12_Member	GO:1901214	GO Biological Processes	regulation of neuron death	-2,71545	4/313	2185,2821,5582,6648	PTK2B,GPI,PRKCG,SOD2
12_Member	GO:2000377	GO Biological Processes	regulation of reactive oxygen species metabolic process	-2,70311	3/147	873,2185,6648	CBR1,PTK2B,SOD2
12_Member	WP4666	WikiPathways	Hepatitis B infection	-2,64569	3/154	2185,5582,10971	PTK2B,PRKCG,YWHAQ
12_Member	GO:0034284	GO Biological Processes	response to monosaccharide	-2,63772	3/155	2185,5211,6648	PTK2B,PKL,SOD2

Accession	Category	Gene	GO Term	Biological Process	Cellular Component	Molecular Function	Score	Log P	Pathway
12_Member	KEGG Pathway	hsa05161	Hepatitis B				-2,58339	-0,876 3/162	2185,5582,10971
12_Member	GO Biological Processes	GO:0046777	protein autophosphorylation				-2,41466	-0,737 3/186	817,2185,5582
12_Member	GO Biological Processes	GO:0080135	regulation of cellular response to stress				-2,21298	-0,567 5/692	2023,2185,5582,6648,7143
12_Member	GO Biological Processes	GO:1903050	regulation of proteolysis involved in cellular protein catabolic process				-2,19606	-0,554 3/223	2185,4130,5582
12_Member	GO Biological Processes	GO:0051054	positive regulation of DNA metabolic process				-2,15402	-0,518 3/231	2185,5582,6950
12_Member	GO Biological Processes	GO:1903362	regulation of cellular protein catabolic process				-2,0232	-0,404 3/258	2185,4130,5582
13_Summary	Hallmark Gene Sets	M5926	HALLMARK MYC TARGETS V1				-4,65397	-2,607 5/200	6141,6426,6428,6950,10971,4670,10657
13_Member	Hallmark Gene Sets	M5926	HALLMARK MYC TARGETS V1				-4,65397	-2,607 5/200	6141,6426,6428,6950,10971
13_Member	WikiPathways	WP411	mRNA processing				-2,80726	-1,084 3/133	4670,6426,6428
13_Member	KEGG Pathway	hsa0340	Spliceosome				-2,70311	-0,979 3/147	4670,6426,6428
13_Member	GO Biological Processes	GO:0043484	regulation of RNA splicing				-2,64569	-0,931 3/154	6426,6428,10657
13_Member	GO Biological Processes	GO:0006403	RNA localization				-2,47503	-0,781 3/177	6426,6428,6950
13_Member	Reactome Gene Sets	R-HSA-72163	mRNA Splicing - Major Pathway				-2,43443	-0,752 3/183	4670,6426,6428
13_Member	Reactome Gene Sets	R-HSA-72172	mRNA Splicing				-2,38248	-0,709 3/191	4670,6426,6428
13_Member	GO Biological Processes	GO:0006397	mRNA processing				-2,12191	-0,497 4/458	4670,6426,6428,10657
13_Member	Reactome Gene Sets	R-HSA-72203	Processing of Capped Intron-Containing Pre-mRNA				-2,08903	-0,460 3/244	4670,6426,6428
14_Summary	Reactome Gene Sets	R-HSA-4420097	VEGFA-VEGFR2 Pathway				-4,61823	-2,582 4/99	808,2185,5829,26999,1778,4130,4131,10382,26999,382,490,6648,7143,2782,2821,5339,6950,4670,817
14_Member	Reactome Gene Sets	R-HSA-4420097	VEGFA-VEGFR2 Pathway				-4,61823	-2,582 4/99	808,2185,5829,26999
14_Member	GO Biological Processes	GO:0051493	regulation of cytoskeleton organization				-4,56111	-2,535 7/525	1778,2185,4130,4131,5829,10382,26999
14_Member	Reactome Gene Sets	R-HSA-194138	Signaling by VEGF				-4,46969	-2,452 4/108	808,2185,5829,26999
14_Member	GO Biological Processes	GO:1902903	regulation of supramolecular fiber organization				-4,40336	-2,399 6/375	2185,4130,4131,5829,10382,26999
14_Member	GO Biological Processes	GO:0090066	regulation of anatomical structure size				-3,78051	-1,864 6/487	490,2185,4131,6648,7143,26999
14_Member	Canonical Pathways	M15	PID LYSPHOSPHOLIPID PATHWAY				-3,73549	-1,826 3/65	2185,2782,5829
14_Member	GO Biological Processes	GO:0051495	positive regulation of cytoskeleton organization				-3,47918	-1,610 4/195	1778,2185,4131,5829
14_Member	GO Biological Processes	GO:0009612	response to mechanical stimulus				-3,42936	-1,574 4/201	2185,2821,4131,5339
14_Member	GO Biological Processes	GO:0032271	regulation of protein polymerization				-3,42936	-1,574 4/201	2185,4131,10382,26999
14_Member	Canonical Pathways	M124	PID CXCR4 PATHWAY				-3,18511	-1,377 3/100	2185,2782,5829
14_Member	Reactome Gene Sets	R-HSA-1500931	Cell-Cell communication				-2,8702	-1,113 5/486	1778,2185,4131,5829,6950
14_Member	Reactome Gene Sets	R-HSA-9006934	Signaling by Receptor Tyrosine Kinases				-2,73778	-1,110 3/129	2185,5339,5829
14_Member	WikiPathways	WP3929	Chemokine signaling pathway				-2,56088	-0,855 3/165	808,2185,4670,5829,26999
14_Member	GO Biological Processes	GO:0032535	regulation of cellular component size				-2,53586	-0,833 4/351	2185,2782,5829
14_Member	GO Biological Processes	GO:1902905	positive regulation of supramolecular fiber organization				-2,48194	-0,787 3/176	2185,4131,5829
14_Member	GO Biological Processes	GO:0001667	ameboid-type cell migration				-2,43443	-0,752 3/183	2185,5339,5829
14_Member	KEGG Pathway	hsa04062	Chemokine signaling pathway				-2,37615	-0,704 3/192	2185,2782,5829
14_Member	GO Biological Processes	GO:0032970	regulation of actin filament-based process				-2,36511	-0,694 4/392	817,2185,5829,26999
14_Member	GO Biological Processes	GO:0043254	regulation of protein-containing complex assembly				-2,33034	-0,665 4/401	2185,4131,10382,26999
14_Member	GO Biological Processes	GO:0034330	cell junction organization				-2,08094	-0,453 4/473	2185,4131,5339,7143
14_Member	GO Biological Processes	GO:0044089	positive regulation of cellular component biogenesis				-2,01944	-0,402 4/493	1778,2185,4131,5829
14_Member	GO Biological Processes	GO:0034329	cell junction assembly				-2,01865	-0,402 3/259	2185,4131,5339
15_Summary	GO Biological Processes	GO:0030162	regulation of proteolysis				-4,49158	-2,470 8/743	2023,2185,2821,4130,4155,5582,25824,26999,10971
15_Member	GO Biological Processes	GO:0030162	regulation of proteolysis				-4,49158	-2,470 8/743	2023,2185,2821,4130,4155,5582,25824,26999
15_Member	Reactome Gene Sets	R-HSA-5628897	TP53 Regulates Metabolic Genes				-3,36183	-1,517 3/87	2821,10971,25824
15_Member	GO Biological Processes	GO:0045861	negative regulation of proteolysis				-2,5403	-0,836 4/350	2821,4130,5582,25824

15_Member	GO:0052548	GO Biological Processes	regulation of endopeptidase activity	-2,23826	-0.585	4/426	2821,4155,25824,26999	GPI,MBP,PRDX5,CYFP2
15_Member	GO:2000116	GO Biological Processes	regulation of cysteine-type endopeptidase activity	-2,16438	-0.526	3/229	2821,25824,26999	GPI,PRDX5,CYFP2
15_Member	GO:0052547	GO Biological Processes	regulation of peptidase activity	-2,13566	-0.502	4/456	2821,4155,25824,26999	GPI,MBP,PRDX5,CYFP2
16_Summary	GO:0060249	GO Biological Processes	anatomical structure homeostasis	-3,95382	-2,002	5/281	490,2185,4130,4155,5213	ATP2B1,PTK2B,MAP1A,MBP,PFKM
16_Member	GO:0060249	GO Biological Processes	anatomical structure homeostasis	-3,95382	-2,002	5/281	490,2185,4130,4155,5213	ATP2B1,PTK2B,MAP1A,MBP,PFKM
17_Summary	GO:0006887	GO Biological Processes	exocytosis	-3,25946	-1,435	4/223	5332,9066,9145,115827,490,2185,4155,6428,10376	PPP3CB,SYT7,SYNGR1,RAB3C,ATP2B1,PTK2B,MBP,SRSF3,TUBA1B
17_Member	GO:0006887	GO Biological Processes	exocytosis	-3,25946	-1,435	4/223	5332,9066,9145,115827	PPP3CB,SYT7,SYNGR1,RAB3C
17_Member	GO:0140352	GO Biological Processes	export from cell	-3,13844	-1,338	5/423	490,532,9066,9145,115827	ATP2B1,PPP3CB,SYT7,SYNGR1,RAB3C
17_Member	GO:0045055	GO Biological Processes	regulated exocytosis	-2,875	-1,116	3/128	5332,9066,9145	PPP3CB,SYT7,SYNGR1
17_Member	GO:0034097	GO Biological Processes	response to cytokine	-2,65821	-0,940	6/799	2185,4155,5532,6428,9145,10376	PTK2B,MBP,PPP3CB,SRSF3,SYNGR1,TUBA1B
17_Member	GO:0032940	GO Biological Processes	secretion by cell	-2,44574	-0,760	4/372	5332,9066,9145,115827	PPP3CB,SYT7,SYNGR1,RAB3C
17_Member	GO:0046903	GO Biological Processes	secretion	-2,04368	-0,421	4/485	5332,9066,9145,115827	PPP3CB,SYT7,SYNGR1,RAB3C
18_Summary	R-HSA-1592230	Reactome Gene Sets	Mitochondrial biogenesis	-3,25006	-1,429	3/95	509,808,6648,5213,5339,873	ATP5F1C,CALMB,SOD2,PFKM,PLEC,CBR1
18_Member	R-HSA-1592230	Reactome Gene Sets	Mitochondrial biogenesis	-3,25006	-1,429	3/95	509,808,6648	ATP5F1C,CALMB,SOD2
18_Member	GO:0015980	GO Biological Processes	energy derivation by oxidation of organic compounds	-3,12004	-1,323	4/243	509,5213,5339,6648	ATP5F1C,PFKM,PLEC,SOD2
18_Member	GO:0045333	GO Biological Processes	cellular respiration	-2,45454	-0,766	3/180	509,5339,6648	ATP5F1C,PLEC,SOD2
18_Member	hsa05208	KEGG Pathway	Chemical carcinogenesis - reactive oxygen species	-2,19606	-0,554	3/223	509,873,6648	ATP5F1C,CBR1,SOD2
19_Summary	GO:0050770	GO Biological Processes	regulation of axonogenesis	-2,64569	-0,931	3/154	4131,4155,7143,2185,4134,10382	MAP1B,MBP,TNR,PTK2B,MAP4,TUBB4A
19_Member	GO:0050770	GO Biological Processes	regulation of axonogenesis	-2,64569	-0,931	3/154	4131,4155,7143	MAP1B,MBP,TNR
19_Member	GO:0120035	GO Biological Processes	regulation of plasma membrane bounded cell projection organization	-2,40698	-0,731	5/622	2185,4131,4134,4155,7143	PTK2B,MAP1B,MAP4,MBP,TNR
19_Member	GO:0031345	GO Biological Processes	negative regulation of cell projection organization	-2,40168	-0,726	3/188	4134,4155,7143	MAP4,MBP,TNR
19_Member	GO:0031344	GO Biological Processes	regulation of cell projection organization	-2,35754	-0,689	5/639	2185,4131,4134,4155,7143	PTK2B,MAP1B,MAP4,MBP,TNR
19_Member	GO:0051129	GO Biological Processes	negative regulation of cellular component organization	-2,23393	-0,582	5/684	4131,4134,4155,7143,10382	MAP1B,MAP4,MBP,TNR,TUBB4A
19_Member	GO:0010975	GO Biological Processes	regulation of neuron projection development	-2,22059	-0,572	4/431	2185,4131,4155,7143	PTK2B,MAP1B,MBP,TNR
20_Summary	GO:0045862	GO Biological Processes	positive regulation of proteolysis	-2,45826	-0,767	4/369	2023,2185,4155,26999,10376,23092	ENO1,PTK2B,MBP,CYFP2,TUBA1B,ARHGAP26
20_Member	GO:0045862	GO Biological Processes	positive regulation of proteolysis	-2,45826	-0,767	4/369	2023,2185,4155,26999	ENO1,PTK2B,MBP,CYFP2
20_Member	R-HSA-9012999	Reactome Gene Sets	RHO GTPase cycle	-2,15889	-0,522	4/449	2185,10376,23092,26999	PTK2B,TUBA1B,ARHGAP26,CYFP2



Mitochondrial fission in Huntington's disease mouse striatum disrupts ER-mitochondria contacts leading to disturbances in Ca^{2+} efflux and Reactive Oxygen Species (ROS) homeostasis

Marta Cherubini^{a,b,c,1}, Laura Lopez-Molina^{a,b,c,1}, Silvia Gines^{a,b,c,4}

^a Departament de Biomedicina, Facultat de Medicina, Institut de Neurociències, Universitat de Barcelona, Barcelona, Spain

^b Institut d'Investigacions Biomèdiques August Pi i Sunyer (IDIBAPS), Barcelona, Spain

^c Centro de Investigación Biomédica en Red sobre Enfermedades Neurodegenerativas (CIBERNED), Madrid, Spain



ARTICLE INFO

Keywords:
Huntington's disease
Mitochondria
MAMs
ROS
Fission
Calcium dysregulation

ABSTRACT

Mitochondria-associated membranes (MAMs) are dynamic structures that communicate endoplasmic reticulum (ER) and mitochondria allowing calcium transfer between these two organelles. Since calcium dysregulation is an important hallmark of several neurodegenerative diseases, disruption of MAMs has been speculated to contribute to pathological features associated with these neurodegenerative processes. In Huntington's disease (HD), mutant huntingtin induces the selective loss of medium spiny neurons within the striatum. The cause of this specific susceptibility remain unclear. However, defects on mitochondrial dynamics and bioenergetics have been proposed as critical contributors, causing accumulation of fragmented mitochondria and subsequent Ca^{2+} homeostasis alterations. In the present work, we show that aberrant Drp1-mediated mitochondrial fragmentation within the striatum of HD mutant mice, forces mitochondria to place far away from the ER disrupting the ER-mitochondria association and therefore causing drawbacks in Ca^{2+} efflux and an excessive production of mitochondria superoxide species. Accordingly, inhibition of Drp1 activity by Mdivi-1 treatment restored ER-mitochondria contacts, mitochondria dysfunction and Ca^{2+} homeostasis.

In sum, our results give new insight on how defects on mitochondria dynamics may contribute to striatal vulnerability in HD and highlights MAMs dysfunction as an important factor involved in HD striatal pathology.

1. Introduction

Mitochondria are dynamic organelles that provide energy to cells and buffer intracellular calcium (Ca^{2+}). In neurons, which critically depend on mitochondria function due to their high-energy demands, mitochondria can travel from the soma to dendritic and axonal processes to supply local necessities of Adenosine triphosphate (ATP) and Ca^{2+} maintenance. To ensure a proper distribution, mitochondria dynamically undergo shape changes modulated through regulated fission and fusion events (Frederick and Shaw, 2007; Campello and Scorrano, 2010).

Mitochondria are not isolated structures but interact with other organelles. The best characterized inter-organelle crosstalk is between mitochondria and endoplasmic reticulum (ER). These contact sites called *mitochondria-associated membranes* (MAMs) are specialized regions that act as a signaling hub to regulate cellular Ca^{2+} homeostasis (Rustio et al., 1994; Rizzuto et al., 1998; Csordás et al., 2006). Indeed, it has been reported that ER releases calcium in this specialized membrane hotspots directed towards mitochondria in order to maintain cellular bioenergetics and mitochondrial dynamics and therefore, cellular lifespan (Szabadkai et al., 2006; Rowland and Voeltz, 2012). These contact sites are characterized by a proteome enriched in

Abbreviations: AD, Alzheimer's disease; ATP, Adenosine triphosphate; Drp1, Dynamin-related protein 1; DAPI, 4',6-diamidino-2-phenylindole; ER, Endoplasmic Reticulum; FCCP, Trifluoromethoxy carbonylcyanide phenylhydrazone; GRP75, Glucose-regulated protein 75; HD, Huntington's Disease; IP3R3, Inositol 1,4,5-trisphosphate receptor 3; MAMs, Mitochondria-Associated membranes; MAP-2, Microtubule-associated protein-2; Mfn2, Mitofusin-2; Mdivi-1, Mitochondrial division inhibitor 1; mHtt, mutant Huntingtin; PCR, Polymerase Chain reaction; PLA, Proximity Ligation Assay; PFA, Paraformaldehyde; PTP, Permeability transition pore; ROS, Reactive oxygen species; SERCA, Sarcoplasmic Ca^{2+} -ATPase; TG, Thapsigargin; TMRM, Tetramethylrhodamine, methyl ester; VDAC1, Voltage-dependent anion-selective channel 1; WT, Wild type

* Corresponding author at: Dept of Biomedical Science, School of Medicine, University of Barcelona, Casanova 143, Barcelona 08036, Spain.

E-mail address: silviagines@ub.edu (S. Gines).

¹ These authors contribute equally to this work.

<https://doi.org/10.1016/j.nbd.2020.104741>

Received 25 June 2019; Received in revised form 26 November 2019; Accepted 8 January 2020

Available online 10 January 2020

0969-9961/© 2020 The Authors. Published by Elsevier Inc. This is an open access article under the CC BY-NC-ND license

(<http://creativecommons.org/licenses/by-nc-nd/4.0/>).



Article

Pyk2 Regulates MAMs and Mitochondrial Dynamics in Hippocampal Neurons

Laura López-Molina^{1,2,3}, Joaquín Fernández-Irigoyen⁴, Carmen Cifuentes-Díaz^{5,6,7}, Jordi Alberch^{1,2,3,8}, Jean-Antoine Girault^{5,6,7}, Enrique Santamaría⁹, Silvia Ginés^{1,2,3} and Albert Giral^{1,2,3,8,*}

- ¹ Departament de Biomedicina, Facultat de Medicina, Institut de Neurociències, Universitat de Barcelona, 08036 Barcelona, Spain; laura.lopezmo12@ub.edu (L.L.-M.); alberch@ub.edu (J.A.); silviagines@ub.edu (S.G.)
- ² Institut d'Investigacions Biomèdiques August Pi i Sunyer (IDIBAPS), 08036 Barcelona, Spain
- ³ Centro de Investigación Biomédica en Red sobre Enfermedades Neurodegenerativas (CIBERNED), 28031 Madrid, Spain
- ⁴ Proteomics Platform, Navarrabiomed, Hospital Universitario de Navarra (HUN), Universidad Pública de Navarra UPNA, IdISNA, 31008 Pamplona, Spain; joaquin.fernandez.irigoyen@navarra.es
- ⁵ Inserm UMR-S 1270, 75005 Paris, France; carmen.diaz@inserm.fr (C.C.-D.); jean-antoine.girault@inserm.fr (J.-A.G.)
- ⁶ Sorbonne Université, 75005 Paris, France
- ⁷ Institut du Fer à Moulin, 75005 Paris, France
- ⁸ Production and Validation Centre of Advanced Therapies (Creatio), Faculty of Medicine and Health Science, University of Barcelona, 08036 Barcelona, Spain
- ⁹ Clinical Neuroproteomics Unit, Navarrabiomed, Hospital Universitario de Navarra (HUN), Universidad Pública de Navarra UPNA, IdISNA, 31008 Pamplona, Spain; enrique.santamaría.martinez@navarra.es
- * Correspondence: albertgiral@ub.edu



Citation: López-Molina, L.; Fernández-Irigoyen, J.; Cifuentes-Díaz, C.; Alberch, J.; Girault, J.-A.; Santamaría, E.; Ginés, S.; Giral, A. Pyk2 Regulates MAMs and Mitochondrial Dynamics in Hippocampal Neurons. *Cells* **2022**, *11*, 842. <https://doi.org/10.3390/cells11050842>

Academic Editor: Dmitri Rasakov

Received: 7 January 2022
Accepted: 25 February 2022
Published: 1 March 2022

Publisher's Note: MDPI stays neutral with regard to jurisdictional claims in published maps and institutional affiliations.



Copyright © 2022 by the authors. Licensee MDPI, Basel, Switzerland. This article is an open access article distributed under the terms and conditions of the Creative Commons Attribution (CC BY) license (<https://creativecommons.org/licenses/by/4.0/>).

Abstract: Pyk2 is a non-receptor tyrosine kinase enriched in hippocampal neurons, which can be activated by calcium-dependent mechanisms. In neurons, Pyk2 is mostly localised in the cytosol and dendritic shafts but can translocate to spines and/or to the nucleus. Here, we explore the function of a new localisation of Pyk2 in mitochondria-associated membranes (MAMs), a subdomain of ER-mitochondria surface that acts as a signalling hub in calcium regulation. To test the role of Pyk2 in MAMs' calcium transport, we used full Pyk2 knockout mice (Pyk2^{-/-}) for *in vivo* and *in vitro* studies. Here we report that Pyk2^{-/-} hippocampal neurons present increased ER-mitochondrial contacts along with defective calcium homeostasis. We also show how the absence of Pyk2 modulates mitochondrial dynamics and morphology. Taken all together, our results point out that Pyk2 could be highly relevant in the modulation of ER-mitochondria calcium efflux, affecting in turn mitochondrial function.

Keywords: hippocampus; calcium; ER-mitochondria contact sites; neuron

1. Introduction

Proline-rich tyrosine kinase 2 (Pyk2) is a Ca²⁺-activated non-receptor tyrosine kinase belonging to the focal adhesion kinase (FAK) family [1]. Pyk2 is enriched in hippocampal adult neurons and plays an important role in neuronal plasticity and hippocampal-related memory [2]. In neurons, Pyk2 is mostly localised in the cytosol and dendritic shafts [3,4]. However, we and others have previously demonstrated that following neuronal activation, Pyk2 translocates to other subcellular compartments, such as the nucleus or the excitatory synapses [5,6]. Indeed, several studies have suggested Pyk2 as a key regulator in synaptic plasticity involved with both LTP and LTD [2,7,8]. In this line, we and others have shown that this role of Pyk2 in synaptic plasticity is compromised in different neurodegenerative disorders, such as Alzheimer's disease and Huntington's disease [2,7–9].

Besides this nuclear and synaptic localisation, following Ca²⁺ entry into the cell via the transient receptor potential (TRP) channel, Pyk2 can be phosphorylated and partially

